Imperial College London

Multi-Fidelity Probabilistic Optimisation of Composite Structures

By

Kwangkyu (Alex) Yoo

Thesis submitted in part fulfilment of the requirements

for the degree of Doctor of Philosophy of Imperial College London

Department of Aeronautics

Faculty of Engineering

Imperial College London

2021

Declaration of Originality

I hereby confirm that the work presented in this thesis is my own. All else is appropriately referenced.

Copyright Declaration

"Because the patriarchs were jealous of Joseph, they sold him as a slave into Egypt. But God was with him and rescued him from all his troubles. He gave Joseph wisdom and enabled him to gain the goodwill of Pharaoh king of Egypt. So Pharaoh made him ruler over Egypt and all his palace."

- Acts 7:9- 10, NIVUK

Acknowledgements

I would like to express my utmost glory to God in the highest for the careful guidance and exquisite intervention he has given me over the last four years. Thanks to God's provision, I was able to step out of my comfort zone in South Korea, followed by running for this long journey in the UK.

I would also like to express my deepest and earnest appreciation to my supervisors, Professor Ferri Aliabadi and Dr Omar Bacarreza, for their invaluable support and tailored supervision during my PhD. They have provided me with uncounted theoretical knowledge and intellectual insight for professional academic development. They always allowed me to reach out to them every time I needed advice. It is a blessing that I have worked with them for my PhD.

I am grateful to the academic staff in the department, Dr Zahra Sharif Khodaei and Dr Errikos Levis, for providing me with career advice and teaching opportunities. Thanks to them, I have gained a wealth of experience that will be valuable in my future career as an independent academic researcher.

I am perpetually thankful to my family, particularly my parents, Kiho and Mihyang, my parents-in-law, Beomseung and Jinju, my sister Boram, and my sister-in-law Yena, for their countless encouragement and formidable support over the last four years. I would not have been able to accomplish as much as I did without their backing.

I want to express my unconditional thank to my friends at Imperial, namely Andres, Cheng, Dimitrios, Francisco, Hanxun, Janos, Karim, Massimiliano, Natalia, Yingwei, Yu and Valentin. I would especially like to thank Julia, Llewellyn, Max and Nick for the kind-hearted proofreading of my writing and intensive training in my English speaking. I would love to thank my Korean friends, particularly Chanhui, Chungsun, Kyoungmin, Youni and Younmo, for their immeasurable moral support. Without these beautiful friends, it is hardly an exaggeration to say that completing PhD would not have been much enjoyable. Finally, I am thankful to my friends at Lighthouse London Church, notably Davide, Elias, Kate, Kristin, Jamie, Mohyin and Rebekah, for the faithful and thoughtful prayers when I was stranded on hardship.

Last but definitely not least, I want to express my ultimate love to my wife, Dr Ye Seol Lauren Lee, for the worthwhile support and unwavering confidence she has delivered to me over the last eight years. She has empowered me to be resilient and courageous to go through this PhD. I am absolutely delighted to dedicate this PhD thesis to my lovely wife, Dr Ye Seol Lauren Lee.

Abstract

In this thesis, novel multi-fidelity modelling-based probabilistic optimisation methods are presented to address the computational challenge of stochastic design philosophies applied to complex aircraft composite structures. Novel multi-fidelity formulations developed in this thesis, blending High-Fidelity Model (HFM) and Low-Fidelity Model (LFM), are shown to significantly improve computational efficiency by making use of machine learning techniques, such as Artificial Neural Networks (ANN) and Non-linear Auto-Regressive Gaussian Process (NARGP). To further improve the computational efficiency compared to the conventional probabilistic optimisation methods, a multi-level optimisation approach and a new sampling strategy to collect training data points are incorporated into the multi-fidelity formulations for the first time. In the developed optimisation methods, the HFM covers part of the design space whilst the LFM explores the whole design space to fill the lack of high-fidelity information. This improvement enables the multi-fidelity formulations to request a much smaller number of high-fidelity information causing considerable computational costs. Several engineering examples such as aircraft mono-stringer composite panels are used to demonstrate the accuracy and computational efficiency of the developed methods when used with different reliability and robustness analysis techniques, including Monte Carlo Simulation (MCS), the First-Order Reliability Method (FORM) and the Second-Order Reliability Method (SORM). The composite panels are subjected to mechanical and thermomechanical loads to show the broad range of potential applications. It is shown that the newly developed multi-fidelity probabilistic optimisation methods offer substantial computational time savings ranging from 50 % to 70 % and levels of error typically less than 1 % when compared with traditional probabilistic optimisation methods. Results demonstrate that the newly developed multi-fidelity probabilistic optimisation methods herein provide significant computational benefits and accurately predict the influence of uncertainties associated with design and manufacturing stages. As a result, the presented methods confidently carry out reliability-based and robust design optimisation of large-scale and complex aircraft composite structures.

Contents

List of Figures

List of Tables

1 Introduction

Innovative and sustainable design technologies are associated with improvements in energy efficiency and reductions in carbon emission, due in part to the increased use of composite materials and the fundamental advantages that they offer, specifically their high strength and lightweight (1). Structures using these materials are widely employed in a vast range of infrastructure manufacturing industry, such as aircraft, renewable energy, naval architecture and automobile. However, traditional design approaches do not consider design uncertainties that every engineering system holds across the entire lifecycle. These uncertainties emanate from design, manufacturing, operation and ageing, which can deteriorate the performance quality of a structure. The design process without considering the uncertainties may also lead either to premature structural failure or a conservative design based on high safety factors. Hence, it is desirable to define a probability of success and sensitivity to variations, referred to as reliability and robustness, respectively. The probability in this context implies that the design breaks down to satisfy particular criteria, referred to as the probability of failure. Failure does not necessarily represent the structural collapse catastrophically, but it suggests that the structure is not able to offer the structural performance aimed. Reliability analysis estimates the probability of failure of each structural element. In contrast, robustness involves how stable the performance quality of the designed structure is regarding the variations in the manufacturing process or environmental condition. These variations associated with manufacturing and operation cause extra costs across the lifecycle, including unscheduled inspection, repair and maintenance (2). The assessment of estimating robustness is named robustness analysis (3). These reliability and robustness analyses provide many benefits to engineers at the early stage of the design process. Reliability analysis allows engineers to comprehend how different engineering parameters affect the reliability of their structure designed, as well as establish a design philosophy to improve its overall probability of success. Robustness analysis enables engineers to account for possible variations influencing the performance quality as well as obtain a more stable design without removing/minimising their sources (4).

Even though reliability and robustness are significant for every structure, it is essentially important in the infrastructure manufacturing industry for the sake of improving energy efficiency by reducing the structural weight. This can tackle the inefficiencies of traditional design approaches caused by the use

of large safety factors that are introduced by international standards and specifications for each design field. These factors generally deliver a conservative and deterministic design to provide required safety levels. For instance, aircraft structures are required by the Federal Aviation Administration (FAA) to incorporate a safety factor of 1.5 for external loads on the structures whilst adding additional factors to escalate the level of safety concerning material properties, manufacturing effects, temperature effects, etc (5).

Probabilistic design optimisation incorporates these reliability and robustness analyses into its optimisation process, and it considers the statistical characteristics caused by the uncertainties associated with design and manufacturing stages. Therefore, it enables the final design to deliver more reliable and robust engineering features to the industry where seeks ways to preserve a specified safety while achieving lightweight, fuel efficiency and net-zero emissions; an international goal (Net Zero by 2050) announced by the International Energy Agency (IEA) (6). Such optimisation process accommodates different methods to carry out either reliability or robustness analysis depending on the objectives of optimisation. In general, Monte Carlo Simulation (MCS) is one of the typical statistical methods to estimate the reliability or robustness. The reliability can also be predicted by non-statistical methods, including the First-Order and Second-Order Reliability Methods, FORM and SORM, respectively (7). These two methods require the approximation of a limit state function using the first-order and second-order Taylor series expansions. More details of these methods can be discovered in many books on reliability and robustness analyses (8,9).

Reliability and robustness analyses require a massive number of experimental tests on the structure to investigate the effect of design uncertainties. However, these experimental tests are impossible because of high cost, execution time and trained workforce requested. Numerical methods, particularly the Finite Element Method (FEM) for structural design, can be exploited to obtain as accurate solutions as experimental tests while not requesting those substantial resources. Even if the FEM can provide a certain level of reduction in time, the estimation of reliability and robustness at every single design point is still a challenging work due to its high computational cost for using the FEM simulations. Note that reliability and robustness analyses using MCS expects tens of thousands of the FEM simulations to reach the converged statistical result of each design point (8). For example, if the probabilistic optimisation using Genetic Algorithm (GA) consist of 12 populations and 20 generations while MCS for robustness analysis requires 10,000 simulations for each population, the total number of the FEM simulations reaches 2,400,000. Even though a structural problem is simple enough to take a few seconds to execute a single FEM simulation, the total computational time for the probabilistic optimisation is nearly one month. As engineering problems in composite structures become more complex and large-scale structures having many design variables under complicated physics, the time for completing a FEM simulation to analyse them used to take more than a few hours. This suggests that the total simulation time can be more than some months or even some years depending on the problem features.

Many model approximation methods running on behalf of the FEM model have been developed to deal with this prohibitive computational challenge, which the models are called a surrogate model or a metamodel (10,11). This enables engineers to carry out reliability and robustness analyses for the probabilistic design optimisation precisely with improved computational efficiency, cutting down the FEM simulation time from a few hours to microseconds. Multi-fidelity model introduced in computer science is holding attention in structural optimisation because it offers more significant computational gains than the surrogate model while maintaining its accuracy (12). Specifically, the multi-fidelity model is expected to conduct the complex and large-scale composite design problems that their computational cost for even classical surrogate modelling is prohibitive.

1.1 Composite Structure in Aircraft Design

Composite structures are widely used in different manufacturing industry, including aircraft, wind turbines, automobile, etc. The recent development in composite materials, including lightweight and multifunction provides many engineering advantages to the industry and results in a dramatic increase in the usage of the materials for their products. As the design approach for environmentally friendly and sustainable development is incentivised to tackle global climate change, aircraft engineering is particularly leading the development of composite structures to accomplish an innovative aircraft design; reduced fuel consumption obtained by lightweight (13). The primary part of using these composite structures in aircraft encompasses fundamental elements to large systems. It is not surprising that the Boeing 787 Dreamliner and the Airbus A350 XWB consist of around 50 % and 53 % composite structures, respectively. These percentages are rising to even further boost weight reduction in aircraft fuselage (commonly 20 % lighter than aluminium) while achieving higher strength and expanded lifespan (14).

One of the most appealing uses of the composite structures is for designing the stiffened panel, which is an essential structural element for aircraft design. This stiffened panel allows a thin skin to carry extreme loading in both tension and compression using longitudinal stringers across the panel at a certain distance. Design for the stiffened composite panel should aim to maximise its strength, stiffness and buckling load. It should be noted that the buckling load does not mean the maximum load that the structure can carry. This implies that the structure can hold several times the amount of the buckling load before the structural failure, referred to as the non-linear post-buckling strength. This post-buckling strength capability offers impressive potential for both weight and cost savings. Hence, designing a composite panel that will work under the buckling load all the times is a very conservative approach. A more lightweight composite structure can be designed if the extra strength under the post-buckling regime is given (4,14,15). Furthermore, thermomechanical loading has been drawn attention in

aeronautics because of a massive increase in the industrial needs for high-speed and lightweight aircraft. This loading may cause untimely structural collapse when the aircraft is subjected to extreme surroundings. In particular, the consideration of thermal loading and mechanical loading can improve the composite aircraft design since the lightweight structures are typically susceptible to buckling under extreme conditions caused by high-speed operation (16–18).

A comprehensive coverage of the mechanics of composite structures can be found in a book by Jones (1). In addition, overviews of the non-linear post-bucking and thermomechanical buckling that are more specific to the work presented in this thesis can be found in the following Chapters 5 and 6.

1.2 Probabilistic Design Optimisation

Industrial manufacturing processes for composite structures are inherently more complex than conventional metals and alloys. This involves significant uncertainties in mechanical properties, geometry, or loading conditions associated with the entire lifecycle (19). One of the major challenges concerning traditional composite design approaches is that the final design does not adequately represent these uncertainties but presume them by using large safety factors, hence resulting in conservative design. These uncertainties assumed by the use of safety factor result in the designed structure being inefficient, leading to increasing raw materials for manufacturing and rising fuel consumption for operating. The weight of aircraft is particularly important to reduce carbon emissions from aviation while being able to maintain fundamental design requirements and capabilities. Hence, an innovative aircraft design approach should aim to minimise the structural weight whilst providing a high safety level, achieved by considering the uncertainties associated with designing and manufacturing processes.

An essential task would be necessary that can estimate the accurate statistical characteristics of the structural performance caused by the uncertainties in engineering parameters such as geometry, material properties and external loading. For example, insufficient understanding of unpredictable features and errors of the computational model can be the uncertainties at the early design stage. In the manufacturing stage for composite structures, a broad spectrum of flaws can lead to significant variations in material properties and geometry. However, traditional deterministic design optimisation methods do not have an action for the statistical measurement; hence they used to make the structure over-optimised across the whole lifecycle. Even if these deterministic approaches find a global design working very well at the design point, it might show a poor performance out of the design point as well as a higher probability of failure. Thus, this design cannot be guaranteed as a reliable or robust design due to the absence of significant influence of the uncertainties (20).

An approach to deal with the above drawback is the probabilistic design optimisation methods, including Reliability-Based Design Optimisation (RBDO) and Robust Design Optimisation (RDO) (15). These methods are classified depending on the different philosophies for which each optimisation method aims. The purpose of RBDO is to minimise the probability of failure by accounting for the design uncertainties so that the final design has a higher level of reliability using a probabilistic approach (14). In comparison, RDO aims to reduce the variability of the structural responses regarding unexpected deviations induced by the uncertainties (4). A robust design found by RDO holds an improved performance quality during the lifecycle compared with a deterministic design. These two probabilistic design optimisation methods principally incorporate reliability and robustness analyses into their process. MCS can be exploited by estimating both reliability and robustness, while FORM and SORM are employed to predict the probability of failure. The procedure begins with searching the entire design space to get potential design points. Once obtained, reliability and robustness analyses are used to estimate the statistical characteristics of the design points related to the aim of probabilistic design. This is the primary feature of the probabilistic design optimisation methods compared with the traditional deterministic approaches. By exploiting the probabilistic philosophy during the optimisation process of aircraft structural elements using the composite structures, engineers are allowed to understand the statistical nature led by the design uncertainties associated with the design and manufacturing process.

Although the probabilistic design optimisation offers a reliable and robust structural design with improved efficiency over the whole lifecycle, it has not been placed in the infrastructure design area due to its tremendous computational resources required (21).

A comprehensive overview and theoretical background of probabilistic design optimisation can be found in a book by Choi (8). In addition, outlines of RBDO and RDO and comparison between them to highlight the work presented in this thesis can be discovered in Chapter 2.

1.3 Surrogate Modelling

Surrogate modelling that is also known as metamodeling aims to approximate computationally expensive FEM models for structural optimisation (10). This modelling allows the FEM models to be represented by a computationally cheap alternative model. The alternative model enables the probabilistic design optimisation to deal with the prohibitive computational challenge for evaluating the influence of the design uncertainties. The computational time using a surrogate model is a lot faster than that of the original FEM model, usually from hundreds to tens of thousands of times faster, while offering acceptable accuracy identical to the FEM model. This facilitates significant improvements in the probabilistic design optimisation process by reducing the total optimisation time from a couple of

weeks to several hours and preserving the solution accuracy of less than 1 % error. Such surrogate model is created by collecting experimental observations or numerical simulations. When enough information is collected, the surrogate modelling method creates a surrogate model by training and testing the collected data. This modelling process could be struggling with running many simulations since the quality of the surrogate model relies on the amount of training data (22). It is not surprising that such modelling process still offers extensive overall savings concerning the total number of computational simulations. Therefore, the surrogate modelling methods have been applied to the probabilistic optimisation due to their advantage regarding computational efficiency. One drawback of surrogate modelling is that they sometimes request an affordable number of simulations for training when the optimisation problem has many design variables. For example, if the optimisation problem involves complex and large-scale composite structures, the run time for a single FEM model would sometimes take more than few hours despite using the HPC resources. There are many types of surrogate modelling methods; some of the most commonly employed methods are Gaussian Process (GP) and Artificial Neural Networks (ANN).

An inclusive summary and theoretical knowledge of the surrogate modelling that are more specific to the work introduced in this thesis can be found in Chapter 3.

1.4 Multi-Fidelity Modelling

Multi-fidelity modelling, which arises from surrogate modelling, has been introduced in computer science, and it has drawn significant attention amongst the optimisation research community since the last three decades (23). The multi-fidelity modelling aims to gain more computational efficiency from the traditional surrogate modelling method. A general surrogate model is created using a High-Fidelity Model (HFM) that brings accurate solutions while being computationally expensive. In contrast, a multi-fidelity model is trained using both a HFM and a Low-Fidelity Model (LFM), which is not accurate but computationally inexpensive. Multi-fidelity models constructed by blending different fidelity models can provide output solutions as precise as those of the general surrogate models using only the HFM while reducing the computational cost similar to the LFM. The ideal concept of multi-fidelity modelling is to use a small number of the HFM and a large number of the LFM to achieve a specific reduction in the total training time. The fidelities to define the HFM and the LFM depend on how the HFM can be simplified by the LFM, such as physics and numerical accuracy. The multi-fidelity models are usually constructed using the surrogate modelling methods to obtain more computational gains compared to the multi-fidelity models using the high- and low-fidelity FEM models.

One remarkable advantage of multi-fidelity modelling is to deal with the computational challenge of the probabilistic design optimisation for complex and large-scale composite structures that the

traditional surrogate modelling method cannot manage. Suppose the multi-fidelity models can provide acceptable accuracy with computational efficiency to the design area of composite structures. In that case, they allow engineers to examine the statistical estimation caused by the design uncertainties at the early design stage without conducting expensive experiments and time-consuming simulations.

Prior to the work introduced in this thesis, multi-fidelity probabilistic design optimisation for composite structures was not researched by the engineering and science community. Given that the importance of composite structures under the non-linear post-buckling regime and thermomechanical loading, the significant necessity of the probabilistic design optimisation to consider the design uncertainties, and also the incredible benefits by the use of surrogate modelling and multi-fidelity modelling, a novel methodology that embraces these different approaches would provide a suitable answer to technical challenges that the industry seeks to tackle.

A comprehensive explanation and theoretical background of the multi-fidelity modelling can be found in a book by Forrester (11). Overviews of the multi-fidelity models to highlight the work presented in this thesis can be discovered at the following Chapter 3.

1.5 Aims and Objectives

The primary objective of the work presented in this thesis is to develop novel multi-fidelity modelling-based probabilistic design optimisation methods for composite structures, demonstrate them using the design problems of a mono-stiffened stringer composite panel, and broaden their application area, particularly to designing large-scale composite structures. The main objectives can be summarised in five sub-objectives.

1. **To develop a multi-fidelity RBDO framework for composite structures integrating with the use of surrogate modelling.** Multi-fidelity models that consist of both a HFM and a LFM defined by different FEM mesh sizes are constructed using response correction functions. Then multi-fidelity surrogate models are created using ANN. The multi-fidelity RBDO framework involves the multi-fidelity modelling process and the reliability methods, such as MCS, FORM and SORM. This framework is demonstrated by the engineering examples of a mono-stringer stiffened composite panel considering uncertainties in geometry and applied load for the first time. These examples evaluate the developed multi-fidelity RBDO framework regarding improvements in solution accuracy and computational time savings compared to the traditional high-fidelity surrogate modelling technique. The framework is presented in Chapter 4.
2. **To develop a multi-fidelity modelling formulation covering different design spaces between the HFM and the LFM.** The main drawback of the traditional multi-fidelity modelling methods, in which the HFM has to share the same design space with the LFM, is

addressed if the HFM and the LFM have a different number of design variables. The HFM has a few design variables to reduce the number of high-fidelity FEM simulations for training. At the same time, the LFM explores the entire design space sharing the design variables in the HFM. The multi-fidelity formulation incorporates multi-level optimisation into the modelling process to complement a lack of information led by the HFM not carrying all design variables. This delivers more computational efficiency followed by surrogate modelling based on ANN, making it particularly suitable for large-scale problems having many design variables. This new multi-fidelity formulation is presented in Chapter 5.

3. **To develop a multi-fidelity RDO framework for composite structures under the non-linear post-buckling regime when the HFM has a smaller number of design variables than the LFM.** The developed multi-fidelity formulation is integrated with the RDO process. Then it is demonstrated by two optimisation problems, deterministic optimisation and RDO, of a mono-stiffened stringer composite panel undergoing mechanical shortening beyond the linear buckling. The design uncertainties in geometry parameters are considered, and MCS predicts the statistical characteristics using the Sobol sampling technique for each design point. The developed framework can improve accuracy and computational cost over both conventional surrogate modelling and different multi-fidelity modelling methods. Comparison between robust and deterministic design is highlighted in terms of the variability of output responses relying on the consideration of design uncertainties. This developed multi-fidelity RDO framework is presented in Chapter 5.
4. **To develop a multi-fidelity modelling formulation utilising different sampling levels between the HFM and the LFM while considering non-linear correlations between them.** This multi-fidelity formulation can offer acceptable multi-fidelity models that take care of the non-linear correlations between different fidelity models in a complex structural problem. This new formulation involves both a non-linear information fusion algorithm and multi-level optimisation. Specifically, the formulation enables the HFM to supervise a part of the entire design space using high-fidelity information collected densely from the selected design spaces. Simultaneously, the HFM provides high-fidelity information of other design variables collected sparsely while not increasing the sampling size for the high-fidelity training dataset. The LFM explores the whole design space for engineers to explore the solution spaces of other design variables associated with the selected design variables in the HFM. This novel multi-fidelity formulation is presented in Chapter 6.
5. **To develop a multi-fidelity probabilistic optimisation framework for composite structures subjected to thermomechanical loading.** The developed multi-fidelity formulation is incorporated with the RBDO process. Then it is demonstrated by a numerical example of a mono-stiffened stringer composite panel under mechanical and thermal loadings for the first time. The RBDO process aims to maximise the critical temperature changes undergoing an

inevitable mechanical shortening while satisfying the target reliability. In this example, the constructed multi-fidelity model carries ten input parameters to consider the design uncertainties in both material properties and geometry during the optimisation process. The optimal designs are found using successive high-fidelity corrections at the end of each optimisation level. The accuracy and computational time savings are highlighted by comparing with different traditional methods and a surrogate model computationally equivalent to the multi-fidelity model. This developed multi-fidelity optimisation framework is presented in Chapter 6.

1.6 Author's Published Work

The follows are a list of author's research achievement. This includes research articles submitted or published in international journals and work presented at international conferences. A link to the author's ResearchGate profile is link.

1.6.1 International Journals

1. Kwangkyu Yoo,; Omar Bacarreza,; M. H. Ferri Aliabadi,; Multi-fidelity Probabilistic Optimisation of Composite Structures under Thermomechanical Loading using Gaussian Processes, *Computers & Structures*, Volume 257, 2021, 106655, https://doi.org/10.1016/j.compstruc.2021.106655.
2. Kwangkyu Yoo,; Omar Bacarreza,; M. H. Ferri Aliabadi,; Multi-fidelity Robust Design Optimisation for Composite Structures based on Low-fidelity Models using Successive High-fidelity Corrections, *Composite Structures*, Volume 259, 2021, 113477, https://doi.org/10.1016/j.compstruct.2020.113477.
3. Kwangkyu Yoo,; Omar Bacarreza,; M. H. Ferri Aliabadi,; A Novel Multi-Fidelity Modelling-Based Framework for Reliability-Based Design Optimisation of Composite Structures, *Engineering with Computers*, 2020, https://doi.org/10.1007/s00366-020-01084-x.

1.6.2 International Conferences

1. Marij Qureshi,; Kwangkyu Yoo,; M.H. Ferri Aliabadi,; Assessment of Algorithms for the Probabilistic Optimisation of Composite Panels, *International Conference on Fracture and Damage Mechanics, American Institute of Physics (AIP) Proceedings*, Mallorca, Spain, September 2020.

2. Kwangkyu Yoo,; Omar Bacarreza,; M. H. Ferri Aliabadi,; Reliability-Based Design Optimisation of Composite Structure using Multi-fidelity Modelling, *European Conference for Aerospace Sciences*, Madrid, Spain, July 2019.
3. Kwangkyu Yoo,; Omar Bacarreza,; M. H. Ferri Aliabadi,; Reliability Analysis of Composite Structures using Multi-Fidelity Modelling, *International Conference on Advances in Aerospace Structures, Systems & Technology*, London, UK, May 2019.

1.7 Thesis Overview

A chapter-by-chapter summary of this thesis is as below:

- **Chapter 2: Fundamental Concepts of Structural Optimisation.** This chapter will introduce the fundamental concepts of structural optimisation, including optimisation methods, probabilistic design optimisation. It will also describe the basic concepts of reliability and robustness analyses, such as MCS, FORM and SORM.
- **Chapter 3: Multi-Fidelity Models.** This chapter will introduce both surrogate modelling and multi-fidelity modelling. This includes methods to build training datasets, such as Random sampling, Optimal Latin Hypercube sampling and Sobol sampling, as well as typical surrogate modelling methods, such as ANN and GP. A simple numerical example of probabilistic optimisation using high-fidelity surrogate modelling will also be introduced. Finally, standard multi-fidelity modelling methods, such as response correction methods, space mapping method and autoregressive method, will be discussed.
- **Chapter 4: Multi-Fidelity Modelling-Based Reliability-Based Design Optimisation for Composite Structures.** This chapter will introduce a multi-fidelity formulation using ANN when the HFM and the LFM share the same design space during the probabilistic optimisation process. The developed formulation is incorporated into the RBDO process and utilised to carry out MCS, FORM and SORM. Two numerical examples will be discussed to demonstrate the presented multi-fidelity RBDO framework. The work presented in this chapter has been published in article 3 from section 1.6.1.
- **Chapter 5: Multi-fidelity Robust Design Optimisation based on Low-Fidelity Models using Successive High-Fidelity Correction.** This chapter will introduce a multi-fidelity formulation using ANN that covers different design spaces between two fidelity models. The formulation is based on the LFM having more design variables and the HFM having fewer ones to carry out large-scale composite design problems with improved computational efficiency. The developed formulations will be discussed by carrying out both deterministic optimisation

and RDO of composite structures under the non-linear post-buckling regime. The work presented in this chapter has been published in article 2 from section 1.6.1.

- **Chapter 6: Multi-fidelity Probabilistic Optimisation of composite structures for thermomechanical loading using Gaussian Process.** This chapter will introduce a multi-fidelity formulation using GP that considers non-linear correlations between the HFM and the LFM. The formulation allows the HFM to collect the training data points with different sampling levels, such as dense and sparse sampling, while the LFM samples the training data points as dense as possible. An engineering example regarding composite structures under thermomechanical loading will be discussed to demonstrate the developed optimisation framework. The work presented in this chapter has been published in article 1 from section 1.6.1.
- **Chapter 7: Conclusions and Future Research.** The final chapter will summarise the conclusion found from the research work found in this thesis. Potential further research topics will also be suggested.

2 Fundamental of Structural Optimisation

This chapter will summarise the fundamental concepts on which the research presented in this thesis is based. This chapter will introduce the basic optimisation methods, such as gradient methods, direct methods and evolutionary methods, that can be used to conduct probabilistic design optimisation. Multi-objective optimisation for probabilistic design will then be presented, including Reliability-Based Design Optimisation (RBDO) and Robust Design Optimisation (RDO). This will highlight a comparison of RBDO and RDO as well. The theory behind the consideration of design uncertainty will then be shown by how to define the uncertainty in structural design optimisation. Reliability analysis and robustness analysis will be discussed how they assess the uncertainty, such as Monte Carlo Simulation (MCS), the First-Order Reliability Method (FORM), and the Second-Order Reliability Method (SORM).

2.1 Optimisation Methods for Probabilistic Design

A vast number of optimisation methods have been developed in the field of structural optimisation over a few decades. These optimisation methods aim to minimise specified objective functions by adjusting a set of design variables while not violating given design constraints. In general, there are not particular types of optimisation methods that are developed to achieve probabilistic design. However, some research has efficient optimisation methods for probabilistic design that provide adequate performance accuracy and efficiency (24). The optimisation methods are categorised in several ways, such as gradient-based methods, direct methods and evolutionary methods. Gradient-based methods require the derivative information of problem functions to decide optimised search directions. Direct methods are derivative-free methods that do not calculate the derivatives of function in their direction search scheme. Evolutionary methods use the information of function values in the optimisation process. More details

of these methods can be found in many works of literature on the topic of optimisation methods for probabilistic design (25–32).

2.1.1 Gradient-Based Methods

Gradient-based methods use the derivatives of problem functions to determine the search direction for the optimum points. Many methods have been developed for this optimal search direction, including simple steepest descent, conjugate gradient, etc (33). These methods decide the direction using the first order or the second order Taylor approximation depending on the characteristic of the problem to calculate the derivatives at each step. The use of derivatives for the search direction scheme requires the problem functions to be twice continuously differentiable in the feasible design space to provide more accurate values. At the same time, the design variables in the problem should be continuous in the design ranges to offer proper values. The main advantage of these methods converges extremely quick compared to different methods because they usually need a small number of simulations iterated. However, the gradient-based methods employ local information such as function values and their gradients during the search direction scheme. This could result in convergence to a local minimum satisfying given conditions. There are many gradient-based methods developed so far, such as the Mixed Integer Sequential Quadratic Programming (MISQP), Non-linear Programming, Sequential Quadratic Programming (SQP), Large Scale Generalised Reduced Gradient (LSGRG), etc (34). Each method has its characteristic depending on the problem, design space, CPU resources, features, etc. The LSGRG is known for the potentials that are suited well for non-linear design spaces and many design variables that can be utilised to the probabilistic design optimisation of large-scale problems. This method adapts the search direction to remain active constraints precisely and follows the constraints to improve the design. The method divides the gradient calculations of possible search directions that ensure parallelisation in contrast with typical gradient-based methods.

2.1.2 Direct Methods

As direct methods do not take the derivatives of the problem functions, they search some points in a local design space to determine the direction and then decrease the size of the local searched area to converge. There are typical direct methods such as Hooke-Jeeves method, Downhill Simplex method, etc (35). The Hooke-Jeeves method investigates points around the current point using the perturbation of each design variable at a time until an improvement is achieved. When there is no more improvement in design tracking the favourable direction, variable perturbation is reduced gradually until convergence criteria are satisfied. In contrast, the Downhill Simplex method is a geometrically intuitive algorithm providing the capability to search in every direction by building a multi-dimensional body. As this

method continues, the simplex leads to a downward path toward the minimum region through the series of steps. This method obtains a reasonable probability of discovering the global minimum when the initial steps are large. The initial simplex will then cover a broader range of the design space and reduce the possibility of getting stuck in a local minimum. Even though direct methods are intuitive and straightforward enough to carry out, they show weak performance in the discontinuous design space. In addition, convergence can be extremely slow in complex large-scale problems and may not even converge to a stationary point.

2.1.3 Evolutionary Methods

Evolutionary methods are inspired by nature. The main characteristic of these methods does not require the derivatives of problem functions but function values. This enables the problem functions not to be differentiable and continuous across the entire design space in contrast with the general requirement of gradient-based methods. The approach of evolutionary methods includes randomness for the search process, whereas gradient-based methods determine the search direction calculated by derivatives (36). These methods seek to run a number of simulations without calculating derivatives to explore the entire design space as much as possible and develop solutions gradually in comparison with previous ones. Many evolutionary methods using this idea have been developed and demonstrated so far, including Genetic Algorithm (GA), Particle Swarm Optimization (PSO), Non-dominated Sorting Genetic Algorithm-II (NSGA-II), etc (34). The methods commonly provide much better coverage of design space. Thus, they ensure a global minimum point concerning objective functions while not getting trapped in different local minimum points. Given that these gradient free optimisation methods do not take derivative tests to reach a minimum but explore the design space to discover the best fitness value, the optimal point could be evaluated using mathematical conditions such as Karush-Kuhn-Tucker (KKT) conditions. An additional helpful feature of the methods can manage various types of problems having continuous, integer, and mixed variables since they do not care about differentiable conditions. Their major drawback is more computationally expensive than gradient-based methods since a large number of simulations are required to discover the area having the global minimum point. However, this drawback can be resolved using parallelisation, one of the benefits of these methods.

It is not surprising that the GA is the most well-known among evolutionary methods. The primary mechanism of this algorithm mimics genetic operations that consist of some critical parameters, such as population, generation, etc (25). The population is a set of design points and also represents possible solution points. The generation shows how many iterations the GA carries out during the optimisation process. The total number of design points considered depends on these two parameters. The GA allows the population of design points to be gradually improved over consecutive generations. The GA process begins with an initial population that are randomly selected in the whole design space. In this set of

design points, a subset is chosen randomly, and then random processes generate new design points using the selected subset. The following sets of design points provide better fitness values because the subset of the previous set is used. This process is terminated until a stopping condition or a maximum allowable iteration is satisfied. This process is accomplished through three main genetic operators, such as selection, crossover and mutation. The selection process is to reproduce an old design point depending on the fitness values for the generation of a new population. In the crossover process, the selected design points of the new population exchange the characteristics between themselves. The mutation allows additional randomness to safeguard the process by mutating a design variable in each design point using another random value. The NAGA-II is a more advanced GA in order to deal with multi-objective problems (37). It employs each objective separately while the standard genetic operation of mutation and crossover are conducted. By the end of the optimisation process, a Pareto front is generated by selecting feasible non-dominated design points where each design point obtains the best combination of objective values. The improvement in one objective is not possible without losing one or more of the other objectives. This algorithm has been considered as a method for multi-objective probabilistic design optimisation due to its excellent performance.

2.2 Multi-Objective Probabilistic Optimisation

Multi-objective optimisation, which is also called multi-criteria optimisation or vector optimisation, is an optimisation process able to minimise several objective functions systematically and simultaneously. In contrast with single-objective optimisation to find a solution minimising the objective function, the way of determining a solution concerning the several objective functions should be defined (38). The different objective functions of this process conflict with each other, which means the improvement in one objective might degrade others. Several constraints can also be considered that feasible solutions having every optimal solution have to satisfy. Equation (2.1) shows a general form of multi-objective optimisation.

$$\begin{aligned} &\min_{d} F(x) = \left(f_1(d), \cdots, f_p(d)\right) \\ &subject\ to \quad g_i(x) \leq 0, \qquad i = 1, \cdots, I \\ &\qquad\qquad h_j(x) = 0, \qquad j = 1, \cdots, J \\ &where \quad F : \mathbb{R}^n \rightarrow \mathbb{R}^p \end{aligned} \tag{2.1}$$

where F is a vector including all p objective functions, d and x are design variables' vector and the whole optimisation variables, g_i and h_j are inequality and equality constraint functions, $\mathbb{R}^n$ and $\mathbb{R}^p$ are the vectors of inputs and objectives, respectively.

The optimal solutions in multi-objective optimisation problems can be characterised by a mathematical concept of dominance or partial ordering (39). The idea of dominance between two solutions, d_1 and d_2 in $\mathbb{R}^n$, is explained in equation (2.2). If d_1 dominates d_2, two conditions should be necessarily considered. Firstly, $d_1$is not worse in any objectives. The value of the objective function for d_1 is less or equal to the value of the objective function for d_2, regarding all the required objective functions. Secondly, there must be at least one objective for which d_1 is rigorously greater.

$$\begin{aligned} &\forall i \in \{1, \cdots, p\}, \qquad f_1(d_1) \leq f_2(d_2) \\ &\exists i \in \{1, \cdots, p\}, \qquad f_1(d_1) < f_2(d_2) \end{aligned} \tag{2.2}$$

This process gives rise to a set of optimal solutions that is defined as Pareto optimality. The definition is that a feasible vector d^* is Pareto optimal if the vector d^* is not dominated by a different possible solution. Equation (2.3) represents that d^* is Pareto optimal if no objective can be improved without sacrificing more than one objective of the other objectives. The set of Pareto optimal is prescribed as Pareto optimal set, and it provides the optimal solutions of multi-objective optimisation problems.

$$Pareto\ optimal\ set = \{d^* \in \mathcal{F} \mid \nexists d \in \mathcal{F}: F(d) < F(d^*)\} \tag{2.3}$$

The main difference in multi-objective probabilistic optimisation is that the optimisation process considers the uncertainties of design variables for the entire structural lifecycle. This consideration enables the final design to become a more reliable or robust design depending on the defined objectives and constraints. There are two types of probabilistic optimisation, such as Reliability-Based Design Optimisation (RBDO) and Robust Design Optimisation (RDO) (15,20). RBDO carries the probability of failures as a constraint, whereas RDO takes the mean and standard deviations of objective functions. These two types will be introduced in the following sections in details.

2.2.1 Reliability-Based Design Optimisation (RBDO)

In general, RBDO integrates the reliability analysis with deterministic optimisation so that the optimisation process assesses the design constraints caused by the uncertainties of random design variables. This optimisation process ensures that the final design satisfies a specific probabilistic constraint as far as a prescribed reliability level. When an optimisation problem focuses on the occurrence of disastrous failure of a structural system, the optimisation problem is defined as RBDO (9,14). In RBDO, the reliability analysis evaluates a limit state function to calculate the probability of failure. A constraint is imposed to safeguard that failure does not exceed an adequate critical value. This limit state function is related to the constraints used in the deterministic optimisation, with the distinction that constraints may be violated having some acceptable probability. A typical RBDO problem can be expressed as

$$\begin{aligned} &minimise && F(d) \\ &subject\ to && g_m(d) \le 0, && m = 1, \cdots, M \\ & && P[G_n(d,x) \le 0] - P_{f,n} \le 0, && n = 1, \cdots, N \end{aligned} \tag{2.4}$$

where d and x are the design variable's vector and random variable's vector, respectively, and F is the objective functions. g_m is *m-th* deterministic constraint and G_n represents the *n-th* probabilistic constraint. $P[\ ]$ implies the probability of the constraint being satisfied and P_f is the acceptable probability of failure. P_f mainly indicates the prescribed reliability level β_t when a normal distribution represents the random variables.

The reliability analysis in this optimisation process is the essential part of determining the probability of failure, which can be predicted using Monte Carlo Simulation (MCS), the First Order Reliability Method (FORM) and the Second Order Reliability Method (SORM) (8). MCS is based on different sampling methods, while the FORM and SORM exploit the derivatives of the limit state function. This reliability assessment considering the design uncertainties requires thousands of function evaluations leading to significantly high computational cost that is not a critical issue for deterministic optimisation. Different advanced numerical techniques have been developed to address the computational cost that is challenging with current technologies.

2.2.2 Robust Design Optimisation (RDO)

RDO combines the concept of robustness into deterministic optimisation that may produce over-optimised design solutions caused by the ignorance of design uncertainties (40). Robust design aims to improve the quality of products concerning unexpected deviations that are led by variation at different phases of the structure's lifecycle. This means that the structural performance of the robust design should be less sensitive to random variations. Even though the design solutions found by a conventional deterministic optimisation work well at design points, they could present inferior performance close or out of the design points. It is not surprising that the design solution, which results from the deterministic optimisation, will not be the robust solution providing minimum sensitivity to the design uncertainties. The structural performance is represented using objective functions or constraints, and it may be under wide scatter at different service phases. This scatter may considerably decrease the structural quality and lead to variations from the required performance. They may also increase the structural costs for inspection, repair and maintenance. In that sense, well-optimised design solutions provide structures that reduce operating costs as well as the scatter of structural performance. These structures work consistently in the presence of unexpected variations during the overall service lifecycle. The robustness

of structures is one of the essential characteristics to be considered in the design stages to shrink the scatter of structural performance.

One possible way is to reduce or exclude the spread of the input parameters, which may either be nearly impossible or increase the structure's total costs. Another way is to discover a design in which the structural performance is insensitive to the deviation of input parameters while not removing the sources of the parameters' variations. The robust structural design approach describes the design quality of the structure using the mean value and variation of the structural performance. An evident approach is to specify the optimality requirements using the expected values of response performance. However, the design determined by the minimum expected value of the objective functions may still be susceptible to the variation of the probabilistic input parameters having uncertainties. This draws attention to the robust structural design that balances mean performance against some measure of the variability. This design is achieved by multi-objective optimisation, which is a trade-off between the mean performance and some measure of the variability (4). The general mathematical formulation of RDO can be given as

$$\begin{aligned} &minimise && \{\mu(f(X)), \sigma(f(X))\} && \\ &subject\ to && g_i(X) \le 0 && i = 1, \cdots, I \\ & && h_j(X) = 0 && j = 1, \cdots, J \\ & && \sigma(f(X)) \le \sigma_M^+ && \\ & && x_l^{(L)} \le x \le x_l^{(U)} && l = 1, \cdots, L \end{aligned} \tag{2.5}$$

where X is the design and random variables' vector, $\mu(f(X))$ and $\sigma(f(X))$ are the first (mean) and second (standard deviation) statistical moments of the objective function, respectively. g_i is i^{th} inequality constraint, h_j is j^{th} equality constraint, σ_M^+ is the upper limit for the standard deviation of the structural performance and, $x_l^{(L)}$ and $x_l^{(U)}$ are the lower and upper bounds for the l^{th} design variables.

2.2.3 Difference between Reliability-Based Design and Robust Design

As discussed in the previous section, Reliability-Based Design Optimisation (RBDO) and Robust Design Optimisation (RDO) aim to incorporate design uncertainties into the design optimisation process. These two optimisation approaches presume that design hazard is defined by combining the probability of an undesired event and its consequence. They put forth different design domains relying on the purpose of each optimisation. Figure 2.1 highlights the design domains of RBDO and RDO using two principal elements, such as event's consequence and frequency. A design could target a structural

system encountering an extremely severe environment that leads to structural failure and collapse. This design is placed in the domain of RBDO, where the concept of reliability level is considered by a critical constraint. In contrast, a design could be optimised that a circumstance does not cause significant failure but deteriorate the structural performance through frequent fluctuations. In terms of design domain, RBDO is more likely associated with structural safety in extreme design condition, whereas RDO relates with structural performance in operating condition.

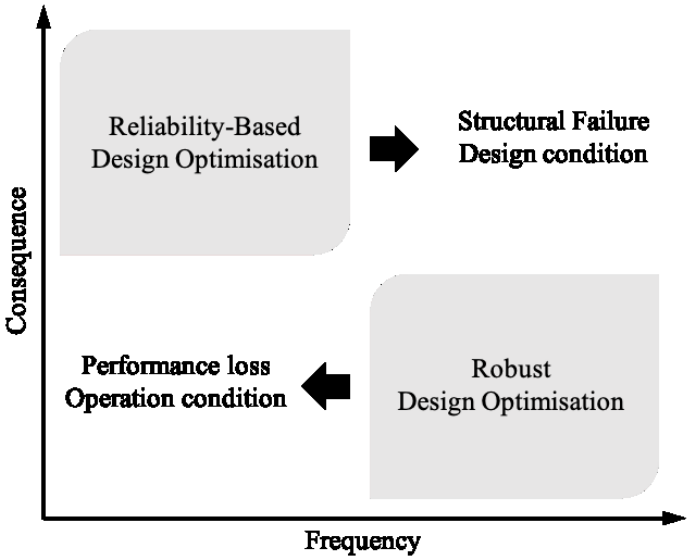

Figure 2.1: Design domains depending on design target (41)

Both RBDO and RDO combine the prediction of possible influence caused by design uncertainties with the optimal design process; however, these two approaches have different interest areas to the objective function's distribution. RBDO aims to meet reliability requirements based on the probability distributions of the random design variables (14,24). The objective functions of RBDO should be minimised while not violating the probability constraints. RDO reduces the variation of structural performance (4,42). This approach includes minimising the variance of objective functions. Simultaneously, constraints can also be characterised by the allowable standard deviations. In RBDO, stochastic analysis predicts the likelihood of extreme events illustrated using the tail of the objective function's distribution. The reliability analysis, which is the main part of RBDO, measures the reliability index associated with the probability of failure (43). This process leads to high computational costs to compute the reliability of each design point. Stochastic analysis in RDO calculates the effect of statistical moments about different design points. The robustness assessment of RDO concerns the variation of structural performance regarding unanticipated events.

highlights the aim of RBDO, which reduces the probability of rare extreme events in the tail of the probability distribution function. Limit state function is a primary constraint that shows the boundary

between safe and failure region. RBDO generally diminishes the tail area across the limit state function so that the structure obtains a required reliability level. In contrast,

Figure 2.3 illustrates how RDO ensures insensitive design. This design process reduces the variance of the objective function that provides more narrow distribution around the mean value of the function.

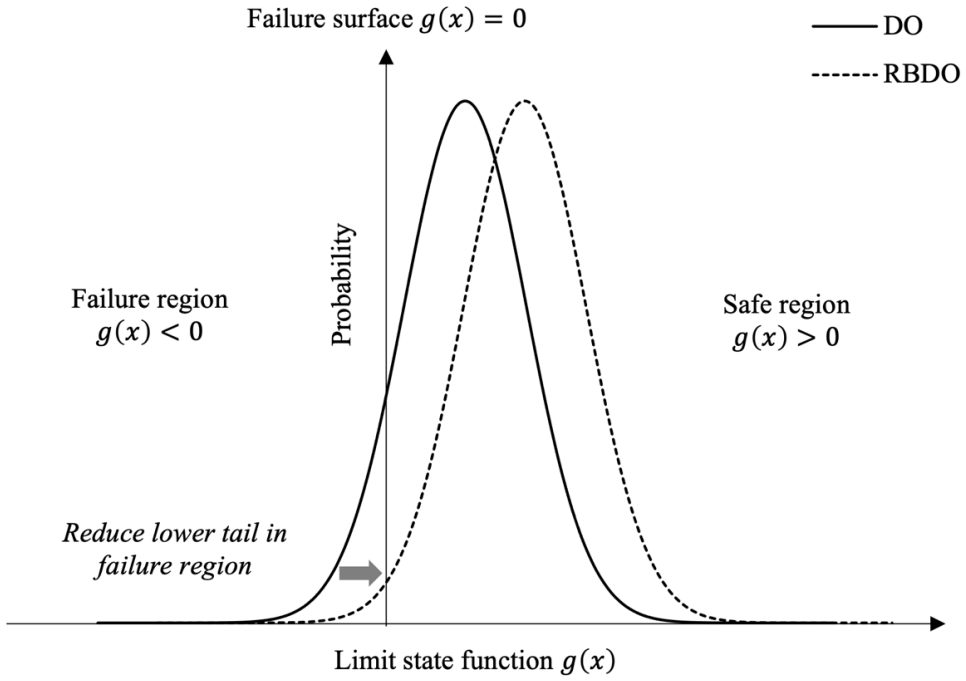

Figure 2.2: RBDO strategy

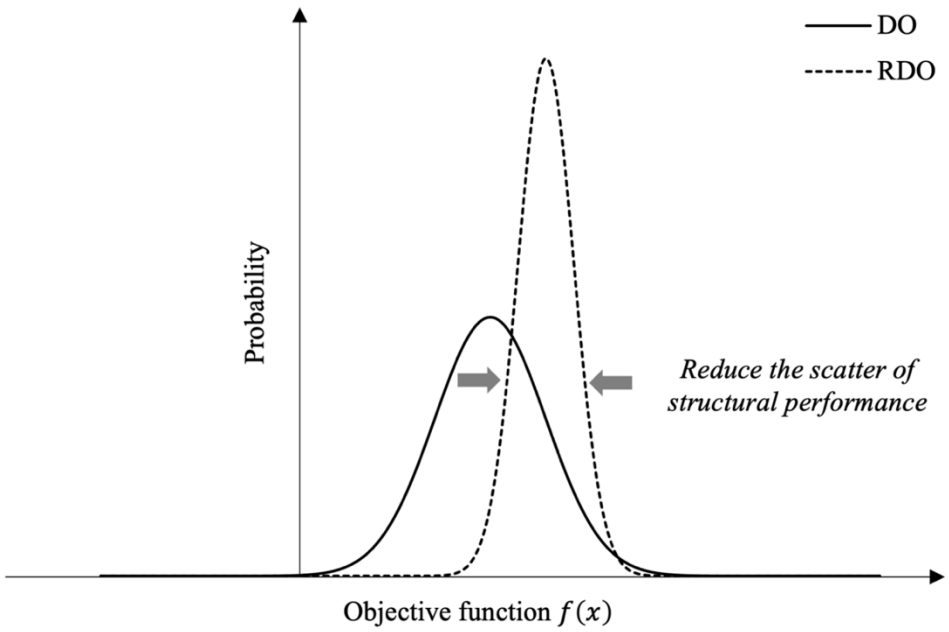

Figure 2.3: RDO strategy

Both clearly show how two approaches offer different design solutions compared with traditional deterministic optimisation. When robust design and reliable design are found, it is meaningful to evaluate whether the final chosen design is feasible in an engineering way.

Figure 2.4 highlights how a feasible design can be obtained using the probabilistic design approach. If the objective function of a robust design (service condition) is much smaller than that of a reliable design (extreme condition), the final design will be similar to a conservative design caused by large safety factors. If the objective function of a robust design is adjacent to a reliable design's one, the final design will be a good design that reduce the difference in structural performance between the service and extreme conditions. Suppose the objective function of a robust design is better than that of a reliable design's one. This does not make sense that the mean value of objective function for operating condition is higher than that of extreme condition.

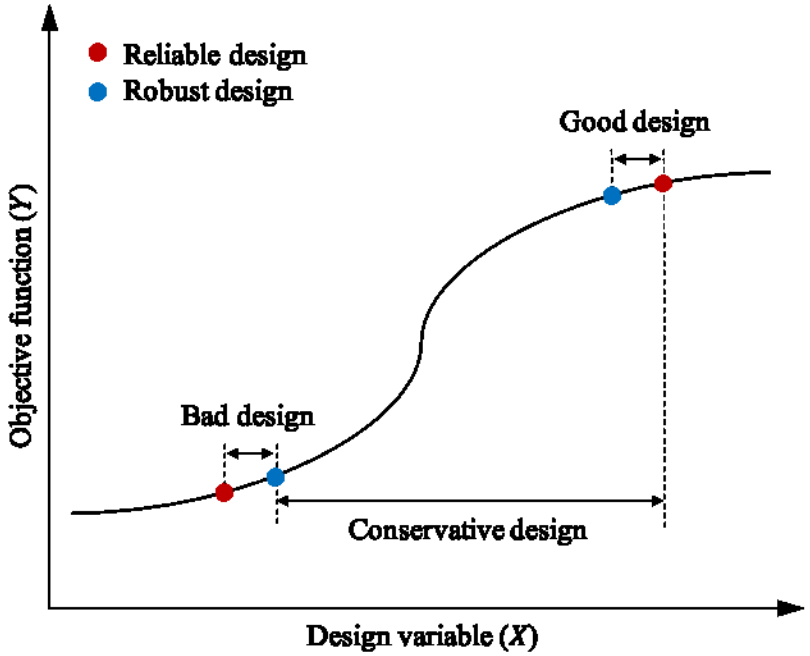

Figure 2.4: Reliable design and robust design

2.3 Design Uncertainty Consideration

As design requirements are getting more complex and comprehensive, many design approaches have been widely developed to answer the need for advanced probabilistic assessment technology considering the design uncertainties. In particular, the consideration of these uncertainties enables the design approaches to deal with the random nature of design parameters. This consideration ensures that the design quality is more improved compared to different design approaches based on safety factors. Probabilistic design obtained using the consideration of design uncertainties safeguards the deviation

of performance caused by system variations. This probabilistic design can resolve the knowledge shortage about the spread of structural performance that is the primary concern in the design based on safety factors (5).

As can be seen in Figure 2.5, the sources of uncertainty are commonly categorised by the product's lifecycle, such as design, manufacturing, service/operation and ageing. In the design stage, the uncertainties are usually inaccuracies in models and insufficient information caused by different level of understanding the structural system. These uncertainties in models and information associate with how precise the models are created and how much engineers perceive the system, respectively. Tolerances and material defects are considered as the uncertainties for the manufacturing stage, followed by the design stage. The tolerances include changes in geometry when the final design is manufactured or assembled in production lines. In particular, the material defects are crucial for manufacturing composite structures since the misalignment of fibre orientation and the presence of void in the matrix influence the overall mechanical properties of composite structures. The operation stage has different uncertainties, such as environmental variation and loading condition that are more likely associated with structural performance for a product's service process. Finally, the decay of material properties may lead to the efficiency loss of the structural system through the ageing stage.

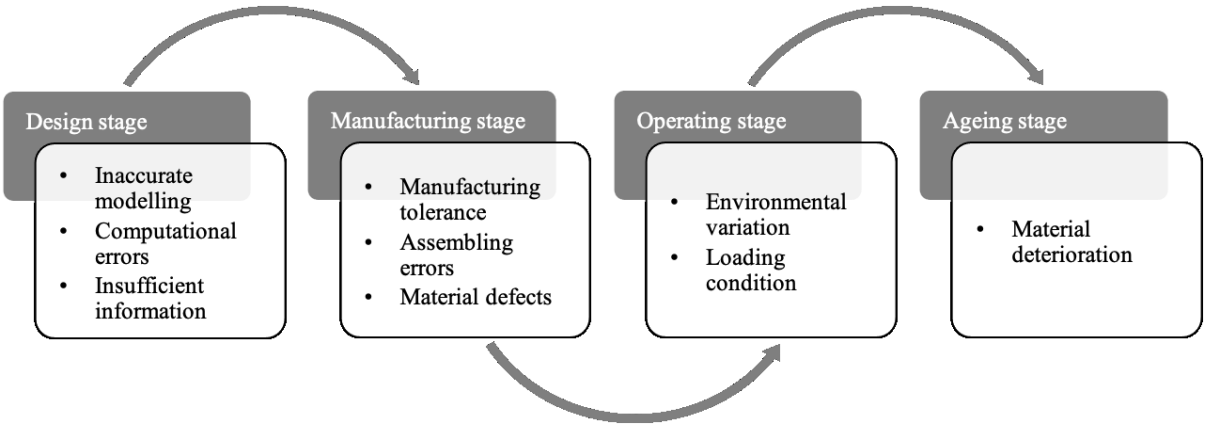

Figure 2.5: Uncertainties through the entire lifecycle

Conventional design approaches of optimisation, which are also known as deterministic design, do not explain any uncertainties in the structural system. These design approaches may provide an over-optimised design. The design may not give adequate capability close or out of the design points despite presenting perfect performance at the design points. In contrast, modern probabilistic design approaches of optimisation account for these uncertainties that can be expected for the entire lifecycle. This consideration ensures that the design approaches can predict how much the uncertainties affect the design objectives, and offer more statistically reliable and robust designs. There are two analysis types to assess the uncertainties associated with the whole lifecycle, such as reliability and robustness (44). In Reliability-Based Design Optimisation (RBDO), reliability analysis is an essential process to predict

the probability of failure caused by the design uncertainties. In general, a structural design produced by a deterministic design approach based on safety factors shows a larger probability of failure compared to a probabilistic design considering the uncertainties. This ensures that the reliable design provides a certain confidence level, not violating a prescribed probabilistic constraint across the whole lifecycle since RBDO examines the effect of the uncertainties. Conversely, Robust Design Optimisation (RDO) carries robustness analysis during the process to calculate the statistical variance of the structural performance. This analysis enables the optimisation process to minimise the sensitivity of the objective function concerning arbitrary changes in the random variable in the system. These two analyses will be discussed further in the following sections.

2.3.1 Reliability Analysis

Reliability analysis is one of the approaches to consider uncertainties across the entire lifecycle of products (45). It becomes more significant in the field of structural design because it provides many benefits. This analysis mainly allows engineers to realise how the uncertainties in different design variables impact the probability of failure of their structures. At the same time, it enables designers to understand where the most critical design region is in the whole design space and improve the level of reliability in the system. There are two types of methods depending on how they predict the structure's reliability, such as statistical methods and non-statistical methods (46). Monte Carlo Simulation (MCS) represents the statistical methods, whilst the First-Order Reliability Method (FORM) and the Second-Order Reliability Method (SORM) are included in the non-statistical methods. The FORM and SORM utilise the first-order and second-order Taylor series expansions, respectively, to approximate a limit state function.

2.3.1.1 Theory

Reliability analysis considers the uncertainties of design variables and computes the probability of structural failure corresponding to the reliability index. The reliability analysis evaluates whether a limit state function that is a prescribed constraint exceeds a specific value. The limit state function means that a structure cannot carry out its design purpose when the structure experiences more than a particular allowable limitation. If the probability of failure regarding the limit state function is greater than the specific required value, the structure does not provide acceptable confidence associated with the reliability level. The limit state can be classified by two sorts, including ultimate and serviceability limit states (8).

The ultimate limit state is represented by the phenomenon of structural collapse such as corrosion, fatigue, deterioration, plastic mechanism, progressive collapse, fracture, etc. These limit states have a very low possibility of occurrence and dangerous consequences. In comparison, the serviceability limit state is related to the disruption of structures. For example, there are excessive deflection, excessive vibration, drainage, leakage, local damage, etc. Such limit states have a higher possibility of occurrence and less harmful consequences.

In general, the limit state function shows the margin of safety between resistance and the load of structures. The limit state function can be defined as

$$g(Z) = R(X) - S(X) \tag{2.6}$$

$$P_f = P[g(Z) < 0] \tag{2.7}$$

where $g(Z)$ is the limit state function, P_f is the probability of failure, Z is a vector of design variables that influence the limit state function, while $X(X \subseteq Z)$ is a vector of design variables that affects R and S, R is the resistance and S is the loading of the structure.

If the value of $g(Z)$ is less than zero, the structure is in the failure region. If the value of $g(Z)$ equals to zero and is larger than zero, the structure is in the failure surface and the safe region, respectively. The reliability index β indicating a confidence level not violating the prescribed limit state is expressed as

$$\beta = \frac{\mu_g}{\sigma_g} \tag{2.8}$$

where μ_g and σ_g are the mean and standard deviation of the limit state function.

The reliability index is the distance of the mean value of limit state from the safe surface and it is an appropriate measurement of reliability. When the limit state function is normally distributed, the probability of failure is described as

$$P_f = P\{g(Z) < 0\} = \int_{-\infty}^{0} f_z(Z)dZ = 1 - \phi(\beta) = \phi(-\beta) \tag{2.9}$$

where $f_z(Z)$ is the joint probability density function of Z, P_f are calculated using integrating over the failure region $(g(Z) < 0)$, β is the reliability index and $\phi(\cdot)$ is the standard normal cumulative distribution function.

All design variables in equation (2.9) are presumed to be independent of each other. It can be challenging to calculate the integral in the equation if the failure surface is non-linear or if there are many random variables in the limit state function. When the reliability index is calculated, the

probability of failure and the probability of success are obtained. There are three numerical methods, including Monte Carlo Simulation (MCS), the First-Order Reliability Method (FORM), and the Second-Order Reliability Method (SORM), that can carry out the reliability analysis. MCS is the most straightforward in those three methods and evaluates the limit state function using randomly sampled design points from the distribution of the random design variables in the limit state function. In contrast, FORM and SORM simplifies the limit state function using the first-order and second-order Taylor series expansions, respectively, so that they can approximate the failure surface. Thus, FORM and SORM require much shorter calculation time, but they are not accurate compared to MCS.

2.3.1.2 Monte Carlo Simulation (MCS) for Reliability Analysis

MCS is a simple random sampling method or a statistical trial method based on randomly generated sampling sets for design variables (9). It is a powerful mathematical method for specific events that are the result of the stochastic process. MCS consists of the creation of random design variables and the statistical analysis of their outcomes. When a distribution type for random design variables is determined, MCS builds up a sampling set from the determined distribution. Then, MCS runs simulations using the created sampling set. There are several parameters for a random sample, such as the number of sampling points and distribution type, etc. The basic process of MCS is extended to the reliability analysis of structures. Firstly, sampling sets of random design variables are collected using the probability density function. Then, the mathematical model of limit-state is set up, and this model evaluates failures in the sampled sets. Next, many simulations are conducted using the created sampled sets of the random design variables. Finally, the probabilistic characteristics of structural response are estimated.

As can be seen in equation (2.6), the limit state function $g(Z)$ to be evaluated is made up of $R(X)$ and $S(X)$ that usually are Finite Element Model (FEM) or Boundary Element Model (BEM) in the area of structural design having unknown probability distributions. If a vector X consists of random design variables having known probability distributions that affect S and R, the variables in X is sampled by their probability distributions. Then the outcomes of $S(X)$ and $R(X)$ concerning the sampled X are obtained. This process is continued repeatedly until the probability of distribution of $g(Z)$ is estimated precisely. If a total sampling number, N_{Total}, for the random design variables in X have been accomplished, the number of samples for which $g(Z_i) < 0$ or $S(X_i) > R(X_i)$ $(i = 1, 2, \dots, N_{Total})$ can be found, where X_i and Z_i are the i^{th} sample for the random design variables in X and Z, respectively. This number is called by $N_{Failure}$. When N_{Total} simulations are carried out, the probability of failure is computed by

$$P_f = \frac{N_{Failure}}{N_{Total}} \tag{2.10}$$

The probability of success, P_s, also known as reliability, can be calculated as

$$P_s = 1 - P_f \tag{2.11}$$

MCS is generally used to validate whether different approximation methods, such as FORM and SORM, offer acceptable results. This process provides the most accurate estimation through a large number of simulations.

2.3.1.3 First-Order Reliability Method (FORM)

There are several ways to approximate the limit state function using Taylor expansion. FORM starts from the First-Order Second Moment (FOSM) method and then it has been developed by Hasofer-Lind (HL) method and Hasofer Lind – Rackwitz Fisseler (HF-RF) method (8). HL-RF method, generally known as FORM, is used in this work.

FOSM method, also called the Mean Value FOSM (MVFOSM), makes the functional relations straightforward and mitigates the complexities to calculate the probability of failures of structures. The meaning of "first-order" is the first-order expansion of the limit state function. Random design variables for reliability analysis are defined by the first moment (mean) and second moment (variance).

In Figure 2.6, the MVFOSM method approximates the limit state function using the first-order Taylor series expansion at the mean value. The approximation at the mean value using statistically independent variables X is expressed as

$$\tilde{g}(X) = g(\mu_X) + \nabla g(\mu_X)^T \left(X_i - \mu_{X_i}\right) \tag{2.12}$$

where $\mu_X = \left\{\mu_{x_1}, \mu_{x_2}, \cdots, \mu_{x_n}\right\}^T$, and $\nabla g(\mu_X) = \left\{\frac{\partial g(\mu_X)}{\partial x_1}, \frac{\partial g(\mu_X)}{\partial x_2}, \cdots, \frac{\partial g(\mu_X)}{\partial x_n}\right\}^T$ is the gradient of the limit-state function.

The mean value of approximate limit state function $\tilde{g}(X)$ is written as

$$\mu_{\tilde{g}} = E[g(\mu_X)] = g(\mu_X) \tag{2.13}$$

The standard deviation of the approximate limit-state function is given as

$$\sigma_{\tilde{g}} = \sqrt{Var[\tilde{g}(X)]} = \sqrt{[\nabla g(\mu_X)^T]^2 Var(X)} = \left[\sum_{i=1}^{n} \left(\frac{\partial g(\mu_X)}{\partial x_i}\right)^2 \sigma_{x_i}^2\right]^{1/2} \tag{2.14}$$

Finally, the reliability index β is calculated as

$$\beta_{MVFOSM} = \frac{\mu_{\tilde{g}}}{\sigma_{\tilde{g}}} \tag{2.15}$$

As can be seen from equation (2.15), it is the same as equation (2.8) if the limit state function is linear. If the limit state function is not linear, the approximated limit state surface is computed by linearising the original limit state function at the mean value.

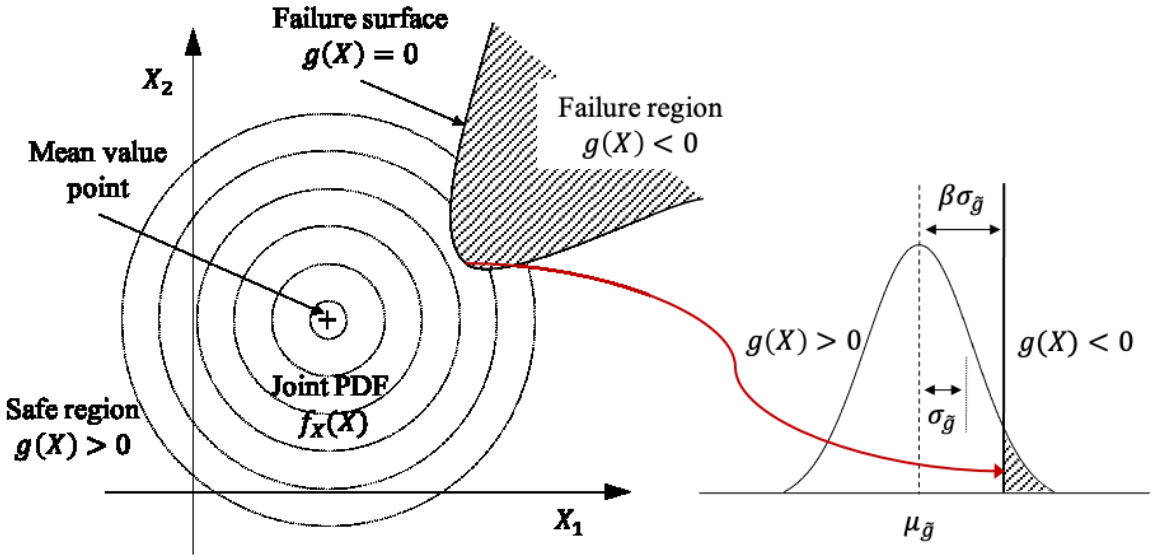

Figure 2.6: Mean Value First-Order Second Moment Method

The reliability index corresponding to the probability of failure is a mathematical optimisation to search for the point on the failure surface, $g(X) = 0$, that shows the shortest distance for the origin point to the surface in the standard normal distribution. Hasofer and Lind improved MVFOSM by the Hasofer and Lind transformation. Here, a vector X of random design variables is transformed into the basic variables into a set of normalised and independent variables U. The standardised form for this transformation is defined as

$$u_i = \frac{x_i - \mu_{x_i}}{\sigma_{x_i}} \tag{2.16}$$

where μ_{x_i} and σ_{x_i} are the mean value and the standard deviation of x_i, respectively. The mean and standard deviation of u_i are zero and one (standard normal distribution), respectively.

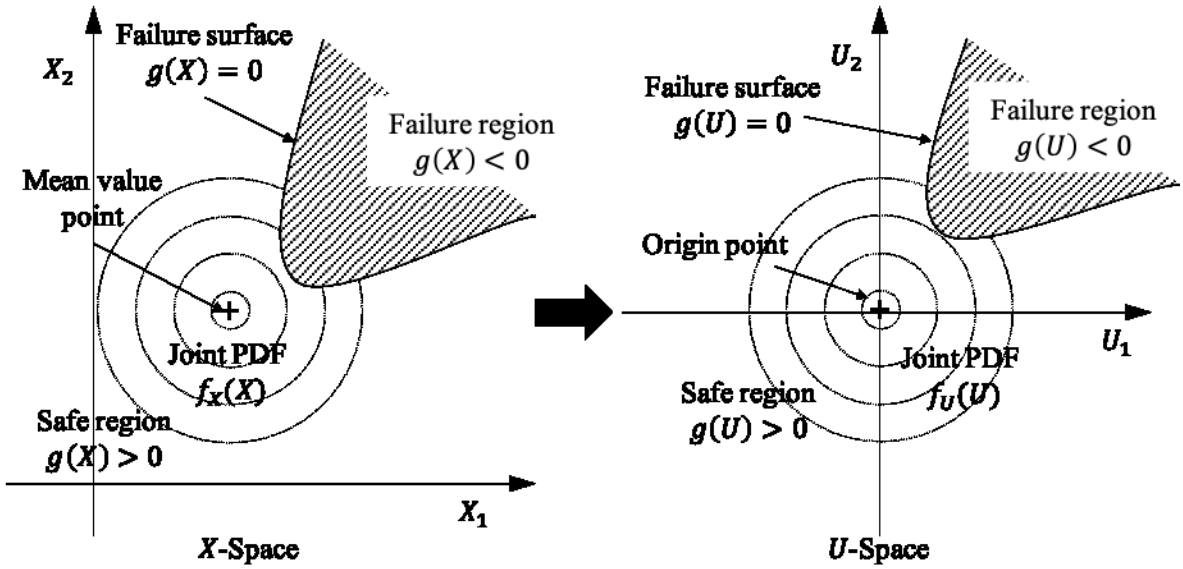

Figure 2.7: Failure surface transformation form X -space to U-space

Through this formulation, the mean value of original space (X-space) is moved to the origin of standard normal space (U-space). The failure surface, $g(X) = 0$, in X-space is transformed to the associated failure surface, $g(U) = 0$, in U-space, as illustrated in Figure 2.7. The reliability index, β, is the shortest distance from the origin to the failure surface, $g(U) = 0$.

$$\beta = \min_{U \in g(U)=0} (U^T U)^{1/2} \tag{2.17}$$

The value of the reliability index is the same with not only the true failure surface but also the tangent hyperplane at the design point. The improvement in this Hasofer-Lind iteration method changes the expansion location from the mean value to the Most Probable Failure Point (MPP). Let presume the limit state function with n-dimensional normally distributed having random design variables X.

$$g(X) = g(\{x_1, \ \dots, x_n\}^T) = 0 \tag{2.18}$$

Based on the formulation of equation (2.16), the limit state function in X-space is mapped into U-space.

$$g(U) = g\left(\{\sigma_{x_1} u_1 + \mu_{x_1}, \dots, \sigma_{x_n} u_n + \mu_{x_n}\}^T\right) = 0 \tag{2.19}$$

The first-order Taylor series of expansion of $g(U)$ at the MPP, U^*, is expressed as

$$\tilde{g}(U) = g(U^*) + \sum_{i=1}^{n} \frac{\partial g(U^*)}{\partial U_i} (u_i - u_i^*) \tag{2.20}$$

The shortest distance from the origin to the approximated failure surface in Figure 2.7 is defined as

$$OP^* = \beta = \frac{g(U^*) - \sum_{i=1}^{n} \frac{\partial g(U^*)}{\partial x_i} \sigma_{x_i} u_i^*}{\sqrt{\sum_{i=1}^{n} \left(\frac{\partial g(U^*)}{\partial x_i} \sigma_{x_i} \right)^2}} \tag{2.21}$$

The direction cosine, which is called the sensitivity factor, is given as

$$cos\theta_{x_i} = cos\theta_{u_i} = -\frac{\frac{\partial g(U^*)}{\partial U_i}}{|\nabla g(U^*)|} = \frac{\frac{\partial g(X^*)}{\partial x_i} \sigma_{x_i}}{\sqrt{\sum_{i=1}^{n} \left(\frac{\partial g(U^*)}{\partial x_i} \sigma_{x_i} \right)^2}} = \alpha_i \tag{2.22}$$

The coordinates of the next point in U-space are calculated as

$$u_i = \frac{x_i - \mu_{x_i}}{\sigma_{x_i}} = OP^* cos\theta_{x_i} = \beta cos\theta_{x_i} \tag{2.23}$$

The corresponding coordinate in X-space is determined by

$$x_i^* = \mu_{x_i} + \beta \sigma_{x_i} cos\theta_{x_i} \tag{2.24}$$

The procedure of the Hasofer-Lind iteration method is shown in Figure 2.8.

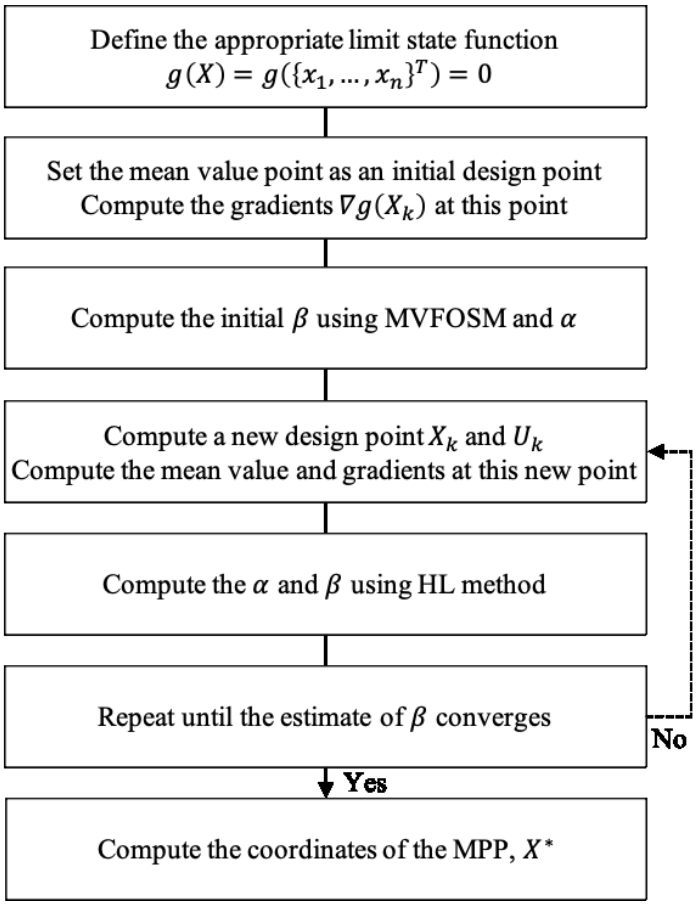

Figure 2.8: Procedure of the Hasofer-Lind iteration method

In the Hasofer-Lind method, random design variables should be represented as normally distributed. If the random design variables are not normally distributed, an additional transformation should be considered to obtain their normal distribution. Rackwitz and Fiessler proposed the transformation, and this advanced method is called the Hasofer Lind-Rackwitz Fiessler (HL-RF) method. Once the distribution of design variables is transformed into a normal distribution, the HF-RF method is identical to the HF method, as shown in Figure 2.9.

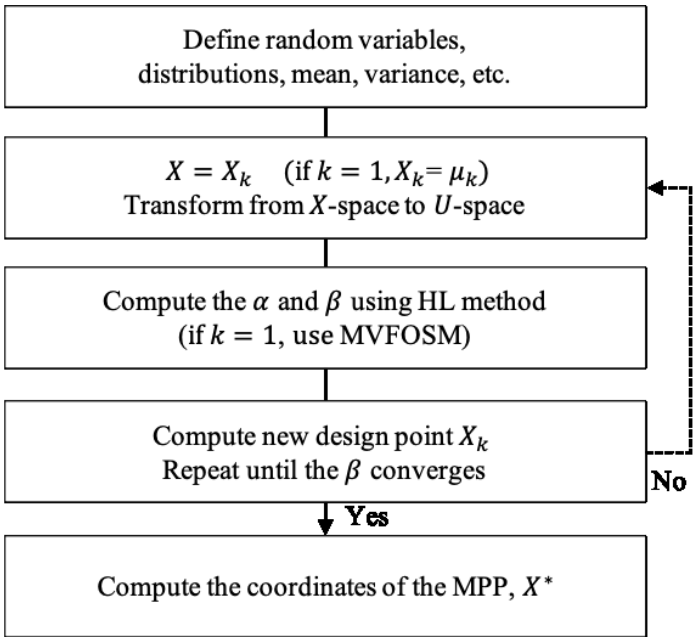

Figure 2.9: Procedure of the Hasofer Lind-Rackwitx Fiessler method

2.3.1.4 Second-Order Reliability Method (SORM)

In general, the First-Order Reliability Method (FORM) provides acceptable results when the limit state surface has only one shortest point, and it is linear near the design point. If the failure surface shows high non-linearity, the reliability index and the probability of failure estimated using FORM might not offer acceptable and accurate results. To deal with this challenge, SORM in Figure 2.10 uses the second-order Taylor series expansion to obtain a more precise approximation that is able to replace the failure surfaces of the original function.

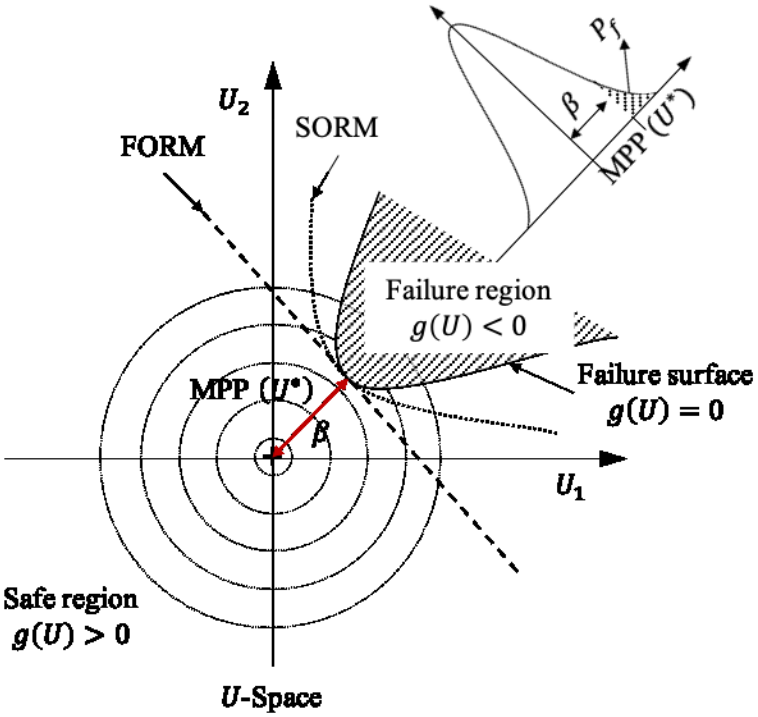

Figure 2.10: Second-Order Reliability Method

The second-order approximation of limit state function, $g(U) = 0$, is derived by the second-order Taylor series expansion at the Most Probable Failure Point (MPP).

$$\tilde{g}(U) = g(U^*) + \nabla g(U^*)^T\,(U - U^*) + \frac{1}{2}(U - U^*)^T \nabla^2 g(U^*)(U - U^*) \tag{2.25}$$

where $\nabla^2 g(U^*)$ is the symmetric matrix of the second derivative of the limit state function.

When the equation (2.25) is divided by $|\nabla g(U^*)|$ and $g(U^*)$ is zero, the equation can be expressed by

$$\tilde{g}(U) = \alpha^T (U - U^*) + \frac{1}{2}(U - U^*)^T B (U - U^*) \tag{2.26}$$

where $\alpha = \frac{\nabla g(U^*)}{|\nabla g(U^*)|}$, and $B = \frac{\nabla^2 g(U^*)}{|\nabla g(U^*)|}$.

The matrix of B is called the Hessian matrix, which is a square matrix of second-order partial derivative of the limit state function. This Hessian matrix leads to substantial computational efforts for the reliability analysis. An orthogonal matrix H is introduced as a form of $Y = HU$ to carry out the rotation from the standard normal U-space to the rotated new standard normal Y-space. The details of the orthogonal matrix are found in textbooks regarding the reliability analysis (8). Equation (2.26) in U-

space can be transformed to Y-space using the definition of direction cosine and the orthogonal matrix H as following.

$$\tilde{g}(Y) = -y_n + \beta + \frac{1}{2}(H^{-1}Y - H^{-1}Y^*)B(H^{-1}Y - H^{-1}Y^*) \tag{2.27}$$

The final matrix in the equation (2.27) can be given using the orthogonal matrix, H.

$$\tilde{g}(Y) = -y_n + \beta + \frac{1}{2}(Y - Y^*)HBH^T(Y - Y^*) \tag{2.28}$$

$$y_n = \beta + \frac{1}{2}\sum_{i=1}^{n-1} k_i y_i'^2 \tag{2.29}$$

where the k_i indicates the curvature of response surface at the MPP and the major computational effort is caused by calculating the second derivatives of limit state function at the MPP.

In particular, if the Finite Difference Method (FDM) to calculate the gradient of the limit state function is considered, a massive computational time might influence the efficiency of reliability analysis. There are two methods to compute the probability of failure using SORM: the Breitung formulation, as can be seen in equation (2.30) and the Tvedt's formulation (8,9).

$$P_f = \phi(-\beta)\prod_{j=1}^{n-1}\left(1 + k_j\beta\right)^{-1/2} \tag{2.30}$$

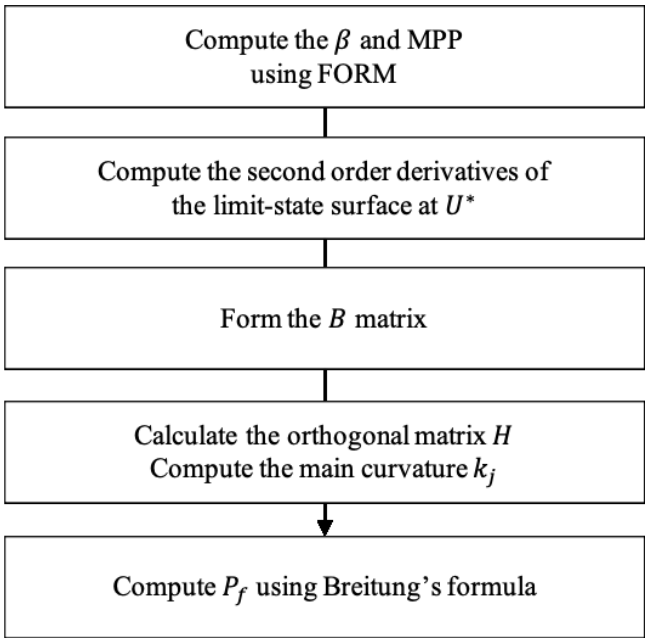

Figure 2.11: Procedure of the Second-Order Reliability Method

2.3.2 Robustness Analysis

The concept of robustness is utilised to quantify the quality of product in manufacturing engineering. When this concept incorporates into the deterministic optimisation process, it ensures that the optimal solution is a robust design. The variation during operating or service condition causes the unpredicted performance deviation in an initial design. This unexpected deviation may cause loss of structures' quality as well as increase different costs for monitoring, inspection, repairs and maintenance. The robustness analysis has drawn attention in structural design to address the quality loss and operational cost rise. The most straightforward way is to decrease or eliminate the scatter of the input parameter, but it is not feasible. The other way is to produce structures that are less sensitive to the variation of input parameters.

2.3.2.1 Theory

The fundamental of robustness in the structural design is that the optimal design is determined not only by the minimum mean value of objective function but also by how much the structural response is scattered to the mean value (3). The global optimal design in deterministic optimisation may be more sensitive than a local design, although the optimisation process finds the minimum mean value of the objective function.

Figure 2.12 highlights the concept of robustness using the distribution of objective function. The figure shows two different distributions concerning the same objective function that has to be minimised through the optimisation process. Each curve illustrates the frequency of the objective function, considering the random perturbation to its mean value. In the figure, two curves that refer to different designs have their mean and variance values. Even though "Design A" presents a smaller mean value of the objective function, its dispersion level to the mean value is larger than "Design B". In comparison, the mean value of "Design B" is greater than "Design A" while "Design B" offers more narrow distribution under the perturbation to the mean value. It is not surprising to note that "Design B" is a much more robust design than "Design A" because "Design B" has smaller sensitivity to variations.

In Figure 2.13, it is made clear that the robust design point may not be consistent with the global optimal value but the local optimal value. However, since the concept of robustness care about the development of insensitive design, the local value can be a robust solution when this solution is the most stable solution to the variation of the design parameters. It is necessary that the designer assures the robustness of the solution, which is not sensitive to the deviation of the design parameters. In that sense, well-optimised design solutions provide structures that minimise operating costs. These structures perform consistently with unexpected variations during the overall service lifecycle. Therefore, the robustness

of structures should be considered in the design parameter stages to reduce the dispersion of structural performance.

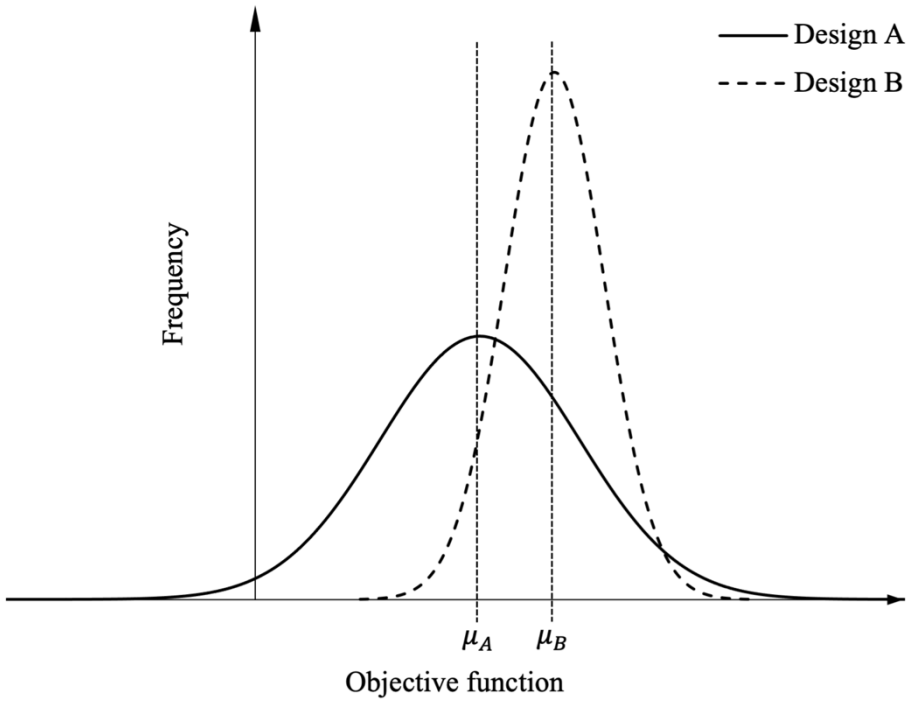

Figure 2.12: Concept of robustness

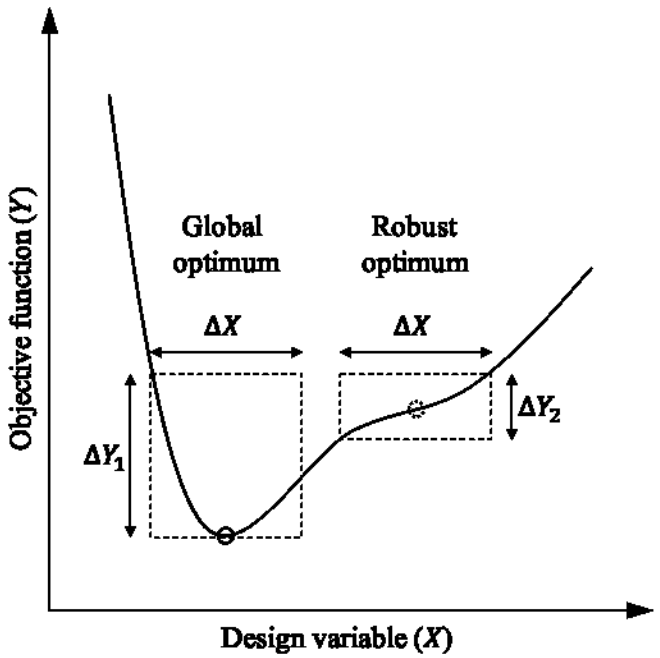

Figure 2.13: Difference between global optimum and robust optimum

2.3.2.2 Monte Carlo Simulation (MCS) for Robustness Analysis

MCS can evaluate not only reliability analysis but also robustness analysis. As discussed in the previous section 2.3.1.2, this method is an uncertainty propagation method that explicitly shows how uncertainties in input parameters influence results. If a probability distribution specifies the uncertainties in design parameters, MCS predicts the statistical characteristics of results propagated by the uncertainties. A large number of simulations regarding all uncertain parameters sampled are conducted to obtain these statistical results. Each simulation result during MCS is stored and then put together as a form of probability distribution (19).

Contrary to the reliability analysis evaluating the limit state function, the robustness analysis requires the mean and variance of the response function. To assess the robustness, random sampling sets regarding input design parameters, $N_{sampled}$, are created and these sets are defined by their mean and standard deviation. Then, the sampling sets are simulated and collected to evaluate the response functions. After that, the expected mean values and variances are obtained using equations (2.31) and (2.32), respectively.

$$\mu_X = E[X] = \frac{1}{N_{sampled}} \sum_{i=1}^{N_{sampled}} f_i \tag{2.31}$$

$$\sigma_X^2 = V[X] = E[(X - \mu_X)^2] = \frac{1}{N_{sampled}} \sum_{i=1}^{N_{sampled}} (f_i - \mu_X)^2 \tag{2.32}$$

where μ_X and σ_X^2 are the mean and standard deviation of the response function f.

In MCS, the greater number of points are sampled, the more accurate solutions are achieved. However, a large number of sampling points to improve the accuracy of solutions leads to substantial computational costs that are necessary to evaluate the response function. This also means that MCS requires many simulations when the dimension of the entire design spaces is large-scale.

3 Multi-Fidelity Models

As the size of the engineering problem becomes more complex and demanding, multi-fidelity models have been utilised in optimisation in the last three decades. Mainly, probabilistic design optimisation requires a large number of computational simulations to evaluate how uncertainties influence outputs. These simulations in structural optimisation, usually based on Finite Element Methods (FEM) or Boundary Element Methods (BEM), are too computationally expensive to use directly for the entire optimisation process. The models for structural optimisation can be defined by two types depending on how accurate they are, such as High-Fidelity Model (HFM) and Low-Fidelity Model (LFM) (47). The HFM having all system information provides acceptable accuracy, but these models are computationally expensive. The LFM is computationally economical but less accurate compared to the HFM. This LFM shows a certain level of similarity regarding the response surfaces of the HFM. Multi-fidelity models combine these two models using appropriate methods relying on the characteristic of problems. The primary aim of multi-fidelity modelling is to offer not only solutions as accurate as those of the HFM but also a lot more economic computational cost. Hence, the multi-fidelity models involve the trade-offs between solution accuracy and computation time savings.

As shown in Figure 3.1, the fidelity is defined in different ways of how the HFM can be simplified by the LFM, such as reduced dimensionality, linearisation, partial convergence, simple geometry, simplified physics, lower refinement, etc (23). They are generally categorised into three types depending on the nature of each fidelity. Physics describes a difference in how the physical model is presumed and implemented. In the beam problem in structural mechanics, for instance, Euler-Bernoulli beam theory can be a physical model of the LFM, whereas Timoshenko beam theory can be that of the HFM. Numerical accuracy refers to how a defined physical model is calculated using different numerical solvers, such as a linear solver or a non-linear solver in Computational Fluid Dynamics (CFD). Numerical accuracy also represents different levels of discretisation or refinement that can be seen by a model with a fine mesh and a model with a coarse mesh in FEM models. Finally, when experiments are carried out as the HFM, computational simulations take the place of the LFM.

The multi-fidelity models constructed by the combination of different fidelity models commonly involve creating surrogate models to obtain more computational benefits. The surrogate models are sorts of approximation that has an explicit form between design input parameters and output parameters. These models have been widely used to deal with computational challenges through creating a black-box model of a complex system (10). The multi-fidelity models can be constructed without the surrogate models; however, the computational cost caused by the use of the HFM and the LFM directly for the optimisation process may still lead to computational burden. These multi-fidelity models based on the surrogate models are constructed by deterministic and non-deterministic methods based on how to estimate the parameters to build the surrogate models. The deterministic methods estimate the coefficients of presumed basis functions that minimise the error between sampling design points and the functions. These deterministic methods build up the surrogate models of HFM and LFM and compare the response surfaces between them. In comparison, the non-deterministic methods consider the uncertainty of either the functions or coefficients and minimise the uncertainty using the sampling design points. They employ a statistical inference method, such as the Bayesian framework or Gaussian Process (GP), to hold the uncertainties in parameters without using the expensive standard Monte Carlo Simulations (23).

The application area of multi-fidelity models has been broadened due to its inheritance of computational efficiency. The vast majority of the application area has been deterministic optimisation and uncertainty quantification (48). It has scarcely carried out probabilistic optimisation considering design uncertainty except for simple structure design problems covering a small design space. In specific, the multi-fidelity models are utilised in different structural mechanics problems, and the primary fidelities are the structure's dimensionality and the discretisation's level.

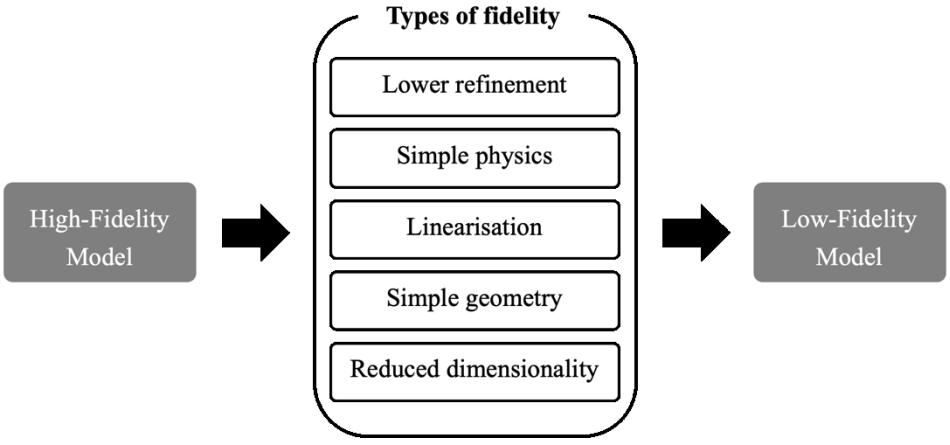

Figure 3.1: Examples of fidelity between HFM and LFM

This chapter will discuss the fundamental theory of surrogate modelling to construct multi-fidelity models such as different sampling techniques, surrogate modelling methods, validation methods and model improvements using sequential design. The probabilistic optimisation of a simple structure will

be introduced using the surrogate models. At the end of this chapter, the formulation of different multi-fidelity methods will be discussed, such as response correction methods, space mapping and Auto-Regressive (AR).

3.1 Surrogate Model

Computation-intensive design problems in engineering structures cause the enormous computational cost to run. This computational cost is still challenging despite constant development in computing technologies because the complexity of computer models created using the Finite Element Method (FEM) is also increasing. This high cost can be addressed using high-performance computing. However, these design problems based on complex computer models require a large number of calculations, often taking from hours to even days to run one single simulation (21). Such problems encompass different engineering fields, including structural design optimisation. In particular, Monte Carlo Simulations (MCS) to carry reliability analysis and robustness analysis require thousands of simulations to predict the statistical characteristics correctly. It is not possible to use the computer models directly for running the simulations needed if a single simulation requires more than hours to run.

Surrogate modelling is a method to improve the overall computation efficiency and reach an acceptable accuracy compared with complex computer models. Surrogate models replace the computationally expensive models at the same time provide an excellent understanding of the relationship between input design parameters and output system performance. The number of input-output data from the complex computer models and where they are collected in the entire design space are crucial to obtain the acceptable accuracy of the surrogate model and the computation efficiency to build the model. Surrogate models can support different engineering area, as highlighted in Figure 3.2 (22). They approximate the complex computer models across the whole design space to reduce the computational cost. Such models enable engineers to explore the design space as well as improve the knowledge regarding the design problems. Finally, the surrogate models can be utilised to find optimal solutions for different optimisation problems that require computationally extensive efforts. In particular, the surrogate models can be used to take the place of the computationally expensive FEM models for probabilistic applications that demand a vast number of simulations to consider design uncertainties.

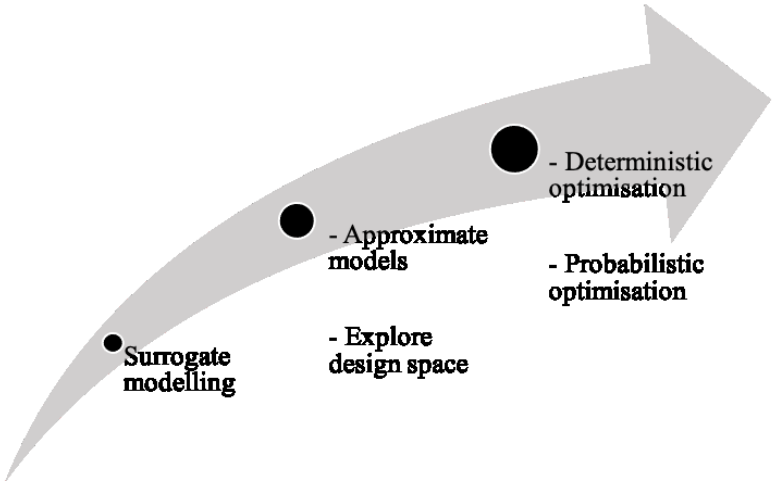

Figure 3.2: Application area of surrogate model

There are several common types of surrogate modelling, including Artificial Neural Networks (ANN), Response Surface Method (RSM) and Gaussian Process (GP) (12). The number of design points to build the surrogate models depends on the dimension of the design space. If a design problem covers many design variables, the computational cost to train the surrogate model using the FEM simulations also rises dramatically.

3.1.1 Sampling Techniques

Sampling techniques are important to create a surrogate model efficiently that represents an original model. If these sampling techniques choose appropriate design points in the design space, the surrogate model is trained accurately, and it replaces the broad range of characteristics of the original model. The input matrix X is the sampled design points that are used to train a surrogate model. The matrix Y is the output corresponding to these design points. These two matrices can be expressed as:

$$X = \begin{bmatrix} \mathrm{x}_1 \\ \mathrm{x}_2 \\ \vdots \\ \mathrm{x}_n \end{bmatrix} = \begin{bmatrix} x_{11} & x_{12} & \cdots & x_{1m} \\ x_{21} & x_{22} & \cdots & x_{2m} \\ \vdots & \vdots & \ddots & \vdots \\ x_{n1} & x_{n2} & \cdots & x_{nm} \end{bmatrix} \tag{3.1}$$

$$Y = \begin{bmatrix} \mathrm{y}_1 \\ \mathrm{y}_2 \\ \vdots \\ \mathrm{y}_n \end{bmatrix} = \begin{bmatrix} y(\mathrm{x}_1) \\ \vdots \\ y(\mathrm{x}_n) \end{bmatrix} \tag{3.2}$$

where n and m are the number of sampled design points and the design space dimension, respectively. If the system has one output value from the expensive model, the output Y will be a $(n \times 1)$ vector. If the system has p output values, the output Y will be a $(n \times p)$ matrix.

The quality of a surrogate model relies on how to sample the design points to set up the input matrix X. Many sampling methods have been developed to explore the entire design space using space-filling approaches. These approaches aim to collect the design points as evenly distributed as possible while minimising the distance or cluster between different design points. Design of Experiments (DOE) is a method to determine the location of the design points that significantly influences the surrogate model's accuracy. DOE is a process having the general target of maximising the amount of information obtained from a limited number of sampling points. Such sampling points estimate performance variability caused by changes in design input parameters. When DOE build a design matrix with input and output data, the design matrix indicates the values of uncertain design parameters. The vast majority of these sampling techniques are simple random sampling, Optimal Latin Hypercube Sampling (OLHS) and Sobol sampling (49). Each technique has its advantages and disadvantages in terms of space-filling capability, computational time and complication. These methods are introduced and discussed as follows.

3.1.1.1 Simple Random Sampling

Simple random sampling is the basic sampling techniques where the design points to be sampled are selected from a specific design range or a probability distribution. This is the most straightforward sampling method compared to different ones. With this sampling method, each design point is selected using a pseudo-random number generator, and every possible design point has the same chance to be sampled. However, this sampling method using the random nature can lead to irregular dispersion in the design space, such as clusters of design points and far distance between different design points. Figure 3.3 shows the uneven dispersion of design points caused by simple random sampling. This can result in poor accuracy of the surrogate model because the design points cannot cover the design space adequately. The surrogate model can provide good accuracy in some areas having many design points while offering inaccurate solutions in other areas having few design points.

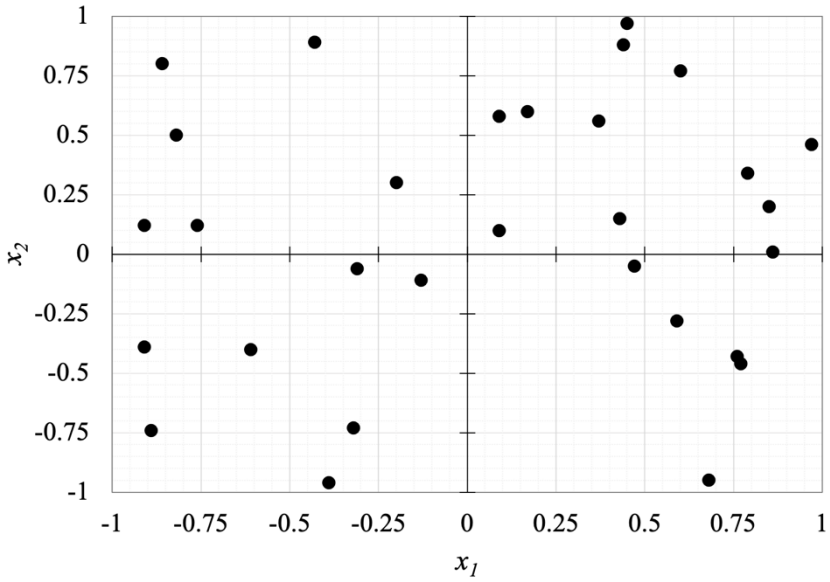

Figure 3.3: Distribution of design points using simple random sampling

3.1.1.2 Optimal Latin Hypercube Sampling (OLHS)

OLHS is a more advanced sampling technique that comes from Latin Hypercube Sampling (LHS). LHS denotes a multivariable sampling method that confirms a non-overlapping design. It is an experimental design that effectively selects the design points in the whole design space. In this method, the distribution for each design variable is divided into an equal interval of probability without overlapping. Each equally divided probability interval has only one design point. These design points in every interval are randomly combined with rearranging them for each point with the different design points. The regularity of uniform probability intervals guarantees that each input design parameter has every portion of its design space. It reduces both response sensitivities and expensive computational cost to sample the design points. The disadvantages of LHS are that the design points are not reproducible since they are combined at random, and the small number of design points increases the possibility of dropping some areas in the whole design space.

OLHS also breaks down the design space with the uniform interval of probability, and these design points in each interval are combined. However, it does not randomly combine the design points like LHS, but an optimisation process is adopted to an initial matrix created by LHS. A new matrix is obtained by swapping the order of design points in a column of the design matrix, and then the overall distance between the design points is evaluated. This optimisation process aims to create a matrix where the design points are scattered as evenly as possible within the design space defined by the lower and upper ranges. There are many different optimality criteria to reach such evenly spread design points.

One of these methods is the max-min distance criteria that involves maximising the minimum distance between other design points as expressed in equations (3.3) and (3.4).

$$\left(\max\left(\text{sum}\left(\min_{1\leq i,j\leq n, i\neq j} d(\mathrm{x_i}, \mathrm{x_j})\right)\right)\right) \tag{3.3}$$

where $d(\mathrm{x_i}, \mathrm{x_j})$ is the distance between two different design points $\mathrm{x_i}$ and $\mathrm{x_j}$, n is the required number of design points.

$$d(\mathrm{x_i}, \mathrm{x_j}) = d_{ij} = \left[\sum_{k=1}^{m} \left|\mathrm{x}_{ik} - \mathrm{x}_{jk}\right|^2\right]^{\frac{1}{2}} \quad where\ i \neq j \tag{3.4}$$

where m is the number of design variables

Equation (3.4) evaluates all design points $i, j = 1, 2, \ldots, n$ except $i \neq j$ and delivers the distance matrix d for the optimised design matrix. OLHS provides an excellent opportunity to train the surrogate model using the outstanding space-filling capability. As illustrated in Figure 3.4 and Figure 3.5, OLHS collects the design points in the entire design space more evenly distributed than LHS.

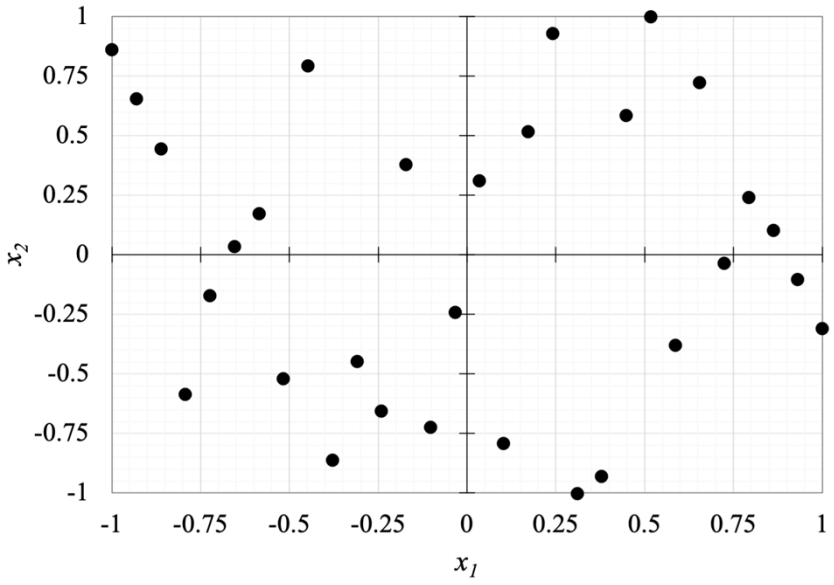

Figure 3.4: Distribution of design points using Latin hypercube sampling

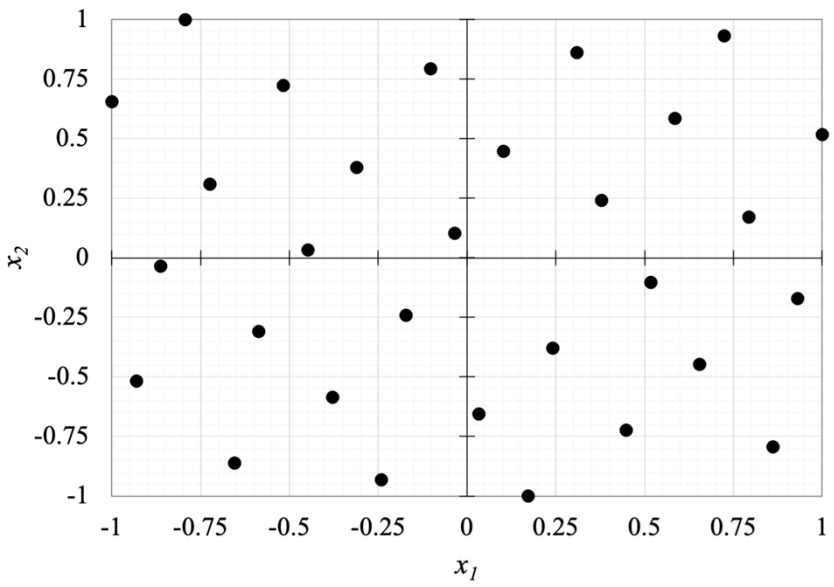

Figure 3.5: Distribution of design points using optimal Latin hypercube sampling

3.1.1.3 Sobol Sampling

Sobol sampling, a quasi-random sequence, provides more uniformly distributed design points than simple random sampling and Latin hypercube sampling methods. This sampling method selects the design points under consideration of earlier sampled design points whilst evading the presence of clusters and large spaces between different design points. The method allows surrogate models to offer a good quality of accuracy using a smaller number of design points than simple random sampling and OLHS. Such Sobol sequence consists of considerably complicated mathematical formulations compared with different sampling methods while providing more robust results having a smaller variation (49).

3.1.2 Surrogate Modelling Methods

Surrogate models aim to deal with a large number of computational simulations that evaluate objective functions and constraints for different optimisation problems. These models allow to carry out these optimisation problems using affordable computational cost. Such surrogate models are created by observations, such as experiments or numerical simulations. They have an explicit mathematical form concerning the relationship between input and output parameters. There are several different methods to construct the surrogate models. This section will introduce two of the most typical methods that work with computer experiments, such as Artificial Neural Networks (ANN) and Gaussian Process (GP).

3.1.2.1 Artificial Neural Networks (ANN)

ANN is a network of simple elements that are called neurons. These neurons take input data and change their activations according to the input data. Then they produce output associated with the input data and activation. There are three components to ANN, such as neurons, weight and activation function (50). In particular, Radial Basis Functions (RBF), a type of ANN, uses radial units as activation function. The output of this network is a linear combination of input and neuron parameters. This network architecture comprises three layers, including an input layer, a hidden layer having the RBF activation function and an output layer. The input layer is the vector of real numbers $\mathrm{x} \in R^n$, and the output layer is the scalar function of the input vector. The basic idea of the RBF is that these functions depending on the distance from a centre vector are radially symmetric. One of the advantages of the RBF is that the interpolation problem is not sensitive to the dimension of design space in which the data points lie. This enables multivariable functions to be approximated using a linear combination of single-variable functions (51). All inputs are connected to each hidden layer in the basic form, as shown in Figure 3.6. The input parameter is used as input data to RBF, and the output data of this network is a linear combination of RBF' outcomes.

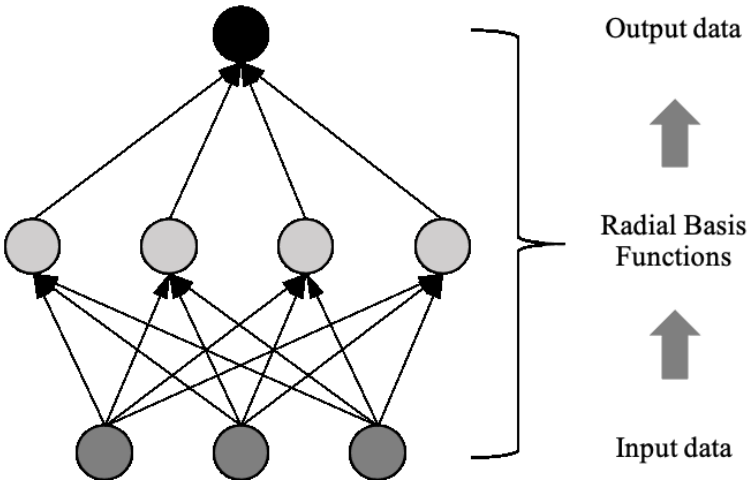

Figure 3.6: Basic form of the radial basis functions

A basic RBF model is mathematically expressed as

$$h(\mathrm{x}) = \sum_{n=1}^{N} w_n \cdot exp(-\gamma \|\mathrm{x} - \mathrm{x}_n\|^2) \tag{3.5}$$

where N is the number of neurons in the hidden layer. $h(\mathrm{x})$ and w_n are hypothesis and the weight of neuron i, respectively. $\|\mathrm{x} - \mathrm{x}_n\|$ is the radial distance between input and centre point of neuron n, the norm is typically calculated by the Euclidean distance.

As shown in equation (3.5), each pair $(\mathrm{x_n}, \mathrm{y_n})$ in the design space influences $h(\mathrm{x})$ based on the radial distance $\|\mathrm{x} - \mathrm{x_i}\|$. The learning algorithm is to find the weights $w_1, w_2, \ldots, w_n$ from the equation using training data $D = (\mathrm{x_1}, \mathrm{y_1}),\ (\mathrm{x_2}, \mathrm{y_2}), \ldots, (\mathrm{x_n}, \mathrm{y_n})$. These weights minimise errors between $h(\mathrm{x_n})$ and $\mathrm{y_n}$. Table 3.1 shows that the basis function in the equation (3.5), $exp(-\gamma\|\mathrm{x} - \mathrm{x_n}\|^2)$, can be changed into different basis functions ϕ (52).

Table 3.1: Typical radial basis functions

Name	Basis function
Linear	$\phi = \|\mathrm{x} - \mathrm{x}_n\|$
Cubic	$\phi = \|\mathrm{x} - \mathrm{x}_n\|^3$
Thin-plate spline	$\phi = \|\mathrm{x} - \mathrm{x}_n\|^2 \ln(\gamma\|\mathrm{x} - \mathrm{x}_n\|)$
Gaussian	$\phi = exp(-\gamma\|\mathrm{x} - \mathrm{x}_n\|^2)$
Multi-quadric	$\phi = \sqrt{\|\mathrm{x} - \mathrm{x}_n\|^2 + \gamma^2}$
Inverse multi-quadric	$\phi = \frac{1}{\sqrt{\|\mathrm{x} - \mathrm{x}_n\|^2 + \gamma^2}}$

Equation (3.5) consists of N equations in N unknowns; thus, the solution can be calculated by

$$\begin{bmatrix} exp(-\gamma\|x_1 - x_1\|^2) & \cdots & exp(-\gamma\|x_1 - x_N\|^2) \\ \vdots & \ddots & \vdots \\ exp(-\gamma\|x_N - x_1\|^2) & \cdots & exp(-\gamma\|x_N - x_N\|^2) \end{bmatrix} \begin{bmatrix} w_1 \\ \vdots \\ w_N \end{bmatrix} = \begin{bmatrix} y_1 \\ \vdots \\ y_N \end{bmatrix} \tag{3.6}$$

$$\begin{bmatrix} w_1 \\ \vdots \\ w_N \end{bmatrix} = \begin{bmatrix} exp(-\gamma\|x_1 - x_1\|^2) & \cdots & exp(-\gamma\|x_1 - x_N\|^2) \\ \vdots & \ddots & \vdots \\ exp(-\gamma\|x_N - x_1\|^2) & \cdots & exp(-\gamma\|x_N - x_N\|^2) \end{bmatrix}^{-1} \begin{bmatrix} y_1 \\ \vdots \\ y_N \end{bmatrix} \tag{3.7}$$

$$W = \phi^{-1} Y \tag{3.8}$$

where ϕ is the matrix of the basis function.

When the vector of weights is obtained, the surrogate model created using RBF can represent the complex computer model and provide outputs concerning different input data that are not used to train the model.

As can be seen in equations (3.6) and (3.7), the value of γ in the Gaussian basis function affects the outcomes of the surrogate model. When the value of γ is small, the Gaussian function has a wide distribution, whereas the function having a large value of γ has a narrow distribution. This γ makes a significant difference depending on where the design points are and how sparse they are between different design points. Figure 3.7 and Figure 3.8 display how the value of γ influences interpolating with Gaussian functions (53). For example, if three points are selected from the red curve in Figure 3.7, the total contribution of the three interpolations passes precisely through the points. However, the small grey curves are the contribution according to each of them. The red curve is determined by adding all multiplication, which are weight w_n and corresponding Gaussian $exp(-\gamma\|\mathrm{x} - \mathrm{x}_n\|^2)$ together. This

curve gives correctly the output data, such as y_1, y_2 and y_3. This width appointed by the small value of γ ensures a successful interpolation that provides a reasonable prediction between two different points. In contrast, the large value of γ leads to an incomplete interpolation between different points because each curve drops rapidly, although the red curve in Figure 3.8 gives the correct output data at the selected points. However, the interpolation of three grey curves is inferior enough not to deliver a good prediction between different points due to the narrow distribution. The two figures show that the value of γ matters about the distance between the points sampled because that it affects the interpolation.

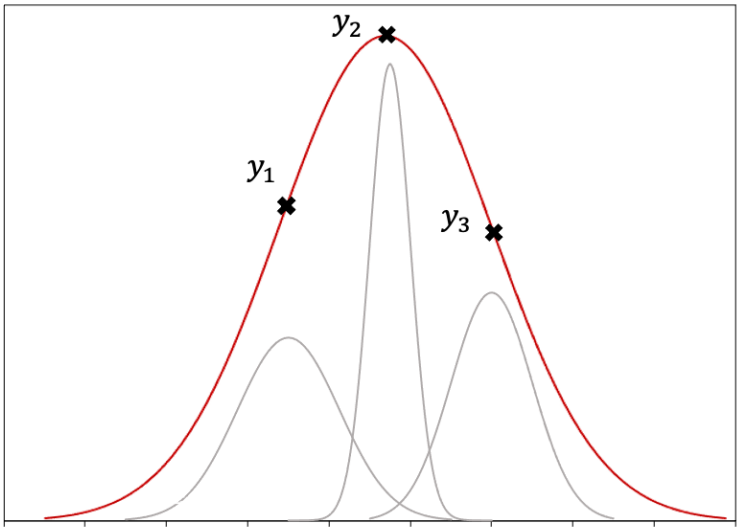

Figure 3.7: RBF with a small value of γ

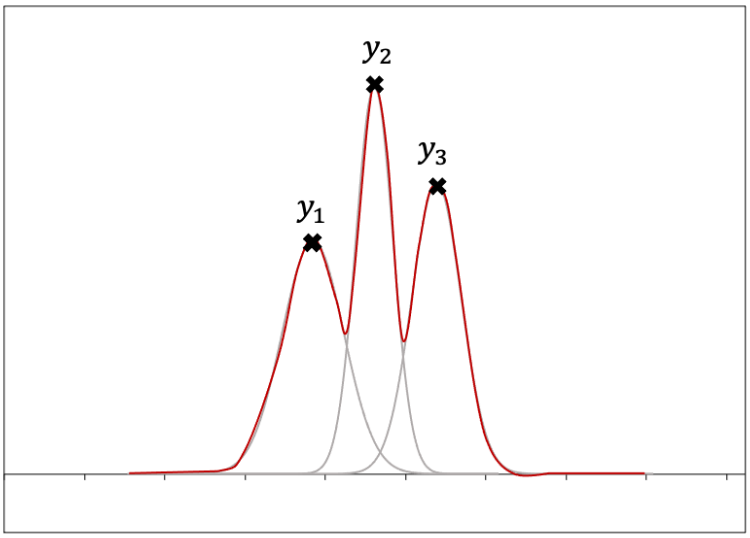

Figure 3.8: RBF with a large value of γ

3.1.2.2 Gaussian Process (GP)

GP regression describes a supervised learning problem that both training and testing data sets consist of input and output pairs of observations $D = \{\mathrm{x_i}, \mathrm{y_i}\} = (\mathrm{x_1}, \mathrm{y_1}),\ (\mathrm{x_2}, \mathrm{y_2}), \ldots, (\mathrm{x_n}, \mathrm{y_n})$. GP defines a collection of random variables that are a finite number of which have a joint Gaussian distribution (54). Such GP is expressed using its mean function and covariance function

$$\mu(\mathrm{x}) = E[f(\mathrm{x})] \tag{3.9}$$

$$k(\mathrm{x}, \mathrm{x}') = E\big[\big(f(\mathrm{x}) - \mu(\mathrm{x})\big)\big(f(\mathrm{x}') - \mu(\mathrm{x}')\big)\big] \tag{3.10}$$

where $\mu(\mathrm{x})$ and $k(\mathrm{x}, \mathrm{x}')$ are the mean function and the covariance function, respectively. $f(\mathrm{x})$ is a Gaussian process written as $f(\mathrm{x}) \sim GP(\mu(\mathrm{x}), k(\mathrm{x}, \mathrm{x}'))$

The definition of GP requires consistency, which is also called the marginalisation property. This property explains that if GP states $(y_1, y_2) \sim N(\mu, \sigma)$, it also has to state $y_1 \sim N(\mu_1, \sigma_{11})$ where σ_{11} is the related submatrix of σ. This safeguards the examination of a greater set of variables does not affect the distribution of the subset.

The covariance function $k(\mathrm{x}, \mathrm{x}')$ is a positive definite kernel that represents the dependence structure of GP. This function characterises the covariance between different random variables. The covariance matrix $cov\big(f(\mathrm{x}), f(\mathrm{x}')\big)$ based on the squared exponential covariance function that is a popular covariance function is written as

$$cov\big(f(\mathrm{x}), f(\mathrm{x}')\big) = k(\mathrm{x}, \mathrm{x}') = exp\left(-\frac{1}{2}|\mathrm{x} - \mathrm{x}'|^2\right) \tag{3.11}$$

where $f(\mathrm{x})$ and $f(\mathrm{x}')$ are GP concerning x and x′, respectively. $|\mathrm{x} - \mathrm{x}'|$ stands for the Euclidean norm between x and x′.

It should be noted that a function of the input data defines the covariance between the output data of GP regression. This covariance in equation (3.11) is nearly unity between the input data in close distance and drops when the distance goes far. If the term of $|\mathrm{x} - \mathrm{x}'|$ in the equation is replaced by $|\mathrm{x} - \mathrm{x}'|/\theta$ for a positive characteristic length-scale θ that can be assumed by the distance to move in the input space before the function value can change considerably, the length-scale can be a parameter to control the oscillation frequencies of the GP regression model. Also, the process variance σ^2 of the random function can be added to control the range of variation of the model. Finally, the covariance matrix based on the squared exponential covariance function can be expressed by equation (3.12). The length scale, also known as hyperparameters, should be optimised because they are essential to creating an excellent surrogate model using GP. The process to find these optimal values are called hyperparameter estimation.

$$cov\big(f(\mathrm{x}), f(\mathrm{x}')\big) = \sigma^2 k(\theta, \mathrm{x}, \mathrm{x}') = \sigma^2 exp\left(-\frac{1}{2\theta^2}|\mathrm{x} - \mathrm{x}'|^2\right) \tag{3.12}$$

When the observations are noise-free, $\{(\mathrm{x}_i, \mathrm{y}_i)|i = 1, \dots, n\}$, the training data provides the function information to be incorporated in the GP regression model. The joint distribution of the training output data sets Y and the test output data sets Y_* based on the prior is expressed as

$$\begin{bmatrix} Y \\ Y_* \end{bmatrix} \sim N\left(0, \begin{bmatrix} K(X,X) & K(X,X_*) \\ K(X_*,X) & K(X_*,X_*) \end{bmatrix}\right) \tag{3.13}$$

where $K(X, X_*)$ is the $(n \times n_*)$ covariance matrix consisting of all combinations of n training data points and n_* testing data points. Similarly, $K(X,X)$, $K(X_*,X)$ and $K(X_*,X_*)$ denotes the covariance matrixes of their components.

The prior appoints an evaluation to specify pairwise correlation between different input data points and manifests prior knowledge on the characteristics of the function to be estimated. This joint prior distribution should be defined to accommodate the function along with the observed design data points so that the posterior distribution is obtained over the function. This posterior distribution corresponds to conditioning the joint Gaussian prior distribution on the design data points, and it can be given as

$$Y_*|X_*, X, Y \sim N\big(K(X_*,X)K(X,X)^{-1}Y, K(X_*,X_*) - K(X_*,X)K(X,X)^{-1}K(X,X_*)\big) \tag{3.14}$$

New output data Y_* concerning testing input data points X_* can be taken from the joint posterior distribution using the mean and covariance matrix. This conditional distribution provides the predictive equations for the GP regression model as

$$p(Y_*|\, X, Y, X_*) = N\big(Y_*|\mu_*(X_*), \sigma_*^2(X_*)\big) \tag{3.15}$$

$$\mu_*(X_*) = K(X_*,X)K(X,X)^{-1}Y \tag{3.16}$$

$$\sigma_*^2(X_*) = K(X_*,X_*) - K(X_*,X)K(X,X)^{-1}K(X_*,X)^T \tag{3.17}$$

Predictions are estimated using the posterior mean μ_*, while the variance associated with these predictions is computed using the posterior covariance σ_*^2.

In order for the GP regression model to predict the response at new testing points X_*, the hyperparameters of the length-scale θ and the process variance σ^2 in equation (3.12) have to be found appropriately. Different methods to optimise these parameters, such as maximum likelihood estimation, has been developed in the past (54). The maximum likelihood estimation used here is a popular method to estimate the parameters, and the maximum log-likelihood of the GP regression model can be expressed by

$$\log p(Y|X) = -\frac{1}{2}\log|K| - \frac{1}{2}Y^T K^{-1} Y - \frac{n}{2}\log 2\pi \tag{3.18}$$

where K is $K(X,X)$ and n is the number of training data points.

3.1.3 Validation of Surrogate Models

When a surrogate model is constructed using ANN or GP, the surrogate models should be validated whether it provides not only the computational efficiency but also accurate solutions. There are two popular validation methods to evaluate the created surrogate model, including the separation and cross-validation methods (55). As shown in Figure 3.9, the separation method requires two different datasets, training and testing datasets, which are determined using sampling techniques, such as simple random sampling, optimal Latin hypercube sampling, etc. The training data set is to create the surrogate model using global approximation methods, such as ANN and GP. Once the surrogate model is constructed, the testing dataset assesses the surrogate model's accuracy by comparing output values between the original model and the surrogate model. The testing dataset is a hidden dataset that is considered only once, and this dataset should not be available until the surrogate model is created using the training dataset. This describes that the testing dataset is not considered in the data training process creating the surrogate model.

In contrast to the separation method, the cross-validation method consists of different phases. Each phase subdivides a sampled dataset into the training dataset and the testing dataset. Then the surrogate model created using the training dataset is validated using the testing dataset. This error analysis is also called the leave-one-out cross-validation method since each phase requires at least a single design point in the testing dataset. The more points are added to each cross-validation phase, the more significant time is taken to validate the model. Figure 3.10 shows the general phase of the cross-validation method.

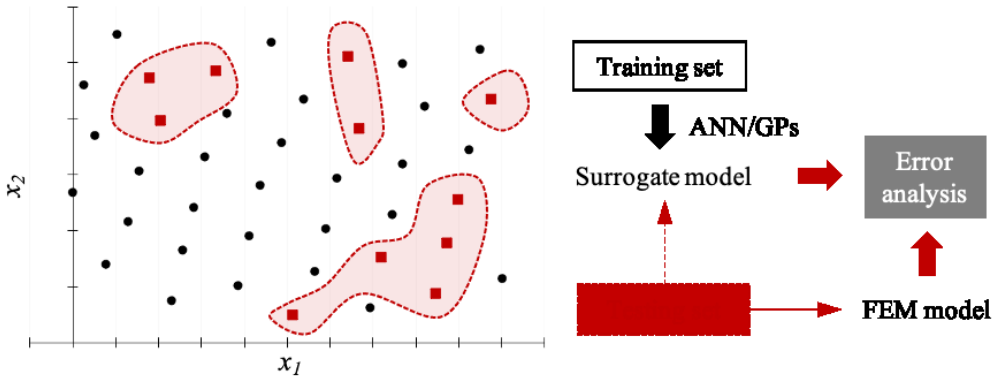

Figure 3.9: Separation method

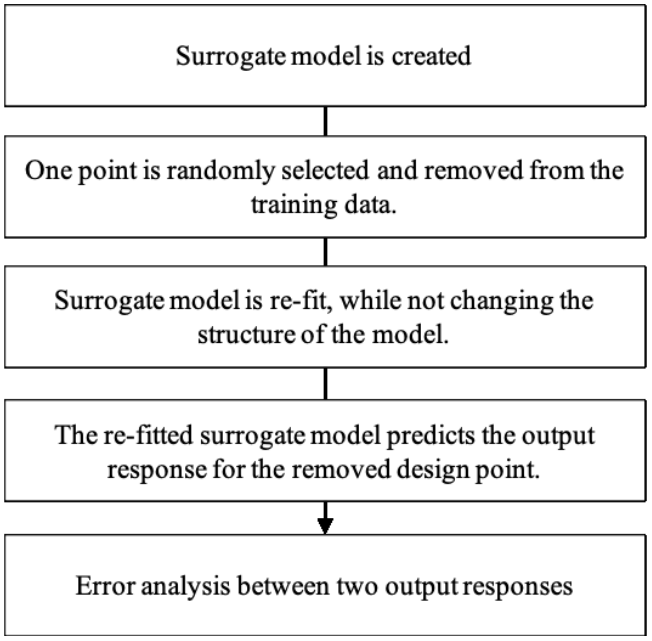

Figure 3.10: Cross-validation method

The differences measured by these two validation methods can be quantified using proper error analysis. There are many error analysis types, such as average, maximum, root mean square and R-squared error analyses. The root mean square error analysis used here calculates the squared differences between the actual output value from the original model and the predicted output value from the surrogate model. These squared differences are normalised using the difference between the maximum and minimum actual output values in the design range. The root mean squared error is computed as

$$Error = \frac{\sqrt{\frac{\sum_{k=1}^{n}(Actual\ output - Predicted\ ouput\ )^2}{n}}}{Maximum\ actual\ output - Minimum\ actual\ ouput} \tag{3.19}$$

where n is the number of testing design points.

3.1.4 Sequential Design

The computational time to obtain the actual output values corresponding to the sample design points takes an enormous contribution to constructing the surrogate model. A sequential sampling process enables designers to improve the accuracy of approximation as well as computational efficiency. As shown in Figure 3.11, this sampling process aims to add more sampling points to the surrogate modelling process to advance the quality of the training dataset (56). The sequential sampling method begins from the initial sampling set to initialise the surrogate modelling process that is collected by a sampling technique. Then this method selects additional sampling points for this initial set using the max-min scaled distance approach. This approach collects new sampling points that maximise the

minimum distance between two different sampling points in the following sampling set. When the accuracy of the surrogate model using the updated training dataset has satisfied the required level, the iterative sampling process can be terminated. Unless the process reaches the specific accuracy, the process carries on using more new sampling points until it fulfils the tolerance requirement. In this manner, the sequential design ensures that the surrogate model having an acceptable accuracy can be created using more computationally efficient than different sampling approaches.

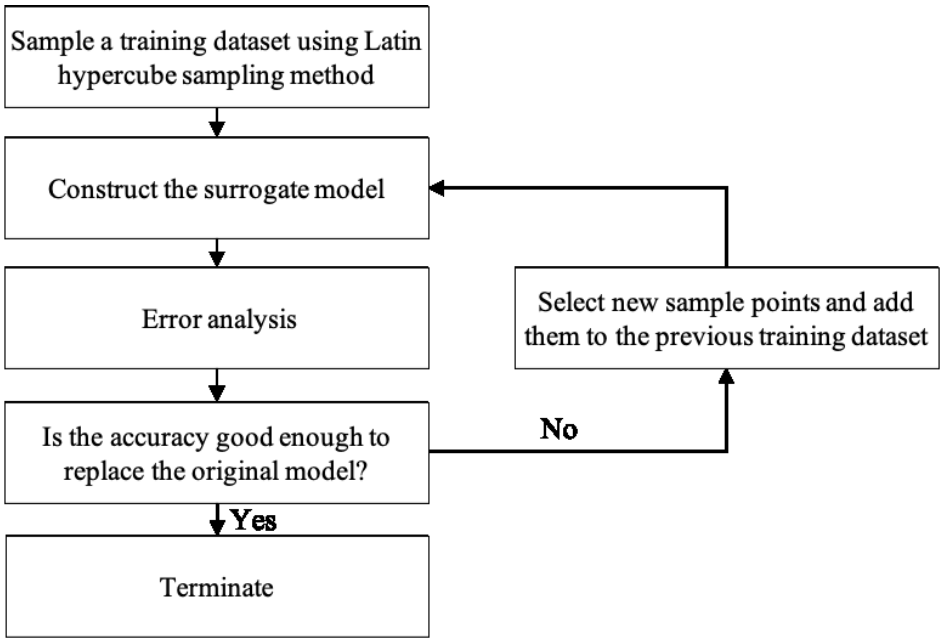

Figure 3.11: Sampling procedure for sequential design

3.1.5 Numerical Example - Surrogate Modelling-Based Probabilistic Optimisation

In this numerical example, Reliability-Based Design Optimisation (RBDO), one type of probabilistic optimisation method, is carried out for the isotropic steel plate's design. This example clearly shows how the surrogate models are utilised in the probabilistic optimisation process. The isotropic steel drain cover illustrated in Figure 3.12 was optimised in the RBDO process that considers the uncertainty of design variables. The objective of the optimisation problem is to minimise both the drain cover's cost related to its mass and the vertical displacement under the uniformly distributed pressure. The maximum stress was defined by a constraint to ensure that the material does not violate half of its yielding point for safety. The height of the drain and the thickness of the steel plate are considered design variables. The Finite Element Method (FEM) model of the drain cover was created using Abaqus and Isight (57,58). The problem definition, including dimension, material properties, loading condition and optimisation is described in Table 3.2. It should be noted that the pressure load is defined by the total

force that gives the total magnitude of pressure applied over the entire surface. The reliability analysis, which is an essential part of RBDO, was conducted using the First-Order Reliability Method (FORM) because this method is computationally affordable to the use of the FEM model. This allows seeing how the surrogate model obtains many computational gains through the comparison with the use of the FEM model. The gradient of the constraint was calculated using the step size of 1 % of the finite difference method. The iteration for the Most Probable Point (MPP) stopped until the convergence of the reliability index is 0.1 %. The design uncertainties of drain height and plate thickness were determined by the coefficient of variations, which are 0.3 and 0.1, respectively. The constraint was 160.0 GPa that is half of the yield stress of steel.

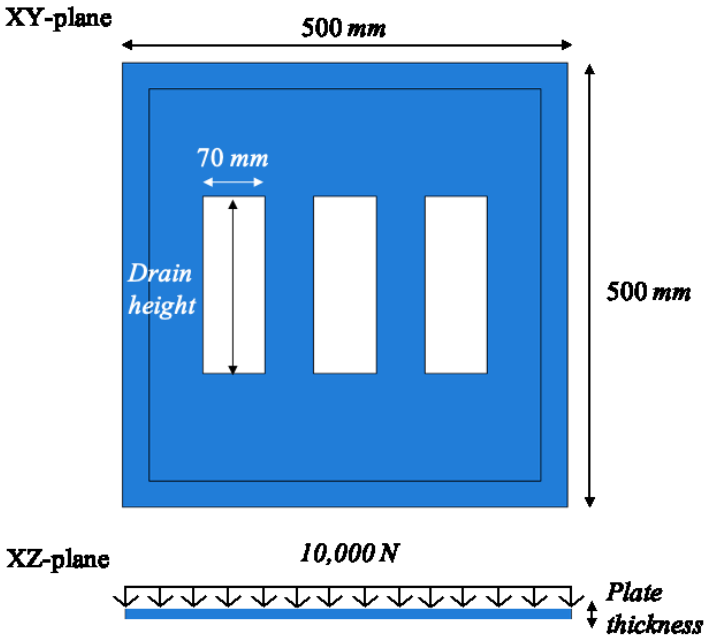

Figure 3.12: Isotropic steel drain cover having two design variables

Table 3.2: Problem definition

Description		Value
Material properties	Young's modulus (GPa)	138
	Poisson's ratio	0.3
Dimension	Outer dimension (mm)	500 × 500
	Drain width (mm)	70
Pressure load	Total force distribution (N)	10,000
Design Variables	Drain height (mm)	$187 < L < 313$
	Plate thickness (mm)	$3.75 < t < 6.25$
Optimisation method	NSGA-II	$Generation$: 5 $Population$: 8
Constraint	Maximum von Mises stress	160.0 GPa
Objectives	Cost (referring the steel price per unit mass)	$minimise$
	Maximum out-of-plane displacement (mm)	$minimise$

Figure 3.13 describes the process of how to create the surrogate model for this optimisation problem. When Optimal Latin Hypercube Sampling (OLHS) samples enough number of design points in the design range, the FEM solver calculates the output values concerning the sampled design points to set up the design matrix. In this example, Radial Basis Functions (RBF) with a basis function of Gaussian created the surrogate model, and the created surrogate model was evaluated using a testing dataset as shown in Table 3.3. The sequential sampling method was also considered to improve the quality of the surrogate model.

Table 3.4 presents the RBDO results using FORM whilst comparing them between the FEM and surrogate models. The optimal solutions of each model were selected by the same vertical displacement in the Pareto front. The costs of the two selected optimal solutions show nearly similar between the FEM model and surrogate model. The reliability index and the probability of failure have also very similar results. This means that the surrogate model offers trustworthy accuracy in comparison with the FEM model. Most notably, substantial computational gains are achieved by the use of the surrogate model. The optimisation time using the FEM model was over 28 hours, whereas that of the surrogate model was less than an hour. In the surrogate modelling method, the vast majority of the computational cost was caused by the FEM simulation to create the design matrix using the input and output values. The actual optimisation time was considerably fast while providing a nearly identical accuracy level to the FEM model.

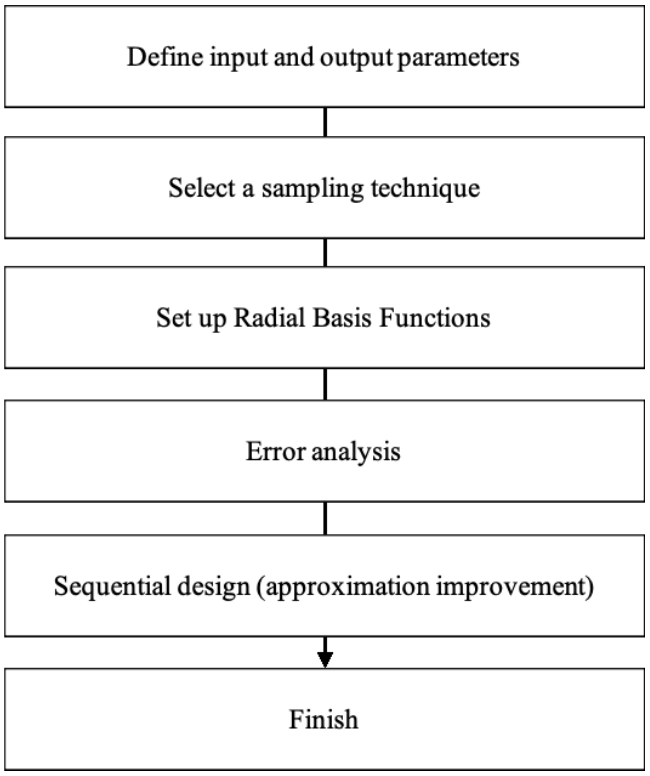

Figure 3.13: Surrogate modelling process

Table 3.3: Validation of surrogate model using the separation method

Testing data point	Drain height (L)	Plate thickness (t)	Output	Surrogate model	FEM model	Error analysis (%)
1	190	5.5	Cost	124.8	124.8	0.00
			Displacement (Dips.)	2.9	2.9	0.06
			Maximum von Mises stress (VMS)	117.0	117.2	0.17
2	160	6	Cost	139.4	139.3	0.03
			Disp.	2.2	2.1	0.94
			VMS	98.0	97.5	0.17
3	182	4.75	Cost	108.4	108.4	0.00
			Disp.	4.14	4.14	0.00
			VMS	146.6	146.8	0.12
4	220	3.8	Cost	84.1	84.2	0.07
			Disp.	6.8	6.7	0.19
			VMS	206.1	193.3	6.64
5	280	6.2	Cost	130.7	130.8	0.11
			Disp.	2.6	2.7	0.92
			VMS	107.2	105.1	2.00

Table 3.4: RBDO result comparison between the FEM model and surrogate model

Parameter	Model	
	FEM model	Surrogate model
Drain height (mm)	175.6	204.6
Plate thickness (mm)	5.4	5.5
von Mises stress (GPa)	121.0	120.0
Cost (£)	122.9	123.2
Vertical displacement (mm)	3.0	3.0
Reliability index	2.0	1.9
Probability of failure	0.04	0.06
Computational time (hours)	28:44:08	00:40:41

3.2 Multi-Fidelity Modelling Methods

The main idea of multi-fidelity modelling is to create a surrogate model that allows Low-Fidelity Models (LFM) to replace High-Fidelity Models (HFM) using proper mathematical corrections. These correction methods are multiplicative correction, additive correction, comprehensive correction and space mapping. The first three methods correct the LFM using the difference or ratio of the response surfaces between the HFM and the LFM. Space mapping discovers a transformation function of input variables that can be mapped from the high-fidelity space to the low-fidelity space. Conversely, Auto Regressive (AR) calculates the correlation between different fidelity models, and then it constructs a multi-fidelity model (23,59).

The construction of a multi-fidelity model requires data from both the HFM and the LFM. The data can be expressed as

$$X_{HF} = \begin{bmatrix} \mathrm{X}_{HF,1} \\ \mathrm{X}_{HF,2} \\ \vdots \\ \mathrm{X}_{HF,n_{HF}} \end{bmatrix} = \begin{bmatrix} x_{HF,11} & x_{HF,12} & \cdots & x_{HF,1m} \\ x_{HF,21} & x_{HF,22} & \cdots & x_{HF,2m} \\ \vdots & \vdots & \ddots & \vdots \\ x_{HF,n_{HF}1} & x_{HF,n_{HF}2} & \cdots & x_{HF,n_{HF}m} \end{bmatrix} \tag{3.20}$$

$$X_{LF} = \begin{bmatrix} \mathrm{X}_{LF,1} \\ \mathrm{X}_{LF,2} \\ \vdots \\ \mathrm{X}_{LF,n_{LF}} \end{bmatrix} = \begin{bmatrix} x_{LF,11} & x_{LF,12} & \cdots & x_{LF,1m} \\ x_{LF,21} & x_{HF,22} & \cdots & x_{LF,2m} \\ \vdots & \vdots & \ddots & \vdots \\ x_{LF,n_{LF}1} & x_{LF,n_{HF}2} & \cdots & x_{LF,n_{HF}m} \end{bmatrix} \tag{3.21}$$

where n_{HF} and n_{LF} are the number of design points from the HFM and the LFM, respectively. m is the number of design variables. The output vectors form the HFM and the LFM are written as

$$Y_{HF} = \begin{bmatrix} \mathrm{Y}_{HF,1} \\ \mathrm{Y}_{HF,2} \\ \vdots \\ \mathrm{Y}_{HF,n_{HF}} \end{bmatrix} = \begin{bmatrix} \mathrm{Y}_{HF}(\mathrm{X}_{HF,1}) \\ \mathrm{Y}_{HF}(\mathrm{X}_{HF,2}) \\ \vdots \\ \mathrm{Y}_{HF}(\mathrm{X}_{HF,n_{HF}}) \end{bmatrix} \tag{3.22}$$

$$Y_{LF} = \begin{bmatrix} \mathrm{Y}_{LF,1} \\ \mathrm{Y}_{LF,2} \\ \vdots \\ \mathrm{Y}_{LF,n_{LF}} \end{bmatrix} = \begin{bmatrix} \mathrm{Y}_{LF}(\mathrm{X}_{LF,1}) \\ \mathrm{Y}_{LF}(\mathrm{X}_{LF,2}) \\ \vdots \\ \mathrm{Y}_{LF}(\mathrm{X}_{LF,n_{LF}}) \end{bmatrix} \tag{3.23}$$

where Y_{HF} and Y_{LF} are the outputs from the HFM and the LFM, respectively.

In general, these multi-fidelity methods that have been developed so far share the same design space with different fidelity models.

3.2.1 Response Correction Methods

Response correction methods aim to create a surrogate model for the LFM to represent the response surface of the HFM. There are three methods depending on how each method corrects its LFM in the case where $n_{HF} = n_{LF}$ (47). Firstly, the estimated response of the HFM using the multiplicative correction to improve the response of the LFM can be written as

$$\hat{Y}_{HF}(X) = \beta(X) \cdot Y_{LF}(X) \tag{3.24}$$

where $\hat{Y}_{HF}$ is the estimated response of the HFM, $\beta(X)$ is a surrogate model of response ratios between the HFM and the LFM, X is a vector of independent design variables, $Y_{LF}(X)$ is the response of the LFM.

Secondly, the estimated response of the HFM using the additive correction to correct the response of the LFM can be expressed as

$$\hat{Y}_{HF}(X) = Y_{LF}(X) + \delta(X) \tag{3.25}$$

where $\delta(X)$ is a surrogate model of response differences between the HFM and the LFM.

Finally, the comprehensive methods use both multiplicative and additive corrections. A popular comprehensive method is

$$\hat{Y}_{HF}(X) = \beta(X) \cdot Y_{LF}(X) + \delta(X) \tag{3.26}$$

where β is the surrogate model of multiplicative correction, and δ is the surrogate model of additive correction.

Many methods fix the multiplicative correction β as a constant value and employ a surrogate model of additive correction (60). However, some comprehensive correction methods work with the β that is not constant either. Equation (3.27) displays a new comprehensive correction method that has been proposed using a weighting function based on the traditional correction methods.

$$\hat{Y}_{HF}(X) = w(X) \cdot \beta(X) \cdot Y_{LF}(X) + (1 - w(X)) \cdot (Y_{LF}(X) + \delta(X)) \tag{3.27}$$

where $w(X)$ is a weighting function.

3.2.2 Space Mapping

The space mapping method aims to cover different design spaces between the HFM and the LFM so that a small number of high-fidelity simulations are evaluated during the multi-fidelity modelling process (61,62). This process continues optimising the multi-fidelity model based on low-fidelity simulations until the stopping criteria of the optimisation is satisfied. For the multi-fidelity model to deal with different design spaces, a mapping function is necessary between the HFM and the LFM. Parameter estimation is crucial to establish the mapping function giving an appropriate relationship between two different sets of design variables. This method ensures that the low-fidelity design variables can be a subset of the high-fidelity ones. Similarly, the high-fidelity design variables can be an interpolation of the low-fidelity ones. Figure 3.14 illustrates how the space mapping constructs the multi-fidelity model. The primary idea is to obtain a suitable model using the proper mapping function that provides not only more computationally efficient than the HFM but also as least more accurate than the LFM. The space mapping consists of four steps to create the multi-fidelity model, as shown in Figure 3.15.

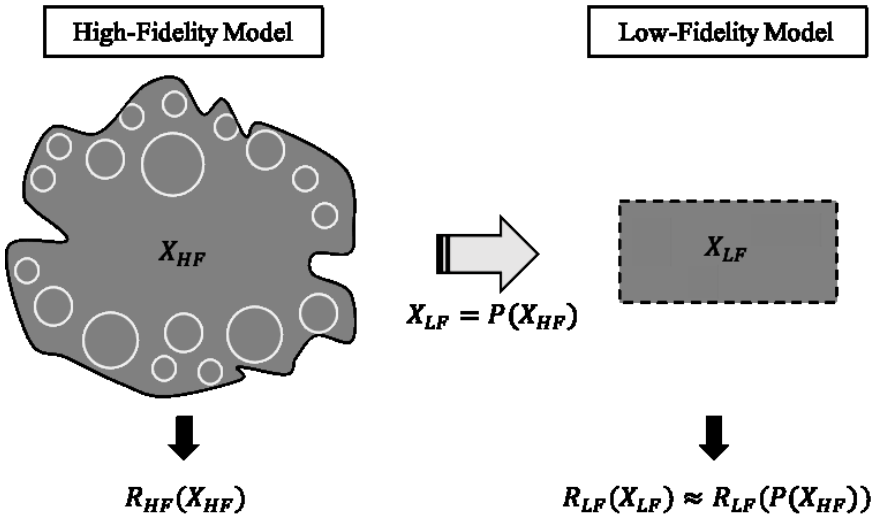

Figure 3.14: Space mapping method

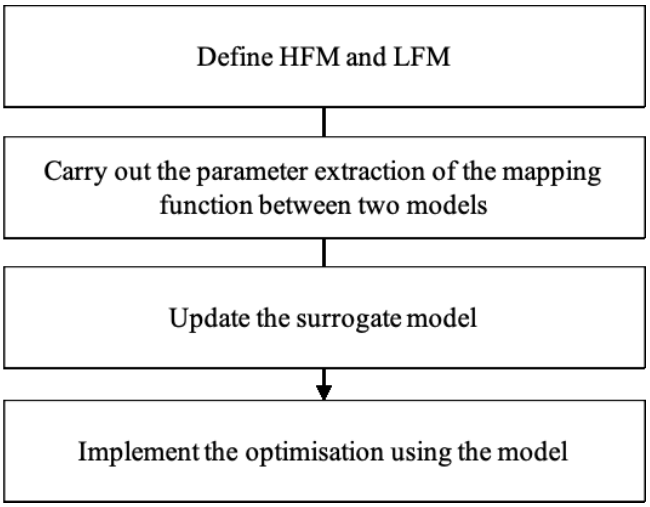

Figure 3.15: Procedure of space mapping method

The space mapping method aims to solve the optimisation problem that is generally given as

$$X^* \triangleq arg \min_X U\big(R(X)\big) \tag{3.28}$$

where $R \in \mathbb{R}^{m\times 1}$ is the vector of m responses of the model, X is the vector of n input variables, and U is an objective function. X^* is the optimal solution to be found.

As shown in Figure 3.14, the design variables of the HFM and the LFM are defined by X_{HF} and $X_{LF} \in \mathbb{R}^{n\times 1}$, respectively. The corresponding vectors of response are defined by R_{HF} and $R_{LF} \in \mathbb{R}^{m\times 1}$, respectively. A mapping function P between the HFM and the LFM input variables is expressed by

$$X_{LF} = P(X_{HF}) \tag{3.29}$$

Then, the response vectors in a region of interest can be written as

$$R_{LF}\big(P(X_{HF})\big) = R_{HF}(X_{HF}) \tag{3.30}$$

The mapping function allows us not to run a large number of high-fidelity simulations but to exploit only low-fidelity simulations during the optimisation process. The LFM having a smaller number of design variables than the HFM enables the multi-fidelity model to explore the whole design space with affordable computational cost. At the end of the optimisation process, they find the optimal solution X_{LF}^{*} in the low-fidelity design space, and it can be transformed by the optimal solution X_{HF}^{*} in the high-fidelity design space using the inverse mapping function as follows.

$$X_{HF}^{*} \triangleq P^{-1}(X_{LF}^{*}) \tag{3.31}$$

The parameter extraction to set up the mapping function is a sub-optimisation problem that is expressed by

$$X_{LF}^{(j)} \triangleq arg \min_{X_{LF}} \left\| R_{HF}\left(X_{HF}^{(j)}\right) - R_{LF}(X_{LF}) \right\| \tag{3.32}$$

where j is the number of iteration to find the parameters of the mapping function.

The error of the parameter extraction is defined by

$$\epsilon \triangleq \left\| R_{HF}\left(X_{HF}^{(j)}\right) - R_{LF}\left(X_{LF}^{(j)}\right) \right\| = \min_{X_{LF}} \left\| R_{HF}\left(X_{HF}^{(j)}\right) - R_{LF}(X_{LF}) \right\| \tag{3.33}$$

The parameters satisfying the equations (3.32) and (3.33) enable the HFM's design variables to be transformed to the LFM's design variables. Then, the optimisation problem can be carried out in the low-fidelity design space that takes more economical computational time to find the optimal solution. If a mapping function between two different design spaces is linear, the relationship between them can be presumed by

$$X_{LF} = P^{(j)}(X_{HF}) = A^{(j)}X_{HF} + B^{(j)} \tag{3.34}$$

where $A^{(j)} \in \mathbb{R}^{n\times m}$ and $B^{(j)} \in \mathbb{R}^{n\times 1}$.

3.2.3 Auto Regressive (AR)

The AR framework is an advanced GP regression model that constructs multi-fidelity models using different fidelity models (11). In contrast to the response correction methods, this framework can work in the case where $n_{HF} \neq n_{LF}$. The AR regression model utilises the correlation between the information datasets of the most accurate expensive model, the HFM, and the less accurate cheap model, the LFM. These two different information datasets are used in the AR framework, the set of high-fidelity data $(X_{HF},\ Y_{HF})$ where X_{HF} is $(n_{HF} \times m)$ matrix and Y_{HF} is a column vector of length n_{HF}, and the other

set of low-fidelity data $(X_{LF},\ Y_{LF})$ where X_{LF} is $(n_{LF} \times m)$ matrix and Y_{LF} is a column vector of length n_{LF}. In this framework, the high-fidelity design points X_{HF} need to be a subset of the low-fidelity design points X_{LF}, $(X_{HF} \subset X_{LF})$. A more detailed explanation of the mathematical formulations can be found in (63,64).

The AR regression model consists of a scaling parameter and GP regression models to approximate the HFM using the LFM. The model can be written as

$$f_{HF}(X) = \rho f_{LF}(X) + f_{\delta}(X) \tag{3.35}$$

where $f_{HF}(\cdot)$ and $f_{LF}(\cdot)$ represent the GP created using the data from the high-fidelity and low-fidelity datasets, respectively. ρ is a scaling parameter that quantifies the correlation between two different fidelity outputs. Another GP $f_{\delta}(X)$ represents the difference between $f_{HF}(X)$ and $\rho f_{LF}(X)$.

In GP regression modelling, the covariance matrix $cov\big(f(\mathrm{x}), f(\mathrm{x}')\big) = \sigma^2 k(\mathrm{x}, \mathrm{x}')$ is a simple form. In the AR regression framework, the covariance matrix is more complex because of the correlation between different fidelity models. This matrix can be represented as

$$\begin{aligned} cov(Y_{LF}, Y_{LF}) &= cov(f_{LF}(X_{LF}), f_{LF}(X_{LF})\ ) \\ &= \sigma_{LF}^2 k(\theta_{LF}, X_{LF}, X_{LF}) \end{aligned} \tag{3.36}$$

$$\begin{aligned} cov(Y_{HF}, Y_{LF}) &= cov(f_{HF}(X_{HF}), f_{LF}(X_{LF})\ ) \\ &= \rho\sigma_{LF}^2 k(\theta_{LF}, X_{LF}, X_{HF}) \end{aligned} \tag{3.37}$$

$$\begin{aligned} cov(Y_{HF}, Y_{HF}) &= cov(f_{HF}(X_{HF}), f_{HF}(X_{HF})\ ) \\ &= cov(\rho f_{LF}(X_{HF}) + f_{\delta}(X_{HF}), \rho f_{LF}(X_{HF}) + f_{\delta}(X_{HF})\ ) \\ &= \rho^2 cov\big(f_{LF}(X_{HF}), f_{LF}(X_{HF})\big) + cov\big(f_{\delta}(X_{HF}), f_{\delta}(X_{HF})\big) \\ &= \rho^2\sigma_{LF}^2 k(\theta_{LF}, X_{HF}, X_{HF}) + \sigma_{\delta}^2\ k(\theta_{\delta}, X_{HF}, X_{HF}) \end{aligned} \tag{3.38}$$

Thus, the complete covariance matrix having a dimension of $(n_{LF} + n_{HF}) \times (n_{LF} + n_{HF})$ is generated by

$$K = \begin{bmatrix} \sigma_{LF}^2 k(\theta_{LF}, X_{LF}, X_{LF}) & \rho\sigma_{LF}^2 k(\theta_{LF}, X_{LF}, X_{HF}) \\ \rho\sigma_{LF}^2 k(\theta_{LF}, X_{HF}, X_{LF}) & \rho^2\sigma_{LF}^2 k(\theta_{LF}, X_{HF}, X_{HF}) + \sigma_{\delta}^2\ k(\theta_{\delta}, X_{HF}, X_{HF}) \end{bmatrix} \tag{3.39}$$

where σ_{LF}^2 and σ_{δ}^2 are the process variances. θ_{LF} and θ_{δ} are the hyperparameters corresponding to the covariance functions for the LFM and the difference data, respectively. These parameters and the scaling parameter ρ can be obtained using the maximum log-likelihood estimation.

Predictions μ_{*HF} and variance σ_{*HF}^2 concerning test input data points X_* can be taken from the joint posterior distribution using the mean and covariance matrix. This multi-fidelity posterior distribution provides the predictive mean and variance at the high-fidelity level represented by

$$p(f_{HF}|\, Y_{HF}, X_{HF}, f_{*LF}) = N\left(f_{HF}|\, \mu_{*HF}(X_*), \sigma^2_{*HF}(X_*)\right) \tag{3.40}$$

$$\mu_{*HF}(X_*) = \rho\mu_{*LF}(X_*) + \mu_\delta + K(X_*, X_{HF})K^{-1}(X, X)[Y_{HF} - \rho\mu_{*LF}(X_{HF}) - \mu_\delta] \tag{3.41}$$

$$\sigma^2_{*HF}(X_*) = \rho^2\sigma^2_{*LF}(X_*) + K(X_*, X_*) - K(X_*, X_{HF})K^{-1}\, K(X_*, X_{HF})^T \tag{3.42}$$

Where $K(X_*, X_{HF}) = \begin{bmatrix} \rho'(\sigma'_{LF})^2 k(\theta'_{LF}, X_{LF}, X_*) \\ (\rho')^2(\sigma'_{LF})^2 k(\theta'_{LF}, X_{HF}, X_*) + (\sigma'_\delta)^2 k(\theta'_\delta, X_{HF}, X_*) \end{bmatrix}$ is a column vector of length $(n_{LF} + n_{HF})$. The superscript $(')$ represents hyperparameters estimated.

4 Multi-Fidelity Reliability-Based Design Optimisation for Composite Structures

Reliability-Based Design Optimisation (RBDO) provides many advantages because it enables engineers to consider uncertainties in different design variables used to design and manufacture a composite structure. The conventional design approach for composite structure design may cause the final design to be conservative that involves using safety factors to hinder structural failures. In contrast to the design approach, RBDO allows engineers to understand how the design uncertainties affect their structural reliability or the probability of failure. At the same time, they ensure not only the most critical design area but the improvement in the reliability of the structures. RBDO includes the reliability assessment having statistical methods or non-statistical methods. Monte Carlo Simulation (MCS) is a statistical method that evaluates the limit state function directly during the optimisation process. The First-Order Reliability Method (FORM) and the Second-Order Reliability Method (SORM) calculate the reliability using first-order and second-order Taylor series expansions to approximate the limit state function. MCS generally offers the most accurate value among the three methods since it uses the limit state function itself without approximation. SORM using higher order approximation is more accurate than FORM when the limit state function is particularly highly non-linear. More details of these reliability methods are introduced in many books and works of literature (8,9).

There have been many research works for the development and application of RBDO in structural optimisation, such as isotropic and composite structures. The reliability analysis, particularly the essential part of RBDO, has been actively considered in various structural design problems (43,65). One remarkable example is Morse et al. (43), where the reliability analysis of a 2D rectangular isotropic plate with a centre hole subjected to uniaxial tension was conducted. The reliability indexes, which represent the probability of success, were compared by different reliability methods, such as MCS, FORM and SORM. The result comparison showed that the two approximation methods obtained similar results to MCS. The optimisation process combined with the reliability analysis, also known as RBDO, has been widely used in the design area of composite structures (20,66). One notable example is Lopez

et al. (14). They developed an advanced RBDO process for a more complex composite structure, a multi-stiffened stringer composite panel. This optimisation process found the stacking sequence of the composite panel to maximise the ultimate load in the post-buckling regime. The hybrid mean value algorithm using the first-order approximation to find the Most Probable failure Point (MPP) was used. This algorithm proposed a next upcoming point during the reliability analysis depending on the type of the limit-state function between convex and concave. Based on the initial stacking sequence provided by DO, the reliability analysis evaluated the reliability of the composite panel associated with uncertainties in material properties.

In general, RBDO is computationally expensive due to considering design uncertainties at every design point to evaluate if each design violates the limit state function. In general, the reliability analysis using MCS requires a significant number of high-fidelity Finite Element Method (FEM) simulations of more than hundreds or even thousands until the results are converged. Even though a single high-fidelity FEM simulation requires a few seconds to run, the entire optimisation may take several days or weeks to run the total number of FEM simulations. Surrogate modelling, also called metamodeling, have been drawn attention to address this substantial computational cost caused by assessing the design uncertainties in probabilistic design approaches. Wang et al. (10) introduced surrogate modelling approaches as essential tools to conduct the optimisation. In particular, they showed that surrogate models have a significant role in Multi-Objective Optimisation (MOO). These models improve the computational performance as well as provide an understanding of the effects of design variables. There are many types of surrogate models that have been exploited concerning RBDO. Hassanien et al. (65) applied a surrogate model that is created by the Response Surface Method (RSM) to conduct the reliability analysis of dented pipes. Scarth et al. (67) created a surrogate model using support vector machines with Gaussian Process (GP) to drive RBDO of a composite aircraft structure. Bacarreza et al. (67) used Radial Basis Function (RBF) to create a surrogate model of a composite stiffened panel. Sampling techniques contribute significantly to the performance of the surrogate model since an increase in computational cost might be caused by an inappropriate sampling process. The sequential sampling method was developed to offer better sampling performance than other techniques (56,68).

Although the use of surrogate models reduces computation time, composite structures may require several hours to simulate even a single FEM model relying on the characteristic of a problem. The concept of multi-fidelity models has been introduced in structural optimisation to address this computational challenge. Multi-fidelity models, which are created by the use of High-Fidelity Model (HFM) and Low-Fidelity Model (LFM), provide results of similar accuracy to surrogate models only based on the HFM while providing a noticeable reduction in computational cost. Many research works have been carried out to apply the multi-fidelity models to structural optimisation. The vast majority of this application has been confined to the area of DO, which does not consider the uncertainty of design variables. Vitali et al. (47) introduced the concept of multi-fidelity models through crack propagation

in a composite structure. The idea is to use the ratio and the difference between the LFM and the HFM. Alexandrov et al. (69) combined the HFM and the LFM using the multiplicative correction function. This multiplicative correction function is constructed by Taylor-series approximation, and it makes the LFM follow the response of the HFM. In Goldfeld et al. (70), the optimisation of buckling analysis for a laminated shell was conducted using the multi-fidelity models using the LFM. Response correction surfaces which are a ratio between the HFM and the LFM, are built by various polynomial functions to create the multi-fidelity models. The LFM was changed to a high-order polynomial response surface with improved accuracy and computation time savings through this approximation. Due to its many advantages, the multi-fidelity models have replaced the extensive use of FEM simulations in different DO problems. However, its application in the probabilistic optimisation of composite design has received little attention. Before the work presented in this thesis, no work has been performed by the research community on the topic of RBDO of composite structures using the multi-fidelity models.

The main objectives of the work introduced in this chapter were to develop a multi-fidelity formulation for reliability analysis and RBDO of composite structures for the first time. The developed multi-fidelity formulation considers the effect of design uncertainties using different reliability methods. In particular, this work showed that the multi-fidelity formulation can be applied to approximate the limit state function using FORM and SORM while providing nearly identical results to MCS. The multi-fidelity formulation incorporating the RBDO process constructs two types of multi-fidelity models depending on how to use FEM models, such as direct and indirect multi-fidelity models. It provides not only similar accuracy to the conventional high-fidelity surrogate modelling but also offers considerable computation time savings. For the first time, the proposed multi-fidelity framework was demonstrated by the reliability analysis and RBDO of a mono-stringer stiffened composite panel to see how much computational gains are obtained.

This chapter begins by introducing the mathematical formulation of the multi-fidelity method used in this work. It will then describe how the multi-fidelity formulation implements both structural reliability analysis and RBDO framework. At the end of this chapter, two engineering examples of rising complexity will demonstrate the multi-fidelity modelling framework to show the potential for large scale problems. The accuracy and computation time savings were evaluated and compared with the results of the conventional surrogate models using only HFM. The work shown in this chapter is based on the research work presented by Yoo et al. in (24).

4.1 Multi-Fidelity Modelling Method for the Same Design Space between Fidelity Models

As described in the previous chapter, the response correction methods require the same training data points between the HFM and the LFM to construct multi-fidelity models. The primary feature of these methods shares the same dimension of design spaces. This enables an accurate response correction function to be created using the information from the same design points of two different fidelity models. The response correction methods allow the inaccurate LFM to represent the response surface of the accurate HFM using the same design points collected by a proper sampling technique. In this work, the multiplicative and additive correction functions were used (47). Two types of multi-fidelity models, depending on how the LFM works with the multi-fidelity method, are constructed using the response correction methods, such as direct and indirect multi-fidelity models.

In this multi-fidelity modelling method, both the HFM and the LFM require the same number of design points ($n_{HF} = n_{LF}$) and share the same dimension of design spaces with each other. This enables the response correction methods to build a proper response correction surface using each information coming from the HFM and the LFM. Two matrixes of the ratio and the difference can be created depending on the number of responses using the information. These two matrixes can build each surrogate model for the ratio and the difference. These surrogate models offer the appropriate correction corresponding to different design points so that the LFM improves their accuracy to represent the HFM. These models can be created as Artificial Neural Networks (ANN) as described in sections 3.1.2.1.

The direct type of multi-fidelity model requires the surrogate model of a response correction surface chosen. This type involves directly calling the response of the LFM during the multi-fidelity modelling process. Two different multi-fidelity models can be created using these two surrogate models as follows.

$$\hat{Y}_{MF1}(X) = \beta(X) \cdot Y_{LF}(X) \tag{4.1}$$

$$\hat{Y}_{MF2}(X) = Y_{LF}(X) + \delta(X) \tag{4.2}$$

where X is n design points for training with input design parameters. MF1 and MF2 denote the direct multi-fidelity models using different response correction functions, respectively. β and δ are the surrogate models of ratio and difference between the HFM and the LFM. Y_{LF} is the response directly calculated using the low-fidelity FEM model.

The indirect type of multi-fidelity model uses two different surrogate models of the LFM and a response correction surface. The indirect type involves approximating the LFM using ANN. This enables $Y_{LF}(X)$ to be replaced by a surrogate model of the LFM to reduce computation time if even the LFM is computationally expensive. Another two different multi-fidelity models are expressed below.

$$\hat{Y}_{MF3}(X) = \beta(X) \cdot \hat{Y}_{LF}(X) \tag{4.3}$$

$$\hat{Y}_{MF4}(X) = \hat{Y}_{LF}(X) + \delta(X) \tag{4.4}$$

where $\hat{Y}_{LF}$ is the surrogate model of the LFM. MF3 and MF4 denote the indirect multi-fidelity models. β and δ are the surrogate models of the ratio and difference between the HFM and the LFM, respectively.

4.2 Multi-Fidelity Modelling-Based Reliability Analysis

A reliability analysis aims to evaluate a limit state function as a constraint and calculate the reliability of a structure. The probability of failure refers to how the structure has reliability under a specific restricted condition. In general, this analysis ensures that powerful computation resources are provided because it needs to calculate the influence caused by uncertainties in design variables. The multi-fidelity modelling-based reliability analysis developed in this work defines the limit state function. This can be represented as

$$g_{MF}(Z) = R_{MF}(X) - S_{MF}(X) \tag{4.5}$$

$$P_{f,MF} = P[g_{MF}(Z) < 0] \tag{4.6}$$

where $g_{MF}(X)$ is the limit-state function using the multi-fidelity models, $P_{f,MF}$ is the probability of failure using the multi-fidelity models, X is a vector of all design variables under consideration, R_{MF} and S_{MF} are the resistance and the loading of structure, respectively, which come from the multi-fidelity models.

If the value of $g_{MF}(X)$ is less than zero, the structure is not in the safe region. If the value of $g_{MF}(X)$ equals zero or is more than zero, the structure is in the failure surface or the safe area, respectively. In this work, MCS, FORM and SORM calculate the probability of failure using the multi-fidelity models blending two different fidelity models.

Firstly, MCS using the multi-fidelity models predicts the probability of failure after $N_{total,MF}$ multi-fidelity simulations are carried out. This can be expressed by

$$P_{f,MCS,MF} = \frac{N_{f,MF}}{N_{total,MF}} \tag{4.7}$$

where $N_{f,MF}$ and $N_{total,MF}$ are the number of failure and the total multi-fidelity simulations conducted. $P_{f,MCS,MF}$ is the probability of failure using MCS predicted by the multi-fidelity models.

When MCS estimates the statistical characteristics for the reliability analysis, Sobol sampling was used to collect the design points that consider the influence caused by the design uncertainties. As described in sections 3.1.1.3, Sobol sampling provides more uniformly distributed design points than the simple random sampling since this sampling technique aims to reduce the variance of statistical predictions for MCS. In particular, Sobol sampling offers more robust statistical results than even the Latin Hypercube sampling for the reliability analysis (49).

In contrast to MCS, FORM and SORM approximate the limit state function using the first- and second-order Taylor expansion series to compute the probability of failure, respectively. The calculation of derivatives of the limit state function is essential to decide the accuracy of the solution and the computational costs to predict a reliability index. There are two typical methods to calculate the derivatives of the limit state function, Finite Difference Method (FDM) and Implicit Differentiation Method (IDM) (43). In this work, the FDM is applied to calculate the probability of failure.

The principle of the FDM is that derivatives in the partial differential equation are approximated by the linear combination of response values defined by a finite grid (71). The FDM is a relatively challenging method because the sensitivities may be hugely susceptible to the step size chosen. This implies that rounding errors or truncation errors become considerable, relying on the step size. However, the FDM provides a distinct advantage of calculating derivatives for complex problems, for which analytical solutions do not exist.

There are three standard methods to evaluate the first-order derivatives using the FDM: the forward difference, the backward difference, and the central difference schemes. The first-order forward finite difference scheme is expressed by

$$\left(\frac{\partial S_{MF}(X)}{\partial X}\right)_i = \frac{S_{MF}(X_i + \Delta X_i, X_{-i}) - S_{MF}(X)}{\Delta X_i} \tag{4.8}$$

The first-order backward finite difference scheme is expressed by

$$\left(\frac{\partial S_{MF}(X)}{\partial X}\right)_i = \frac{S_{MF}(X) - S_{MF}(X_i - \Delta X_i, X_{-i})}{\Delta X_i} \tag{4.9}$$

The first-order central finite difference scheme is expressed by

$$\left(\frac{\partial S_{MF}(X)}{\partial X}\right)_i = \frac{S_{MF}(X_i + \Delta X_i, X_{-i}) - S_{MF}(X_i - \Delta X_i, X_{-i})}{2\Delta X_i} \tag{4.10}$$

The second-order finite difference scheme determines the derivatives using the central scheme as follows.

$$\left(\frac{\partial^2 S_{MF}(X)}{\partial X^2}\right)_i = \frac{S_{MF}(X_i + \Delta X_i, X_{-i}) - 2S_{MF}(X) + S_{MF}(X_i - \Delta X_i, X_{-i})}{(\Delta X_i)^2} \tag{4.11}$$

Where ΔX_i is the step size and X_{-i} is the vector of design variable eliminating the variable X_i. The magnitude of the step size ΔX_i affects the accuracy of the derivatives of $S_{MF}(X)$. A small step size will cause substantial rounding error, whereas a large step size will cause substantial truncation error. It was found that the proper value of step size is in the range of between 0.01 % and 0.1 % using a sensitivity analysis. The step size in this range offered accurate derivatives of $S_{MF}(X)$; hence, a value from the range was selected as the step size in this work.

FORM calculates the reliability indexes presenting the shortest distance from the origin point to the failure surface in the standard normal distribution. This method transforms the mean value point of the original space (X-space) to the origin of normal space (U-space). This transformation enables the Taylor expansion point to be moved from the mean value point to the Most Probable failure Point (MPP). The first-order Taylor series of expansion of $g_{MF}(U)$ at MPP U^* using the multi-fidelity models is defined as

$$\tilde{g}_{MF}(U) = g_{MF}(U^*) + \sum_{i=1}^{n} \frac{\partial g_{MF}(U^*)}{\partial U_i}(U_i - U_i^*) \tag{4.12}$$

The shortest distance, also known as the reliability index, from the origin to the failure surface using the multi-fidelity models is written as

$$\beta_{MF} = \frac{g_{MF}(U^*) - \sum_{i=1}^{n} \frac{\partial g_{MF}(U^*)}{\partial X_i}\sigma_{X_i}U_i^*}{\sqrt{\sum_{i=1}^{n}\left(\frac{\partial g_{MF}(U^*)}{\partial X_i}\sigma_{X_i}\right)^2}} \tag{4.13}$$

This process is iterated until the estimate of reliability index β_{MF} using the multi-fidelity models converges in specific tolerance criteria. When the limit-state function is the normal distribution function, the probability of failure using the multi-fidelity models is defined as

$$P_{f,FORM,MF} = 1 - \phi(\beta_{MF}) = \phi(-\beta_{MF}) \tag{4.14}$$

where $P_{f,FORM,MF}$ is the probability of failure using FORM predicted by the multi-fidelity models, and $\phi(\cdot)$ is the standard normal cumulative distribution function.

Compared to FORM, SORM requires the second-order derivatives to approximate the failure surface to provide more accurate results under the highly non-linear failure surface. The second-order approximation of limit-state function $g_{MF}(U) = 0$ is derived by the second-order Taylor series expansion at the MPP using the multi-fidelity models.

$$\tilde{g}_{MF}(U) = g_{MF}(U^*) + \nabla g_{MF}(U^*)^T\,(U - U^*) + \frac{1}{2}(U - U^*)^T \nabla^2 g_{MF}(U^*)(U - U^*) \tag{4.15}$$

where $\nabla^2 g_{MF}(U^*)$ is the Hessian matrix, which is the symmetric matrix of the second derivative of the limit-state function. The Hessian matrix creates additional computational cost during the reliability analysis; however, it ensures that SORM provides a more accurate reliability index in a non-linear limit-state function.

$$P_{f,SORM,MF} = \phi(-\beta_{MF}) \prod_{j=1}^{n-1} \left(1 + k_j \beta_{MF}\right)^{-1/2} \tag{4.16}$$

where $P_{f,SORM,MF}$ is the probability of failure using SORM predicted by the multi-fidelity models and the k_i indicates the curvature of the response surface at the MPP.

4.3 Multi-Fidelity Reliability-Based Design Optimisation Framework

The conventional form of RBDO is introduced in equation (2.4). This RBDO process requires computationally intensive models or a surrogate model using many high-fidelity design points. A novel multi-fidelity modelling-based RBDO framework to address this computational challenge caused by the traditional optimisation process is developed in this work, as illustrated in Figure 4.1. This framework can be divided into two stages: the multi-fidelity modelling process and the multi-fidelity RBDO process.

Before the RBDO process begins, the multi-fidelity modelling process should be conducted to construct multi-fidelity models having adequate quality. The modelling process defines the HFM and the LFM based on the discretisation level of the FEM model, which is commonly used in structural optimisation. The type of fidelity can be determined relying on the characteristic of optimisation problems. Then, the sampling technique, which is the Optimal Latin Hypercube Sampling (OLHS) method in this work, collects appropriate design points to set up the design matrix having all input design parameters in the entire design space. The collected design points are employed to set up the input and output datasets of the two different fidelity models using a FEM solver. ANN based on RBF using these datasets creates three surrogate models of the LFM, the ratio and the difference between the two fidelity models, respectively. The three surrogate models should be evaluated using a proper error analysis, such as root mean square error analysis, to show a specified level of accuracy in this framework. After the models are validated, the multi-fidelity models are constructed using the combination of these three surrogate models and one low-fidelity FEM model depending on the direct or the indirect multi-fidelity models. The direct multi-fidelity model requires the response of the composite structures directly from the low-

fidelity FEM models during the multi-fidelity modelling process. Conversely, the indirect type calls for the response from the surrogate model using the low-fidelity training datasets. Both models exploit the surrogate models of response correction surfaces so that the LFM represents the nature of the high-fidelity response.

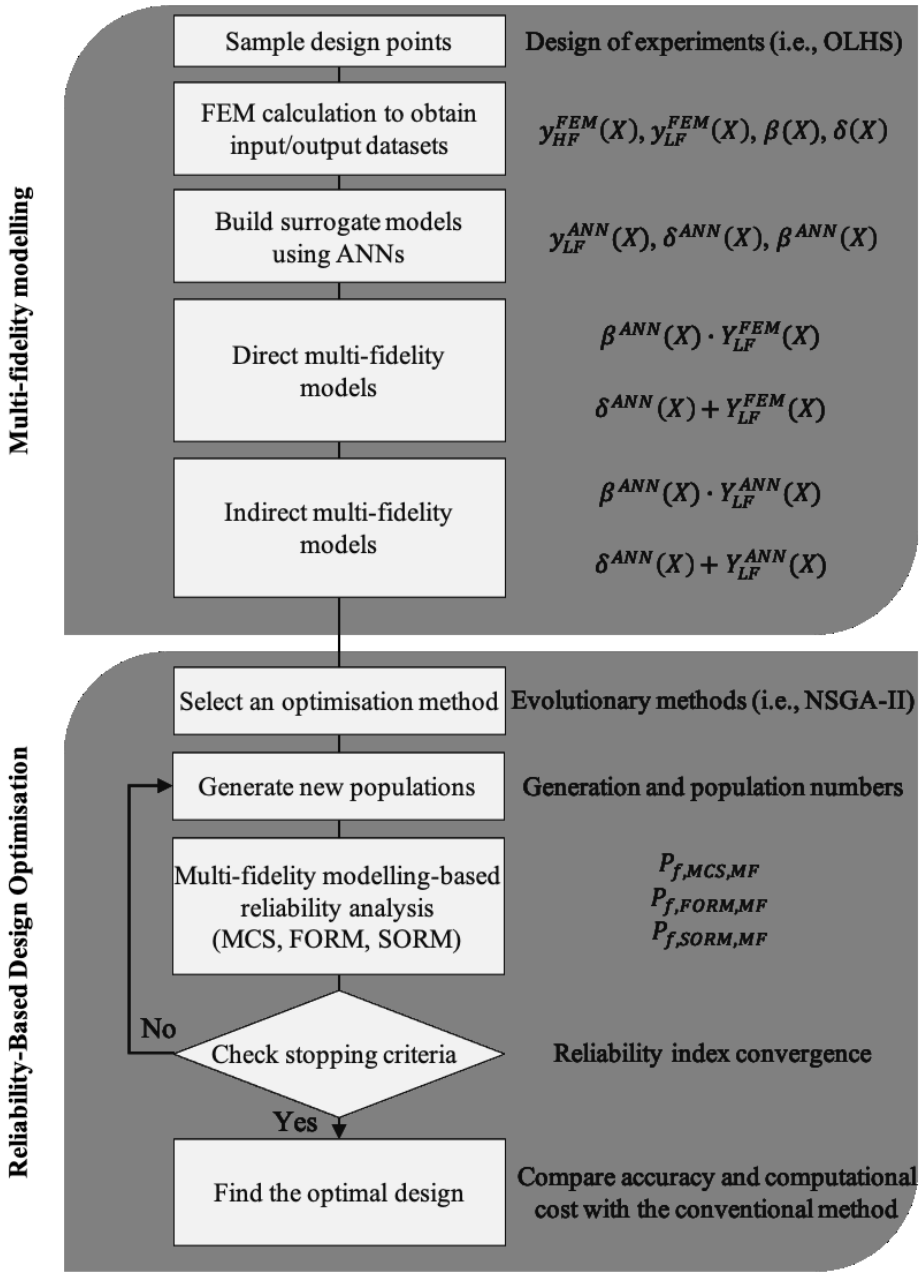

Figure 4.1: Multi-fidelity modelling-based reliability-based design optimisation framework

After this modelling process, the RBDO process begins to find the optimal design while exploring the whole design space using the constructed multi-fidelity models. There are many optimisation methods to conduct the RBDO process, and a proper optimisation method can be determined by engineering according to the problem characteristics. In particular, evolutionary methods, described in sections 2.1.3, work well with the probabilistic design optimisation of composite structures because these methods are

suitable to catch the global reliable solution in the non-linear solution space (34). When a proper optimisation method is chosen, three reliability methods, such as MCS, FORM and SORM, predict the probability of failure regarding each design point offered by the optimisation method. When the specified stopping criteria are satisfied, the optimal solutions, which are found using the multi-fidelity models, are evaluated by accuracy and computation time savings compared with the conventional RBDO process using high-fidelity modelling based surrogate models.

4.4 Numerical Examples

This section demonstrates the developed multi-fidelity models using two numerical examples concerning the design of composite structures. A short outline of each numerical example is described as follows.

- Numerical example 1: Multi-fidelity modelling-based reliability analysis. This numerical example is based on work shown in Yoo et al. (24). This example aims to demonstrate how multi-fidelity modelling approaches can be used to carry out different reliability methods, such as MCS, FORM and SORM, while increasing the efficiency of conventional high-fidelity reliability analysis for a composite structure.
- Numerical example 2: Multi-fidelity reliability-based design optimisation. This numerical example is based on work shown in Yoo et al. (24). This example aims to show the potential if multi-fidelity modelling approaches are utilised to the RBDO of composite structures for the first time. The efficiency caused by the use of multi-fidelity models is introduced as well.

4.4.1 Model Description

The composite structure considered in this work is a mono-stiffened stringer composite panel, as shown in Figure 4.2. The geometry of this composite panel is parameterised by $X1, X2, X3$ and $X4$ that represent stringer foot length, stringer height, the horizontal distance between stringer top and foot, and stringer top length, respectively. The material properties and dimension of the panel are denoted in Table 4.1. The composite panel consists of the skin and the stringer. It is clamped at both the right-hand and left-hand ends, but the left-hand end is free to move in the loading direction (z-direction in Figure 4.2). There are no constraints on two either side of the skin. The composite panel was analysed in the linear-buckling regime to obtain the maximum first buckling load. In the example of the reliability analysis, the linear buckling was considered when the applied load has eccentricity regarding the centre of mass of the stringer (y-direction in the figure). In the example of RBDO, the load was applied to the centre of mass without eccentricity. In these two examples, a HFM and an LFM should be defined first

to create the multi-fidelity models. The level of discretisation of FEM models was considered as a type of fidelity in this work. The FEM models are built and calculated using Abaqus/CAE. The mesh convergence study was conducted to select both the HFM and the LFM with different accuracy and computational costs. As shown in Figure 4.3, the mesh size was determined that the HFM and the LFM are 4.0 mm and 30.0 mm, respectively. The accuracy difference between the two models was 10 %, and the computation time of the LFM was 80 % more efficient than the HFM.

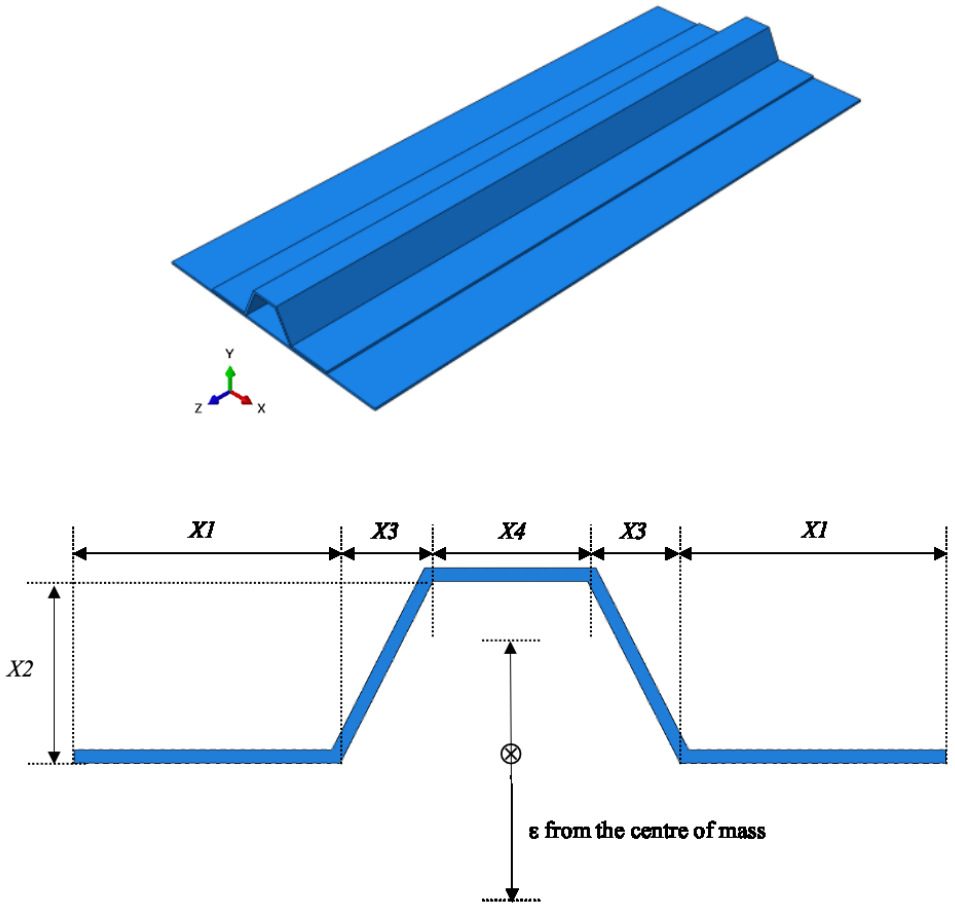

Figure 4.2: Mono-stringer stiffened composite structure having four geometry parameters

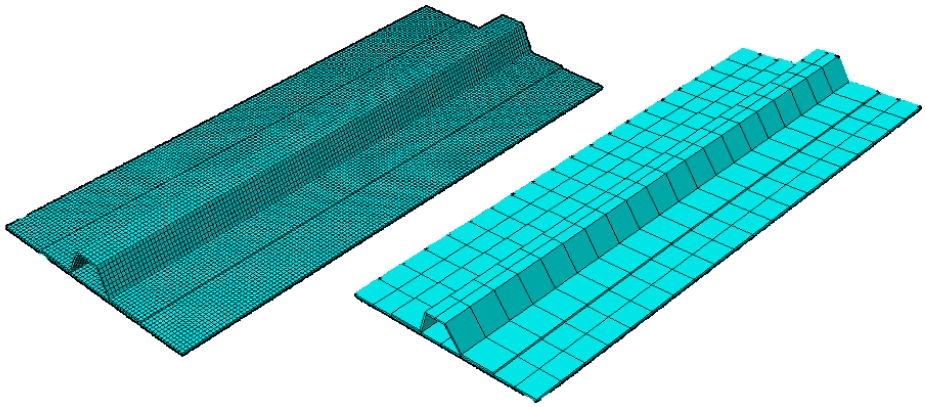

Figure 4.3: The HFM with 4.0 mm mesh size (left) and the LFM with 30.0 mm mesh size (right)

Table 4.1: Material properties and dimensions of the composite structure

Parameter	Value	
Longitudinal modulus of elasticity (GPa)	E_{11}	139.0
Transversal modulus of elasticity (GPa)	$E_{22} = E_{33}$	8.1
Poisson's ratio	ν	0.33
Out-of-plane shear modulus (GPa)	$G_{12} = G_{13}$	3.1
In-plane shear modulus (GPa)	G_{23}	4.8
Skin and stringer thickness (mm)	t	2.208
Skin and stringer layup $(degree)$		[45/-45/0/0/90/0]$_{sym}$
Panel length (mm)	L	600.0
Panel width (mm)	W	250.0

4.4.2 Multi-Fidelity Modelling-Based Reliability Analysis

The multi-fidelity reliability analyses using MCS, FORM and SORM were performed on the mono-stringer stiffened composite panel. The composite panel was loaded by a compressive axial load having eccentricity. Five random variables, four parameters defining the geometry and one load eccentricity, were considered. The limit-state function, which is made up of five random variables and one constraint, can be written as

$$g_{MF}(X) = P_{cr,c} - P_{cr,e,MF}(X1, X2, X3, X4, \varepsilon) \tag{4.17}$$

where $P_{cr,c}$ is the minimum buckling load as a constraint, $P_{cr,e,MF}$ is the first buckling load from the multi-fidelity model, ε is the eccentricity from the centre of mass.

The structure fails when $g_{MF}(X) < 0$. Each random variable has a probability distribution having mean and standard deviation, as seen in Table 4.2.

Table 4.2: Probability distribution of random design variables

Parameter	Probability distribution	Mean	Standard deviation
Stringer foot ($X1$)	Normal	43 mm	0.215
Stringer height ($X2$)	Normal	30 mm	0.15
Distance between stringer top and foot ($X3$)	Normal	15 mm	0.075
Stringer top ($X4$)	Normal	25 mm	0.125
Eccentricity (ε)	Normal	0 mm	9.09

4.4.2.1 Multi-Fidelity Modelling

In this example, ANN was used to create three surrogate models of the LFM, and two correction response surfaces of the ratio $\beta(X)$ and the difference $\delta(X)$ between the two fidelity models. The design points to create the surrogate models using ANN were obtained using Optimal Latin Hypercube Sampling (OLHS). The sampling range was determined by the value of each random variable's cumulative distribution function from 0.5 % to 99.5 %. The reason is that the sampling points are highly concentrated in the high probability region of each random variable and less concentrated in the low probability region. Once OLHS collects the design points, the HFM and the LFM using the FEM solver calculate the corresponding output values to each design point. Then the training datasets to create the three different surrogate models are obtained. The training dataset having 11 points was sampled using OLHS because it is the minimum number of sampling points for ANN to create the surrogate models having four design variables. In order to evaluate the quality of the surrogate models, the test dataset having thirty points were also sampled from each variable's cumulative distribution function from the same sampling range. ANN created the three surrogate models: the LFM, the ratio, and the difference between the two fidelity models. These models were validated by the separation method using the test dataset. The multi-fidelity models were constructed using these surrogate models and the low-fidelity FE model, as shown in Table 4.3.

The direct multi-fidelity models, MF1 and MF2 in Table 4.3, spend expensive computation time to conduct the reliability analysis because they call the first buckling load from the low-fidelity FEM models. It should be noted that the computation time of the low-fidelity FEM models is not cheap when it comes to thousands of FEM simulations for the reliability analysis. To provide more computation time savings, the surrogate models of MF1 and MF2 were also generated using the training dataset having 40 points. The test dataset has 20 points from the same range of cumulative distribution function. The indirect multi-fidelity models, MF3 and MF4, were created without calling the low-fidelity FEM models.

Table 4.3: Multi-fidelity models

Model	Output approximation
MF1	$Y_{MF1}(X) = \beta^{ANN}(X) \cdot Y_{LF}^{FEM}(X)$
MF2	$Y_{MF2}(X) = \delta^{ANN}(X) + Y_{LF}^{FEM}(X)$
MF3	$Y_{MF3}(X) = \beta^{ANN}(X) \cdot Y_{LF}^{ANN}(X)$
MF4	$Y_{MF4}(X) = \delta^{ANN}(X) + Y_{LF}^{ANN}(X)$

4.4.2.2 Results and Discussion

In this section, the multi-fidelity models were used to conduct the reliability analysis of the composite panel to the linear buckling under eccentric load. The reliability analysis was carried out using MCS, FORM and SORM. A minimum buckling load constraint of 20 kN was applied, and it is drawn in each figure using a dashed red line. If the buckling load of each simulation is less than this constraint, the composite panel is supposed to fail. Surrogate models using a different number of HFM were also generated to see how accurate the multi-fidelity models are and find the equivalent number of HFM that show a similar accuracy level to the multi-fidelity models.

The accuracy of multi-fidelity models is evaluated by comparing mean and standard deviation at the mean value point. As shown from Table 4.4 to Table 4.6, the reliability analysis results using the multi-fidelity models are very close to the result of a HF100. The HF100, which is a surrogate model using 100 of the HFM, is presumed by the most accurate value. In addition, a HF11 is also a surrogate model that uses the minimum number of HFM for ANN to create the surrogate model. As the number of HFM to generate the surrogate model decreases, the surrogate models do not produce accurate solutions compared to the HF100. These mean and standard deviation are calculated by the outcomes of design points of MCS using Sobol sampling, whereas FORM and SORM calculate these two values using output and gradient at the mean value point. Table 4.4 and Figure 4.4 show that the mean and standard deviation of the HF100 are 27.88 kN and 7.13, respectively. These values are used as the most accurate value to evaluate the accuracy of the created multi-fidelity models. The difference of mean values between the HF100 and the HF11 is 6.1 %, while the differences to the direct multi-fidelity models, MF1 and MF2, are smaller at 2.5 %. However, the indirect multi-fidelity models, MF3 and MF4, show similar differences to the HF11, which are 5.5 % and 6.0 %, respectively. The standard deviation of the HF100 using MCS is 7.13. The standard deviation of MF1 and MF2 at the mean value point are 6.72 and 6.05, respectively, whereas the MF3 and MF4 show the values of 6.40 and 6.51, respectively. Figure 4.5 and Figure 4.6 show that the MF1 and MF2 show similar levels of accuracy to the HF100, although the standard deviation of the MF2 is smaller. Table 4.5 and

Table 4.6 clearly show that the mean and standard deviation are identical between FORM and SORM since they use the same output and gradient at the mean value point. The means of FORM and SORM

at the mean value point are slightly smaller than the mean of MCS, but the standard deviation is nearly the same with MCS. Interestingly, the difference error of the mean of the HF11 using FORM and SORM is over 11 % compared to the mean of the HF100. When the number of HFM used to generate the surrogate model is more than 40, the differences concerning the HF100 are less than 1 %. The MF1 and MF2 provided better accuracy than the MF3 and MF4. In particular, the standard deviation of the MF1 was more accurate than the HF50. It can be seen from Table 4.4 to Table 4.6 that the reliability indexes from SORM are closer to the MCS results than the FORM results. It suggests that SORM can provide a more accurate solution in the failure domain than FORM because SORM takes into account the curvature of the limit-state function using second-order derivatives. It is found that the reliability index of the MF1 is much more accurate to the HF100 compared to even the HF50. Although the MF2 provided the accurate mean, its reliability index is not correct because the standard deviation is smaller than other multi-fidelity models. The MF3 and MF4 show similar levels of reliability indexes between the HF11 and HF20.

In order to evaluate computation time savings, the computation time of each model was normalised by the computation time of the HF100 using MCS. The average FEM simulation time for the HFM and the LFM was 47 seconds and 10 seconds, respectively. The average computation time for one surrogate model was 0.0057 seconds, and this computation time was calculated over 1,000,000 runs. The computation time of each reliability analysis using different models was calculated by multiplying the simulation number and the average computation time. The computation time savings are compared in Figure 4.7. The MF1 and MF2 were constructed by 11 of the HFM and 51 of the LFM, while the MF3 and the MF4 were built by 11 of HFM and 11of LFM. It is interesting to note that there were notable computation time savings in the use of multi-fidelity models. In particular, the computation time of both the MF1 and the MF2, which presented highly accurate solutions, is about 45 % of the HF100 using MCS. The computational cost of these two models is also cheaper than the HF40 having the equivalent accuracy. It is seen that FORM and SORM do not show a significant difference in computation time than MCS because this problem converges to a small number of MCS. Suppose the problem is more complex, or the reliability analysis is conducted using only high-fidelity FE models. In that case, the computation time savings through the multi-fidelity models will increase a lot more. This comparison clearly highlights that the multi-fidelity model provides not only accurate solutions that are similar to the HFM having many design points but also computation time that is a lot more economical than the HFM.

Table 4.4: Reliability analysis results using MCS

	HF11	HF20	HF30	HF40	HF50	HF100	HF11+LF11			
							MF1	MF2	MF3	MF4
Mean	29.57	29.20	29.56	27.99	27.97	27.88	28.58	28.58	29.41	29.55
Standard deviation	6.59	6.85	6.14	6.17	6.47	7.13	6.72	6.05	6.40	6.51
Reliability index	1.60	1.44	2.17	1.81	1.59	1.35	1.41	1.75	1.60	1.60
Error (%)	6.1	4.7	6.0	0.4	0.3	-	2.5	2.5	5.5	6.0

Table 4.5: Reliability analysis results using FORM

	HF11	HF20	HF30	HF40	HF50	HF100	HF11+LF11			
							MF1	MF2	MF3	MF4
Mean	29.54	29.04	29.44	26.47	26.36	26.48	27.31	27.46	29.30	29.52
Standard deviation	6.73	6.89	4.96	4.87	6.12	7.18	6.64	4.76	6.57	6.74
Reliability index	1.51	1.55	2.61	2.23	1.74	1.32	1.44	2.06	1.52	1.50
Error (%)	11.56	9.66	11.72	0.03	0.46	-	3.13	3.70	10.64	11.47

Table 4.6: Reliability analysis results using SORM

	HF11	HF20	HF30	HF40	HF50	HF100	HF11+LF11			
							MF1	MF2	MF3	MF4
Mean	29.54	29.04	29.44	26.47	26.36	26.48	27.31	27.46	29.30	29.52
Standard deviation	6.73	6.89	4.96	4.87	6.12	7.18	6.64	4.76	6.57	6.74
Reliability index	1.55	1.56	2.61	2.23	1.74	1.35	1.48	2.06	1.56	1.54
Error (%)	11.56	9.66	11.72	0.03	0.46	-	3.13	3.70	10.64	11.47

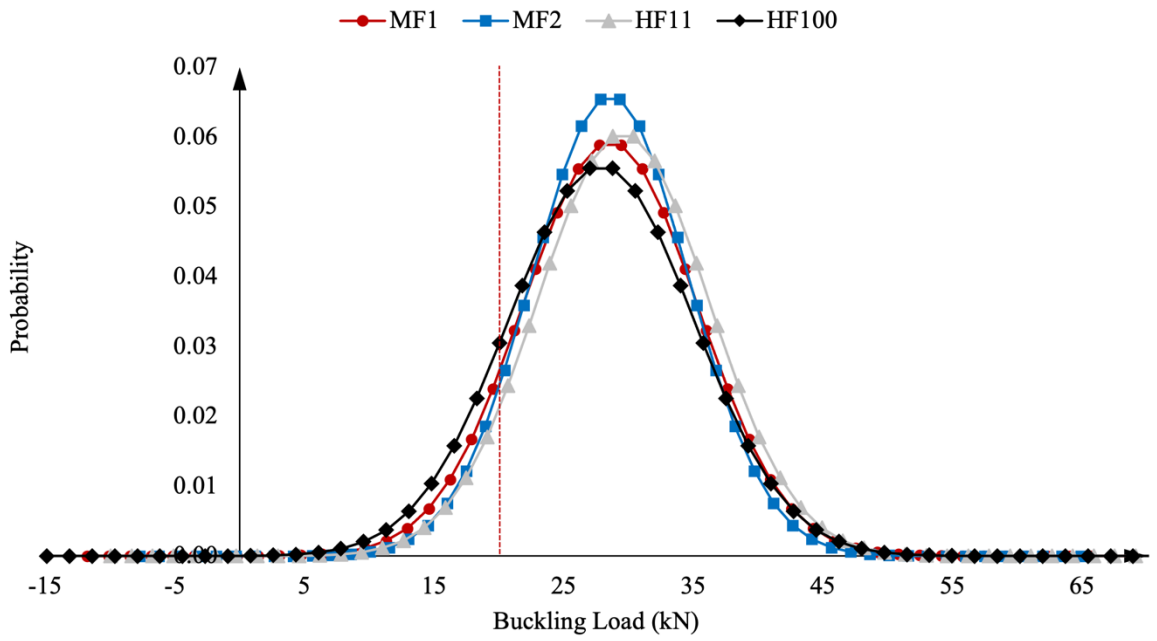

Figure 4.4: Reliability analysis result using MCS

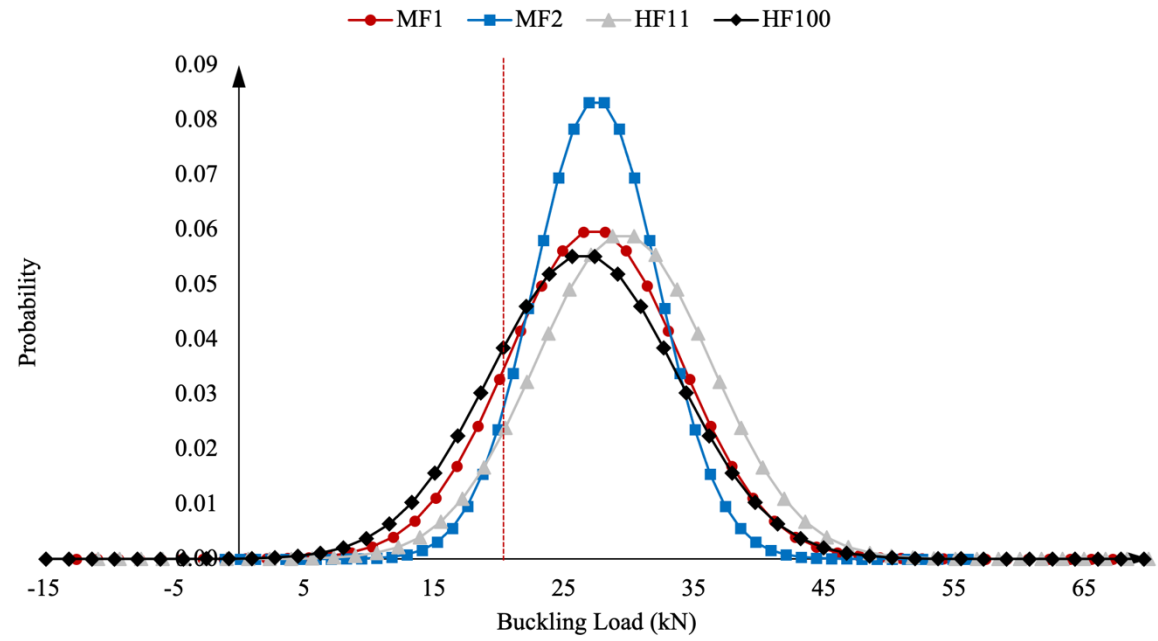

Figure 4.5: Reliability analysis results using FORM

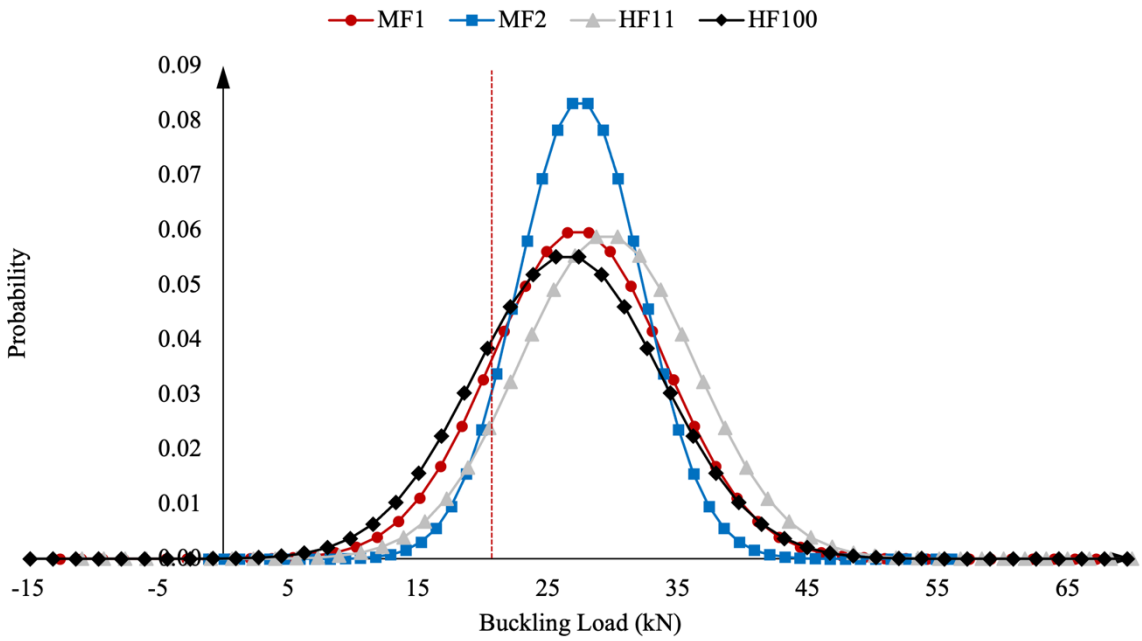

Figure 4.6: Reliability analysis results using SORM

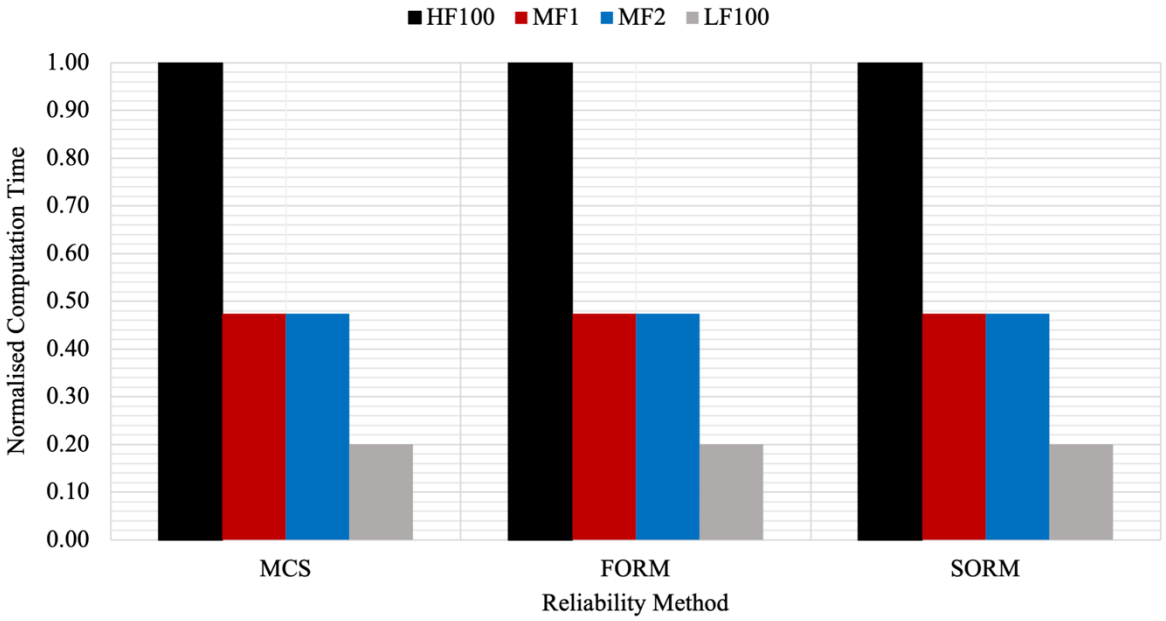

Figure 4.7: Computation time to different multi-fidelity models

4.4.3 Multi-Fidelity Modelling-Based Reliability-Based Design Optimisation

In this section, a multi-objective probabilistic optimisation is carried out. It is demonstrated that the multi-fidelity models provide accurate solutions and high computation time savings compared to the

surrogate model of the HFM. Multi-fidelity RBDO is conducted to validate the concept of multi-fidelity models in a probabilistic optimisation process, requiring a number of simulations to consider design uncertainties. The four geometric design variables of the same composite panel have their own uncertainty, as shown in Table 4.2. NSGA-II is used, which is a multi-objective evolutionary optimisation method.

4.4.3.1 Problem Definition

In general, RBDO includes reliability analysis in its optimisation process, and this example involves considering the uncertainties of four geometry parameters of the composite panel. RBDO process ensures that the optimal design meets the requirement of a specific probabilistic constraint defined by a prescribed reliability index β. In this example, random design variables are characterised by a normal distribution, a probability failure $P_{f,MF}$ is related to the prescribed reliability index β_{MF} as $P_{f,MF} = \Phi(-\beta_{MF})$. As mentioned before, there are three methods to calculate the reliability of structure such as MCS, FORM and SORM. In particular, MCS was conducted by the Sobol sampling method because the simple random sampling requires a vast number of simulations during the optimisation process. In Table 4.7, the number of simulations for MCS using the Sobol sampling is 20 % less than that of the simple random sampling. At the same time, the mean and standard deviation of the statistical result are nearly identical to each other. To ensure the accuracy of FORM and SORM, the step size of the FDM was set as 0.001, and the convergence tolerance was determined by 0.0001. The constraints of this optimisation process are the maximum mass and the target probability of failure that are 1.0 kg and 0.00135, respectively. The objective functions are to maximise the first buckling load and to minimise the structure mass. Parameter studies using NSGA-II were carried out to set the population size and generation number, and then they were determined by 12 and 60, respectively. The details of the multi-fidelity models are described in the next section.

Table 4.7: Sobol sampling vs. Simple random sampling

	MCS Sobol Sampling	MCS Random Sampling
Simulation number	150	600
Probability of success	1.0000	0.9967
Mean	53.76	53.77
Standard deviation	0.28	0.28
Minimum	53.12	52.93
Maximum	54.45	54.58

4.4.3.2 Multi-Fidelity Modelling

The minimum number of design points for ANN to create the surrogate models was 10 because there are four geometric design variables. The multi-fidelity models were constructed using 10 of the HFM and 10 of the LFM. The surrogate models using 100 of the HFM, known as HF100, were also created to evaluate the performance of the multi-fidelity models. OLHS is employed to build the training and test datasets. In particular, a total of 300 design points, 100 for the training dataset and 200 for the test dataset, were collected to create the surrogate models of the HF100. Total 30 design points, 10 for the training dataset and 20 for the test dataset, were also sampled to create two surrogate models having the HFM and the LFM, respectively. These training and test datasets also were used to generate the two correction factors, $\beta(x)$ and $\delta(x)$, for the LFM to represent the response surfaces of the HFM. The design points for the training dataset were determined by the range from -20 % to 20 % concerning the mean of each design variable. The design points for the test dataset were selected by the broader range from -25 % to 25 % in order to evaluate the quality of the surrogate model. Through the training dataset from the sampling range, two direct multi-fidelity models and two indirect multi-fidelity models are constructed, as can be seen in Table 4.3. Each model has four inputs having geometries and two outputs having mass and buckling load.

Table 4.8 highlights that the two direct multi-fidelity models, MF1 and MF2, showed better quality than the two indirect multi-fidelity models, MF3 and MF4. The HF100 presented nearly the same response as the high-fidelity FEM models, whereas an HF10 which consists of 10 of the HFM, showed significant differences compared to the four different multi-fidelity models. All models provided the correct mass because the response surface of mass is simple for the multi-fidelity models to represent. It is interesting to note that the MF1 and MF2 provided more accurate results of buckling load and mass than the HF10, even though the computation time of these two models was slightly more expensive due to the extra LFMs to improve the quality of the multi-fidelity models. The increase in this extra computation time caused by the LFMs is worth it since the multi-fidelity models provide more accurate results than the HF10. If the number of the HFM increases until the accuracy is similar to the multi-fidelity models, the computation time caused by this increase should be much higher than that of the multi-fidelity models. It is seen that the errors of the indirect multi-fidelity models were higher than the direct multi-fidelity models because these indirect multi-fidelity models use the surrogate models based on the design points from the LFM. These four multi-fidelity models were validated to conduct the RBDO process as an alternative model to the HFM.

Table 4.8: Multi-fidelity models validation

Model	Fitness error	
	Buckling load	Mass
MF1	0.0101	0.0009
MF2	0.0107	0.0009
MF3	0.0155	0.0034
MF4	0.0155	0.0034
HF10	0.0159	0.0029
HF100	0.0034	0.0006

4.4.3.3 Results and Discussion

In Figure 4.8 and Figure 4.9, the optimisation results of the multi-fidelity models using FORM are compared to the results of the high-fidelity modelling-based surrogate model (HF100). The results using MCS and SORM are not presented in this example because they are nearly the same as the results using FORM. As shown in these figures, the Pareto Fronts show the optimal design results that are satisfied with the desired objectives and constraints. It should be noted that the slope of the Pareto Front line is changed when the structure mass is around 0.94 kg. It means that the first buckling load increases gradually until the mass reaches 0.94 kg. However, when the mass is more than 0.94 kg, the buckling load does not rise as much as the structure mass increases. It is determined that the design geometries around the mass of 0.94 kg are the reasonable design values in the given design space.

Table 4.9 and Figure 4.10 show the comparison of chosen geometries when the mass of the composite panel is 0.94 kg that the linear buckling load is the economically maximum value. The result of the HF100 is the most accurate value because this model consists of enough HFM that provide the correct first buckling load. It is worth noting that the chosen optimal geometry values from the multi-fidelity models are nearly identical to those from the HF100. The mean and standard deviation of the multi-fidelity models are similar to those of the HF100 in the same mass. Figure 4.10 and Figure 4.11 show the probabilistic distribution of each multi-fidelity model and the optimal geometric design from RBDO. The direct multi-fidelity models, MF1 and MF2, have almost the same mean and standard deviation. The probabilistic distributions of indirect multi-fidelity models, MF3 and MF4, have a little different mean of first buckling loads, although they have nearly the same standard deviation. Therefore, the accuracy of all multi-fidelity models was validated.

Computation time savings, as well as accuracy, are the main goals of this study. It is essential to show how much computation time savings can be achieved by using the multi-fidelity models. In order to be able to compare the computation time of each model reasonably, the required simulation number of each model during this optimisation process is compared. The average computation time of HFM and LFM using Abaqus/CAE was calculated over 100 runs, respectively. This computation time was 47

seconds and 10 seconds, respectively. The computation time of one surrogate model was assumed by total simulation time divided by the total simulation number used in the whole optimisation process. The total simulation time using Intel Core i7-6700 CPU @ 3.40GHz and the number of simulations using all surrogate models were 7,036 seconds and 1,229,085, respectively. The computation time of one surrogate model was 0.0057 seconds. To ensure the computation time of each model, it was calculated by the combination of the simulation number of surrogate models, high-fidelity FEM models and low-fidelity FEM models. As shown in Figure 4.12, all computation time is normalised by the computation time of the HF100 using MCS, which is the most computationally expensive. This figure clearly shows that the multi-fidelity models require a lot less computational cost than the HF100. In three reliability methods that calculate the probability of failure, MCS is the most computationally expensive. FORM is a little cheaper than SORM because SORM requires more simulation for a second-order Taylor expansion at the failure domain. The direct multi-fidelity models, MF1 and MF2, are slightly more expensive than the indirect multi-fidelity models, MF3 and MF4, because the direct models call the low-fidelity FEM models when they create the surrogate models. In particular, all multi-fidelity models show a similar level of computation time to the LF100, which consists of 100 low-fidelity FEM models. It should be noted that the computation time of the multi-fidelity models is reduced by at least 70 % compared to the HF100. If the optimisation is conducted using the high-fidelity FEM models without the surrogate models, the multi-fidelity models will save the computation time a lot more than 70 %.

Table 4.9: Initial and chosen geometry of the composite panel

Model	X1	X2	X3	X4	Mean	STD	Mass
	$[mm]$	$[mm]$	$[mm]$	$[mm]$	$[kN]$	[-]	$[kg]$
Initial	43.0	30.0	15.0	25.0	53.76	-	0.90
HF100	51.6	24.3	18.0	30.0	73.86	0.40	0.94
MF1	51.6	24.5	18.0	30.0	72.87	0.36	0.94
MF2	51.5	24.4	18.0	30.0	72.83	0.36	0.94
MF3	51.6	24.5	18.0	30.0	73.45	0.39	0.94
MF4	51.6	24.6	18.0	30.0	72.67	0.36	0.94

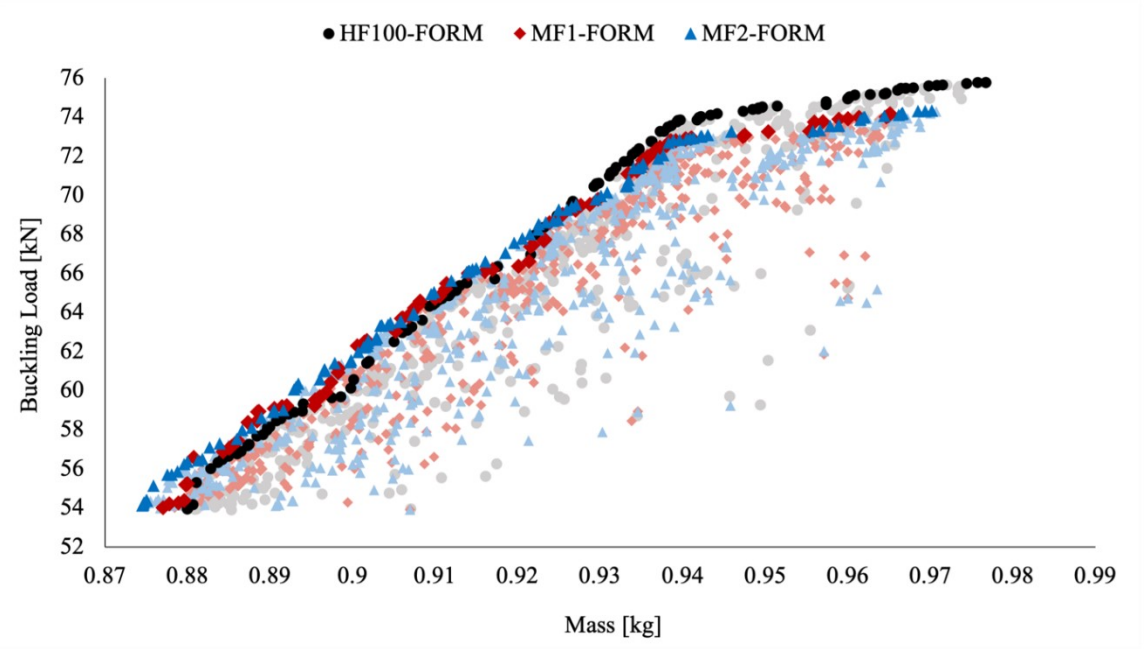

Figure 4.8: Comparison to RBDO results using FORM (HF100 vs. Direct multi-fidelity models)

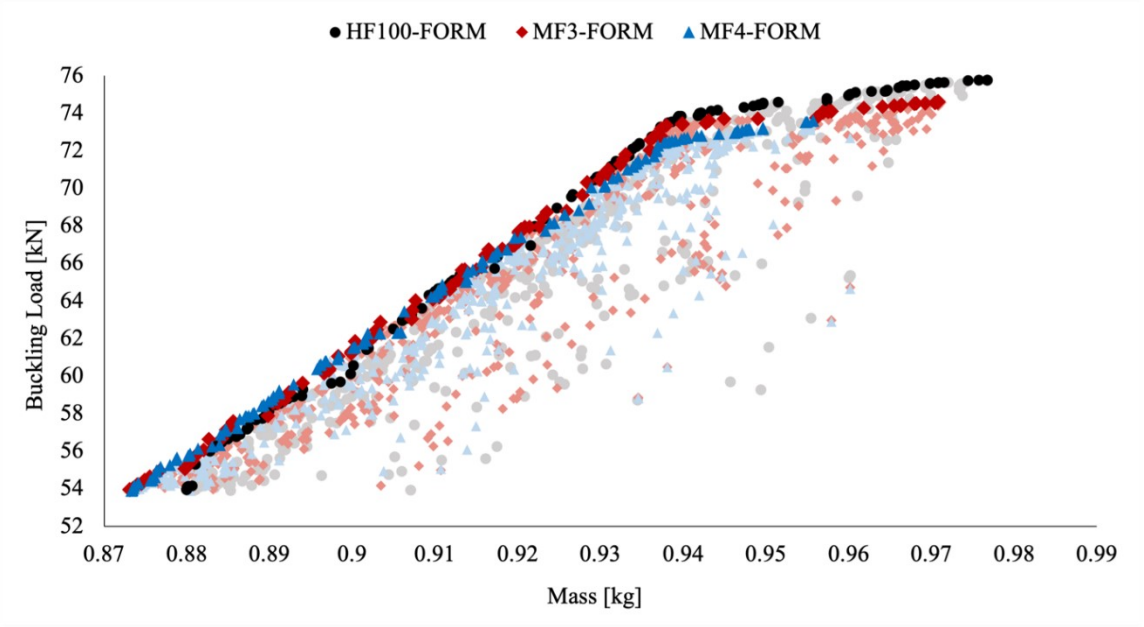

Figure 4.9: Comparison to RBDO results using FORM (HF100 vs. Indirect multi-fidelity models)

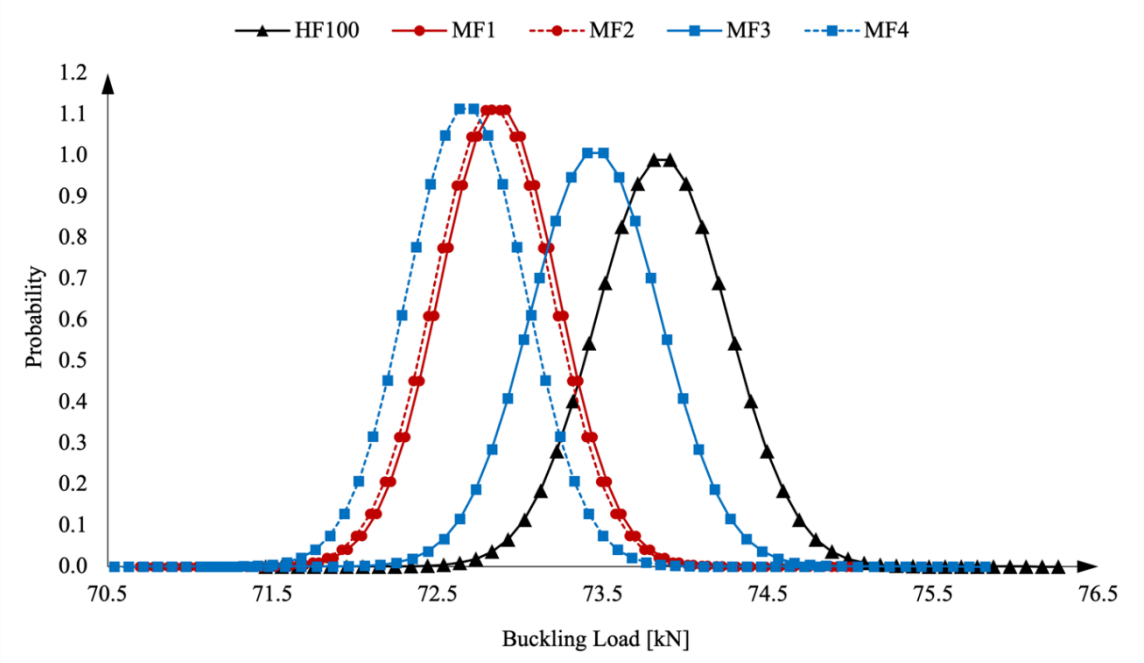

Figure 4.10: Reliability-based design optimisation results

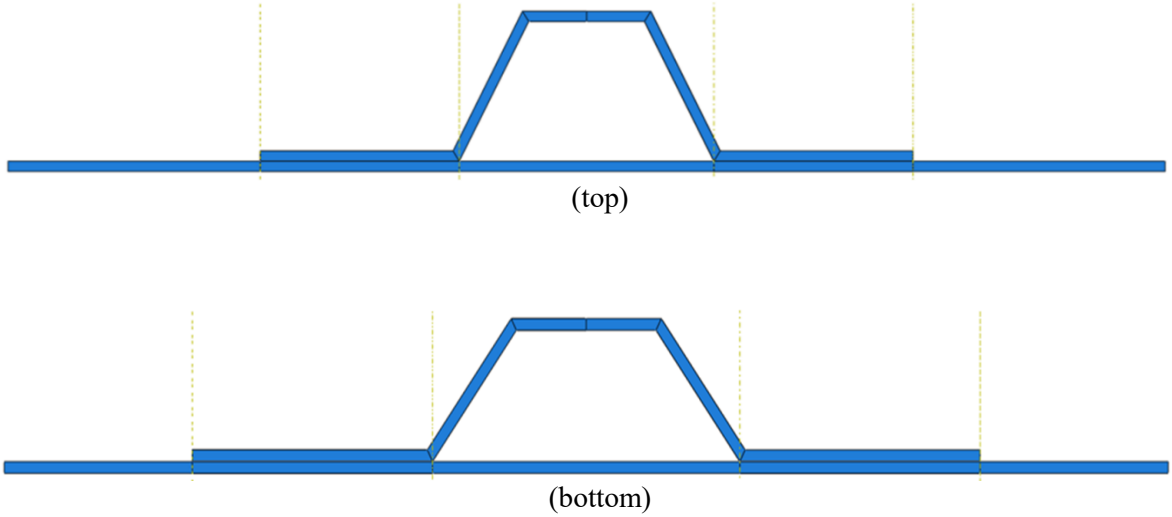

Figure 4.11: Mono-stringer stiffened panel geometry optimised for maximum linear buckling load based on 0.94 kg: (top) Initial model and (bottom) RBDO model (MF1)

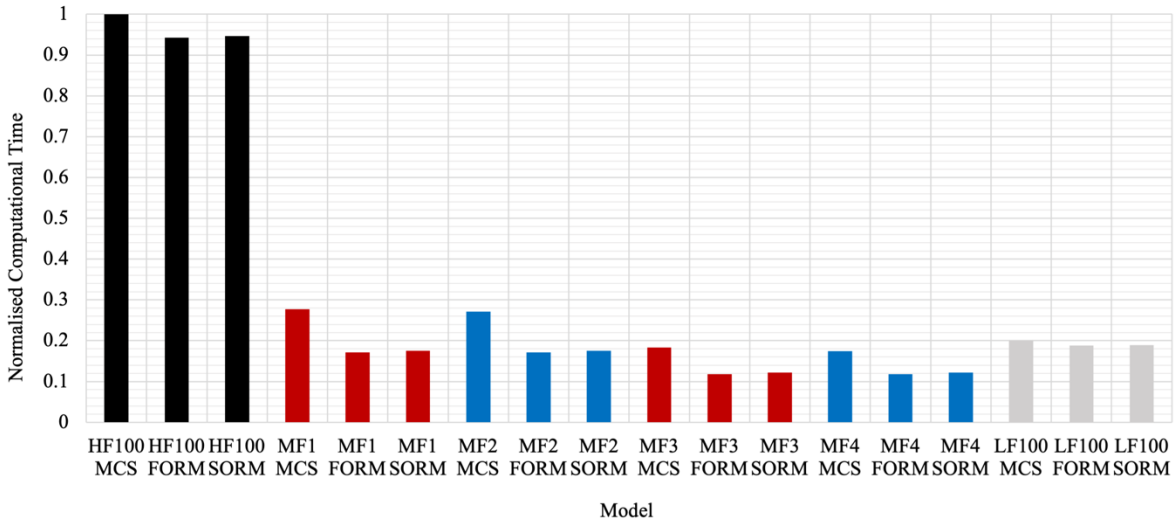

Figure 4.12: Computation time concerning different multi-fidelity models

4.5 Summary

In conclusion, the multi-fidelity formulation was developed for reliability analysis and RBDO of composite structures to consider the influence of uncertainties in design variables. This formulation enables the multi-fidelity models to offer remarkable accuracy nearly identical to the HFM as well as significant computational time savings similar to the LFM. This is accomplished by creating the response surfaces of ratio and difference between two different fidelity models. These two models covering the same design spaces requires the same number of design points to train the surrogate model using ANN. The direct and indirect multi-fidelity models depending on the use of the low-fidelity FEM models during the modelling process are constructed. Then these models are employed in the developed multi-fidelity RBDO process.

Two numerical examples demonstrated the performance of the multi-fidelity models: reliability analysis and RBDO. The multi-fidelity reliability analyses considering design uncertainties were conducted using MCS, FORM and SORM that calculate the reliability of structure under the given limit-state function. In the example of multi-fidelity reliability analysis, the direct multi-fidelity models, particularly the model using the ratio response surface, provided a highly accurate solution. The computational cost of the multi-fidelity models is equivalent to the use of 40 high-fidelity FEM models. These multi-fidelity models furnished computation time savings of over 50 % compared to the conventional computationally expensive method using only HFM. The concept of multi-fidelity modelling was also applied to the probabilistic multi-objective optimisation problem. The direct and indirect multi-fidelity models provided very close optimisation solutions to the results of the conventional method. The computation time using MCS was decreased by at least 70 %, and this time

savings were a lot larger when FORM and SORM were used in the optimisation process. These results suggest that the new multi-fidelity framework can be applied to reliability analysis and RBDO of composite structures having design uncertainties. This framework provides a certain level of accuracy and considerable computation time savings compared to the conventional method using only HFM.

5 Multi-Fidelity Robust Design Optimisation based on Low-Fidelity Models using Successive High-Fidelity Correction

It is well acknowledged that composite structures draw attention in different industrial areas because they provide remarkable strength, stiffness and energy savings consistent with both an environmentally friendly design and a cost-effective operation. The manufacturing process of composite structures is complex and carries various uncertainties that influence the quality and performance of the final design. The variation in design parameters, in general, provokes unexpected deviations across the entire lifecycle, including design, manufacturing, service, and ageing. Robust Design Optimisation (RDO), one type of probabilistic design optimisation, is an essential design approach since it considers how the uncertainties associated with design and manufacturing could affect product quality and performance. The main idea of RDO was proposed by Taguchi Genichi (3), and such idea aims to provide more stable output performance regarding the variation of design parameters, such as geometry, service environment and material property. RDO allows the final design not to be an extremely conservative design based on excessive safety factors or worst-case scenarios because it minimises the variation of product performance caused by the design uncertainties. Hence, RDO improves the quality of the design product by stabilising the deviations of response behaviour without removing their design sources and minimising the effect of the design uncertainties (44).

RDO has been studied and applied to various engineering design fields, such as structural design using Finite Element Method (FEM) (4,20,72–74) and aerodynamic design using Computer Fluid Dynamics (CFD) (67,75–77). In general, RDO requires computationally expensive efforts to find robust design solutions because many computational simulations have to be conducted to calculate the effect caused by the design uncertainties. This is a typical challenge to be addressed in the area of probabilistic design optimisation. Likewise, RBDO in the previous chapter, the use of the surrogate model has been actively developed to tackle the computational challenge caused by carrying out the process of RDO (22). Most

of them approximate the expensive computation models using Artificial Neural Networks (ANN), Kriging, polynomial regression and Response Surface Method (RSM) (4,67,78–80). One notable example concerning RDO of composite structures using the surrogate model is Bacarreza et al. (4), where the RDO framework of a composite stiffened panel under non-linear progressive failure analysis was presented using ANN. The quality of the created surrogate model was evaluated by the cross-validation error method to determine whether the model provides the computation time savings and an acceptable level of accuracy. This model was applied to conduct a robustness analysis considering the design uncertainties of the composite stiffened panel. This work allows the concept of RDO to be implemented in the design of composite structures under non-linear damage progressive problems. It shows the potential to extend the application area of RDO using the surrogate model.

As discussed in Chapter 4, there are different types of multi-fidelity modelling methods that have been developed to improve the computational efficiency of conventional high-fidelity surrogate modelling methods. When a problem becomes large-scale and complex, the computational cost to create the surrogate model is still extremely expensive because a large number of High-Fidelity Models (HFM) have to be simulated using a numerical solver. However, the computational cost for running even a single high-fidelity FEM simulation of the composite structure is too high to neglect when the problem has non-linear response behaviour or many design variables. Multi-fidelity modelling methods developed so far have been used to conduct optimisation and uncertainty propagation using the combination of both HFM and Low-Fidelity Models (LFM). In particular, the vast majority of the way of combining two different fidelity models uses response correction methods for the LFM to represent the response behaviour of the HFM (12,23,47). Different multi-fidelity modelling methods, such as the Co-kriging method, have been applied to aerodynamic optimisation problems (63,75,81). Even though these multi-fidelity modelling methods provide acceptable accuracy and computational efficiency compared to the conventional high-fidelity surrogate modelling methods, they have been demonstrated using mathematical examples, aerodynamic design optimisation and structural design optimisation of isotropic materials. The primary limitation of these methods is difficult to take care of large-scale problems having many design variables. In order to create the response correction functions, such as the ratio or difference between the HFM and the LFM, many high-fidelity simulations should be conducted using a FEM or CFD solver to build a correct response surface. This causes tremendous computational burdens when the system has many design variables. It should be noted that the number of high-fidelity simulations needs to be the same as that of low-fidelity simulations to construct a multi-fidelity model using the response correction methods.

The main objective of this work was to develop a novel multi-level multi-fidelity modelling-based RDO framework. It aims to apply to the probabilistic optimisation problem when the HFM and the LFM have a different number of design variables so that the computational cost to construct the multi-fidelity model is reduced. This developed multi-fidelity RDO framework requires a smaller number of high-

fidelity FEM simulations compared to the conventional multi-fidelity modelling methods, which require the same number of FEM simulations between the HFM and the LFM. To achieve this research objective, the HFM has a fewer number of design variables during the optimisation process, while the LFM has more design variables to explore the whole design space sharing the same design variables with the HFM. Multi-level optimisation was also considered to gain more computational efficiency by dividing the optimisation problems into several subproblems. This framework drives using the LFM covering the whole design space while updating the optimal solutions using high-fidelity corrections. Its applications demonstrated this approach to both Deterministic Optimisation (DO) and RDO of a mono-stringer stiffened composite panel under the post-buckling regime. Finally, the robust design and deterministic design were compared by conventional optimisation methods using the HFM. The performance of this new framework was evaluated in terms of optimisation solution accuracy and computation time savings.

This chapter will first explain the concept of the multi-fidelity modelling method that covers different design spaces between the HFM and the LFM. Then it will introduce the developed multi-fidelity formulation and how this formulation implements the probabilistic design optimisation. At the end of this chapter, two numerical examples of DO and RDO will be conducted to design a composite structure to demonstrate the new multi-fidelity optimisation framework. The work presented in this chapter is based on work presented by Yoo et al. in (42).

5.1 Multi-Fidelity Modelling Method for Different Design Spaces between Fidelity Models

As discussed in Chapter 3, the traditional multi-fidelity methods developed so far can be divided by how they allow the LFM to represent the response behaviours. The majority of these multi-fidelity methods set up the response correction function, such as multiplicative, additive and comprehensive correction methods. These methods require the same number of high-fidelity FEM simulations as that of low-fidelity FEM simulations. Some methods using Gaussian Process (GP), including Co-kriging, require a smaller number of high-fidelity FEM simulations than low-fidelity FEM simulations. However, the design variables in the HFM and the LFM have to be identical to each other. These traditional methods may cause significant computational challenges when the optimisation problem is large-scale or has many design variables. The space mapping method creating a proper transformation function between different design spaces has not been used in the field of structural optimisation so far due to its limitation. The limitation will be described in the following section.

5.1.1 Space Mapping Method in Structural Optimisation

The space mapping method allows different fidelity models to cover different design spaces, and it constructs the multi-fidelity model. This method builds a mapping function between the HFM having all design variables and the LFM having a few design variables. The mapping function enables the optimisation results obtained in the low-fidelity design space to be transformed into the high-fidelity design space using the inverse mapping function. The idea of the space mapping method was proposed to design the microwave circuit at first (62). Then its application scope has expanded to the field of aerodynamic design (82). However, this method has scarcely applied to the area of structural optimisation. The only example found in (83) used the space mapping method to conduct a DO of a steel beam structure with two design variables subjected to a uniformly distributed load. However, the space mapping method considered in the vast majority of related literature shared the same number of design variables between the HFM and the LFM (84). Even though the HFM and the LFM have a different number of design variables, the fidelity is not the level of discretisation but numerical solvers (82).

This section demonstrated whether the space mapping method is available to construct a proper multi-fidelity model for structural optimisation when the HFM and the LFM have a different number of design variables. The numerical example is the same as the isotropic steel plate presented in Chapter 3, but it has more design variables, as shown in Figure 5.1. The drain cover has four design variables, such as horizontal drain, vertical drain, drain depth and plate thickness. This DO problem aims to minimise the mass and vertical displacement under a uniformly distributed load. The constraint is the maximum allowable stress of the drain cover. The Finite Element Method (FEM) model of the drain cover was created using Abaqus (57). The design ranges of each variable are described in Table 5.1.

Table 5.1: Design range of each variable

Parameter	Value
Drain height (mm)	$144 < V < 216$
Drain width (mm)	$56 < H < 84$
Drain depth (mm)	$24 < D < 36$
Plate thickness (mm)	$4 < T < 6$

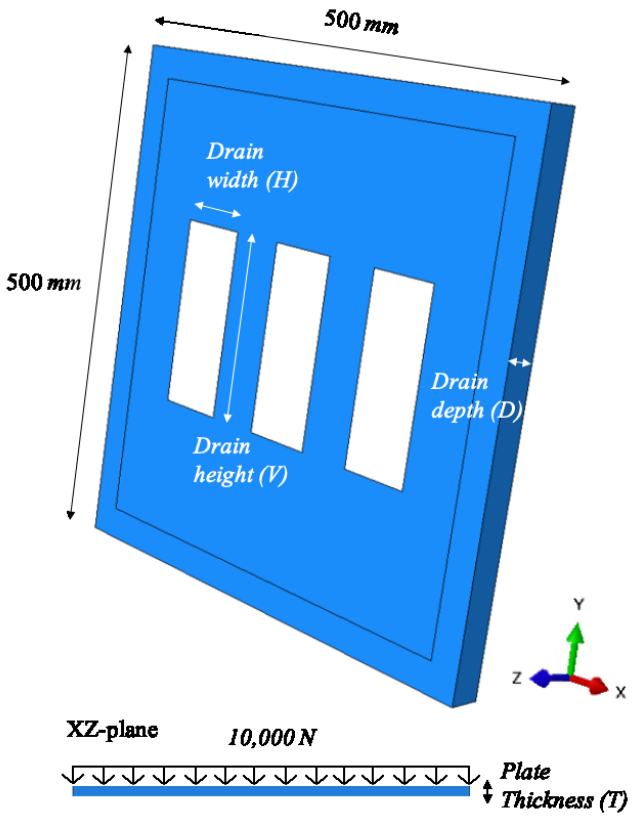

Figure 5.1: Isotropic steel strain cover having four design variables

In this example, the HFM has four design variables (H, V, D, T), while the LFM has two of them (v, t). These two variables for the LFM were determined by more dominant input design variables to the objective functions than other design variables. Both the high- and low-fidelity FEM models were created using the identical mesh size, whereas they carry different design variables.

As illustrated in Figure 5.2, the optimisation process using the space mapping method consists of two steps, such as a mapping parameter extraction and DO process. Basically, X_{HFM} is a vector of high-fidelity design variables, and the mapping function, P, transforms the X_{HFM} to X_{LFM} that is a vector of low-fidelity design variables. Then, the optimisation problem can find optimal solutions in the low-fidelity design spaces. Finally, the low-fidelity optimal solutions, X^*_{LFM}, are transformed to high-fidelity optimal solutions, X^*_{HFM}, using the inverse mapping function. The parameter extraction is the main step for the space mapping method to build a multi-fidelity model.

In this example, the created mapping function transforms the high-fidelity design spaces having four design variables to the low-fidelity design spaces having two design variables. Firstly, n high-fidelity training points should be collected from the entire design space using Design of Experiments (DoE). Then the output responses are obtained to set up the high-fidelity training dataset. A linear mapping function, P, should be presumed that can be represented as $X_{LFM} = P(X_{HFM}) = B \times X_{HFM} + C$. It should be noted that the dimension of the mapping matrix B and the vector C is (2×4) and (2×1),

respectively, relying on a different number of design variables between the HFM and the LFM. Parameter extraction is a sub-optimisation problem to obtain each mapping parameter of the matrix B and the vector C. This sub-optimisation problem minimises the difference between high-fidelity response, $Y_{HFM}(X_{HFM})$, and low-fidelity response, $Y_{LFM}(X_{LFM}) = Y_{LFM}(B \times X_{HFM} + C)$. The sub-optimisation offers the mapping parameters. Then the surrogate model, $\hat{P}$, of the mapping parameters can be established using ANN. This surrogate model satisfies with $Y_{LFM}\left(\hat{P}(X_{HFM})\right) \cong \hat{Y}_{HFM}(X_{HFM})$ and is used to carry out the optimisation problem until the low-fidelity optimal solutions, X^*_{LFM}, are obtained. Finally, the high-fidelity optimal solutions, X^*_{HFM}, are found using the inverse mapping function.

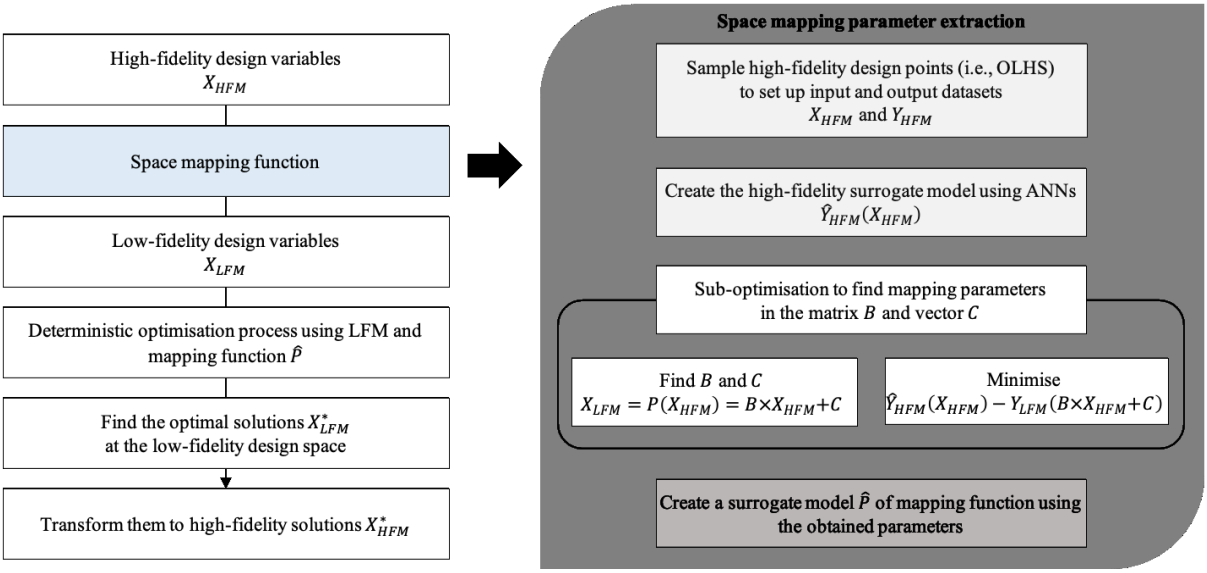

Figure 5.2: Deterministic optimisation process using the space mapping method

Equation (5.1) represents the mapping function of design variables between the HFM and the LFM. The HFM has four design variables, while the LFM has two design variables. The parameter extraction aims to find the mapping parameters in the matrix B and the vector C. Equation (5.2) shows the objectives of the parameter extraction. The first objective is to minimise the difference in responses between the two fidelity models. The second and third objectives are for the low-fidelity design variables not to be far away from the high-fidelity design space. It should be noted that the mapping parameters B_{12} and B_{23}, which are related to V and T in the HFM, are constant at 1.0.

$$X_{LFM} = P(X_{HFM}) = B \times X_{HFM} + C$$

$$\begin{bmatrix} v \\ t \end{bmatrix} = \begin{bmatrix} B_{11} & B_{12} & B_{13} & B_{14} \\ B_{21} & B_{22} & B_{23} & B_{24} \end{bmatrix} \begin{bmatrix} H \\ V \\ T \\ D \end{bmatrix} + \begin{bmatrix} C_1 \\ C_2 \end{bmatrix} \tag{5.1}$$

$$
\begin{aligned}
minimise \quad & \left\| \hat{Y}_{HFM}(X_{HFM}) - Y_{LFM}(B \times X_{HFM} + C) \right\| \\
& B_{11} \cdot H + B_{13} \cdot T + B_{14} \cdot D = 0 \\
& B_{21} \cdot H + B_{22} \cdot V + B_{24} \cdot D = 0
\end{aligned} \tag{5.2}
$$

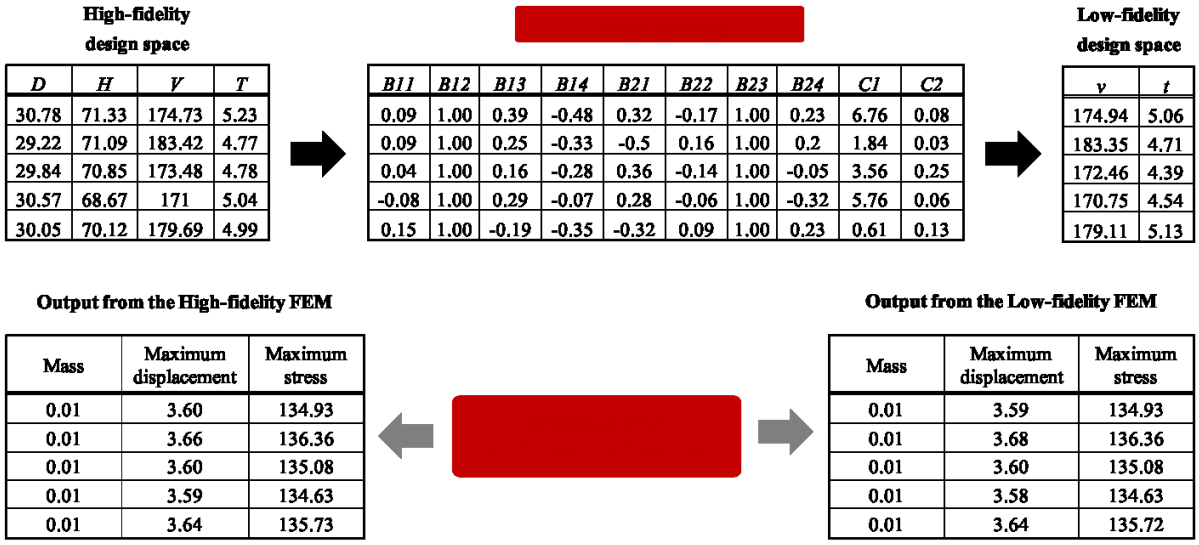

Figure 5.3: Space mapping method between the HFM and the LFM

When the surrogate model of the HFM is created, the parameter extraction is conducted using NSGA-II and finds the mapping parameters, as shown in Figure 5.3. The output responses of the LFM using the mapping function were nearly identical to those of the HFM. However, it should be evaluated whether the inverse mapping function transforms a low-fidelity design point to a correct high-fidelity design point. Equation (5.3) denotes how the high-fidelity design point is obtained using the inverse mapping function. The pseudo-inverse was considered due to the different design spaces of the HFM and the LFM.

$$X_{HFM} = P^{-1}(X_{LFM}) = [[B^T B]^{-1} B^T][[X_{LFM}] - [C]] \tag{5.3}$$

In the first case in Figure 5.3, the inversed high-fidelity design point from the low-fidelity design point was not even close to the original design point but completely different. The inversed design points are out of design space and geometrically impossible values, as described in equation (5.4)

$$X_{HFM\_original} = \begin{bmatrix} 71.33 \\ 174.73 \\ 5.23 \\ 30.78 \end{bmatrix} \neq X_{HFM\_inversed} \begin{bmatrix} 7.89 \\ 123.72 \\ 37.93 \\ -60.82 \end{bmatrix} \tag{5.4}$$

This result shows that the inverse mapping matrix does not provide correct high-fidelity design variables when the design spaces of the HFM and the LFM are different. The matrix $B^T B$ in equation (5.3) is close to a singular matrix, and the matrix $[B^T B]^{-1} B^T$ might provide an incorrect high-fidelity design point. It is not possible for the mapping function to offer reasonable high-fidelity design variables from

low-fidelity design spaces because of information loss between the two fidelity models when the design variables are dependent on the mesh size using the same FEM solver.

5.2 Multi-Fidelity Modelling having a Different Number of Design Variables between HFM and LFM

The multi-fidelity methods developed in computer science provide significant computational efficiency compared to metamodels or surrogate models. Such surrogate models have been widely used in different types of design problems in engineering. However, it is found that the traditional multi-fidelity methods do not allow different fidelity models to carry a different number of design variables. The space mapping method, which covers different design spaces between the HFM and the LFM, was not available for structural optimisation as described in the previous section. The inverse mapping function derived by the pseudo inverse formulation does not provide a correct high-fidelity design point from a low-fidelity design point since the mapping matrix is not with the same number of rows and columns. It should be noted that a composite structure used in large-scale design problems, such as aircraft or wind turbine, has many design variables such as geometry, material properties, etc. For instance, if a structure has more than thirty design variables and each design variable has a wide design range, hundreds of high-fidelity FEM models have to be simulated to construct the response correction function in the same design spaces with the LFM. This requires the same number of design points with the LFM to cover the entire design space and leads to considerable computational cost. Although the traditional multi-fidelity methods offer a certain level of computation time savings, it should be highlighted that the changes in the mesh regarding different geometry parameters in the HFM cause additional computational cost when it comes to large-scale structures.

5.2.1 Multi-Level Optimisation for Multi-Fidelity Modelling

As the engineering system in the field of structural optimisation becomes more complex and enormous, it causes an increase in the number of design variables to consider. As mentioned in the previous section, the computational cost of considering all design variables in high-fidelity FEM simulations is prohibitive to construct even multi-fidelity models.

In order to resolve this challenge, the developed multi-fidelity formulation adapts the concept of multi-level optimisation to improve computational efficiency compared with traditional surrogate methods and other multi-fidelity methods. Multi-level optimisation presents a wide range of benefits when it comes to large-scale optimisation problems. This optimisation approach separates a given large-scale

optimisation problem into several scaled-down problems (85). This approach breaks down the large-scale optimisation problem into several levels of design adjustment corresponding to various collections of design variables. This adaptation ensures that the multi-fidelity formulation can offer significant computational time savings while safeguarding the probabilistic optimisation process against different levels leading to information loss (42).

The selection of levels and the associated design variables depend on the problem characteristics. For instance, if the level is determined by numerical analysis methods, the design variables should be defined by what the numerical solver requires (86). In comparison, if the level is defined by different objective functions, each level should take different design variables which deliver critical impact (87). The level can also be determined by different design approaches, such as preliminary and detailed design (4). These levels provide the large-scale problem to computational efficiency with benefits. It is not surprising that each level has its objectives and constraints, depending on the design variables. In this multi-level optimisation, the designer should decide to find reasonable solutions at each level that maximise the performance of the whole given system. A typical multi-level multi-objective optimisation process can be expressed as equation (5.5):

$$
\begin{aligned}
&\text{Level 1}\\
mininise/maximise \quad & f_i(X) && (i = 1, 2, \dots, I)\\
subject\ to \quad & g_j(X) \le 0 && (j = 1, 2, \dots, J)\\
& h_k(X) = 0 && (k = 1, 2, \dots, K)\\
& x_l^{(L)} \le x_l \le x_l^{(U)} && (l = 1, 2, \dots, L)\\
&\vdots\\
&\text{Level } n\\
mininise/maximise \quad & f_o(Y) && (o = 1, 2, \dots, O)\\
subject\ to \quad & g_p(Y) \le 0 && (p = 1, 2, \dots, P)\\
& h_q(Y) = 0 && (q = 1, 2, \dots, Q)\\
& y_r^{(L)} \le y_r \le y_r^{(U)} && (r = 1, 2, \dots, R)
\end{aligned}
\qquad (5.5)
$$

where X is the design variables, f_i is the i^{th} objective function, g_j is j^{th} inequality constraint, h_k is k^{th} equality constraint, and $x_l^{(L)}$ and $x_l^{(U)}$ are the lower and upper bounds for the l^{th} design variables in *Level 1*. Similarly, Y is the design variables, f_o is the o^{th} objective function, g_p is p^{th} inequality

constraint, h_q is q^{th} equality constraint, and $x_r^{(L)}$ and $x_r^{(U)}$ are the lower and upper bounds for the r^{th} design variables in *Level n*. It should be noted that part of the objectives can be used at a different level.

5.2.2 Multi-Fidelity Formulations Based on the LFM using Successive High-Fidelity Correction

This section introduces a new multi-level multi-fidelity modelling method to address the computational challenge and offer more computational efficiency than the traditional multi-fidelity methods. This multi-fidelity method aims to manage different design spaces between the HFM and the LFM. The multi-level optimisation approach is incorporated into this developed modelling process. This method employs ANN, which uses particularly the radial basis functions introduced in sections 3.1.2.1, to create the surrogate models.

Figure 5.4 represents the main idea of this multi-fidelity modelling method is to use the LFM with successive high-fidelity correction across the optimisation level. Here, the HFM has fewer design variables (one variable in this example) than the LFM at each level to reduce the high-fidelity FEM simulations to construct surrogate models. In contrast, the LFM has more design variables than the HFM at the same level. The multi-fidelity model constructed by these two fidelity models encompasses different dimension of design spaces, and it is utilised at each level of the probabilistic optimisation process. Fundamentally, the optimal solutions of high-fidelity design variables are obtained using the optimisation loop of the HFM. At the same time, the solution spaces of other design variables that are not included in the HFM can be explored by the optimisation loop of the LFM having all design variables. After every optimisation level, both the HFM and the LFM are corrected using the optimal solutions of the multi-fidelity model at each level, and then the updated models move on to the following optimisation level. These updated models are exploited to construct an improved multi-fidelity model that carries new high-fidelity design variables during the following optimisation process. The optimal solutions of the low-fidelity design variables at the previous level are employed by the initial starting points of the next level to discover global solutions efficiently. The LFM can complement information loss in the whole design space caused by the HFM not embracing the entire design space. In this manner, the HFM provides accurate optimal solutions of high-fidelity design variables. The LFM explores the whole solution space of all design variables while sharing the design variables in the HFM.

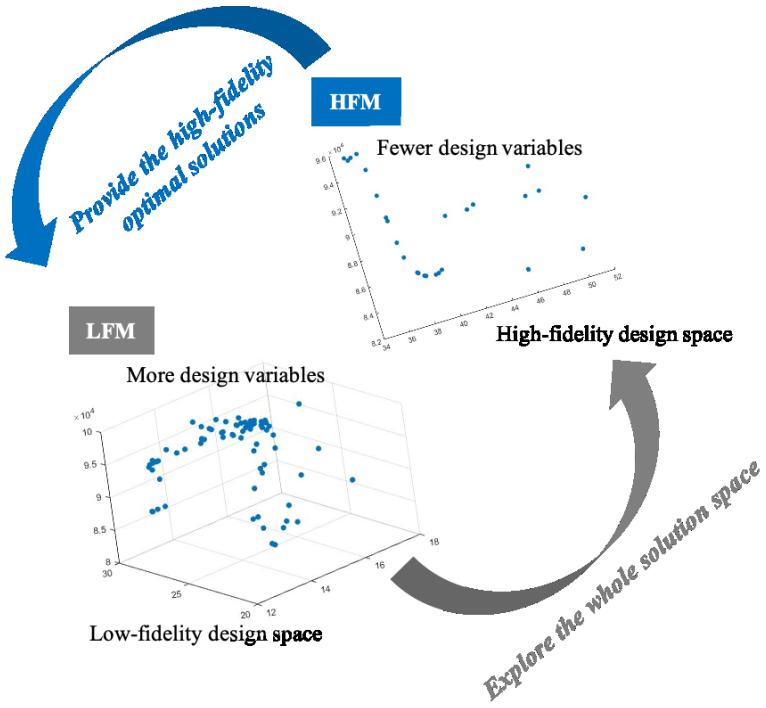

Figure 5.4: Concept of multi-fidelity modelling method having a different number of design variables

As defined in Table 5.2, the formulation highlights how a multi-fidelity model is constructed using a different number of design variables between the HFM and the LFM. At the first level, m design variables in the HFM are selected from all design variables, n. These m selected design variables are defined by $\mathrm{H}^{(\mathrm{I})}$. Other design variables not chosen are fixed at their initial values. In comparison, the LFM has n design variables defined by $\mathrm{L}^{(\mathrm{I})}$. It is not surprising that $\mathrm{H}^{(\mathrm{I})}$ is a subset of $\mathrm{L}^{(\mathrm{I})}$. This enables the constructed multi-fidelity model to explore the whole design space using the LFM. After the optimisation at this level, the optimal solutions are found that are represented by $\hat{\mathrm{H}}^{(\mathrm{I})}$ and $\hat{\mathrm{L}}^{(\mathrm{I})}$ of high-fidelity design variables and low-fidelity design variables, respectively. Then the selected high-fidelity design variables in the first level are updated by $\hat{\mathrm{H}}^{(\mathrm{I})}$ and other design variables not chosen by the HFM are also updated by $\hat{\mathrm{L}}^{(\mathrm{I})}$.

The HFM chooses a different number of design variables in the next level, l, as new design variables $\mathrm{H}^{(\mathrm{II})}$ and the optimised design variables in the first level, $\hat{\mathrm{H}}^{(\mathrm{I})}$, are fixed for this level. The LFM covers the whole design space except for the previous high-fidelity design spaces of $\mathrm{H}^{(\mathrm{I})}$ while sharing the new design high-fidelity design spaces of $\mathrm{H}^{(\mathrm{II})}$. The vector size of low-fidelity design variables should be $(n-m)\times 1$. The constructed multi-fidelity model finds the optimal solutions of design variables specified by $\tilde{\mathrm{H}}^{(\mathrm{II})}$ and $\tilde{\mathrm{L}}^{(\mathrm{II})}$. $\tilde{\mathrm{H}}^{(\mathrm{II})}$ updates the multi-fidelity model while $\tilde{\mathrm{L}}^{(\mathrm{II})}$ offers initial starting points for the following optimisation level. This process is continued until all optimal solutions are found. It should be noted that the selection of the design variables in the HFM does not follow any particular order since the LFM encompasses the whole design space regardless of choice. It was

demonstrated that different selection orders do not affect the optimisation results. This modelling method can be incorporated into the probabilistic optimisation framework where the primary challenge is to deal with substantial high-fidelity FEM simulations.

Table 5.2: Formulations of multi-level multi-fidelity modelling method

	HFM at Level I	LFM at Level I
Design variables	$\mathrm{H}^{(\mathrm{I})} = [x^{(1)}, \cdots, x^{(m)}], \quad (m < n)$ $x^{(m+1)}, \cdots, x^{(n)}$ *are fixed*	$\mathrm{L}^{(\mathrm{I})} = \mathrm{X} = [x^{(1)}, x^{(2)}, \cdots, x^{(n)}]$ $\mathrm{H}^{(\mathrm{I})} \subset \mathrm{L}^{(\mathrm{I})}$
Number of Design variables	m	n (*all design variables*)
Optimal values	$\hat{\mathrm{H}}^{(\mathrm{I})} = [\hat{x}^{(1)}, \cdots, \hat{x}^{(m)}]$	$\hat{\mathrm{L}}^{(\mathrm{I})} = [\hat{x}^{(1)}, \cdots, \hat{x}^{(n)}]$
Corrected HFM &LFM	$\mathrm{X} = [\hat{\mathrm{H}}^{(\mathrm{I})}, \hat{x}^{(m+1)}, \cdots, \hat{x}^{(n)}]$	
	HFM at Level II	LFM at Level II
Design variables	$\mathrm{H}^{(\mathrm{II})} = [\hat{x}^{(m+1)}, \cdots, \hat{x}^{(l)}], \quad l < n$ $\hat{\mathrm{H}}^{(\mathrm{I})}$ *and* $\hat{x}^{(l+1)}, \cdots, \hat{x}^{(n)}$ *are fixed.*	$\mathrm{L}^{(\mathrm{II})} = [\hat{x}^{(m+1)}, \cdots, \hat{x}^{(n)}]$ $\hat{\mathrm{H}}^{(\mathrm{I})}$ *is fixed.* $\mathrm{H}^{(\mathrm{II})} \subset \mathrm{L}^{(\mathrm{II})}$
Number of Design variables	$l - m$	$n - m$
Optimal values	$\tilde{\mathrm{H}}^{(\mathrm{II})} = [\tilde{x}^{(m+1)}, \cdots, \tilde{x}^{(l)}]$	$\tilde{\mathrm{L}}^{(\mathrm{II})} = [\tilde{x}^{(m+1)}, \cdots, \tilde{x}^{(n)}]$
Corrected HFM &LFM	$\mathrm{X} = [\hat{\mathrm{H}}^{(\mathrm{I})}, \tilde{\mathrm{H}}^{(\mathrm{II})}, \tilde{x}^{(l+1)} \cdots, \tilde{x}^{(n)}]$	
	HFM at Level III	LFM at Level III
	Find the $\mathrm{H}^{(\mathrm{III})}$ *and* $\mathrm{L}^{(\mathrm{III})}$ *using the same manner.* $\hat{\mathrm{H}}^{(\mathrm{I})}$ *and* $\tilde{\mathrm{H}}^{(\mathrm{II})}$ *are fixed at this level.*	

5.2.3 Multi-Fidelity Modelling-Based Robust Design Optimisation Methodology

The developed multi-fidelity formulation is integrated with the RDO process, a type of probabilistic optimisation methods. Figure 5.5 shows how the developed optimisation framework combines with the multi-fidelity method introduced in the previous section. The framework consists of the multi-fidelity modelling process and the RDO process using the concept of multi-level optimisation. The primary steps that should be highlighted in this framework are to build a set of high-fidelity design parameters at each level and construct the multi-fidelity model for the RDO process. The framework is implemented as follows.

As shown in the figure and the table, the HFM and the LFM are defined by mesh convergence studies, and then each FEM model using the defined mesh sizes are created. The number of optimisation levels, k in the figure, and the number of design variables in the HFM, m and l in the table, should be determined by engineers depending on the characteristic and size of the optimisation problem. It should

be noted that the HFM has fewer design variables, $H^{(I)}$, while the LFM has all design variables in the first level, $L^{(I)}$. Once the training dataset is obtained using the two FEM models, the multi-fidelity model is constructed by the surrogate models using ANN of both the HFM and the LFM based on the set of design variables, $H^{(I)}$ and $L^{(I)}$, for the first level. The multi-fidelity RDO process is carried out by Monte Carlo Simulations (MCS) using the Sobol sampling technique and offers the optimal solutions for the first level, $\hat{H}^{(I)}$ and $\hat{L}^{(I)}$. The optimal solutions of design variables in HFM, $\hat{H}^{(I)}$, update the HFM while those in LFM, $\hat{L}^{(I)}$, provides starting points for the next level.

For example, there are two models in the first level of the RDO process, the HFM having only one design variable and the LFM having all design variables. Both surrogate models of the two fidelity models are constructed using ANN. It should be noted that other design variables apart from the selected design variable in the HFM are fixed at the initial mean value of each design variable. At the same time, the LFM examines the design spaces of those design variables that are not selected in the HFM. Hence, both the HFM and the LFM cooperate as a multi-fidelity model during the optimisation process. The initial starting points are chosen by sampling techniques to be evenly distributed in the design spaces, such as Optimal Latin Hypercube Sampling (OLHS) and Sobol sampling techniques. The LFM shares the selected design variables of the HFM during the RDO process. When the first level of the RDO process is completed, the chosen design variables in the HFM are corrected by the optimal solutions of the high-fidelity design variables at the level. The optimal solutions of the low-fidelity design variables also correct the other design variables in HFM that are not considered in the first level. These updated HFM and LFM are used in the next level of the RDO process. In this manner, the multi-fidelity optimisation process is continued until the multi-fidelity model finds the optimal solutions of all high-fidelity design variables.

This new multi-level multi-fidelity modelling-based RDO framework enables the use of a considerably smaller number of the HFM compared with conventional multi-fidelity methods. These computational time savings are obtained by the HFM having fewer design variables so that the number of high-fidelity FEM simulations is reduced, which is the main contribution of this multi-fidelity formulation. This method also provides the complementation of information loss using the LFM exploring all design spaces in the optimisation process, which the HFM omits depending on the selection of design variables. It should be highlighted that the proposed method takes more advantage of multi-fidelity modelling than the conventional multi-fidelity methods.

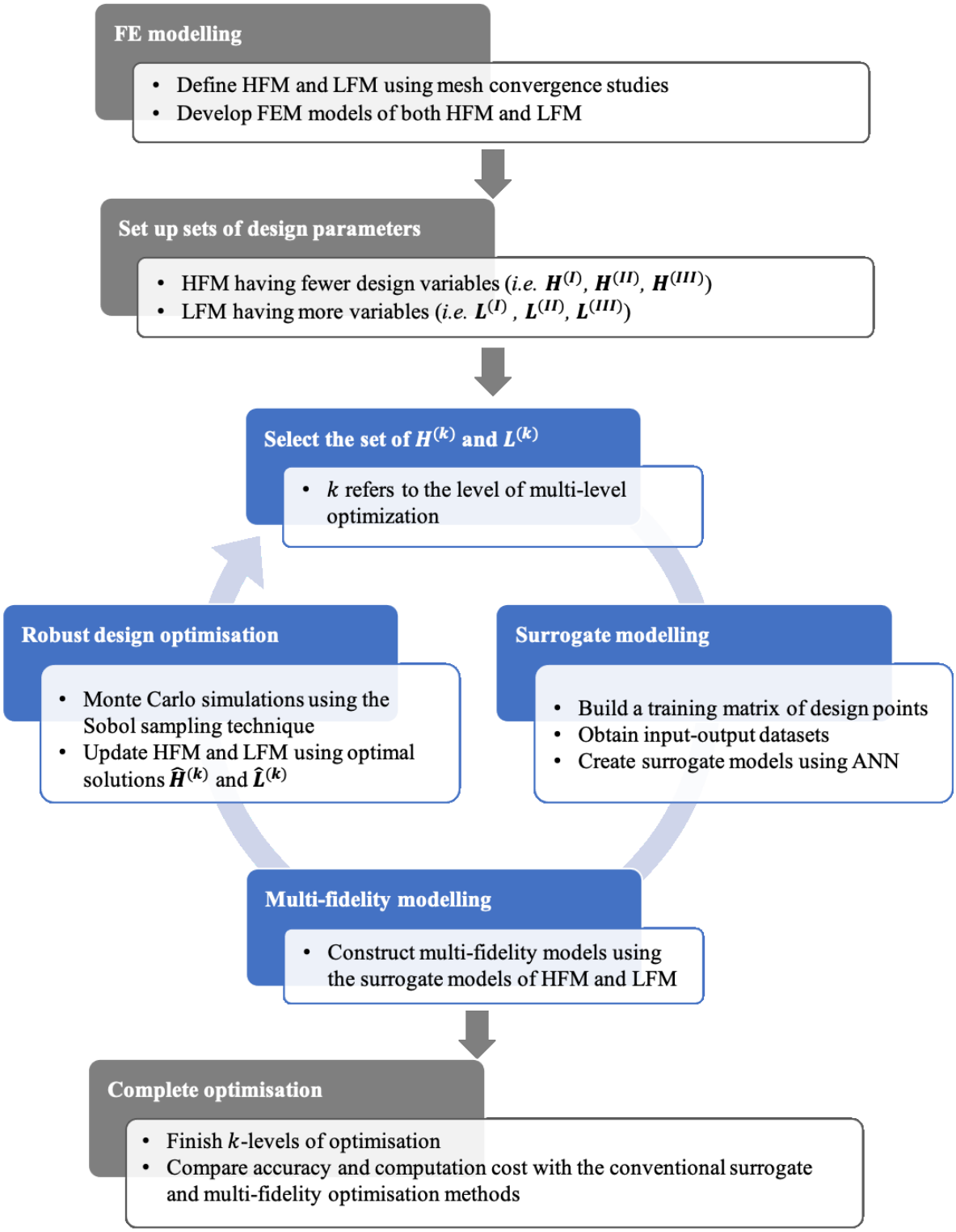

Figure 5.5: Multi-fidelity robust design optimisation framework

5.3 Finite Element Model of Composite Structures under Non-Linear Post-Buckling

In general, stringer-stiffened composite structures are represented by a thin skin structure that should be preserved using longitudinal stringers in compressive loading condition. The composite structures under compression are subjected to mechanical shortening. As the shortening rises along the longitudinal direction, transverse deflection appears all of a sudden at a certain shortening length or load level. This transverse deflection is called linear buckling that was considered in Chapter 4. If a composite structure is loaded beyond the linear buckling, the structure is under a post-buckling regime. Linear buckling is widely used in many industrial design problems because it conveniently provides a structural stability level to designers. However, it is acknowledged that the linear buckling load does not mean the maximum load for the structure to survive. Even though the applied load is a few times bigger than the buckling load, the failure of the structure might not happen even under the post-bucking region (88). The post-buckling strength capacity of the stringer-stiffened composite structures has been studied in the area of probabilistic design because it offers considerable benefits to reduce weight (4,14,15).

A non-linear FEM model is developed in this section in order to demonstrate the multi-fidelity RDO framework using the mono-stringer stiffened composite structure under a non-linear post-buckling regime. In the post-bucking regime, the buckled shape of the structure frequently varies as the compression load increases. Also, mode-switch or mode-jump, known by abrupt changes in the buckling mode, is observed when the compression load increases to a specific value. These structural instabilities found in the post-buckling regime lead to significant numerical challenges, which cannot be entirely caught by the use of quasi-static FEM analysis. The non-linear explicit dynamic analysis is a much better way to analyse the non-linear post-buckling (89). The forecast of the collapse load is considerably demanding because stresses along thickness in composites are sensitive. In general, the non-linear post-buckling analysis of composite structures includes both geometric and material non-linearity. It will mainly introduce how the parameters of constraints and objectives for the optimisation problem are determined. A good design approach for the mono-stringer stiffened structure aims that the stiffener buckles first before the skin is in the yield region. This enables the structure to achieve buckling without damage initiation in the skin.

There are several failure measures based on the stress or strain of a structure. One well-known failure criterion was proposed by Tasi and Wu (90) that can be applied to composite materials to predict the load-carrying capability of a structure. This criterion is useful to estimate the damage initiation of the structural failure process. The maximum stress failure criterion based on this theory is expressed as:

$$I_{Tsai-Wu} = F_1\sigma_{11} + F_2\sigma_{22} + F_{11}\sigma_{11}^2 + F_{22}\sigma_{22}^2 + F_{66}\sigma_{12}^2 + 2F_{12}\sigma_{11}\sigma_{22} < 1.0 \quad (5.6)$$

where $I_{Tsai-Wu}$ is a failure index, F is a Tsai-Wu coefficient, σ is stress, subscripts 1 and 2 refers to the longitudinal and transverse directions, respectively. If the $I_{Tsai-Wu}$ exceeds this criterion, it is presumed that the damage begins.

Each coefficient in equation (5.6) is defined as:

$$F_1 = \frac{1}{X_t} + \frac{1}{X_c}, \qquad F_2 = \frac{1}{Y_t} + \frac{1}{Y_c}, \qquad F_{11} = \frac{-1}{X_t X_c}, \qquad F_{22} = \frac{-1}{Y_t Y_c}, \qquad F_{66} = \frac{1}{S^2} \quad (5.7)$$

where X_t and X_c are maximum tensile and compressive strength in the longitudinal direction, Y_t and Y_c are maximum tensile and compressive strength in the transverse direction, S is the maximum shear strength in the XY plane.

Firstly, the FEM model of the mono-stiffened stringer composite structure is created to see the difference in structural behaviours depending on the use of cohesive elements. When the FEM model accounts for both the geometric and material non-linearity, the model should be created using the cohesive elements to consider progressive failures caused by interfacial debonding between the stringer and skin. Modelling these elements is a challenging task and leads to considerable computational cost due to the tiny element size of the cohesive zone. Suppose a FEM model without the cohesive elements can obtain an acceptable reaction force and failure index regarding the compressive load before the global buckling calculated using a FEM model with cohesive elements. In that case, the composite structure can be optimised geometrically non-linear region. The computational cost without the cohesive elements is a lot cheaper than that with the cohesive elements.

As shown in Figure 5.6, the same mono-stringer stiffened composite structure was considered in Chapter 4. This structure is clamped at both ends, but the left-hand end is free to move in the longitudinal direction (z-direction in the figure), which is the applied loading direction. Pure compression load is applied by increasing uniform displacement at the left-hand end. The material properties are the same as in Table 4.1. The failure parameters to calculate Tsai-Wu indexes are shown in Table 5.3.

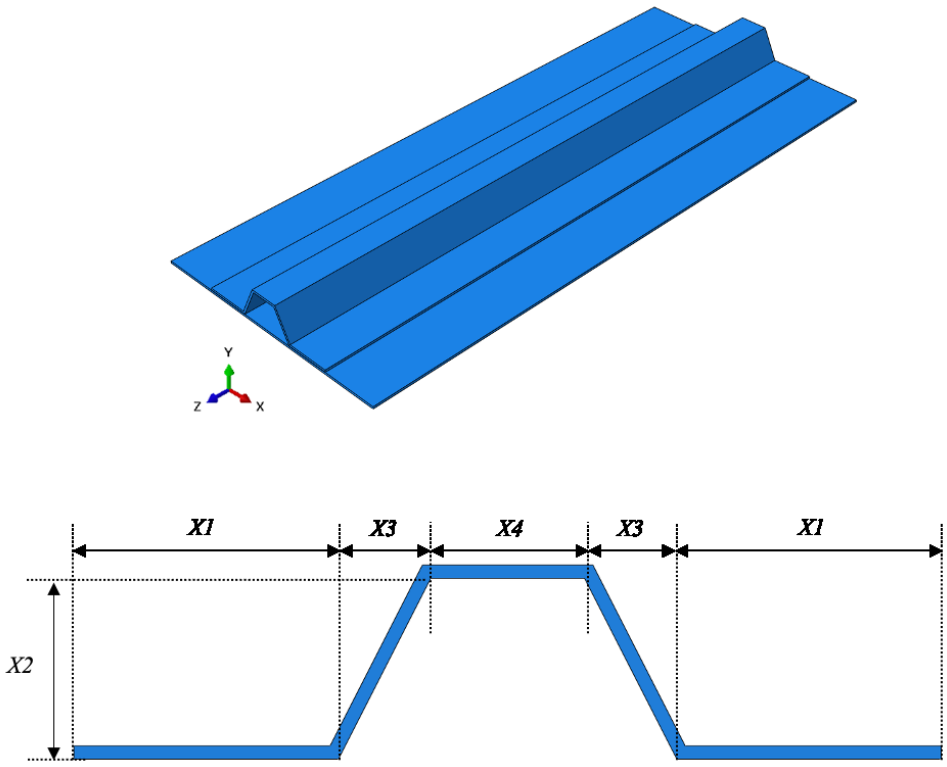

Figure 5.6: Mono-stringer stiffened composite panel

Table 5.3: Damage initiation parameters

Parameter	Value	
Longitudinal tensile strength (GPa)	X_t	2.9
Longitudinal compressive strength (GPa)	X_c	1.66
Transverse tensile strength (GPa)	Y_t	0.058
Transverse compressive strength (GPa)	Y_c	0.025
In-plane shear strength (GPa)	S	0.095

Table 5.7(top) compares the reaction force between two FEM models depending on the use of the cohesive elements. The reaction force between the two different FEM models is nearly identical before the global buckling happens at around the shortening length of 3.12 *mm* following the linear buckling at about the shortening length of 0.5 *mm*. The reaction force at the global buckling in the FEM model with cohesive elements was 134 *kN,* while the FEM model without cohesive elements showed 131 *kN*. The out-of-plane displacement of the panel at the global buckling is shown in Table 5.7(bottom). Hence, the shortening length of 3.0 *mm* is suitable for building up input and output datasets to construct the surrogate models. This shows that the cohesive elements are not necessary to consider when the global buckling is not a primary structural behaviour for the optimisation.

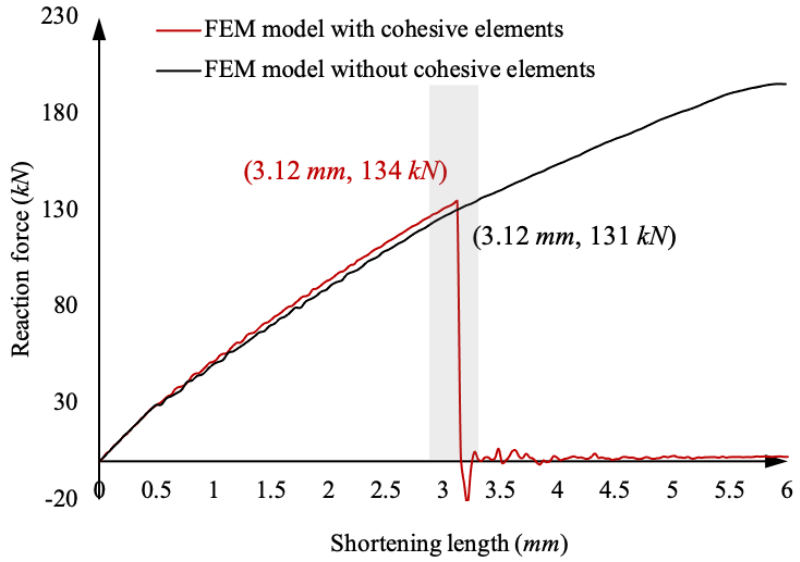

(top)

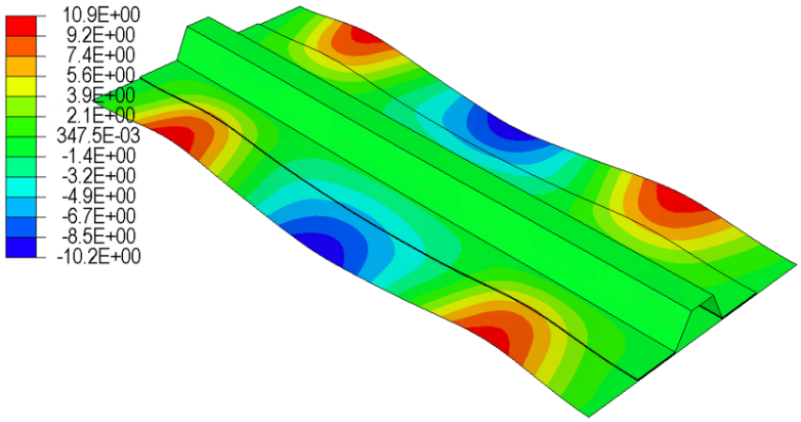

(bottom)

Figure 5.7: Reaction force comparison depending on the use of the cohesive elements (top) and the out-of-plane displacement at the shortening length of 3.12 *mm* (bottom)

The failure index calculated by Tsai-Wu theory is generally considered a constraint $I_{Tsai-Wu} < 1.0$ to track the failure process of the structure (4). It is analysed to see whether this index can be used as a parameter that the multi-fidelity model can manage. As a result, this index is not appropriate to construct a multi-fidelity model as follows.

- Computation time for post-processing: Tsai-Wu indexes should be extracted from all integration points in all lay-ups of each element. That causes enormous post-processing time much longer than high-fidelity FEM simulation time. For example, a single high-fidelity FEM simulation in this problem takes about 40 minutes; however, the computation time for post-processing takes more than 2 hours 30 minutes because the damage imitation has to be found

from millions of integration points in thousands of elements. This is not a reasonable computation time.

- Local value: Tsai-Wu index is a local value that is considerably dependent on the mesh. It is challenging to create a surrogate model using even the HFM because it is not easy to obtain an exact reaction force at the damage initiation point where the Tsai-Wu index equals one. Even though the loading speed for the explicit dynamic analysis decreases, it is not possible to capture the acceptable reaction force using the LFM. Figure 5.8(a) shows the response surface of the reaction force of the LFM having one design variable (*X1).* The low-fidelity surrogate model does not catch the response surface thoroughly because the response values from the FEM model change suddenly at the region between *X1* = 42.55 *mm* and *X1* = 43.45 *mm*. Although the surrogate model represents the responses of the FEM model except for the region, the error of the surrogate model is not good enough to construct the multi-fidelity model. Figure 5.8(b) highlights why the Tsai-Wu index cannot be considered a parameter of the surrogate model. The figure illustrates the maximum Tsai-Wu index regarding the shortening length of two FEM models between *X1* = 42.55 *mm* and *X1* = 43.45 *mm*. When the Tasi-Wu index equals one, the reaction force at the damage initiation point is obtained. However, it is challenging to collect proper reaction forces at the damage initiation point of different FEM models. In the figure, the damage of the FEM model of 42.55 *mm* occurs at the shortening length of 3.54 *mm*. Then corresponding reaction force of the model is obtained. When the FEM model of 43.45 *mm* undergoes a similar shortening length, its reaction force is not obtained since the Tsai-Wu index is about 0.999. Then the reaction force of the model is found at the shortening length of 4.41 *mm*, which leads to a sudden rise in the response surface. Hence, the reaction force at the damage initiation point is not appropriately captured, so adequate surrogate models are not obtained to construct the multi-fidelity model.

The damage initiation was not selected as a constraint based on these parameter studies, but the reaction force was determined as an objective function. The reaction force is not only a global index that can define the HFM and the LFM, but also a parameter to evaluate the global buckling. Hence, material properties were assumed in the linear elastic region, while geometric non-linearity was considered. Delamination that is caused by debonding between stringer and skin was not considered in this section.

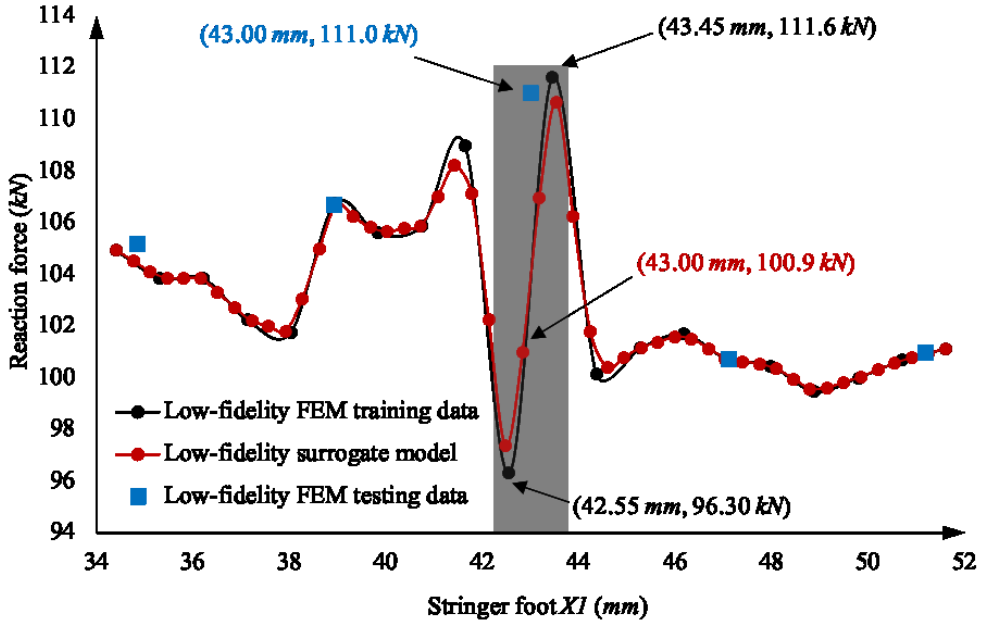

(a)

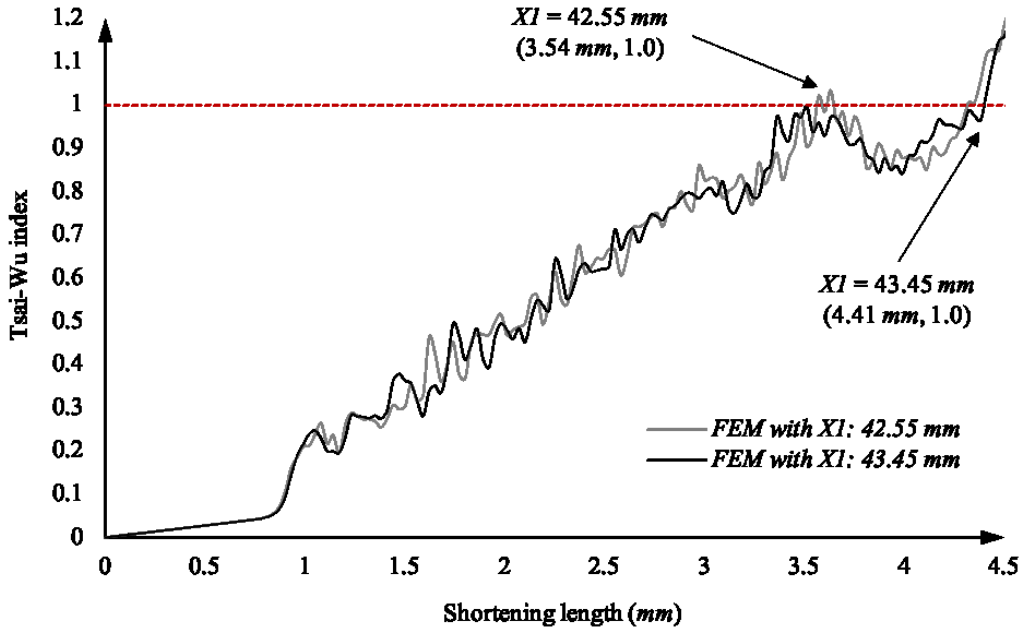

(b)

Figure 5.8: Response surface of the reaction force of LFM having one design variable $X1$ (a) and Tsai-wu index of low-fidelity FEM models between $X1 = 42.55$ *mm* and $X1 = 43.45$ *mm* (b)

5.4 Numerical Examples

Two engineering examples, DO and RDO, were carried out to design a mono-stringer stiffened composite structure using the developed multi-level multi-fidelity probabilistic optimisation method. Firstly, DO that is more straightforward than probabilistic optimisation methods was conducted to evaluate the feasibility of the developed method. Then, RDO was carried out to see whether this new method could be systematically incorporated into the probabilistic optimisation of composite structures considering design uncertainties. In these two engineering examples, the efficiency of the multi-fidelity model covering different design spaces between the HFM and the LFM was evaluated using the conventional optimisation method based on high-fidelity modelling-based surrogate models.

5.4.1 Optimisation of a Mono-Stringer Stiffened Composite Panel under the Non-Linear Post-Buckling Regime

As shown in Figure 5.6, the same mono-stringer stiffened composite structure considered in the example of Chapter 4. It should be noted that only the geometry of the stringer part is to be optimised, and the dimensions of the skin are fixed during the optimisation process. The number of the stringer geometry parameters is four (*X1, X2, X3* and *X4*) to validate the proposed method via a simple optimisation problem. The type of fidelity in these two examples was chosen by the level of discretisation of the FEM model. Figure 5.9 shows that the mesh grid of both the HFM and the LFM was defined by the size of 7.0 *mm* and 20.0 *mm*, respectively. The HFM and the LFM show about 10 % difference in accuracy, while the computational cost of the HFM is ten times higher than that of the LFM. These models were modelled using non-linear explicit dynamic finite element analysis using Abaqus (57). The FEM models consist of 4-node shell elements (S4R).

Two types of examples, i.e. DO and RDO, are conducted to demonstrate the developed multi-fidelity modelling-based probabilistic optimisation method embracing different design spaces between the HFM and the LFM. Each level has the same objective functions and constraints, whereas other design variables are considered at each level. The boundary conditions and loading conditions were not changed at every optimisation level. The optimisation aims to find a composite panel that shows minimum mass and maximum reaction force under the non-linear post-buckling regime. Through these two engineering examples, the potential application area of the developed optimisation method can be broadened to large-scale problems having substantially larger design spaces.

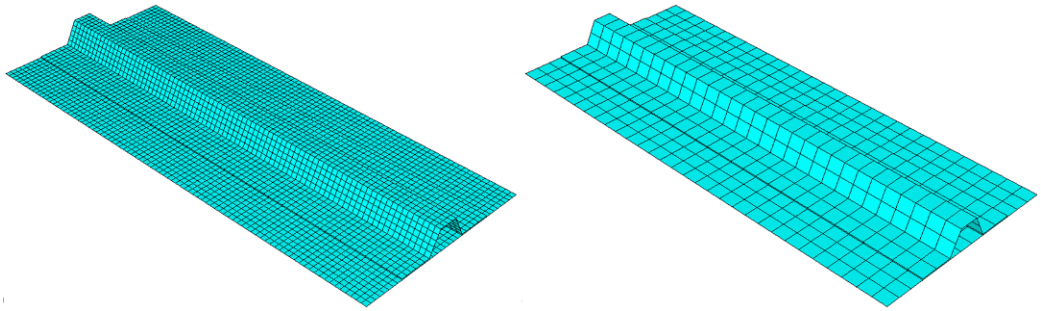

Figure 5.9: The HFM with 7 *mm* mesh size (left) and the LFM with 20 *mm* mesh size (right)

5.4.2 Multi-Fidelity Modelling-Based Deterministic Optimisation

DO was conducted to see if this method provides acceptable solution accuracy and computational time savings. In order to find the best solution, the Pareto front is found first, and then the optimum solution is selected by a decision-maker.

5.4.2.1 Problem Definition

As can be seen in Table 5.4, the mesh size of the HFM and LFM for finite element analysis were defined by of 7.0 *mm* and 20.0 *mm*, respectively. The design spaces of cross-section geometric parameters of the stringer are also denoted. The optimisation was carried out using the NSGA-II algorithm, a multi-objective method suited well for highly non-linear design spaces. The Pareto front is constructed by choosing the feasible non-dominated designs where each design point has the best combination of objective function values. The improvement of the objective is only possible by sacrificing the other objectives. Generation and population numbers for the optimisation process were chosen as of 20 and 12, respectively. These values were accomplished by the convergence study of the objective functions. Hence, the total number of FEM simulations at each level was 240. Different constraints for the HFM and the LFM are defined by the minimum reaction force that originates from the initial model. Both the HFM and the LFM have their objectives in the multi-fidelity modelling-based DO process.

Table 5.5 shows the selected design variables in the HFM at each level and the number of FEM simulations to build the multi-fidelity model. It is not surprising that the number of high-fidelity FEM simulations is dramatically reduced because the LFM examines the whole design spaces. This should compensate for the disparity of solution space caused by a lack of information of which the HFM does not cover the entire design spaces.

Table 5.4: DO – problem definition

Description		Value
Multi-fidelity model	HFM	$Mesh$: 7.0 mm
	LFM	$Mesh$: 20.0 mm
Design variables	Stringer foot	$34.4 \leq X1 \leq 51.6$
	Stringer height	$24.0 \leq X2 \leq 36.0$
	Distance between top and foot	$12.0 \leq X3 \leq 18.0$
	Stringer top	$25.0 \leq X4 \leq 30.0$
Optimisation method	NSGA-II	$Generation$: 20
		$Population$: 12
Constraints	HFM Reaction Force	$RF \geq 124.0\ kN$
	LFM Reaction Force	$RF \geq 130.0\ kN$
Objectives	HFM Mass	$minimise$
	LFM Mass	$minimise$
	HFM Reaction Force	$maximise$
	LFM Reaction Force	$maximise$

Table 5.5: Details of the multi-fidelity model

Level	HFM		LFM	
	Design variable	Number of FEM simulations	Design variable	Number of FEM simulations
I	X1	10	X1, X2, X3, X4	100
II	X2	10	X2, X3, X4	70
III	X3	10	X3, X4	40
IV	X4	10		-

5.4.2.2 Results

There are four objectives in this optimisation problem, and this is not easy to present using a 2D or 3D graph. However, a tabular form can be an option to represent the results concerning different levels and objectives. Table 5.6 shows the results of DO using the multi-fidelity model. This model has four geometric parameters to be optimised; hence the HFM has only one design variable at each optimisation level in this example. Table 5.6 highlights how both the HFM and the LFM embrace the whole design spaces as a multi-fidelity model. As mentioned before, two fidelity models share the design variable of *X1* during the optimisation process at Level I. The results of Level I show optimal values of both the HFM and the LFM that provide the maximum reaction force at the given shortening length. These optimal values correct both the HFM and the LFM; in particular, the optimal value of *X1* is fixed because this value is the best solution obtained from the high-fidelity design spaces. At Level II, the HFM takes the new design variable *X2*. At the same time, *X3* and *X4* are also updated by the optimal values of the LFM at Level II. The LFM has three design variables (*X2, X3* and *X4*) with the fixed value of *X1* from Level I. Similarly, Level II provides the optimal values that are *X2* of the HFM, and *X3* and *X4* of the LFM. They are also used to correct both the HFM and the LFM in Level II, and these updated models are utilised at Level III. In this manner, the final optimal solution is found when Level IV is completed.

Table 5.6: DO results - multi-fidelity model

Level	Design variable		Result				Optimal value (*mm*) for multi-fidelity model correction		Updated HFM by multi-fidelity model
			RF (*kN*)		Mass (*g*)				
	HFM	LFM	HFM	LFM	HFM	LFM	Value from HFM	Value from LFM	
I	X1	X1 X2 X3 X4	126.0	138.1	617	635	*X1*: 47.225	*X2*: 34.470 *X3*: 17.450 *X4*: 27.515	*X1*: 47.225 (Fixed) X3: 17.450 X4: 27.515
II	X2	X2 X3 X4	131.9	140.5	639	641	*X2*: 35.924	*X3*: 17.241 *X4*: 29.728	*X2*: 35.924 (Fixed) X4: 29.728
III	X3	X3 X4	132.9	140.4	642	641	*X3*: 17.493	X4: 29.282	*X3*: 17.493 (Fixed)
IV	X4	-	133.1	-	642	-	*X4*: 30.000	-	*X4*: 30.000 (Fixed)

Table 5.7: DO results accuracy by optimal solution (multi-fidelity vs. high-fidelity)

	Multi-fidelity model	High-fidelity FEM model
Maximum RF (*kN*)	133.1	132.8
Minimum mass (*g*)	642	640

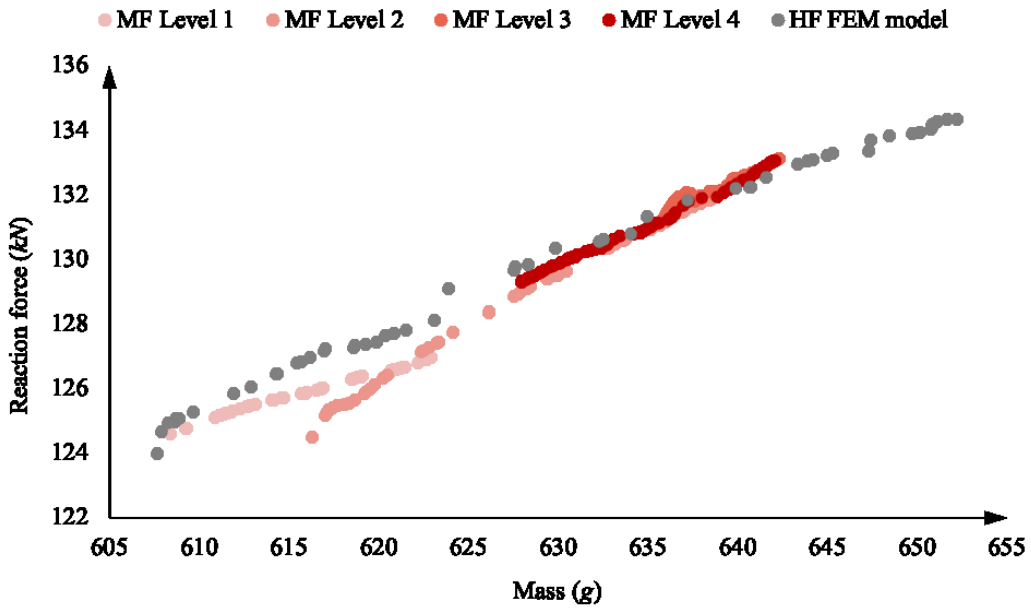

Figure 5.10: DO results comparison by the Pareto front (multi-fidelity vs. high-fidelity FEM)

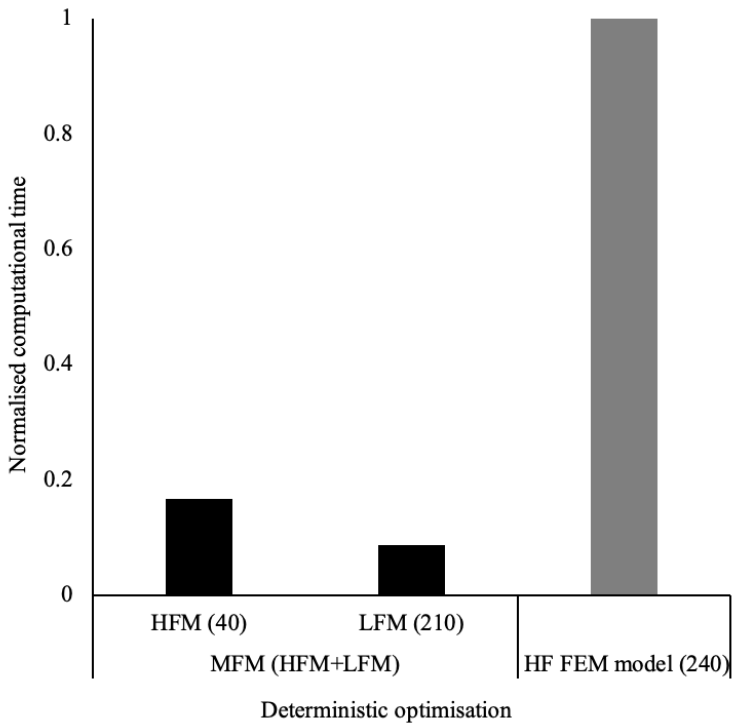

Figure 5.11: DO computation time comparison (multi-fidelity vs. high-fidelity)

Figure 5.10 shows the Pareto front of the optimisation using the multi-fidelity model. As shown in the figure, the Pareto front improves gradually in the direction in which the reaction force increases as the level goes up. The Pareto front of Level I is lower than that of Level II. The Pareto front of Level IV is higher than other levels. Table 5 shows that the maximum reaction force of each level increased from Level I (126.0 *kN*) to Level IV (133.1 *kN*). The conventional DO method using high-fidelity FEM models has the same objectives and constraints, and the Pareto front of this traditional method is shown in Figure 5.10. Table 5.7 presents the comparison of the final chosen solution between the multi-fidelity model and the high-fidelity FEM model to show how accurate the solution of the multi-fidelity model is. The reaction force of the multi-fidelity model indicates good agreement with that of the high-fidelity FEM model corresponding to a mass of 640 *g*.

The proposed multi-fidelity modelling method aims to provide the accuracy of solutions and computation time savings. It is significant to show how much of the computational time savings are obtained using the multi-fidelity model. Unfortunately, not many research works provide a standard guideline for the computational cost of multi-fidelity models (23). In general, the computational cost is defined by the number of high-fidelity FEM simulations because the primary goal of the multi-fidelity modelling method is to reduce the computational cost of the HFM using the LFM (48). In order to evaluate the computational cost of each model acceptably and diminish the computational noise, the total number of FEM simulations to create the multi-fidelity model is calculated and then it is normalised by the number of FEM simulations used for the conventional method (24). Figure 5.11 displays the computational time taken by the proposed method and the traditional method. In the

previous section, 40 design points of the HFM and 210 design points of the LFM were used to construct the multi-fidelity model. The conventional method was performed using 240 high-fidelity FEM models. The developed multi-fidelity model offers about 80 % of computation time savings compared to the traditional method using the high-fidelity FEM models.

5.4.3 Multi-Fidelity Modelling-Based Robust Design Optimisation

Through the benchmark study of DO in the previous section, the feasibility of this developed multi-fidelity modelling-based optimisation method was proven. This enables to broaden to the area of RDO using the developed method. This example aims to demonstrate how computationally economical and accurate this proposed optimisation method is to find a robust design solution.

5.4.3.1 Problem Definition

Table 5.8 shows the problem definition of this example. The details of the stiffened composite panel, the mesh size and the design space are the same as the previous example. The reason for the same design space with DO is that a robust solution might be far from the deterministic solution. Each design variable has its design uncertainty of 0.1 % as manufacturing tolerance (15). These uncertainties are described by the statistical characteristics, which is a form of the normal distribution having mean and standard deviation. The extra constraint was added by a maximum mass of 630 *g*. In particular, the objectives in Table 5.8 presents the features of RDO. Eight objectives for the optimisation process using the multi-fidelity model are to maximise reaction force while minimising mass and the standard deviations of both reaction force and mass. Table 5.5 shows the selection order of the design variable in the HFM at each level and the number of FEM simulations to create the multi-fidelity model. Figure 5.12 illustrates the multi-fidelity RDO framework using NSGA-II. In particular, robustness should be checked at each member of the population of each generation. MCS was utilised to specify the statistical moments of the objectives (mass and reaction force), which are caused by the uncertainties of random design variables. The Sobol sampling technique was considered that provides more uniformly distributed design points and more robust statistical predictions than the descriptive sampling technique (49). The maximum number of sampling points to check the robustness was 1,000. The convergence tolerance was 0.1 % of both mean and standard deviation compared to those associated values calculated every 25 sampled points. Hence, the maximum number of the multi-fidelity model's simulations was 120,000 during the robust optimisation process.

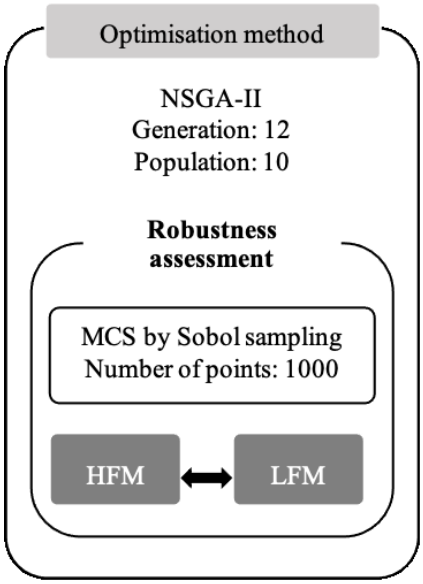

Figure 5.12: RDO structure

Table 5.8: RDO – problem definition

Description		Value
Multi-fidelity model	HFM	$Mesh$: 7.0 mm
	LFM	$Mesh$: 20.0 mm
Design variables	Stringer foot	$34.4 \leq X1 \leq 51.6$
	Stringer height	$24.0 \leq X2 \leq 36.0$
	Distance between top and foot	$12.0 \leq X3 \leq 18.0$
	Stringer top	$25.0 \leq X4 \leq 30.0$
Optimisation method	NSGA-II	$Generation$: 10 $Population$: 12
Analysis type	Monte Carlo simulation	$Sobol\ sampling$: 1000
Design uncertainty	Mean	Standard Deviation (Std. Dev.)
	$X1$	$0.001 \times X1$
	$X2$	$0.001 \times X2$
	$X3$	$0.001 \times X3$
	$X4$	$0.001 \times X4$
Constraints	HFM Reaction Force	$RF \geq 124.0\ kN$
	LFM Reaction Force	$RF \geq 130.0\ kN$
	Mass	$mass \leq 630\ g$
Objectives	HFM Mass	$minimise$
	LFM Mass	$minimise$
	Std. Dev. HFM Mass	$minimise$
	Std. Dev. LFM Mass	$minimise$
	HFM RF	$maximise$
	LFM RF	$maximise$
	Std. Dev. HFM RF	$minimise$
	Std. Dev. LFM RF	$minimise$

5.4.3.2 Results

Table 5.9 describes the optimisation results at each level and how the HFM is corrected by the optimal values from using the multi-fidelity model. In the first level, both the HFM and the LFM share the design variable of *X1* while exploring the entire solution spaces of all design variables using the LFM. Figure 5.13 depicts how this multi-fidelity modelling-based method probes the solution spaces when the HFM and the LFM have a different number of design variables in the optimisation process. Figure 5.13 (a) shows the optimal solution of *X1* using the HFM, which is reliable and accurate. At the same time, (b), (c) and (d) in the figure represent how the proposed multi-fidelity modelling method is implemented to embrace different solution spaces which are not included in the HFM during the optimisation process. It should be highlighted that these sub-figures offer what the different solution spaces are expected by the use of the LFM sharing the same *X1* with the HFM at the first level. As can be seen in the figure, the LFM helps the decision-maker travel the different solution spaces of *X2, X3* and *X4* corresponding to the variation of *X1* of the HFM. This information trade within the multi-fidelity model enables *X2, X3* and *X4* of the HFM to be updated by optimal values of the LFM having all design variables. Table 5.9 highlights that the reaction force of HFM at the given shortening length at each level rises gradually as the optimisation level is escalated.

Table 5.9: RDO results - multi-fidelity model

Level	Design variable		Result RF (*kN*)		Mass (*g*)		Optimal value (*mm*) for multi-fidelity model correction		Updated HFM by multi-fidelity model
	HFM	LFM	HFM	LFM	HFM	LFM	Value from HFM	Value from LFM	
I	X1	X1 X2 X3 X4	127.0	132.6	623	627	*X1*: 50.129	*X2*: 31.589 *X3*: 17.684 *X4*: 20.656	*X1*: 50.129 (Fixed) *X3*: 17.684 *X4*: 20.656
II	X2	X2 X3 X4	128.9	130.5	631	617	*X2*: 33.312	*X3*: 15.082 *X4*: 20.097	*X2*: 33.312 (Fixed) *X4*: 20.097
III	X3	X3 X4	128.8	134.5	630	625	*X3*: 18.000	*X4*: 23.640	*X3*: 18.000 (Fixed)
IV	X4	-	129.0	-	631	-	*X4*: 20.504	-	*X4:* 20.504 (Fixed)

Figure 5.14 illustrates the Pareto front at each level of the RDO process using the multi-fidelity model. As seen in the Pareto front in the figure, the reaction force in the post-buckling regime was improved as the level progressed while the constraint of mass was not violated. Finally, the Pareto front of the fourth level presents the maximum reaction force with a mass of 630 *g* to evaluate the efficiency of the proposed method using an equivalent approach. In the figure, the optimal solutions from the use of the surrogate model based on 200 design points of the HFM are also presented to verify the accuracy of the

multi-fidelity model. It should be noted that these Pareto fronts from both the proposed method and the conventional method show the acceptable range of difference among the optimal solutions.

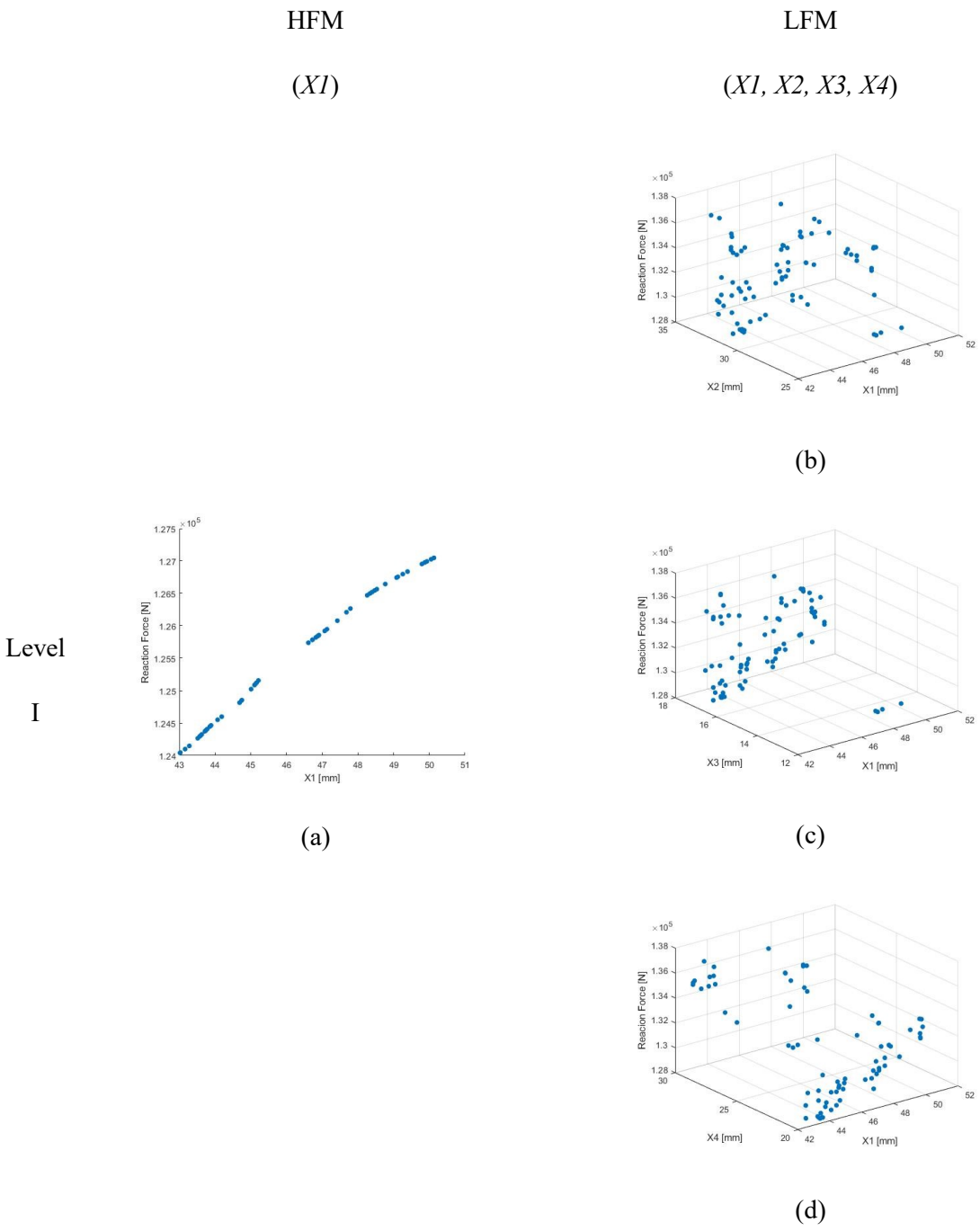

Figure 5.13: Multi-fidelity modelling based optimisation at Level I

Table 5.10 describes the robust results which are chosen by the optimal solutions. This RDO aims to maximise the mean values of mass and reaction force, and minimise the standard deviation values of mass and reaction force. Hence, two optimal robust designs were selected that show the maximum mean of reaction force and the minimum standard deviation of reaction force, respectively. These results were

compared with the results of the conventional high-fidelity surrogate model that have the same mass as those designs from the proposed method. The robust solution of the multi-fidelity model is close enough to that of the high-fidelity surrogate model. Both solutions for different objectives have an acceptable agreement with the solutions of the high-fidelity surrogate model. It should be highlighted that the optimal solutions of the multi-fidelity model are more robust, which the standard deviations of each reaction force are 0.30 and 0.18, respectively, compared to those of the high-fidelity surrogate model. This means that the proposed optimisation method using a lot smaller number of FEM simulations discovers a more robust design. This is also found at the standard deviation of mass.

In general, surrogate models are used to conduct RDO to overcome high computational cost, and these models are a kind of black-box form between design variables and responses. Hence, the final chosen solution that is produced by these surrogate models should be validated using proper calculation, such as a FEM solver or an experiment. Table 5.11 shows the solution accuracy of the surrogate model constructed using ANN. According to the table, the reaction forces of two surrogate models at the optimal design point are nearly identical to those calculated by the FEM solver. It should be remarked that the accuracy of the multi-fidelity model is better than that of the HFM.

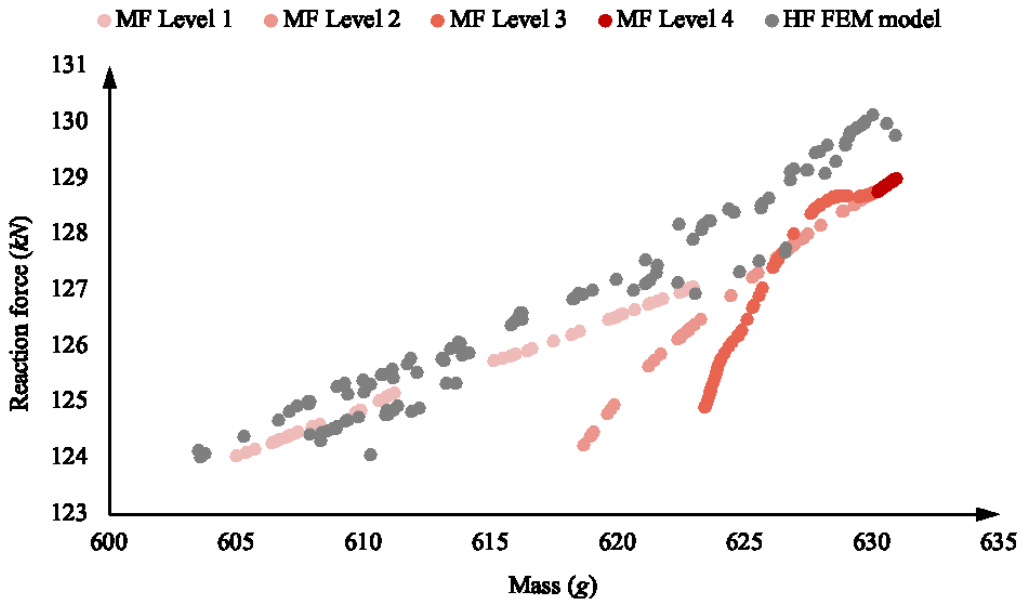

Figure 5.14: RDO result comparison by the Pareto front (multi-fidelity vs. high-fidelity)

Table 5.10: RDO results' accuracy by optimal solution (multi-fidelity vs. high-fidelity)

Model	X1 (*mm*)	X2 (*mm*)	X3 (*mm*)	X4 (*mm*)	RF (*kN*) Mean	Std. Dev.	Mass (*g*) Mean	Std. Dev.
Objective: maximise reaction force								
Multi-fidelity model	50.13	33.31	18.00	20.50	129.0	0.30	631	0.12
HF surrogate model	43.47	35.45	17.34	29.96	130.1	0.48	631	0.16
Objective: minimise standard deviation of reaction force								
Multi-fidelity model	43.01	32.67	15.38	22.28	124.8	0.18	608	0.15
HF surrogate model	40.87	35.44	13.95	24.42	124.7	0.24	611	0.15

Figure 5.15 shows the statistical characteristic of the reaction force depending on the type of optimisation. The optimal design, which is obtained by DO, represents a more significant mean value of reaction force than the robust design. In contrast, the deterministic design is more sensitive with a larger standard deviation. It is worthy to note that the variation of the robust design using the multi-fidelity model is smaller than that of the conventional method. Figure 5.16 illustrates the robust designs of the multi-fidelity model and the high-fidelity surrogate model when the objective function minimises the standard deviation of the reaction force under the post-buckling regime. Both robust designs in the figure have a nearly identical mean value of reaction force, while the dispersion of reaction force obtained by the multi-fidelity model is smaller than that of the conventional method. This is also clearly observed in Table 5.10. It should be noted that the accuracy of this multi-fidelity model is acceptable enough to be applied to RDO considering the design uncertainty of random design variables.

The computational time savings are presented in Figure 5.17. The computational cost to create the multi-fidelity model were normalised by the total computation time of the high-fidelity surrogate model. The developed multi-fidelity model incorporated 40 design points of the HFM and 210 design points of the LFM, while the high-fidelity surrogate model used 200 design points of the HFM. The computation time savings through the use of the multi-fidelity model was about 70 % compared to the computation time of the conventional high-fidelity surrogate method. It is critical to show how much the proposed multi-fidelity method is efficient than the different multi-fidelity methods covering the same number of design variables between the HFM and the LFM. These conventional multi-fidelity methods require the same number of FEM simulations between the HFM and the LFM to construct proper response correction surfaces that are the main component (47). Table 5.5 shows that the LFM having all design variables requires 100 design points of the LFM to construct the surrogate model having good quality. Hence, the HFM having all design variables should also need 100 design points of the HFM to create proper response correction surfaces. Figure 5.17 shows that the multi-fidelity model using the proposed method requires 40 design points of the HFM and 210 points of the LFM. The computational time

savings of the proposed method is about 50 % than the conventional multi-fidelity methods. These savings could be a dramatic improvement in conducting RDO of large-scale composite structures, which require the high computational cost to analyse even a single HFM. The final chosen deterministic and robust designs are illustrated in Figure 5.18.

Table 5.11: The accuracy of the surrogate model (ANN vs. FEM solver)

Model	X1 (*mm*)	X2 (*mm*)	X3 (*mm*)	X4 (*mm*)	RF (ANN)	RF (FEM Solver)	Error (%)
Multi-fidelity model	50.13	33.31	18.00	20.50	129.0 *kN*	129.0 *kN*	0 %
HF surrogate model	43.47	35.45	17.34	29.96	130.1 *kN*	128.2 *kN*	1.5 %

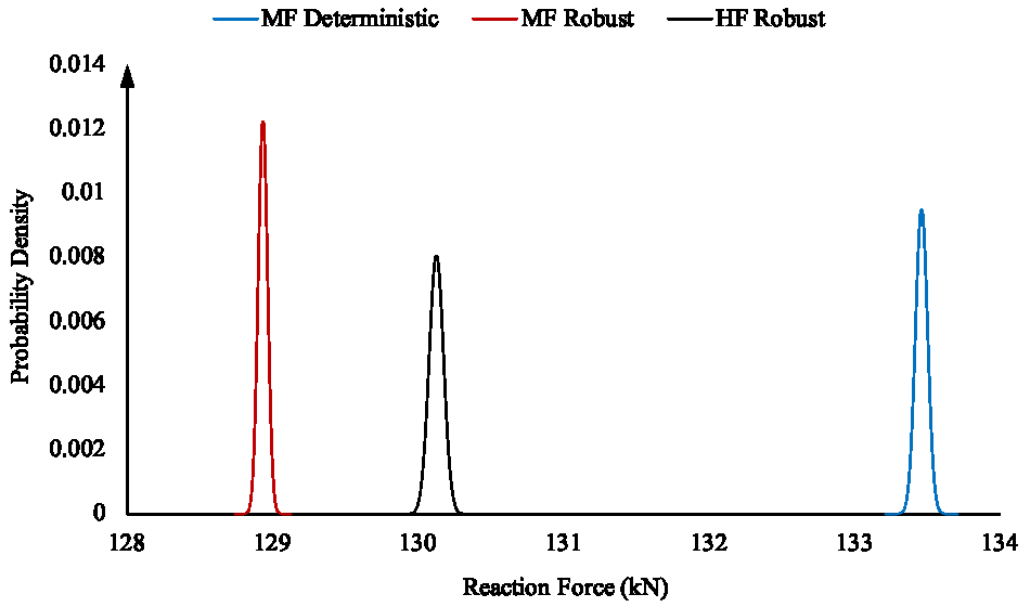

Figure 5.15: Statistical characteristic between DO and RDO: maximum reaction force

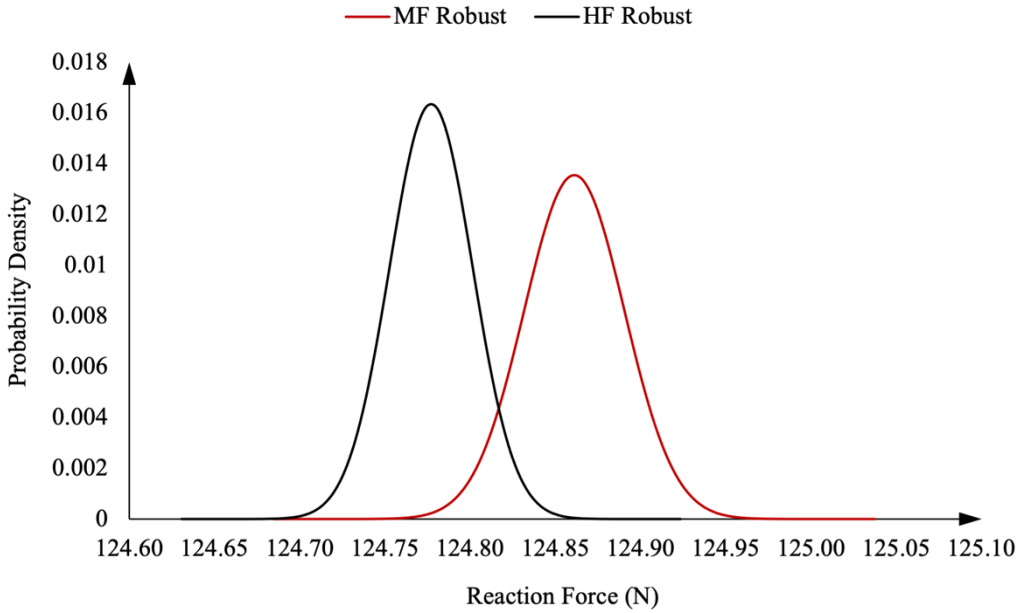

Figure 5.16: Statistical characteristic between multi-fidelity and high-fidelity surrogate model: minimum standard deviation of reaction force

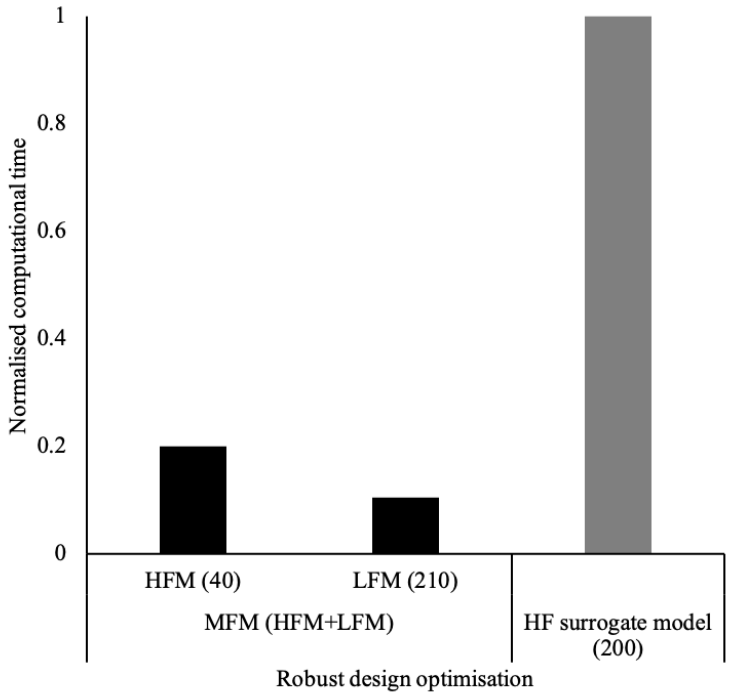

Figure 5.17: RDO computation time comparison (multi-fidelity vs. high-fidelity)

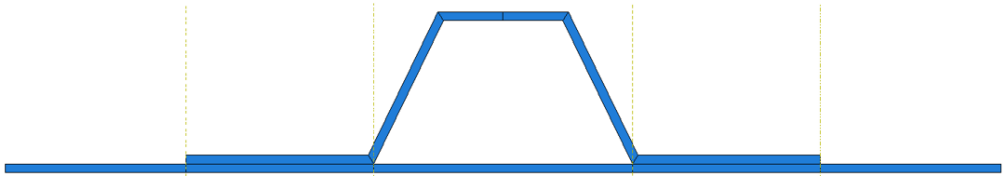

(top)

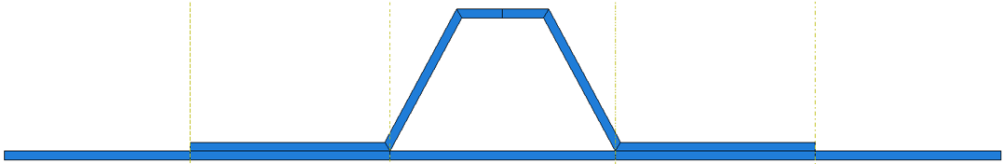

(bottom)

Figure 5.18: Chosen stringer geometry from DO (top) and RDO (bottom): maximum reaction force

5.5 Summary

In this chapter, the multi-level multi-fidelity modelling based optimisation framework is presented. It is demonstrated by RDO of a mono-stringer stiffened composite panel under the non-linear post-buckling regime. It should be noted that the HFM has a fewer number of design variables, whereas the LFM has more design variables in this multi-fidelity modelling method. This is one of the main contributions of this work compared to conventional multi-fidelity modelling methods that require the same number of design variables between the HFM and the LFM to create the correction response function. During this optimisation process, the HFM having fewer design variables provides an accurate solution to correct the multi-fidelity model. At the same time, the LFM having more design variables explores the solution space of all design variables while sharing the design variables with HFM. In particular, the constructed multi-fidelity model using ANN is incorporated with the multi-level optimisation approach to deal with large-scale composite problems with many design spaces. The results of two engineering examples were evaluated in terms of solution accuracy and computational time savings. The optimal solutions of DO and RDO using the multi-fidelity model were nearly identical to those using the conventional method. It should be highlighted that the standard deviation of the optimal solution using the multi-fidelity model was more robust than that of the optimal solution using the conventional high-fidelity surrogate model. Computational efficiency was highlighted by the use of normalisation between the number of FEM simulations to create the multi-fidelity model and the number of FEM simulations to generate conventional high-fidelity surrogate models, as well as a comparison with a traditional multi-fidelity model with the same number of design variables for the HFM and the LFM. The multi-fidelity model was constructed using both 40 design points of the HFM and 210 design points of the LFM. In contrast, the conventional method for DO and RDO used 240 and

200 design points of the HFM, respectively. At least 50 % of computational time savings were obtained using this new multi-level multi-fidelity modelling method. Through these demonstrations, the multi-fidelity modelling based optimisation framework was proven as a new optimisation method that the HFM and the LFM have different design spaces during the optimisation process. The developed multi-fidelity modelling-based probabilistic optimisation framework shows excellent potential for large-scale composite problems considering design uncertainties.

6 Multi-Fidelity Probabilistic Optimisation of Composites for Thermomechanical Loading using Gaussian Process Based on Sparse High-Fidelity Information

Thermomechanical loading may lead to a premature structural collapse in composite materials used in different engineering structures. By comprehensive awareness of the thermomechanical loading behind the structural stability, the stability of a designed composite system can be more precisely secured. As industrial demands for energy efficiency and low carbon emissions are rising, structures using these composite materials are applied to a broad range of engineering fields due to their fundamental advantages providing high strength and lightweight. For example, composite structures are used in aircraft structural design because high-speed and lightweight aircraft requirements are significantly growing. Lightweight structures are generally vulnerable to buckling under extreme environmental conditions. Hence, it is essential that buckling is taken into account at the design stage of composite structures. In particular, thermomechanical buckling should not be ignored since thermal loading can cause considerable damage followed by mechanical loading for a high-speed aircraft. Many design optimisation approaches for composite structures have been developed to consider both thermal and mechanical loading. However, the limitation of these current approaches is only based on Deterministic Optimisation (DO) that could cause conservative composite designs because they do not consider design uncertainties associated with the product's lifecycle.

In common, these uncertainties are considered by the use of safety factors that could result in a waste of material resources caused by increased weight. An ideal optimisation approach to consider the design uncertainties is the probabilistic design optimisation, including Reliability-Based Design Optimisation (RBDO) and Robust Design Optimisation (RDO). These optimisation approaches allow structural optimisation to deliver low carbon emissions and energy efficiency since they bring reliable and robust

design solutions for the entire lifecycle of structures. In specific, RBDO aims to minimise the probability of failure so that the final design satisfies reliability requirements based on the probabilistic characteristics of the design variables. This optimisation approach focuses on the safety of structures when they are exposed to catastrophic and extreme circumstances. So far, the vast majority of research works have considered the thermal buckling behaviours of composite and metallic structures caused by thermal expansions without considering mechanical loading (91–95). Only a few research works have studied the thermomechanical buckling behaviours of composite structures. They have been demonstrated by structural analysis and deterministic design problems that do not consider the design uncertainties (16,18). Although the probabilistic design optimisation has been studied for designing different composite structures (4,14,15,20,24,42), there has not been a research work that carries out the probabilistic design of composite structures under thermomechanical loading. It is not surprising that the computational cost of these design problems is higher than considering a single loading.

In the design area of composite structures, RBDO considers different design uncertainties depending on the objectives of optimisation problems. It highlights how different reliable designs rely on the consideration of design uncertainties compared with deterministic designs. These design uncertainties commonly involve mechanical properties and geometric parameters of structures associated with the design and manufacturing process (14,15,67,96–98). As discussed in previous chapters, the probabilistic design optimisation process encounters significant computational challenges led by statistical calculations regarding the design uncertainties. In particular, RBDO carries out the reliability assessments to obtain a prescribed reliability level, which requires millions of computationally expensive simulations such as Finite Element Method (FEM) simulations. An attempt to reduce the high computational cost caused by considering the design uncertainties involves the use of surrogate models (4,10,99). These models have been widely used in the various probabilistic optimisation process for composite structures while providing a certain level of computational gains. However, the computational cost is still the main obstacle to carry out the RBDO of complex and large-scale composite structures. It is not surprising that even a single FEM simulation in these problems is too computationally expensive to create the surrogate models.

An approach that accounts for the prohibitive computational challenge involves the use of a multi-fidelity modelling approach that offers substantial computational time savings compared with the traditional single-fidelity surrogate modelling approach. This multi-fidelity modelling approach allows hundreds number of computationally economical Low-Fidelity Model (LFM) data points to boost the accuracy of tens of High-Fidelity Model (HFM) data points, accurate but computationally demanding. In particular, the multi-fidelity modelling approach enables the probabilistic optimisation to account for the design uncertainties that conventional surrogate modelling approaches are still struggling with (12,23,48). As introduced in Chapters 4 and 5, traditional multi-fidelity approaches using Artificial Neural Networks (ANN) or Response Surface Method (RSM) require that the HFM and the LFM carry

the same number of training points to build correction response surfaces (24,47). This may lead to additional high-fidelity FEM simulations that designers do not want to count. In contrast, some multi-fidelity approaches allow the HFM and the LFM to embrace a different number of training points since they don't build the correction response surfaces. They are mainly derived using Gaussian Process (GP) (54) and these approaches are combined with the linear autoregressive information fusion scheme (63,64). One notable example is Forrester et al. (63), where a multi-fidelity optimisation using co-kriging was developed to consider the linear correlation between different fidelity levels using GP. The authors demonstrated the multi-fidelity method using composite design problems in which the fidelity is defined by the linearity level of the numerical solver. Another notable example is Perdikris et al. (100,101), where a non-linear information fusion algorithm was presented to capture non-linear correlations during the multi-fidelity modelling process. The algorithm was based on GP regression and the non-linear autoregressive scheme to consider the complex non-linear correlation between different fidelity models. The algorithm offered a lot higher accuracy when the two fidelity models have non-linear correlations across the whole design space. This can contribute to deal with a challenging gap in the response surface caused by different FEM mesh size between the HFM and the LFM. This gap is not captured using even hundreds of the LFM data points when traditional multi-fidelity approaches carry out structural optimisation problems. Due to its many advantages, GP considering linear correlation has found extensive use with different optimisation problems, with notable examples being (63,75). However, its application considering the non-linear information fusion algorithm to the structural optimisation problems has not received attention.

The multi-fidelity modelling approaches for probabilistic optimisation developed so far request that the HFM and the LFM explore the same dimension of design spaces. This causes enormous computational cost when there are many design variables in large-scale composite design problems. As presented in Chapter 5, the multi-level multi-fidelity modelling method allows two different fidelity models to embrace different design spaces during the optimisation process. This method was not suitable to carry out probabilistic design problems that show the non-linear correlation between the HFM and the LFM. The method does not use GP considering the correlation between the two models but uses ANN analysing input-output values to construct the multi-fidelity model. This drawback could be resolved by the use of both GP and the non-linear information fusion algorithm. The improved multi-fidelity method could enable the LFM to represent the response surfaces using the HFM covering part of the entire design space. This research work aims to develop a multi-fidelity probabilistic optimisation of composite structures under thermomechanical loading using GP for the first time. Before the work presented in this thesis, no work has been carried out by the research community on the topic of multi-fidelity probabilistic optimisation of composite structures under thermomechanical loading.

In summary, the work presented in this chapter aimed to develop a novel multi-fidelity methodology for:

- **Formulating a multi-fidelity method.** The multi-fidelity formulation allows the HFM and the LFM to have a different number of design variables during the optimisation process. Specifically, the HFM supervises only a small part of the entire design space, while the LFM encompasses the whole design space. The primary contribution of this formulation allows the high-fidelity training dataset to be collected by different sampling levels, such as dense and sparse. This offers a very efficient means to construct a multi-fidelity model.
- **Combining the non-linear information fusion algorithm with the multi-fidelity modelling formulation.** Previous works on this topic have exclusively involved the use of high-fidelity information covering the same dimension of design space as low-fidelity information. One drawback of this concept causes extra computational cost. The proposed multi-fidelity probabilistic framework avoids this problem by supervising part of the whole design space using densely distributed high-fidelity information while covering the entire design space using sparsely distributed one. Then the non-linear information fusion algorithm using GP calculates the correlation between the HFM and the LFM, and then incorporates the multi-fidelity RBDO framework to construct a more accurate multi-fidelity model.
- **Demonstrating a novel multi-fidelity probabilistic optimisation method.** As part of this approach, a new multi-fidelity methodology is developed. This methodology is demonstrated by the RBDO of composite structures under thermomechanical loading for the first time. The accuracy and computational efficiency are evaluated through this numerical example when the composite structure is loaded by mechanical loading and thermal loading.

This chapter will begin by reviewing the fundamental theory of thermomechanical buckling and non-linear information fusion algorithm. Then, the developed multi-fidelity method will be introduced, including multi-fidelity formulation and RBDO framework. A numerical example of a composite structure under thermomechanical loading is presented towards the end of this chapter. The work presented in this chapter is based on the work presented by Yoo et al. in (102).

6.1 Multi-Fidelity Modelling-Based Probabilistic Optimisation

A novel multi-fidelity modelling method, which blends an HFM and an LFM based on a proper correction using high-fidelity information, has been developed to improve the computational efficiency of the probabilistic optimisation process. Since conventional multi-fidelity modelling approaches involve the HFM embracing the same dimension of design spaces with the LFM, the computational cost of such modelling methods is exceptionally high to carry out the probabilistic design of large-scale composite structures. This requires that the HFM calls for the same number of high-fidelity FEM simulations as the LFM to build correction response surfaces. It should be noted that even mesh

generation for the HFM caused by changes in geometrical random design variables can bring about substantial computational cost. A new multi-fidelity modelling-based probabilistic optimisation to supervise different design spaces between the HFM and the LFM is developed to mitigate the computational cost in this section. This developed method begins with the critical idea about maximising the use of low-fidelity information while minimising the use of high-fidelity information. The number of high-fidelity design points relies on the dimension of design spaces to be covered. When the HFM has a small number of design variables and the LFM has all design variables, the computational cost to construct the multi-fidelity model can be significantly reduced. In particular, the multi-fidelity modelling method is integrated with multi-level optimisation to manage large-scale composite design problems. As introduced in Chapter 5, the multi-level multi-fidelity modelling method for the probabilistic optimisation separately creates two surrogate models of the HFM and the LFM with different design variables (42). This formulation is combined with the RDO of composite structures under the non-linear post-buckling regime without considering the correlation between the two different fidelity models. The proposed multi-fidelity modelling formulation in this section extends the application area to composite structures under thermomechanical loading by considering the correlation between the HFM and the LFM.

6.1.1 Theory of the Non-Linear Information Fusion Algorithm

The presented multi-fidelity modelling method in this chapter employs the non-linear information fusion algorithm (101), which is also called the Non-linear Auto-Regressive Gaussian Process (NARGP), to consider the non-linear correlation between different fidelities. The NARGP is put forth to improve the linear autoregressive GP scheme developed by Kennedy and O'Hagan (64). As discussed in Chapter 3, the autoregressive GP (denoted by AR) is extended by the GP regression to construct a probabilistic model that consists of different fidelity models, such as the HFM and the LFM, as the generalised form is expressed in equation (6.1).

$$f_{HF}(X) = z_{LF}\big(f_{LF}(X)\big) + f_{\delta}(X) \tag{6.1}$$

where f_{HF} and f_{LF} are GP created using the training datasets of the HFM and LFM, respectively. They are usually assigned a zero mean prior $f \sim GP(f|0, k(\mathrm{x}, \mathrm{x}'; \theta))$. k is a proper covariance function defined using hyper-parameters θ that produce a covariance matrix $K_{ij} = k(\mathrm{x}_i, \mathrm{x}_j; \theta)$ between different input data $(\mathrm{x}_i, \mathrm{x}_j)$. These hyper-parameters are obtained using the maximum-likelihood estimation (54). z_{LF} is an unknown function that describes the correlation between the outputs of the HFM and the LFM. f_{δ} is a GP representing the difference between $z_{LF}\big(f_{LF}(X)\big)$ and $f_{HF}(x)$.

The NARGP harnesses the functionality of the linear AR without compromising its analytical compliance and straightforward algorithm structure. In particular, $z_{LF}\left(f_{LF}(X)\right)$, the functional composition of two GP priors, is characterised by the so-called deep GP. This does not allow the posterior of f_{HF} is Gaussian distribution. To deal with this problem, the NARGP substitutes the GP posterior of low-fidelity predictions, $f_{*LF}(x)$, with the GP prior, f_{LF}, put forth by Le Gratiet and Garnier (103). The principal significance of this non-linear information fusion algorithm is that z_{LF} and f_{δ} in equation (6.1) incorporates a function, g_{HF}, as described in equation (6.2).

$$f_{HF}(X) = g_{HF}(X, f_{*LF}(X)) \tag{6.2}$$

where $g_{HF} \sim GP(f_{HF}|0, k_{HF_g}((X, f_{*LF}(X)), (X', f_{*LF}(X'); \theta_{HF}))$ is a GP that is characterised by a covariance k_{HF_g} of low-fidelity predictions between different input data (X, X').

The main difference in comparison with the linear AR in equation (6.1) is that f_{δ} is implicitly taken in equation (6.2). Likewise the linear AR, the NARGP under the assumption of noiseless data implies the Markov property as in equation (6.3), which translates into presuming that given the nearest point of the LFM's posterior, $z_{LF}\left(f_{*LF}(X)\right)$, there is nothing to learn more about $f_{HF}(X)$ from any other output $z_{LF}\left(f_{*LF}(X')\right)$ (64). The assumption of nested training datasets allows the high-fidelity training data, X_{HF}, to be a subset of the low-fidelity training data, X_{LF}.

$$\mathrm{cov}\left\{f_{HF}(X), z_{LF}\left(f_{*LF}(X')\right) | z_{LF}\left(f_{*LF}(X)\right)\right\} = 0, \qquad \forall X \neq X' \tag{6.3}$$

It should be noted that the training of g_{HF} using the HFM becomes more straightforward to conduct the maximum-likelihood estimation because the posterior of the LFM, $f_{*LF}(X_{HF})$, is a known deterministic quantity. The covariance function of g_{HF} also contribute to the improvement in the NARGP. The function is broken down to consider precise correlations between different input data, as shown in equation (6.4).

$$k_{HF_g} = k_{HF_\rho}(X, X'; \theta_{HF_\rho}) \cdot k_{HF_f}(f_{*LF}(X), f_{*LF}(X'); \theta_{HF_f}) + k_{HF_\delta}(X, X'; \theta_{HF_\delta}) \tag{6.4}$$

where k_{HF_ρ}, k_{HF_f} and k_{HF_δ} are the covariance functions of the scaling factor, function value from low-fidelity GP model and the difference between two different data, respectively. θ_{HF_ρ}, θ_{HF_f} and θ_{HF_δ} are the hyper-parameters of each covariance function, which are obtained by the high-fidelity training dataset using the maximum-likelihood estimation as introduced in Chapter 3.

The covariance function is selected by the square exponential function in equation (3.11). Hence, the NARGP in equation (6.2) enables the LFM's posterior, f_{*LF}, to be projected onto a high-fidelity response, f_{HF}, through a flawless mapping. This allows the multi-fidelity model to capture the non-linear correlations between the HFM and the LFM. Then, the posterior distributions from the multi-

fidelity model are the predictive mean, $\mu_{*MF}(X_*)$, and variance, $\sigma^2_{*MF}(X_*)$. They are calculated using Monte Carlo simulation that is expressed by:

$$\begin{aligned} p(f_{*HF}(X_*)) &\coloneqq p(f_{HF}(X_*, f_{*LF}(X))|f_{*LF}, X_*, Y_{HF}, X_{HF}) \\ &= \int p(f_{HF}(X_*, f_{*LF}(X))|Y_{HF}, X_{HF}, X_*)\, p(f_{*LF}(X_*))dX_* \end{aligned} \tag{6.5}$$

where X_* is a new test point, f_{HF} is the GP of the multi-fidelity model, f_{*LF} is the GP model of the LFM, Y_{HF} and X_{HF} are the high-fidelity training (input/output) data points. The multi-fidelity model, which provides the predictive mean, $\mu_{*MF}(X_*)$, is incorporated into the proposed multi-fidelity probabilistic optimisation framework.

6.1.2 Sampling Strategy for High- and Low-Fidelity Information

As shown in Figure 6.1, the formulation aims to maximise the use of the LFM while providing precise corrections using a small number of high-fidelity training data points. Here, the HFM concentrates on the design spaces of few selected variables at each probabilistic optimisation level. In order to facilitate this purpose, an effective sampling strategy has been employed in this work that the principle is based on standard filling sampling strategies such as uniform random sampling or Optimal Latin Hypercube Sampling (OLHS). In general, these space-filling strategies are typically implemented to create a multi-fidelity model due to their nature offering evenly distributed training data points without gaps or clusters in the whole design space. It is not surprising that the performance of multi-fidelity models relies on how to collect the training data points using an appropriate sampling strategy.

Figure 6.1 illustrates the effective sampling strategy consisting of different sampling degrees to obtain the training data points, including dense and sparse sampling. Each sub-figure in the figure shows a plan view of distribution relying on different design variables to highlight such sampling strategy. Figure 6.1(a) presents the distribution of the dense sampling for the selected design variables in the HFM, $\mathrm{H_d}$ in Table 6.1, which refers to collecting evenly enough distributed training data points to embrace the design space of $\mathrm{H_d}$. It should be noted that traditional multi-fidelity modelling methods exploit the training datasets sampled as dense as possible. In comparison, Figure 6.1(b) and (c) display the distribution of the sparse sampling for other design variables in the HFM, $\mathrm{H_s}$ in Table 6.1, which does not thoroughly cover the design space with a biased distribution caused by the insufficient number of training data points. Still, it can provide scarce information within the same sampling size for $\mathrm{H_d}$. Standard regression methods, including GP or artificial neural networks, commonly require the number of training data points ten times more than the dimension of design space (104). For example, if there are three design variables in a structural optimisation problem in Figure 6.1, the number of training data points, also called the dense sampling in this work, should be at least thirty.

This sampling scheme offers a launchpad for the multi-fidelity formulation to reduce the high-fidelity FEM simulations compared with other multi-fidelity modelling methods. Consider the illustrative example with three design variables in Figure 6.1. The HFM focuses on only two design variables ($H_d = [X1, X2]$). In that case, the number of high-fidelity training data points is significantly reduced because they cover two-dimensional design space. Another design variable ($H_s = [X3]$) not selected in H_d is randomly sampled within the number of training data points for H_d, and then added to the high-fidelity training dataset. This allows the high-fidelity training dataset to provide the dense information of the selected design variables, H_d, as well as sparse information of other design variables, H_s, without causing extra computational cost. In the meantime, the LFM exploring the entire design space in Figure 6.1(d), (e) and (f) collects enough information as dense as possible to obtain a good quality. The low-fidelity training dataset shares the high-fidelity training data points, as displayed by a blue box in those sub-figures. This allows the NARGP to calculate the correlations using these constructed high- and low-fidelity training datasets based on equation (6.4). Then, it creates the multi-fidelity model using equation (6.2), which can predict output responses, $\mu_{*MF}(x_*)$, concerning the variation of design variables correctly. It should be highlighted that the number of high-fidelity training data points in this sampling strategy becomes a lot less than thirty, which the traditional methods require.

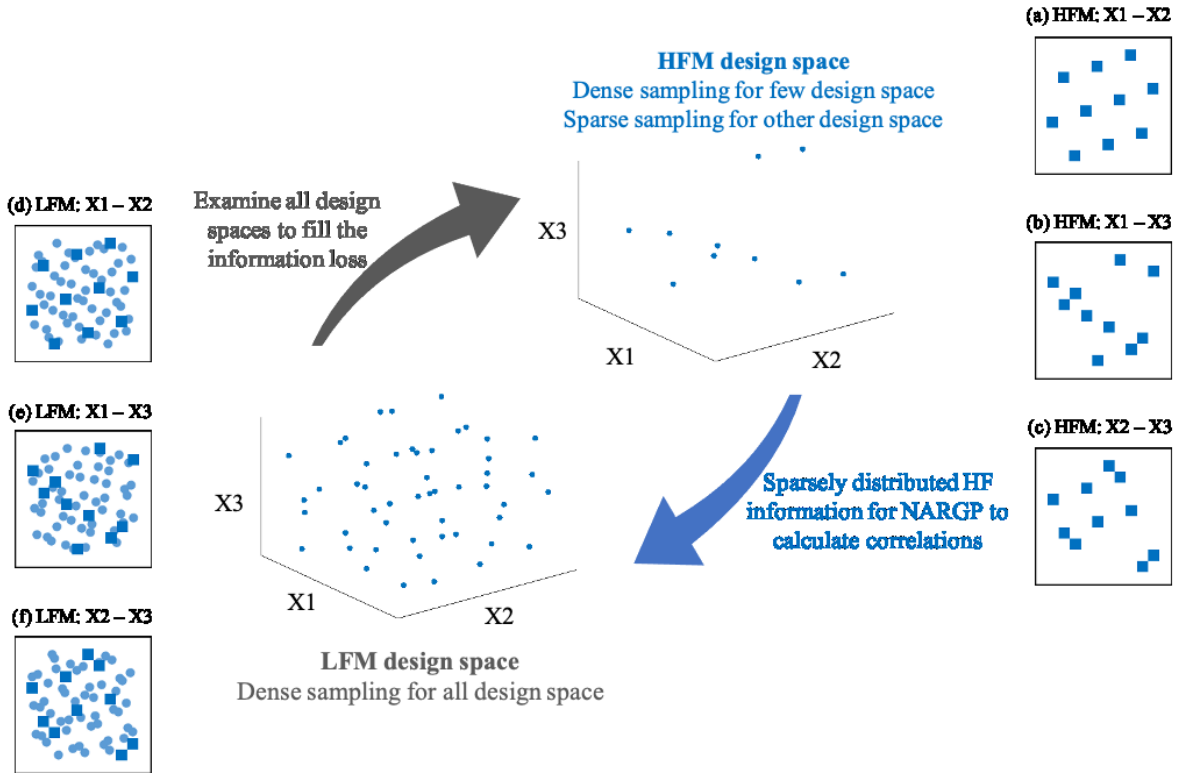

Figure 6.1: Concept of the proposed multi-fidelity modelling approach

Table 6.1: Sampling strategy for the multi-fidelity formulation

Iterate:
Characterise the design and random variables
Select the design variables in the HFM, H_d
Define other design and random variables in the HFM as H_s
Define all design and random variables in the LFM as L_d
Dense sampling H_d: Around five times of the number of design variables in H_d
Sparse sampling H_s: Equal sampling size for H_d
Combine H_d and H_s
Dense sampling L_d: At least five times of the number of design and random variables in L_d
Create a multi-fidelity model using the NARGP
Evaluate the quality of the model
If satisfied, the model is constructed.
If not satisfied, more training data points for the HFM and LFM should be added.
Continue until the quality is acceptable.

6.1.3 Multi-Fidelity Modelling Formulation and Probabilistic Optimisation Process

This section describes how to construct a multi-fidelity model and it introduces the developed multi-fidelity probabilistic optimisation framework. Table 6.2 summarises the workflow that the multi-fidelity modelling formulation constructs the multi-fidelity model using the sampling strategy. Then Figure 6.2 shows the optimisation framework using the constructed multi-fidelity model. The first level of probabilistic optimisation begins with selecting m design variables in the HFM, $H_d^{(I)} = [x^{(1)}, \cdots, x^{(m)}]$ in the table, and the training data points for this $H_d^{(I)}$ should be sampled as dense as the NARGP can represent the response surfaces of $H_d^{(I)}$ accurately. The selected design variables, m $(m < n)$, are chosen by the designer's decision from all design variables, n, depending on the problem size. This enables the NARGP to require a smaller number of high-fidelity training data points compared with different multi-fidelity modelling methods considering all design variables in the HFM. Other design variables in the HFM are defined by $H_s^{(I)} = [x^{(m+1)}, \cdots, x^{(n)}]$ and they are not selected in $H_d^{(I)}$. The training data points for $H_s^{(I)}$ is randomly collected within the sampling size for $H_d^{(I)}$ using the sparse sampling to preserve the size of the high-fidelity training dataset. Then these two sampling sets comprising different sampling degrees are combined as a high-fidelity training input dataset for the first level of probabilistic optimisation. At the same time, low-fidelity training data points for the LFM having n design variables, $L_d^{(I)} = [x^{(1)}, x^{(2)}, \cdots, x^{(n)}]$, are also sampled using the dense sampling to embrace the entire design space completely. Then, two training output datasets corresponding to the high- and low-fidelity training input datasets, respectively, can be constructed using a proper numerical solver (Abaqus CAE in this work). The NARGP creates a multi-fidelity model for the first level of probabilistic optimisation using the two high- and low-fidelity training input/output datasets. Figure 6.1

highlights that the multi-fidelity model based on the sampling strategy can provide the correct solutions of $H_d^{(I)}$ during the first level of probabilistic optimisation process since it comprises enough high-fidelity training data points using the dense sampling. Simultaneously, the multi-fidelity model examines all design variables' solution spaces using both the sparse high-fidelity training data points for $H_s^{(I)}$ and the dense low-fidelity training data points for $L_d^{(I)}$. When the first level of probabilistic optimisation discovers the optimal solutions, the multi-fidelity model for the second level should be constructed using $H_d^{(II)} = [\hat{x}^{(m+1)}, \cdots, \hat{x}^{(l)}]$, $H_s^{(II)} = [\hat{x}^{(l+1)}, \cdots, \hat{x}^{(n)}]$ and $L_d^{(II)} = [\hat{x}^{(m+1)}, \cdots, \hat{x}^{(n)}]$ followed by updating the HFM and LFM with the optimal solutions of the first optimisation level, as described in Table 6.2 and Figure 6.2.

As shown in Figure 6.1, the cooperation between the HFM and LFM enables a multi-fidelity model to embrace the entire design space without a lack of information during the probabilistic optimisation process. Notably, the structure of the NARGP constructs a multi-fidelity model when the training dataset of HFM is a subset of the LFM training dataset. The main contribution of this multi-fidelity formulation is that the HFM focuses on only a small part of the entire design spaces to reduce the sampling size for the high-fidelity training dataset. The HFM also provides sparsely the high-fidelity information of other design variables, $H_s^{(I)}$, while avoiding the requirement of extra high-fidelity FEM simulations. This enables the NARGP to calculate the correlations precisely between the HFM and the LFM based on the sampling strategy to construct the accurate multi-fidelity model. Also, the low-fidelity training dataset using the dense sampling complements the lack of information led by the insufficient high-fidelity information of $H_s^{(I)}$.

Next, the multi-fidelity probabilistic optimisation framework using this proposed multi-fidelity modelling formulation is illustrated in Figure 6.2. Once the NARGP creates the multi-fidelity model using the sampling strategy and the training scheme, the first level of probabilistic optimisation is conducted using the predictions, $\mu_{*MF}(x_*)$, offered by the constructed multi-fidelity model. The optimal solutions, $\hat{H}_d^{(I)}$, of the selected design variables in the HFM, $H_d^{(I)}$, are found. The design variables, $[x^{(1)}, \cdots, x^{(m)}]$, of both the HFM and LFM are updated by the optimal solutions, $X = [\hat{H}_d^{(I)}, \hat{L}_d^{(I)}]$, where $\hat{L}_d^{(I)}$ represents the optimal solutions of other design variables in the LFM, $[x^{(m+1)}, \cdots, x^{(n)}]$. The design variables in $\hat{H}_d^{(I)}$ are fixed and not considered in the second level since their optimal solutions come from the high-fidelity training dataset using the dense sampling. Then, different design variables for the second level, $H_d^{(II)} = [\hat{x}^{(m+1)}, \cdots, \hat{x}^{(l)}]$ where $(l < n)$, are selected. The choice of the HFM's design variables should not necessarily follow any particular sequence because the LFM embraces the whole design space at all times. During the second level of probabilistic optimisation, the optimisation algorithm finds the optimal solutions, $\tilde{H}_d^{(II)}$ and $\tilde{L}_d^{(II)}$, of the design variables, $H_d^{(II)}$ and $L_d^{(II)}$, using a new

multi-fidelity model constructed for this level. These multi-fidelity modelling and probabilistic optimisation process are continued until Level k terminates, which means all optimal solutions are found.

The LFM does not require extra FEM simulations to build up a new training dataset for the next level. This can provide additional computational gains compared to the multi-level multi-fidelity method that should establish the low-fidelity training dataset for each level (42). It is not surprising that even low-fidelity FEM simulations can cause a computational burden when a problem is complex and large-scale. It should be highlighted that the proposed method seeks to harness most of the advantages of multi-fidelity modelling as well as deal with the non-linear correlation between different fidelity models using non-linear data fusion GP. In particular, this method enables the probabilistic design optimisation to broaden its area to the design of composite structures under thermomechanical loading.

Table 6.2: Multi-fidelity modelling process

Optimisation level			HFM	LFM
Level I	Design and random variables	Dense sampling	$\mathrm{H}_{\mathrm{d}}^{(\mathrm{I})} = [x^{(1)}, \cdots, x^{(m)}]$, $m < n$	$\mathrm{L}_{\mathrm{d}}^{(\mathrm{I})} = \mathrm{X} = [x^{(1)}, x^{(2)}, \cdots, x^{(n)}]$
		Sparse sampling	$\mathrm{H}_{\mathrm{s}}^{(\mathrm{I})} = [x^{(m+1)}, \cdots, x^{(n)}]$	
	Number of design and random variables		n $(all\ variables)$	
	Optimal solutions at Level I		$\widehat{\mathrm{H}}_{\mathrm{d}}^{(\mathrm{I})} = [\hat{x}^{(1)}, \cdots, \hat{x}^{(m)}]$	$\widehat{\mathrm{L}}_{\mathrm{d}}^{(\mathrm{I})} = [\hat{x}^{(m+1)}, \cdots, \hat{x}^{(n)}]$
	Updated HFM & LFM		$\mathrm{X} = [\widehat{\mathrm{H}}_{\mathrm{d}}^{(\mathrm{I})}, \hat{x}^{(m+1)}, \cdots, \hat{x}^{(n)}]$	
Level II	Design and random variables	Dense sampling	$\mathrm{H}_{\mathrm{d}}^{(\mathrm{II})} = [\hat{x}^{(m+1)}, \cdots, \hat{x}^{(l)}]$, $l < n$, $\widehat{\mathrm{H}}_{\mathrm{d}}^{(\mathrm{I})}\ is\ fixed.$	$\mathrm{L}_{\mathrm{d}}^{(\mathrm{II})} = [\hat{x}^{(m+1)}, \cdots, \hat{x}^{(n)}]$
		Sparse sampling	$\mathrm{H}_{\mathrm{s}}^{(\mathrm{II})} = [\hat{x}^{(l+1)}, \cdots, \hat{x}^{(n)}]$	
	Number of design and random variables		$n - m$	
	Optimal solutions at Level II		$\widetilde{\mathrm{H}}_{\mathrm{d}}^{(\mathrm{II})} = [\tilde{x}^{(m+1)}, \cdots, \tilde{x}^{(l)}]$	$\tilde{\mathrm{L}}_{\mathrm{d}}^{(\mathrm{II})} = [\tilde{x}^{(l+1)}, \cdots, \tilde{x}^{(n)}]$
	Updated HFM & LFM		$\mathrm{X} = [\widehat{\mathrm{H}}_{\mathrm{d}}^{(\mathrm{I})}, \widetilde{\mathrm{H}}_{\mathrm{d}}^{(\mathrm{II})}, \tilde{x}^{(l+1)} \cdots, \tilde{x}^{(n)}]$	
			$Find\ the\ \mathrm{H}_{\mathrm{d}}^{(\mathrm{III})} and\ \mathrm{L}_{\mathrm{d}}^{(\mathrm{III})}\ using\ the\ same\ manner.$ $\widehat{\mathrm{H}}_{\mathrm{d}}^{(\mathrm{I})}\ and\ \widetilde{\mathrm{H}}_{\mathrm{d}}^{(\mathrm{II})}\ are\ fixed\ at\ this\ level.$	

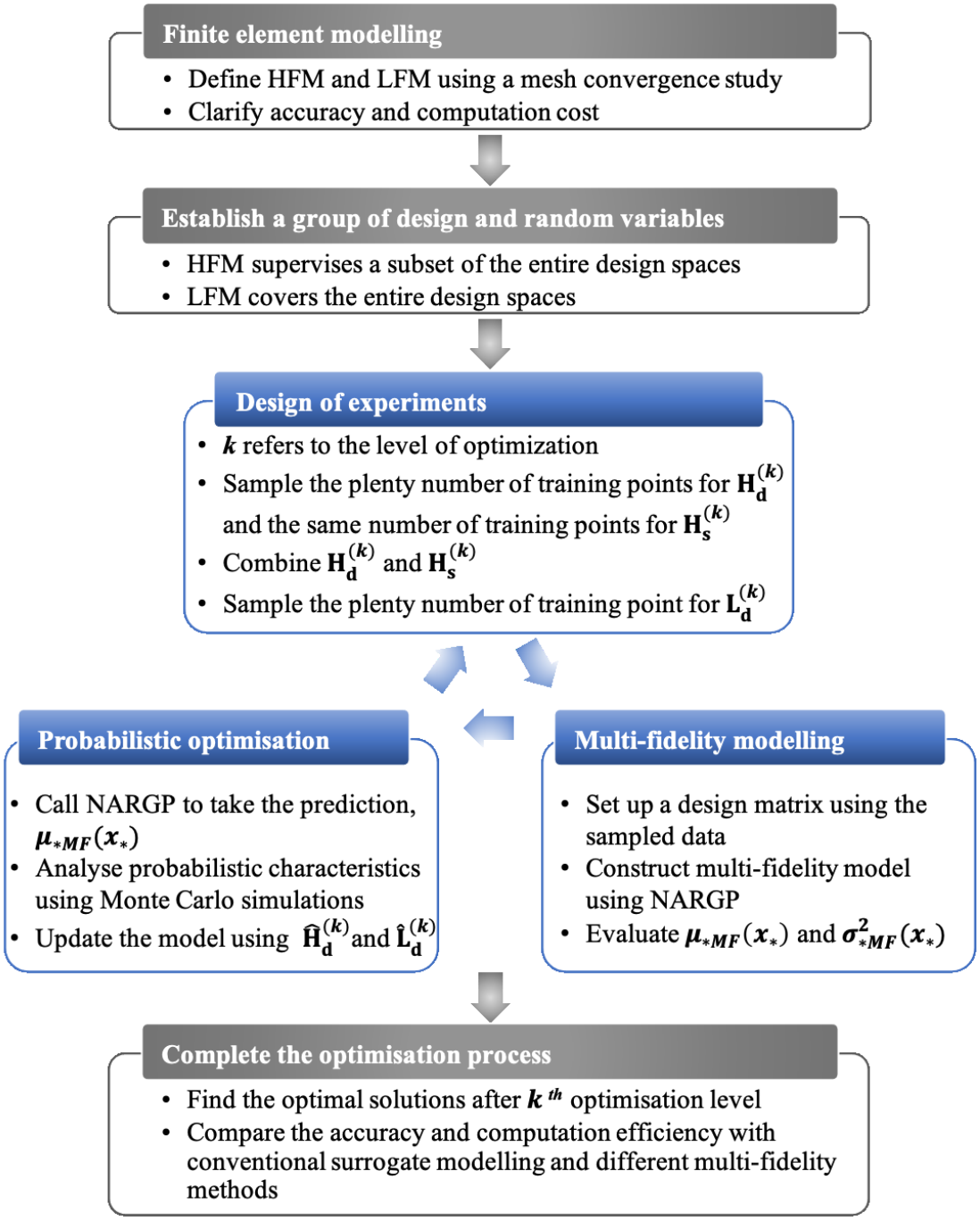

Figure 6.2: Multi-fidelity probabilistic optimisation framework

6.2 Thermomechanical Buckling of Composite Structures

The displacement for a composite structure modelled using three-dimensional shell elements for FEM simulations is based on the first-order deformation plate theory (18), given by equation (6.6)

$$\begin{aligned} u(x,y,z) &= u_0(x,y) + z\phi_y(x,y) \\ v(x,y,z) &= v_0(x,y) + z\phi_x(x,y) \\ w(x,y,z) &= w_0(x,y) \end{aligned} \tag{6.6}$$

where u_0, v_0 and w_0 are the displacements at the middle of the plane along each direction, including x, y and z, respectively. ϕ_x and ϕ_y represents the rotation of the mid-surface in the x and y axis.

The von Karman strain-displacement relationship to consider geometrical non-linearity caused by the large deflections of thin plates is described by equation (6.7).

$$\mathrm{E} = \begin{Bmatrix} \varepsilon_x \\ \varepsilon_y \\ \gamma_{xy} \end{Bmatrix} = \begin{Bmatrix} \dfrac{\partial u}{\partial x} \\ \dfrac{\partial v}{\partial y} \\ \dfrac{\partial u}{\partial y} + \dfrac{\partial v}{\partial x} \end{Bmatrix} + \frac{1}{2} \begin{Bmatrix} \left(\dfrac{\partial w}{\partial x}\right)^2 \\ \left(\dfrac{\partial w}{\partial y}\right)^2 \\ 2\dfrac{\partial w}{\partial x}\dfrac{\partial w}{\partial y} \end{Bmatrix} \tag{6.7}$$

The in-plane strain vector, E, in equation (6.7), is expressed by substituting the equation (6.6).

$$\begin{aligned} \mathrm{E} &= \varepsilon^0 - z\kappa = \varepsilon_m + \varepsilon_\theta - z\kappa \\ &= \begin{Bmatrix} \dfrac{\partial u_0}{\partial x} \\ \dfrac{\partial v_0}{\partial y} \\ \dfrac{\partial u_0}{\partial y} + \dfrac{\partial v_0}{\partial x} \end{Bmatrix} + \frac{1}{2} \begin{Bmatrix} \left(\dfrac{\partial w_0}{\partial x}\right)^2 \\ \left(\dfrac{\partial w_0}{\partial y}\right)^2 \\ 2\dfrac{\partial w_0}{\partial x}\dfrac{\partial w_0}{\partial y} \end{Bmatrix} - z \begin{Bmatrix} \dfrac{\partial \phi_y}{\partial x} \\ \dfrac{\partial \phi_x}{\partial y} \\ \dfrac{\partial \phi_y}{\partial x} + \dfrac{\partial \phi_x}{\partial y} \end{Bmatrix} \end{aligned} \tag{6.8}$$

where ε^0, ε_m, ε_θ and κ represent the in-plane strain vector at the mid-plane, the linear in-plane strain vector, and the non-linear in-plane strain vector and the curvature strain vector, respectively.

In the meantime, transverse shear strains, γ, are expressed as equation (6.9).

$$\gamma = \begin{Bmatrix} \gamma_{yz} \\ \gamma_{xz} \end{Bmatrix} = \begin{Bmatrix} \dfrac{\partial w_0}{\partial y} - \phi_x \\ \dfrac{\partial w_0}{\partial x} - \phi_y \end{Bmatrix} \tag{6.9}$$

In general, equation (6.10) explains the thermo-elastic anisotropic stress-strain relations (1,18). It is recognised that thermal stress is not caused by external loads but is a consequence of restrained geometrical thermal distortion.

$$\{\sigma\} = [C](\{\mathrm{E}\} - \{\alpha\}\Delta T) \tag{6.10}$$

where $[C]$ is a constitutive matrix, $\{\alpha\}$ is the coefficient vector of thermal expansion for a single lamina concerning the in-plane coordinate system and ΔT is a temperature difference.

The stresses of the k-th layer in the laminate layers are calculated using the transformation of coordinates from principal material coordinates, which is represented by equation (6.11)

$$\begin{bmatrix}\sigma_x\\ \sigma_y\\ \tau_{xy}\end{bmatrix}=\begin{bmatrix}\bar{Q}_{11} & \bar{Q}_{12} & \bar{Q}_{16}\\ \bar{Q}_{12} & \bar{Q}_{22} & \bar{Q}_{26}\\ \bar{Q}_{16} & \bar{Q}_{26} & \bar{Q}_{66}\end{bmatrix}\begin{bmatrix}\varepsilon_x-\alpha_x\Delta T\\ \varepsilon_y-\alpha_y\Delta T\\ \gamma_{xy}-\alpha_{xy}\Delta T\end{bmatrix} \tag{6.11}$$

where $\left[\bar{Q}_{ij}\right]$ is the transformed stiffness coefficient matrix. α_x, α_y and α_{xy} are defined as

$$\begin{aligned}\alpha_x &= \alpha_1 cos^2\theta + \alpha_2 sin^2\theta\\ \alpha_y &= \alpha_1 sin^2\theta + \alpha_2 cos^2\theta\\ \alpha_{xy} &= 2(\alpha_1-\alpha_2)sin\,\theta cos\theta\end{aligned} \tag{6.12}$$

where α_1 and α_2 are thermal expansion coefficients, respectively, and θ is the ply angle of the layer.

The entire force and moment resultants for a N-layered laminate composite structure are defined as

$$\begin{bmatrix}N_x\\ N_y\\ N_{xy}\end{bmatrix}=\int_{-t/2}^{t/2}\begin{bmatrix}\sigma_x\\ \sigma_y\\ \tau_{xy}\end{bmatrix}dz=\sum_{k=1}^{N}\int_{z_{k-1}}^{z_k}\begin{bmatrix}\sigma_x\\ \sigma_y\\ \tau_{xy}\end{bmatrix}_k dz \tag{6.13}$$

$$\begin{bmatrix}M_x\\ M_y\\ M_{xy}\end{bmatrix}=\int_{-t/2}^{t/2}\begin{bmatrix}\sigma_x\\ \sigma_y\\ \tau_{xy}\end{bmatrix}z\,dz=\sum_{k=1}^{N}\int_{z_{k-1}}^{z_k}\begin{bmatrix}\sigma_x\\ \sigma_y\\ \tau_{xy}\end{bmatrix}_k z\,dz \tag{6.14}$$

where t is the thickness of the k-th layer. Note that z_k is the directed distance to the bottom of the k-th layer, and z_{k-1} is the directed distance to the top of the k-th layer.

When equation (6.11) is substituted in equations (6.13) and (6.14), the force and moment resultants are obtained that are integrated through the thickness of the composite structure

$$\begin{aligned}\begin{Bmatrix}N\\ M\end{Bmatrix}&=\begin{bmatrix}A & B\\ B & D\end{bmatrix}\begin{Bmatrix}\varepsilon^0\\ \kappa\end{Bmatrix}-\begin{Bmatrix}N_{\Delta T}\\ M_{\Delta T}\end{Bmatrix}\\ Q&=S\gamma\end{aligned} \tag{6.15}$$

$$(\mathrm{N}_{\Delta\mathrm{T}},\mathrm{M}_{\Delta\mathrm{T}})=\sum_{k=1}^{n}\int_{z_{k-1}}^{z_k}[\bar{\mathrm{Q}}]_k\{\alpha\}_k(1,z)\Delta T\,dz \tag{6.16}$$

where the laminate stiffness is defined as $([\mathrm{A}],[\mathrm{B}],[\mathrm{D}])=\sum_{k=1}^{n}\int_{z_{k-1}}^{z_k}\left(\bar{Q}_{ij}\right)_k(1,z,z^2)dz$ with $(i,j=1,2,6)$. $[A],[B]$ and $[D]$ are extensional, bending-extension coupling and bending twisting coupling matrices, respectively. $[S]$ is shear stiffness matrices defined by $\sum_{k=1}^{n}\kappa_p\int_{z_{k-1}}^{z_k}\left(\bar{Q}_{ij}\right)_k dz$ with $(i,j=$

4,5) and κ_p is a shear correction factor. $\{N_{\Delta T}\}$ and $\{M_{\Delta T}\}$ are the thermal forces and thermal moment induced by the temperature changes ΔT, respectively.

The principle of virtual work derives the governing equation for thermomechanical buckling.

$$\delta W = \delta W_{int} - \delta W_{ext} = 0 \tag{6.17}$$

where δW_{int} is the internal virtual work that consists of $\delta W_{int}^{(1)}$ and $\delta W_{int}^{(2)}$ done by linear and thermal geometric stiffness such that

$$\begin{aligned} \delta W_{int}^{(1)} &= \int_A \{\delta\varepsilon_m\}^T\{N\} + \{\delta\kappa\}^T\{M\} + \{\delta\gamma\}^T\{Q\}\, dA \\ &= \int_A [\delta\varepsilon_m^T A\varepsilon_m + \delta\varepsilon_m^T B\kappa + \delta k^T B\varepsilon_m + \delta\kappa^T D\kappa + \delta\gamma^T S\gamma]\, dA \\ &= \{\delta d\}^T[K]\{d\} \end{aligned} \tag{6.18}$$

where $\{d\}$ is the displacement vector and $[K]$ is the linear stiffness matrix.

Thermal geometric stiffness matrix, $[K_{\Delta T}]$, is offered by the work done by a constant thermal force that leads to a small lateral deflection. This internal work is done by the thermal forces, including $N_{\Delta Tx}$, $N_{\Delta Ty}$, and $N_{\Delta Txy}$, caused by the temperature change. The change in strain energy due to the thermal forces is written as equation (6.19).

$$\begin{aligned} \delta W_{int}^{(2)} &= -\int_A \left[\delta\varepsilon_\theta^T N_{\Delta T}\right] dA \\ &= -\int_A \left[N_{\Delta Tx}\delta\left(\frac{\partial w}{\partial x}\right) + N_{\Delta Ty}\delta\left(\frac{\partial w}{\partial y}\right) + N_{\Delta Txy}\delta\left(\frac{\partial w}{\partial x}\right)\left(\frac{\partial w}{\partial y}\right)\right] dA \\ &= -\int_A \delta\begin{Bmatrix}\frac{\partial w}{\partial x}\\ \frac{\partial w}{\partial y}\end{Bmatrix}^T \begin{bmatrix} N_{\Delta Tx} & N_{\Delta Txy} \\ N_{\Delta Txy} & N_{\Delta Ty}\end{bmatrix}\begin{Bmatrix}\frac{\partial w}{\partial x}\\ \frac{\partial w}{\partial y}\end{Bmatrix} dxdy \\ &= -\{\delta d\}^T[K_{\Delta T}]\{d\} \end{aligned} \tag{6.19}$$

Finally, the equation of motion of the composite structure and the eigenproblem for the thermomechanical buckling analysis is obtained, which can be represented as

$$([K] - \lambda[K_{\Delta T}])\{d\} = \{0\} \tag{6.20}$$

$$([K] - \lambda[K_{\Delta T}])\{\Phi\} = \{0\} \tag{6.21}$$

where λ and $\{\Phi\}$ are the critical temperature change and buckling mode shape, respectively.

6.3 Numerical Example

The proposed multi-fidelity probabilistic optimisation framework was demonstrated by the RBDO of a mono-stringer stiffened composite panel under thermomechanical loading. This demonstration shows the potential of the developed multi-fidelity optimisation method to be utilised for the probabilistic design of large-scale composite structures under both mechanical and thermal loading. Notably, the computational efficiency of the presented method was highlighted by comparison with traditional multi-fidelity models and high-fidelity surrogate models.

6.3.1 Mono-Stringer Stiffened Composite Structure under Thermomechanical Loading

The details of the mono-stringer stiffened composite structure is illustrated in Figure 6.3, which is identical to the composite structures considered in previous chapters. This structure is clamped at both ends, but the left-hand end is free to move in the longitudinal direction (z-direction in the figure), which is the applied loading direction. Pure compression load for mechanical shortening is applied by increasing uniform displacement at the left-hand end. The material properties are the same as in Table 4.1. The thermal expansion coefficients of the structure are shown in Table 6.3. It should be noted that only the stringer geometry is to be optimised, while the optimisation process considers the uncertainties of both the geometry and the mechanical properties of both the stringer and the skin. There are no constraints on the two longitudinal edges of the skin. Perfect bonding is assumed between the stiffener and skin to consider their interaction.

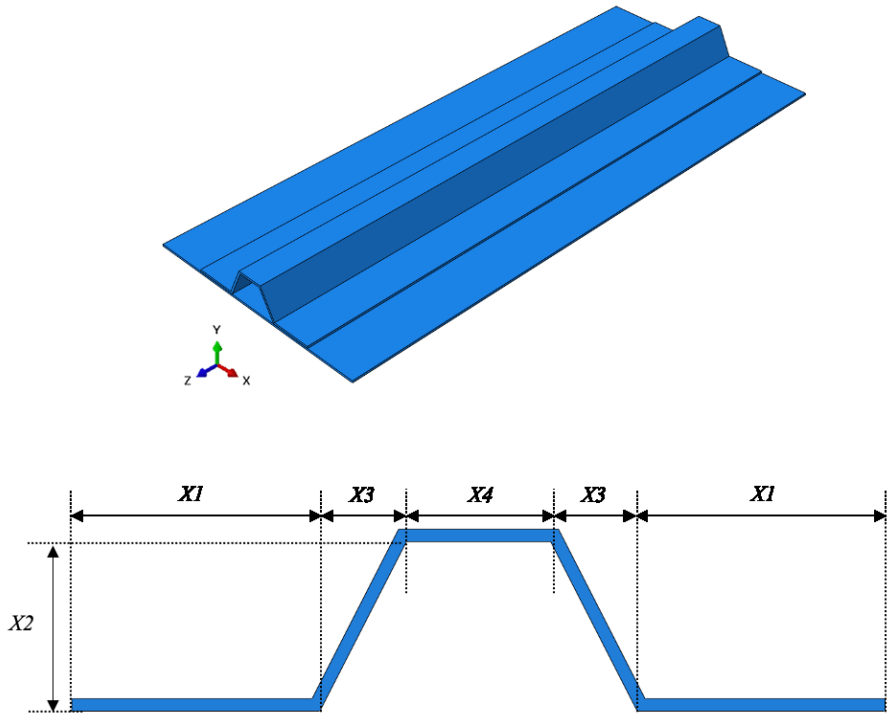

Figure 6.3: Mono-stringer stiffened composite panel

Table 6.3: Thermal expansion coefficient

Parameter	Value	
Longitudinal thermal coefficient (/℃)	α_1	$1.7 \times E^{-6}$
Transverse thermal coefficient (/℃)	α_2	$-1.0 \times E^{-6}$

The thermomechanical buckling analysis depending on different mechanical shortening lengths was conducted to see how significant the critical temperature changes are. Figure 6.4 displays the thermomechanical buckling results for a mono-stiffened stringer panel with the mean geometry values at the design space. As seen in the figure, the composite structure carries mechanical shortening caused by pure compression, and then a thermal buckling analysis is conducted to find the critical temperature change. Table 6.4 shows that the thermomechanical buckling occurs in the vicinity of 95 ℃, which is the normal operating temperature range of regional aircraft when the shortening length is 0.3 mm ($\Delta L/L = 0.05$ %). In this work, the thermomechanical buckling temperature refers to the maximum critical temperature change followed by the shortening, $\Delta L/L = 0.05$ %. The class of fidelity was decided by the level of FEM discretisation. Figure 6.5 illustrates the mesh grid of both the HFM and LFM; the element size was defined as 4.0 mm and 12.0 mm, respectively, through a mesh convergence study for the thermomechanical buckling temperature. It should be highlighted that the LFM shows around 15 % error while demonstrating a computational cost of only about 30 % compared to the HFM. The FEM models are composed of four-node shell elements (S4R).

Table 6.4: Critical temperature changes depending on mechanical shortening

Mechanical shortening (mm)	0	0.1	0.2	0.3
Critical temperature changes (°C)	407	303	200	94.9

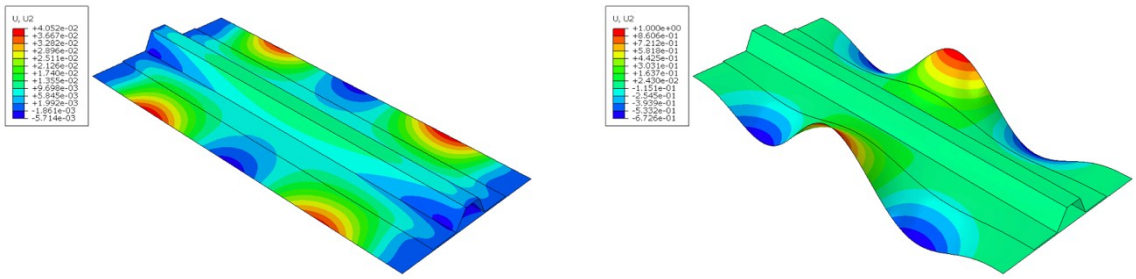

(a) Mechanical shortening (compression) (b) Temperature rise

Figure 6.4: Out-of-plane displacement of composite structures

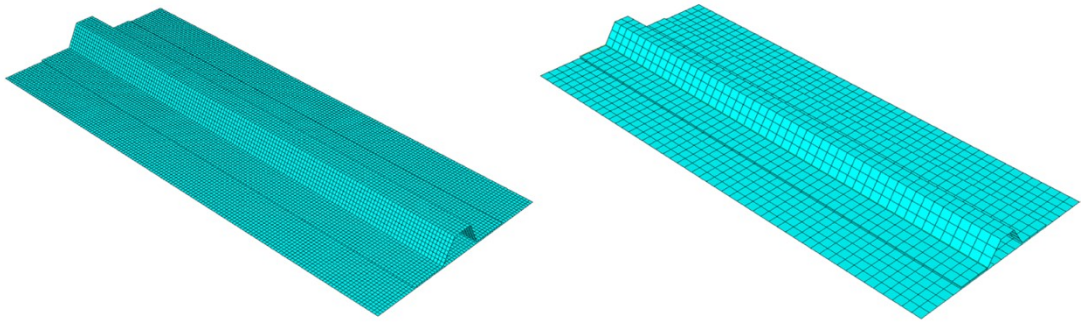

Figure 6.5: 4 mm mesh size for HFM (left) and 12 mm mesh size for LFM (right)

6.3.2 Multi-Fidelity Modelling

A multi-fidelity model using the proposed formulation is constructed to carry out the probabilistic optimisation of composite structures under thermomechanical loading. The input parameters of the multi-fidelity model are the mono-stiffened stringer geometry ($X1, X2, X3$ and $X4$) in Figure 6.3 and the mechanical properties of the composite structure (E_{11}, E_{22}=E_{33}, G_{23}, G_{12}=G_{13}, α_{11} and α_{22}) in Table 4.1 and Table 6.3. These input parameters are defined as the design and random variables that are used for optimisation and reliability analysis, respectively. In this work, the design variables are geometry parameters, whereas the random variables are both geometry and mechanical properties. Outputs are the critical temperature change and the mass of the composite structure. This multi-fidelity model having ten input parameters and two output parameters is constructed using both the HFM and the LFM covering different design spaces. As mentioned before, the NARGP quantifies non-linear correlations between different fidelities to create an accurate multi-fidelity model.

Firstly, the training datasets for the HFM and the LFM should be sampled using OLHS technique that is a sampling technique to collect training data in the given design space as evenly distributed as possible. Table 6.5 shows ten input parameters having each design range that consist of four geometric parameters and six mechanical properties. The geometric parameters primarily influence the output of the composite structure. At the same time, they have uncertainties associated with design and manufacturing that could considerably affect the structure's performance. Apart from these geometric parameters, the uncertainties of the mechanical properties should be considered as well. Table 6.6 clearly shows how the multi-fidelity model is constructed using two different fidelity models that explore supervise different design spaces at each level. The number of FEM simulations to construct the multi-fidelity model are also shown in the table. As mentioned in the previous section, the HFM covers only a part of the whole design space as dense as the sampled high-fidelity dataset can precisely examine the response surfaces of the selected design variables, $X1$ and $X2$ in this work. When the HFM at the first level focuses on the two design variables, ten training data points are enough to create the metamodel concerning these design variables accurately. The same number of training data of other design variables should also be sampled sparsely and added to the high-fidelity training dataset. Although the number of ten training data points is not sufficient to set up other design variables' metamodel, it allows the NARGP to use the high-fidelity information as much as possible in the given training dataset without causing extra high-fidelity FEM simulations. In contrast, the LFM, because it supervises all design variables, requires sixty training data points to supplement the lack of other design variables' information that is not included in the HFM. This training dataset embraces the response surfaces of all design variables as solidly as possible. Once the NARGP constructs the multi-fidelity model, error analysis should be conducted using a test dataset that uses points not included in the training scheme. The created multi-fidelity model at each level predicts the critical temperature change and the mass with less than 1.5 % error in the given design spaces.

When the multi-fidelity model completes the first level of optimisation, this multi-fidelity model provides the optimal solutions of the two selected design variables in the HFM as well as corresponding values of other design variables in the LFM. These optimal solutions update the HFM to choose different design variables that are not considered at the previous level. The LFM is also updated by those optimal solutions that enable a smaller number of design variables than the first level. The corresponding values obtained by the LFM update other design variables that are not considered in HFM. After updating two models, HFM chooses new design variables, $X3$ and $X4$, as shown in Table 6.6. Then, ten new training data points that can correctly establish the chosen design variables' response surfaces are sampled using OLHS as densely as possible. Simultaneously, the same number of training data points of other design variables are also collected sparsely to build up an efficient high-fidelity training dataset. It is not surprising that the LFM at the first level is still precise enough to carry out the next level optimisation since it is made up of sixty training points. This means the LFM requires only

ten additional low-fidelity FEM simulations that are identical to the training data of HFM for this level since the high-fidelity training dataset should be a subset of the low-fidelity training dataset. Figure 6.6 highlights how the HFM and the LFM cooperate using different sampling levels in different design spaces when $X1$ and $X2$ are selected as the HFM's design variables. The high-fidelity training dataset is evenly distributed using the small number of training points in the design space of $X1$ and $X2$. However, it does not seem that the rest of the design spaces, $X3$ and $X4$, are scattered uniformly in the high-fidelity design spaces. The low-fidelity training dataset carefully covers the whole design space without information loss dissimilar to the high-fidelity design spaces. It should be highlighted that this multi-fidelity scheme enables the size of the high-fidelity training dataset to decrease while embracing the entire design space with sparsely distributed high-fidelity information as well as dense low-fidelity information. It should be noted that conventional surrogate modelling approaches require hundreds of training points to consider all design and random variables. Some multi-fidelity modelling methods also demand a significant number of high-fidelity training data points because the HFM encompasses the same design spaces as the LFM. The proposed multi-fidelity modelling methodology provides significant computational time savings compared with other multi-fidelity methods and enables probabilistic optimisation to broaden its application area to large-scale composite structures under thermomechanical loading.

Table 6.5: Design and random variables

Design of experiment input data	Value
Stringer foot (mm)	$34.4 < X1 < 51.6$
Stringer height (mm)	$24.0 < X2 < 36.0$
Distance between top and bottom (mm)	$12.0 < X3 < 18.0$
Stringer top (mm)	$20.0 < X4 < 30.0$
E_{11} (GPa)	$111 < E_{11} < 167$
E_{22}=E_{33} (GPa)	$6.5 < E_{22} < 9.8$
G_{12}=G_{13} (GPa)	$3.8 < G_{12} < 5.8$
G_{23} (GPa)	$2.5 < G_{23} < 3.7$
α_{11} (/°C)	$1.36E^{-6} < \alpha_{11} < 2.04E^{-6}$
α_{22} (/°C)	$-1.2E^{-6} < \alpha_{22} < -0.8E^{-6}$

Table 6.6: Details of the multi-fidelity models

Level	Scatter degree of Training data	HFM		LFM	
		Design and random variable	Number of FEM simulations	Design and random variable	Number of FEM simulations
I	Dense	$X1, X2$	10	$X1, X2, X3, X4, E_{11}, E_{22} = E_{33}, G_{23}, G_{12} = G_{13}, \alpha_{11}, \alpha_{22}$	60
	Sparse	$X3, X4, E_{11}, E_{22} = E_{33}, G_{23}, G_{12} = G_{13}, \alpha_{11}, \alpha_{22}$		-	
II	Dense	$X3, X4$	10	$X3, X4, E_{11}, E_{22} = E_{33}, G_{23}, G_{12} = G_{13}, \alpha_{11}, \alpha_{22}$	10
	Sparse	$E_{11}, E_{22} = E_{33}, G_{23} G_{12} = G_{13}, \alpha_{11}, \alpha_{22}$		-	

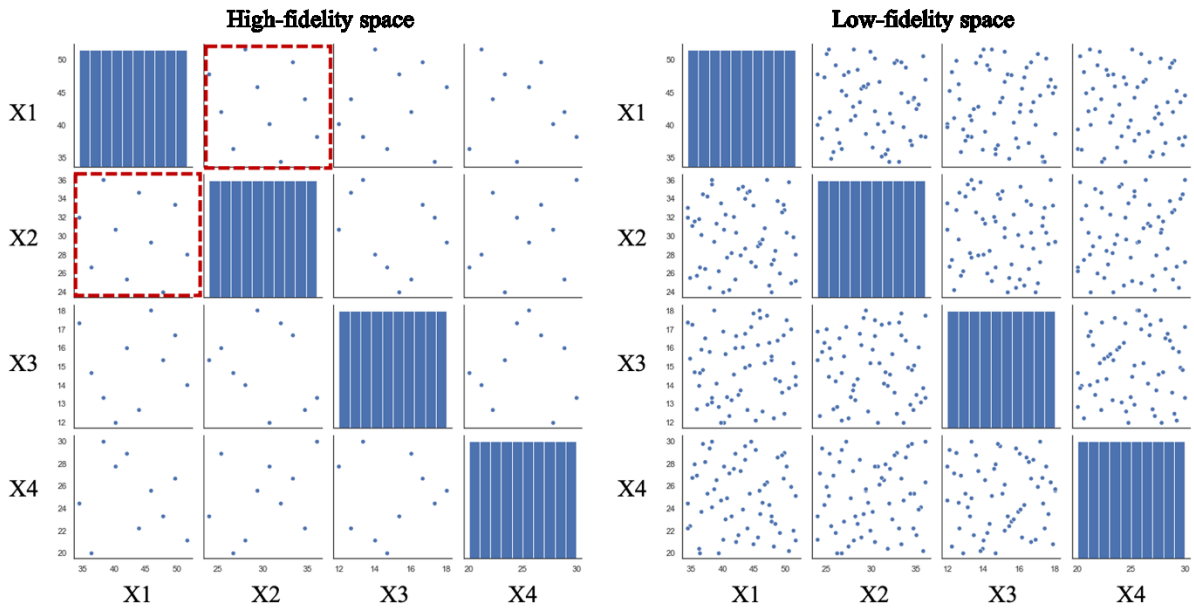

Figure 6.6: Training data distribution between HFM and LFM

6.3.3 Multi-Fidelity Reliability-Based Design Optimisation

RBDO, a type of probabilistic optimisation, was conducted to demonstrate the efficiency and accuracy of the multi-fidelity model constructed using the proposed formulation. In this example, geometric non-linearity were considered, while the material properties were presumed to be in the linear elastic region.

6.3.3.1 Problem Definition

Table 6.7 describes the description of the RBDO problem of the mono-stiffened stringer composite structure under thermomechanical loading. There are four constraints and three objectives. Since this proposed multi-fidelity optimisation approach aims to cooperate with the HFM and the LFM exploring different design spaces, each fidelity model has its constraints and objectives in the optimisation process. They carried typical mass constraints but different constraints regarding minimum critical temperature changes based on the difference between the HFM and the LFM. The reliability index was targeted by the associated value with the probability of failure, 0.135 %. The objective functions were to maximise the critical temperature changes and minimise the mass of the composite structure. It should be highlighted that the composite structure should be under thermal condition followed by a specific mechanical shortening, 0.05 % regarding the longitudinal direction, to include the effect of residual stress.

The discretisation level of FEM models for the HFM and the LFM were defined through a mesh convergence study. It should be noted that the LFM shows 15 % solution error compared to the HFM whilst offering a 70% reduction in computational cost. The design spaces of geometric parameters and material properties are the same as the range of design of experiments in the previous section. As shown in Figure 6.7, the optimisation was conducted using NSGA-II (37), a multi-objective exploratory technique. This optimisation method is suitable for highly non-linear design spaces as well as discontinuous design spaces. The method follows the standard genetic operation of mutation and crossover. Still, the selection process is based on different mechanisms to construct a Pareto set with the best combination of objective values. Generation and population numbers were determined by 12 and 20, respectively, to find optimal solutions correctly. These values were obtained using the convergence check of the Pareto front depending on different combinations of generation and population. In particular, the reliability check to consider the design uncertainties of random design variables is essential in this optimisation process. The uncertainties associated with geometric parameters are commonly assumed by a 0.1 % coefficient of variation concerning its mean values as manufacturing tolerance. The uncertainties of mechanical properties are considered by a random normal distribution with 5 % coefficient of variation (15). All input parameters are presumed to have a truncated Gaussian distribution at three standard deviations. The reliability assessment should be conducted at all populations of each generation. Monte Carlo simulation computes the statistical characteristics of the objective functions, which are induced by the uncertainties of random design variables. Sobol sampling method was incorporated into the Monte Carlo simulation to obtain more homogeneous sampling distribution as well as more robust statistical estimations than other sampling methods (49). It should be noted that the maximum allowable number of multi-fidelity simulations to check the probability of failure was set to 2,000. The convergence tolerance check was carried out at

every 25 sampling points to improve the computational efficiency. The Monte Carlo simulations were halted when both mean and standard deviations satisfy 0.1 % difference with these associated values at the previous convergence test. Hence, the maximum simulation number using the developed multi-fidelity model was 480,000 for the two levels in this RBDO process.

Table 6.7: Reliability-based design optimisation - problem definition

Description		Value
Multi-fidelity model	HFM	$Mesh\ size$: 4.0 mm
	LFM	$Mesh\ size$: 12.0 mm
Optimisation method	$NSGA-II$	$Generation$: 12
		$Population$: 10
Analysis type	$Monte\ Carlo\ simulations$	$Sobol\ samples$: 2000
Design uncertainty	$Mean$	$Standard\ deviation$
	$X1$	$0.001 \times X1$
	$X2$	$0.001 \times X2$
	$X3$	$0.001 \times X3$
	$X4$	$0.001 \times X4$
	E_{11}	$0.05 \times E_{11}$
	E_{22}	$0.05 \times E_{22}$
	G_{12}	$0.05 \times G_{12}$
	G_{23}	$0.05 \times G_{23}$
	α_{11}	$0.05 \times \alpha_{11}$
	α_{22}	$0.05 \times \alpha_{22}$
Constraints under 0.05% mechanical shortening	$mass$	$m \leq 1\ kg$
	$HFM\ \ \Delta T_{cr}$	$\Delta T_{cr,HFM} \geq 50$ ℃
	$LFM\ \ \Delta T_{cr}$	$\Delta T_{cr,LFM} \geq 57.5$ ℃
	$Reliability\ index\ \beta$	$\beta = 3$
Objectives under 0.05% mechanical shortening	$Mean\ mass$	$minimise$
	$Mean\ HFM\ \ \Delta T_{cr}$	$maximise$
	$Mean\ LFM\ \ \Delta T_{cr}$	$maximise$

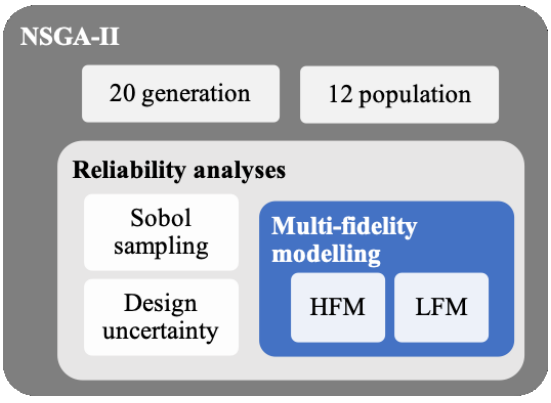

Figure 6.7: Multi-fidelity RBDO framework

6.3.3.2 Results

Table 6.8 represents the RBDO results using the proposed multi-fidelity formulation. This table demonstrates how the multi-fidelity model enables cooperation between two different fidelity models and improves its accuracy at the end of each level. In the table, the HFM has two different sampling degrees of training data, while the LFM is sampled densely as it can produce the response surfaces for all random design variables. At the first level, the HFM carries two design variables, $X1$ and $X2$, while the LFM has all the random design variables. At the same time, the HFM takes other two design variables, $X3$ and $X4$, and six random variables of material properties as a form of sparsely scattered training data that allows the LFM to quantify correlations among all variables. Both the HFM and LFM share the selected design variables of $X1$ and $X2$ during the first level of the optimisation. As shown in Figure 6.8, this enables the multi-fidelity model to scrutinise the solution spaces of other design variables corresponding to those of the selected design variables. When the first level finds the Pareto front satisfied with the objectives and constraints, the optimal solutions should be chosen by the designer's decision. In this work, the optimal solutions were chosen by the allowable temperature range associated with the regional aircraft operation, known from -45 ℃ to 85 ℃. The chosen optimal solutions at the first level update the multi-fidelity model before the next level. The optimal solutions of $X1$ and $X2$ are good enough to be fixed at the next level because they are obtained by dense high-fidelity information. It is not surprising that the corresponding optimal solutions of the LFM at the first level can update other design variables, $X3$ and $X4$, that are not included in the HFM. Hence, this update enables the HFM to take different design variables that are collected as densely as possible. Similarly, as the first level, this updated HFM carries different design variables, $X3$ and $X4$, while the information of six random variables is also included sparsely. The LFM is updated by the optimal solutions of $X1$ and $X2$, while the HFM takes all random design variables except for the fixed $X1$ and $X2$. When this level is finished, the final solution is obtained because there are two levels in this example.

Figure 6.9 illustrates the Pareto fronts of the optimisation results at each level. The Pareto front of the first level is associated with the selected design variables that the HFM mainly supervises for the optimisation process, while the LFM compensates for the lack of high-fidelity information. The second level's Pareto front has a small range since the optimal solutions in the first level's Pareto front updates the multi-fidelity model. It should be highlighted that the second level examines the solution spaces thoroughly based on the chosen solution of the first level and discovers more reliable and better solutions compared to those of the first level. As can be seen in the figure, the Pareto front points at the second level rise to the upward direction and fill the gap in the solution space left from the first level. The figure also includes the Pareto front found from a conventional surrogate modelling approach, which is called a super HFM in this work, to highlight how accurate the proposed multi-fidelity method is. The super HFM consists of 150 high-fidelity FEM simulations to correctly resemble ten random

design variables' response surfaces. This figure shows that the Pareto front of the super HFM is nearly identical to that of the multi-fidelity model.

Table 6.9 displays the mean value and standard deviation of the chosen optimal solutions so that the results of reliability assessments are compared between the multi-fidelity model and the super HFM. It should be noted that the optimal solution of the super HFM is selected as having the same mass as the chosen optimal solution of the multi-fidelity model. The multi-fidelity model has almost the same mean value and acceptable standard deviation as those of super HFM. It is also significant to assess the accuracy of the multi-fidelity model as the solution of the HFM created by the equivalent number of high-fidelity FEM simulations. There could be no advantages of the proposed method unless the multi-fidelity model constructed by the same computational cost is more accurate. Table 6.6 shows that the multi-fidelity model comprises 20 HFMs and 70 LFMs that equate to 40 high-fidelity FEM simulations. Figure 6.10 features the accuracy among three different models: the multi-fidelity model, the super HFM and the equivalent HFM (HFM40). In this figure, the multi-fidelity model's mean value is much closer to the super HFM than that of HFM40 while having the standard deviation similar to the super HFM. This means that the reliability assessments of the proposed multi-fidelity method are more accurate than the equivalent number of high-fidelity FEM simulations in terms of computation time. As the NARGP is incorporated into the multi-fidelity formulation, the constructed multi-fidelity model has a black-box structure between input and output parameters. The chosen optimal solutions should be checked to show if the solutions make sense using proper techniques, such as a FEM solver or an experiment. Table 6.9 shows the critical temperature change using the multi-fidelity model is nearly identical to that of the FEM solver. It should be remarked that the accuracy of the multi-fidelity model is more accurate than that of the super HFM at this design point.

The vast benefit of multi-fidelity modelling methods is that they can reduce the significant computational cost caused by the consideration of uncertainties during the probabilistic optimisation process. Figure 6.11 represents the computational time savings of the proposed multi-fidelity method compared to different probabilistic optimisation methods. All computational costs in this figure are normalised by the total computational cost of the super HFM so that the computational gains are emphasised in a practical way (48). The proposed multi-fidelity model is constructed using both 20 HFM training points and 70 LFM training points. The equivalent computational cost equates to about 40 high-fidelity FEM simulations because the computational cost of LFM is 70 % more economical than HFM’s cost. In contrast, the super HFM requires 150 high-fidelity FEM simulations. It is not surprising that the proposed multi-fidelity optimisation method provides around 75 % of computation time savings. However, it is more significant to show how much computation time savings are obtained by the use of this new method compared with different multi-fidelity methods. Traditional multi-fidelity methods (23)construct a multi-fidelity model using both 60 HFM training points and 60 LFM training points because two different fidelity models have the same number of design variables. The equivalent

high-fidelity FEM simulation number to this model is around 80, which is twice more computationally expensive than the proposed multi-fidelity method. This proposed multi-fidelity method is still more efficient than the multi-level multi-fidelity modelling approach developed before (42). The multi-level multi-fidelity approach uses both 20 HFM training points and 110 LFM training points, which equates to around 55 high-fidelity FEM simulations; hence the proposed multi-fidelity method enables 30 % of computation time savings. Although the LFM is generally computationally cheap, its computational cost can cause a severe burden when it comes to large-scale problems. Therefore, the proposed novel multi-fidelity method allows for considerably significant computational benefits to broaden the application range of the multi-fidelity method to the probabilistic design of large-scale composite structures.

Table 6.8: RBDO results

Level	Scatter degree of training data	Design and random variables used for the HFM and LFM		Result			Optimal design values to update the multi-fidelity model
				Critical temperature change (℃)		Mass (g)	
		HFM	LFM	HFM	LFM		
I	Dense	$X1, X2$	$X1, X2, X3, X4, E_{11}, E_{22} = E_{33}, G_{23}, G_{12} = G_{13}, \alpha_{11}, \alpha_{22}$	87	95	861	$X1$: 34.67 $X2$: 24.10 $X3$: 17.82 $X4$: 27.27
	Sparse	$X3, X4, E_{11}, E_{22} = E_{33}, G_{23}, G_{12} = G_{13}, \alpha_{11}, \alpha_{22}$	-				
II	Dense	$X3, X4$	$X3, X4, E_{11}, E_{22} = E_{33}, G_{23}, G_{12} = G_{13}, \alpha_{11}, \alpha_{22}$	98	110	867	$X1$: 34.67 $X2$: 24.10 $X3$: 18.00 $X4$: 30.00
	Sparse	$E_{11}, E_{22} = E_{33}, G_{23} G_{12} = G_{13}, \alpha_{11}, \alpha_{22}$	-				

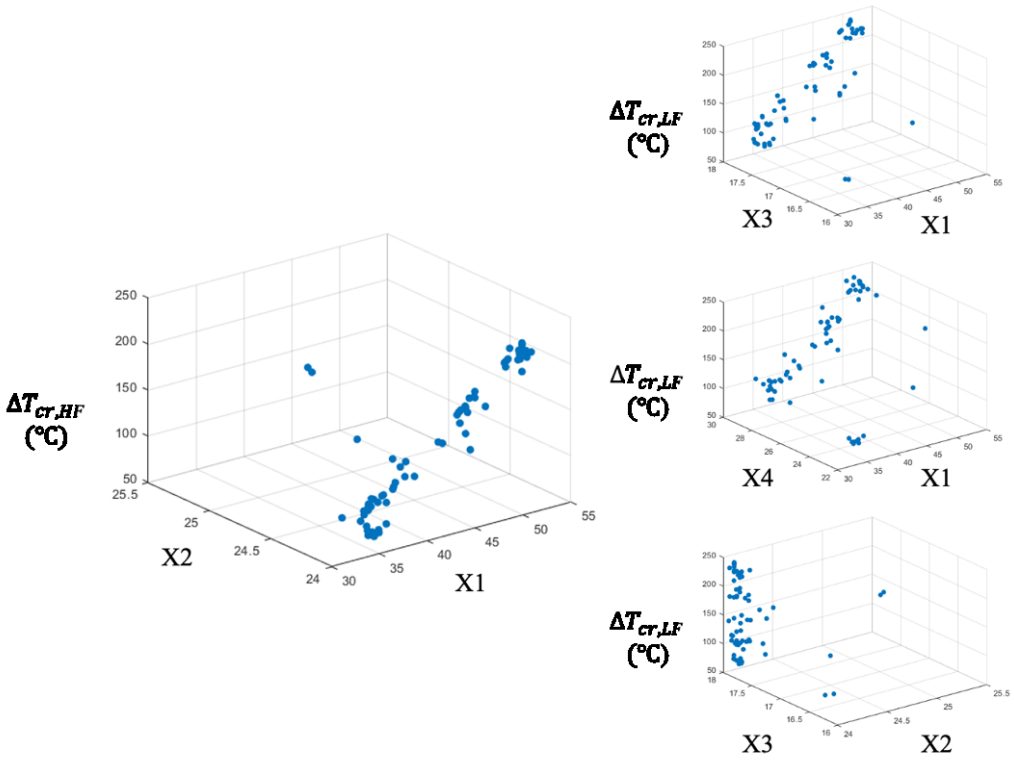

Figure 6.8: Multi-fidelity modelling based RBDO at Level I

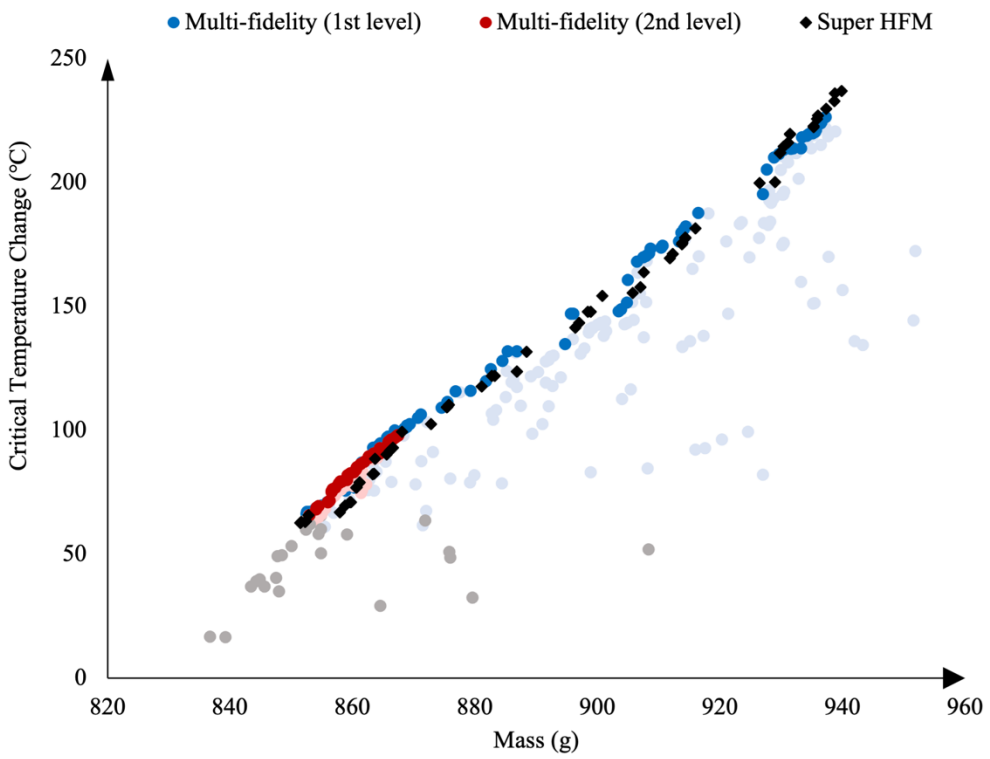

Figure 6.9: RBDO results comparison by Pareto Front between multi-fidelity model vs. super HFM

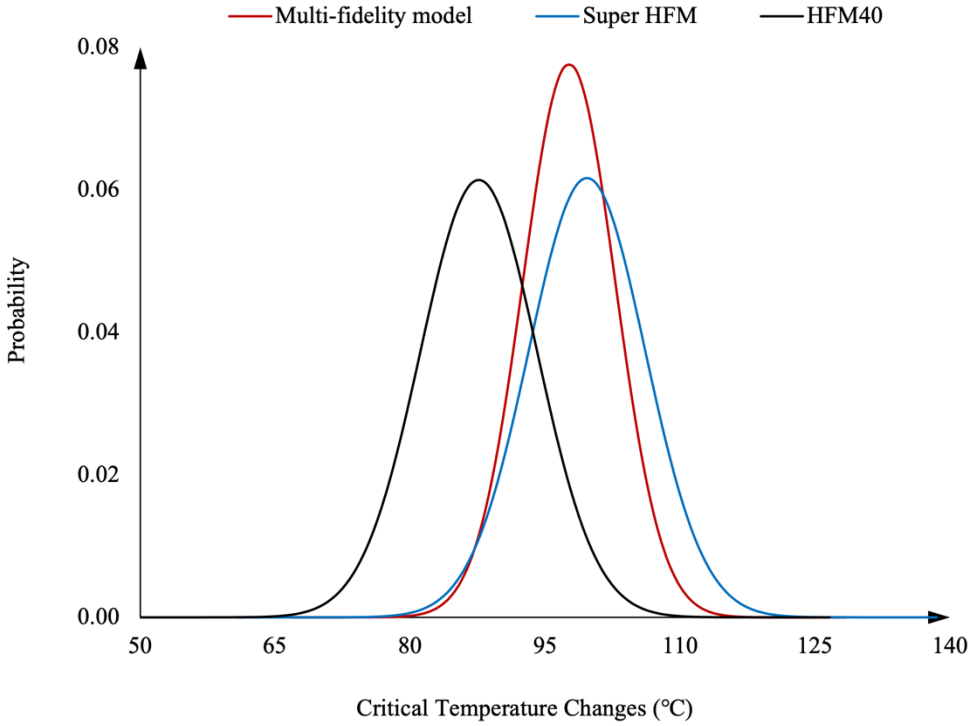

Figure 6.10: Statistical characteristic among three different models

Table 6.9: Design value and FE solver check

Model	Design variables (mm)				Mass (g)	Approximated model ΔT_{cr}(℃)		FEM model ΔT_{cr}(℃)
	$X1$	$X2$	$X3$	$X4$		μ	σ	
Multi-fidelity model	34.67	24.10	18.00	30.00	867	98.1	5.2	98.7
Super HFM	35.35	24.01	17.97	29.08	868	99.5	12.1	98.7
HFM40	37.25	24.01	17.97	23.90	865	87.4	9.3	85.1

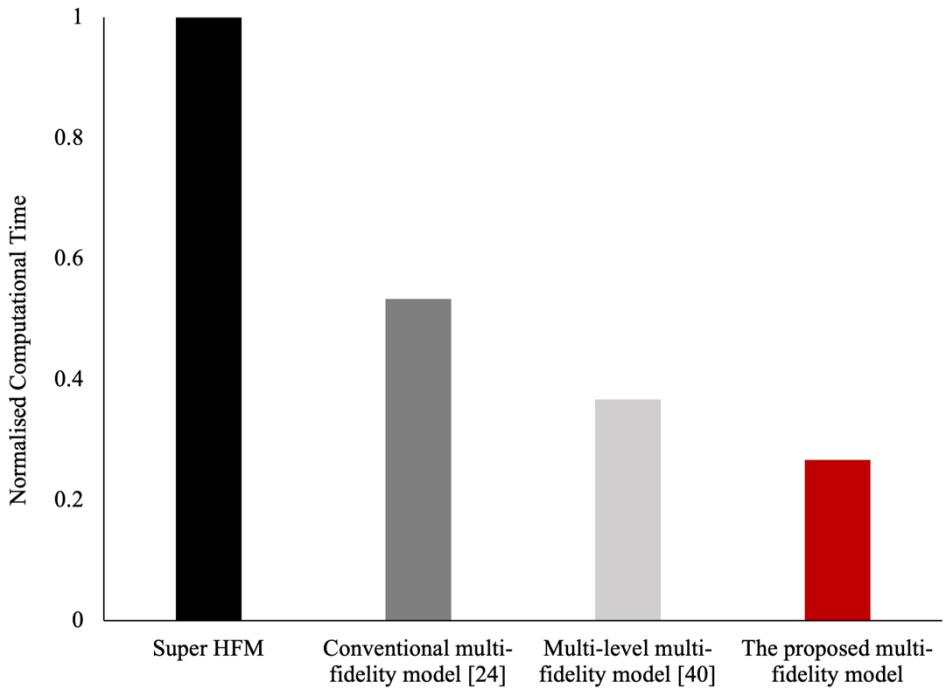

Figure 6.11: Computational efficiency comparison among four different methods

6.4 Summary

In this work, a novel multi-fidelity probabilistic optimisation approach was proposed and demonstrated with a mono-stiffened stringer composite panel under thermomechanical loading. This approach enables the probabilistic optimisation of composite structures while providing considerable computation time savings and reliable solutions. This research work's main contribution is that the HFM supervises a part of the entire design space as dense as possible while examining other design spaces sparsely within not causing extra computational cost. Simultaneously, the LFM takes all design variables for the multi-fidelity model to explore the whole design space. The NARGP is incorporated into this multi-fidelity method because it can quantify correlations between different fidelity models to predict more accurate solutions. This method also cooperates with a multi-level optimisation framework to be utilised for large-scale problems with a vast number of design variables. The proposed method was demonstrated by the RBDO problem of the composite structure under a thermal environment followed by mechanical shortening. The optimal solutions and their reliability assessments obtained by the proposed multi-fidelity method were nearly identical to those of the super HFM, the conventional surrogate modelling approach. They are also more accurate than a surrogate model that used the equivalent number of high-fidelity FEM simulations to the multi-fidelity model in terms of computation time. Compared with a FEM solver, the multi-fidelity model predicts the critical temperature changes more precisely than those of the super HFM for this example. As well as improvements in accuracy,

this proposed method provides significant improvements to computational efficiency. This new method's computational efficiency was highlighted by comparing it with a conventional surrogate method, traditional multi-fidelity method and multi-level multi-fidelity method. It should be noted that the proposed method offers remarkable computation time savings. In particular, this method is 30-50 % more computationally efficient than other multi-fidelity methods. The developed multi-fidelity probabilistic optimisation method is a new optimisation approach that enables the HFM and the LFM to supervise different design spaces while cooperating with each other during the optimisation process. This new multi-fidelity method enables the probabilistic optimisation of complex and large-scale problems, such as for composite structures under thermomechanical loading, to be conducted in a significantly more efficient and accurate manner.

7 Conclusions and Future Work

In this chapter, general conclusions and potential suggestions for both short-term and long-term future work are discussed.

7.1 Summary and Conclusions

As introduced in Chapter 1, the main objectives of the work presented in this thesis were to develop novel multi-fidelity modelling-based probabilistic design optimisation methods for composite structures, including Reliability-Based Design Optimisation (RBDO) and Robust Design Optimisation (RDO). In order to achieve the objectives, new multi-fidelity modelling formulations were formulated to specifically reduce the computational cost associated with the high-fidelity finite element analysis. The newly developed formulations bridged the gap between High-Fidelity Model (HFM) and Low-Fidelity Model (LFM) using machine learning techniques, including Artificial Neural Networks (ANN) and Non-linear Auto-Regressive Gaussian Process (NARGP). Furthermore, a multi-level optimisation approach was developed and a new sampling strategy were integrated into the probabilistic design for the first time. The developed multi-fidelity probabilistic optimisation methods enable the HFM and the LFM to have a different number of design variables during the optimisation process; hence, they offered more computational benefits than traditional surrogate methods and existing multi-fidelity methods. Several engineering examples using aircraft mono-stringer stiffened composite panels under mechanical and thermal loads demonstrated the accuracy and computational efficiency of the developed multi-fidelity probabilistic optimisation methods. Results represent that the developed methods herein significantly reduce the required computational time, allowing for more design variables to be considered early in the design stage of large-scale and complex aircraft composite structures. The results discussed in Chapters 4, 5 and 6 show that this main research aim has been accomplished.

In Chapter 4, a multi-fidelity modelling-based RBDO framework was developed for composite structures for the first time. This framework proved to provide acceptable accuracy and substantial computational efficiency compared with the conventional RBDO optimisation method using the

common high-fidelity surrogate model. The new multi-fidelity framework also assured the capability to carry out different reliability analyses estimating the probability of failure. These were demonstrated in two engineering examples at the end of the chapter highlighting the accuracy and efficiency of the developed framework.

In Chapter 5, a new multi-fidelity modelling-based RDO framework was developed for covering different design spaces between High-Fidelity Model (HFM) and Low-Fidelity Model (LFM). Two engineering examples featuring a mono-stiffened stringer composite panel subjected to the non-linear post-buckling regime were examined. The developed framework integrated with multi-level optimisation convinced extra computational gains compared with the traditional multi-fidelity methods while providing acceptable accuracy.

In Chapter 6, a novel multi-fidelity modelling-based probabilistic optimisation framework was developed for considering the non-linear correlations between the HFM and the LFM using Gaussian Process (GP). An engineering example of the same composite panel under thermomechanical loading was investigated. This new framework employing different sampling degrees to the HFM probed to be more computationally efficient than other different multi-fidelity methods. The accuracy of this framework was further improved with the use of non-linear fusion GP.

As mentioned in Chapter 1, the primary objectives of the work presented in this thesis broke down into five sub-objectives. The conclusions for each of these sub-objectives are summarised as follows.

1. **To develop a multi-fidelity RBDO framework for composite structures integrating with the use of surrogate modelling.** This was introduced in Chapter 4. The developed multi-fidelity method using the Artificial Neural Networks (ANN) provides acceptable accuracy and significant computational efficiency to carry out the RBDO process of composite structures. Firstly, the accuracy of the multi-fidelity models was demonstrated by comparing the conventional high-fidelity surrogate models. Overall, the direct multi-fidelity models that directly called low-fidelity FEM models during the modelling process offer more accurate solutions to carry out the reliability analyses and RBDO process than the indirect multi-fidelity models that called the surrogate model of the LFM. These multi-fidelity models using 11 high-fidelity FEM models proved to be much more accurate than a surrogate model using the same number of high-fidelity FEM models used in the multi-fidelity models. In particular, their accuracy assured to be similar to a surrogate model using the high-fidelity FEM models four times more than the number of high-fidelity FEM models used in the multi-fidelity models. The multi-fidelity models proved to be utilised with different reliability methods such as MCS, FORM and SORM. Although FORM and SORM require the first-order and second-order gradients of the response surfaces, the direct multi-fidelity models provided acceptable accuracy to estimate the probability of failure of the structural system. These multi-fidelity

models also proved to be suitable to conduct the RBDO process since they correctly found the optimal solutions, which are nearly identical to those of the traditional high-fidelity surrogate model. The Pareto fronts between the multi-fidelity and high-fidelity surrogate models were almost similar across the solution space. The mean values and standard deviation of the selected optimal solution based on the equal mass showed a high level of accuracy between the two different models. Secondly, the computational efficiency was evaluated by comparing the total simulation numbers of both FEM and surrogate models for the reliability analyses and RBDO process. Notable computational time savings were achieved by the use of multi-fidelity models. All computational costs were normalised by the computation time for MCS of the surrogate model using one hundred of HFMs. The direct multi-fidelity models were slightly computationally expensive compared with the indirect multi-fidelity models since they directly use the low-fidelity FEM models to offer higher accuracy. When utilising the multi-fidelity surrogate models, the computational costs among MCS, FORM and SORM assured to be comparable due to the inherent computational benefit of the surrogate model. Given that the computational time of the surrogate model using only LFM is similar to those of the multi-fidelity models, it should be highlighted that the developed multi-fidelity probabilistic optimisation framework provides significant computational efficiency as well as high accuracy nearly identical to the traditional high-fidelity surrogate model.

2. **To develop a multi-fidelity modelling formulation covering different design spaces between the HFM and the LFM.** This was introduced in Chapter 5. Overall, the developed formulation allows the HFM and the LFM to have a different number of design variables to provide more computational efficiency than the traditional multi-fidelity methods. These multi-fidelity methods, including the method presented in Chapter 4, require an equal number of FEM simulations between the HFM and the LFM. The main drawback of these methods causes extra high-fidelity FEM simulations associate with the number of design variables in the HFM. Ideally, many low-fidelity simulations and fewer high-fidelity simulations bring more computational benefit to the probabilistic optimisation. The developed multi-fidelity formulation enables the HFM to cover the design spaces of a few selected design variables. At the same time, other design variables not chosen in the HFM are included in the LFM to explore the entire design space. This idea was achieved by incorporating multi-level optimisation into the multi-fidelity formulation. In this formulation, the HFM aims to find accurate optimal solutions of the selected design variables during the probabilistic optimisation process. In contrast, the LFM aims to allow engineers to explore the solution spaces of design variables not included in the HFM. It was found that the HFM discovers the optimal solutions in the high-fidelity design space at the end of each optimisation level. These optimal solutions were used to correct the multi-fidelity models before they carry out the next level. The optimal solutions obtained by the LFM were used by the initial starting points for the next level to find global

solutions efficiently. In conclusion, the multi-fidelity formulation proved to be a more computationally efficient alternative to construct an acceptable multi-fidelity model while preserving a high level of accuracy similar to the traditional surrogate models.

3. **To develop a multi-fidelity RDO framework for composite structures under the non-linear post-buckling regime when the HFM has a smaller number of design variables than the LFM.** This was introduced in Chapter 5. The developed multi-fidelity formulation was incorporated into the RDO framework of composite structures. The framework was demonstrated by two engineering examples of a mono-stiffened stringer composite panel under the non-linear post-buckling regime, deterministic optimisation (DO) and RDO, respectively. It was found that the difference in solution accuracy between the multi-fidelity model and the high-fidelity FEM model for the DO process was only less than 1 %. The computational time savings obtained by the multi-fidelity model was 75 % in comparison with the DO using the high-fidelity FEM model directly. The multi-fidelity methods delivered more computational gains to the RDO process considering the design uncertainties of geometry parameters. Due to a significant number of simulations for the RDO process, the high-fidelity FEM model was not able to be directly used. Still, the traditional high-fidelity surrogate model was used to evaluate the efficiency and accuracy of the developed multi-fidelity methods. It was found that the objective functions obtained by the multi-fidelity model were improved as the optimisation level was progressed. The difference in the optimal solutions having an equal mass between the two models were less than 1 %, while the optimal solution using the multi-fidelity model was more robust than the high-fidelity surrogate model. It was found that more economic computational cost was achieved using the developed multi-fidelity model. The multi-fidelity model required both 40 high-fidelity design points and 210 low-fidelity design points. In contrast, the conventional surrogate model requested 200 high-fidelity design points. It was found that around 70 % of computational time savings were obtained using this multi-level multi-fidelity method. These examples assured that the developed multi-fidelity method shows significant potential for large-scale composite design problems considering the design uncertainties compared to different multi-fidelity methods.
4. **To develop a multi-fidelity modelling formulation utilising different sampling levels between the HFM and the LFM while considering non-linear correlations between them.** This was introduced in Chapter 6. A multi-fidelity modelling formulation was developed to deliver more computational gains as well as more accurate solutions. This approach was able to improve the multi-level multi-fidelity method presented in Chapter 5 that the HFM provides the high-fidelity information regarding the design variables selected. The method was capable of capturing the response surfaces of structural behaviours that show a simple linear trend between different fidelity models. This formulation presented in this chapter was motivated using different sampling levels to collect the high-fidelity information from the entire design

space while collecting the low-fidelity information as much as possible. The sampling strategy was established to collect high-fidelity information using dense sampling and sparse sampling. It was found that this sampling strategy allows the multi-fidelity model to require a smaller number of high-fidelity FEM simulations embracing a part of the entire design space. At the same time, it was found that the high-fidelity training dataset offers sparsely information of other design spaces without causing extra high-fidelity FEM simulations. The non-linear fusion GP was used to consider the non-linear correlation between the HFM and the LFM. Compared to the use of conventional surrogate modelling methods, the use of the non-linear fusion GP constructed a more accurate multi-fidelity model capturing a complex trend between different fidelity models. Both the sampling scheme and the non-linear fusion GP were integrated with multi-level optimisation to bring more computational efficiency to large-scale design problems. In conclusion, it has been demonstrated that this novel multi-fidelity modelling formulation can efficiently and accurately conduct the probabilistic optimisation of composite structures.

5. **To develop a multi-fidelity probabilistic optimisation framework for composite structures subjected to thermomechanical loading.** This was introduced in Chapter 6. The developed multi-fidelity formulation using the non-linear fusion GP was incorporated into the RBDO process. The established framework was demonstrated by an engineering example of a mono-stiffened stringer panel under thermomechanical loading. The composite panel was subject to mechanical loading and thermal loading. The design uncertainties of four geometry parameters and six material properties were considered input parameters to construct the multi-fidelity model. It was found that the multi-fidelity model for each level of the RBDO process scrutinises a part of design spaces while providing sparely high-fidelity information to the LFM. This enabled the multi-fidelity model to be updated using the optimal solutions at the end of each level, as well as be ready to explore different design spaces for the following level. The Pareto front of the multi-fidelity model was compared with the conventional surrogate model using 150 high-fidelity FEM simulations. It was found that the solution spaces are more thoroughly examined as the optimisation level goes up. This offered more reliable and better solutions compared with those of the previous optimisation levels since the design space to be explored by the multi-fidelity model narrowed down. The statistical characteristics of the optimal solution obtained by the multi-fidelity model were nearly identical to those of the optimal solution from the high-fidelity surrogate model. The multi-fidelity model proved to be more accurate than the surrogate model using 40 high-fidelity FEM simulations that equates to both 20 HFMs and 70 LFMs required for constructing the multi-fidelity model. In terms of computational efficiency, it is not surprising that the multi-fidelity model accomplished about 75 % reduction compared to the surrogate model using 150 high-fidelity FEM simulations. It was found that the multi-fidelity model delivers around 50% of computational time savings compared with the traditional multi-fidelity method (47) using both 60 HFMs and 60 LFMs.

This multi-fidelity model proved to be approximately 30 % more computationally efficient than the multi-level multi-fidelity method presented in Chapter 5, requiring both 20 HFMs and 110 LFMs. Given that the computational cost of low-fidelity FEM simulations could lead to a severe challenge when it comes to large-scale design problems, the gains obtained by a smaller number of low-fidelity FEM models can be significant.

7.2 Future Work

Some possible future research works are summarised as follows. These suggested works are divided into two groups, such as short-term and long-term. Short-term research work can be accomplished within one year, while long-term research work requests more than several years.

7.2.1 Short-Term Future Research Work

- In the research work introduced in Chapter 6 of the thesis, the developed multi-fidelity formulation was demonstrated by the probabilistic design optimisation of composite structures under thermomechanical buckling. If the formulation is shown by a more practical engineering problem of large-scale composite structures, its advantages would be strengthened. As presented in Chapter 5, the non-linear post-buckling strength can be a helpful design criterion to achieve more lightweight to reduce fuel consumption while maintaining structural stability. Hence, the multi-fidelity formulation could be implemented to the probabilistic design optimisation of a sizeable multi-stiffened stringer composite panel subjected to the non-linear thermal post-buckling regime.
- Depending on the level of complexity involved, it might be worthy of considering material non-linearity, including damage propagation failure analysis. Suppose the non-linear fusion GP does not construct a multi-fidelity model to capture the response surfaces of a large-scale problem. Then a more advanced multi-fidelity approach, known as Deep GP, can be utilised to boost the quality of the multi-fidelity model. However, an innovative improvement in the multi-fidelity formulation should be put forth to deal with the considerable computational cost caused by the Deep GP.

7.2.2 Long-Term Future Research Work

- The work presented in this thesis was restricted to probabilistic design optimisation considering uncertainties associated with the design and manufacturing process. However, it would be

interesting to broaden the application area of developed research work on the operational and ageing process such as Structural Health Mentoring (SHM).

- The multi-fidelity SHM framework with probabilistic design philosophy could deliver the total solution framework to industry, such as aircraft and offshore wind power. Notably, it would be better to develop new multi-fidelity formulations that require experimental data for high-fidelity information and computational simulations for low-fidelity information. This could contribute to providing remarkable time savings into the virtual design, testing and inspection.

8 Bibliography

1. Jones RM. *Mechanics of composite materials*. Taylor & Francis; 1997.

2. Baker JW, Schubert M, Faber MH. On the assessment of robustness. *Structural Safety*. 2008;30(3): 253–267. https://doi.org/10.1016/j.strusafe.2006.11.004.

3. Taguchi G. *Introduction to quality engineering: designing quality into products and processes*. Quality Resources; 1986.

4. Bacarreza O, Aliabadi MH, Apicella A. Robust design and optimization of composite stiffened panels in post-buckling. *Structural and Multidisciplinary Optimization*. 2015;51(2): 409–422. https://doi.org/10.1007/s00158-014-1136-5.

5. Long MW, Narcosi JD. *Probabilistic design methodology for composite aircraft structure*. DOT/FAA/AR-99/2. 1999 [Accessed 15th April 2021]. http://www.tc.faa.gov/its/worldpac/techrpt/ar99-2.pdf [Accessed 15th April 2021].

6. Bouckaert S, Pales AF, McGlade C, Remme U, Wanner B. *Net-zero by 2050: a roadmap for the global energy sector*. International Energy Agency. 2021 [Accessed 30th May 2021]. https://www.iea.org/reports/net-zero-by-2050 [Accessed 30th May 2021].

7. Rackwitz R. Reliability analysis - a review and some perspectives. *Structural Safety*. 2001;23(4): 365–395. https://doi.org/https://doi.org/10.1016/S0167-4730(02)00009-7.

8. Choi S-K, Grandhi R, Canfield RA. *Reliability-based structural design*. London: Springer; 2006. https://doi.org/10.1007/978-1-84628-445-8.

9. Robert E Melchers ATB. *Structural reliability analysis and prediction*. John Wiley & Sons; 2018. https://doi.org/10.1002/9781119266105.

10. Wang GG, Shan S. Review of metamodeling techniques in support of engineering design optimization. *Journal of Mechanical Design*. 2007;129(4): 370–380. https://doi.org/10.1115/1.2429697.

11. Forrester AIJ, Sobester A, Keane AJ. *Engineering design via surrogate modelling: a practical guide*. John Wiley and Sons; 2008. https://doi.org/10.1002/9780470770801.

12. Peherstorfer B, Willcox K, Gunzburger M. Survey of multi-fidelity methods in uncertainty propagation, inference, and optimization. *SIAM Review*. 2018;60(3): 550–591. https://doi.org/10.1137/16M1082469.

13. Das TK, Ghosh P, Das NCh. Preparation, development, outcomes, and application versatility of carbon fiber-based polymer composites: a review. *Advanced Composites and Hybrid Materials*. 2019;2(2): 214–233. https://doi.org/10.1007/s42114-018-0072-z.

14. López C, Bacarreza O, Baldomir A, Hernández S, H. Ferri Aliabadi M. Reliability-based design optimization of composite stiffened panels in post-buckling regime. *Structural and Multidisciplinary Optimization*. 2017;55(3): 1121–1141. https://doi.org/10.1007/s00158-016-1568-1.

15. Farokhi H, Bacarreza O, Aliabadi MHF. Probabilistic optimisation of mono-stringer composite stiffened panels in post-buckling regime. *Structural and Multidisciplinary Optimization*. 2020;62: 1395–1417. https://doi.org/10.1007/s00158-020-02565-9.

16. Gutiérrez Álvarez J, Bisagni C. Closed-form solutions for thermomechanical buckling of orthotropic composite plates. *Composite Structures*. 2020;233(May 2019): 111622. https://doi.org/10.1016/j.compstruct.2019.111622.

17. Lee HJ, Lee JJ, Huh JS. A simulation study on the thermal buckling behavior of laminated composite shells with embedded shape memory alloy (SMA) wires. *Composite Structures*. 1999;47(1–4): 463–469. https://doi.org/10.1016/S0263-8223(00)00020-9.

18. Yoo K-K, Kim J-H. Optimal design of smart skin structures for thermo-mechanical buckling and vibration using a genetic algorithm. *Journal of Thermal Stresses*. 2011;34(10). https://doi.org/10.1080/01495739.2011.601261.

19. Yao W, Chen X, Luo W, van Tooren M, Guo J. Review of uncertainty-based multidisciplinary design optimization methods for aerospace vehicles. *Progress in Aerospace Sciences*. 2011;47(6): 450–479. https://doi.org/10.1016/j.paerosci.2011.05.001.

20. Sbaraglia F, Farokhi H, Aliabadi MHF. Robust and reliability-based design optimization of a composite floor beam. *Key Engineering Materials*. 2018;774: 486–491. https://doi.org/10.4028/www.scientific.net/KEM.774.486.

21. Viana FAC, Simpson TW, Balabanov V, Toropov V. Metamodeling in multidisciplinary design optimization: how far have we really come? *AIAA Journal*. 2014;52(4): 670–690. https://doi.org/10.2514/1.J052375.

22. Parnianifard A, Azfanizam AS, Ariffin MKA, Ismail MIS, Ale Ebrahim N. Recent developments in metamodel based robust black-box simulation optimization: an overview. *Decision Science Letters*. 2019;8(1): 17–44. https://doi.org/10.5267/j.dsl.2018.5.004.

23. Fernández-Godino MG, Park C, Kim N-H, Haftka RT. Review of multi-fidelity models. *arXiv preprint*. 2016; arXiv:1609.07196v3. https://doi.org/10.1016/j.jcp.2015.01.034.

24. Yoo K, Bacarreza O, Aliabadi MHF. A novel multi-fidelity modelling-based framework for reliability-based design optimisation of composite structures. *Engineering with Computers*. 2020; https://doi.org/10.1007/s00366-020-01084-x.

25. Marler RT, Arora JS. Survey of multi-objective optimization methods for engineering. *Structural and Multidisciplinary Optimization*. 2004;26(6): 369–395. https://doi.org/10.1007/s00158-003-0368-6.

26. Koziel S, Yang X-S. *Computational optimization, methods and algorithms*. Berlin, Heidelberg: Springer Berlin Heidelberg; 2011. https://doi.org/10.1007/978-3-642-20859-1.

27. Andradottir S. A review of simulation optimization techniques. In: *1998 Winter Simulation Conference. Proceedings (Cat. No.98CH36274)*. IEEE; https://doi.org/10.1109/WSC.1998.744910.

28. Haftka RT, Gürdal Z. *Elements of Structural Optimization*. Springer, Dordrecht; 1992. https://doi.org/https://doi.org/10.1007/978-94-011-2550-5.

29. Vanderplaats GN. *Multidiscipline Design Optimization*. Vanderplaats Research & Development; 2007.

30. Arora RK. *Optimization: Algorithms and applications*. Chapman and Hall/CRC; 2015. https://doi.org/10.1017/cbo9780511974076.010.

31. Boyd S, Vandenberghe L. *Convex optimization*. Cambridge University Press; 2004. https://doi.org/10.1017/CBO9780511804441.

32. Qureshi M, Yoo K, Aliabadi MHF. Assessment of algorithms for the probabilistic optimisation of composite panels. In: *AIP Conference Proceedings 2309, 020045*. 2020. https://doi.org/10.1063/5.0034767.

33. Lewis RM, Torczon V, Trosset MW. Direct search methods: then and now. *Journal of Computational and Applied Mathematics*. 2000;124(1–2). https://doi.org/10.1016/S0377-0427(00)00423-4.

34. Zitzler E, Lothar T, Kalyanmoy D. Comparison of multiobjective evolutionary algorithms: empirical results. *Evol.\ Comput.* 2000;8(2): 173–195. https://doi.org/10.1016/S0377-0427(00)00423-4.

35. Kalyanomy DEB AP. A fast and elitist multi-objective genetic algorithm: NSGA-II. *IEEE TRANSACTIONS ON EVOLUTIONARY COMPUTATION*. 2001;6(0): 182–197. https://doi.org/10.1109/4235.996017.

36. Deb K. *Multiobjective optimization using evolutionary algorithms*. Wiley. Wiley; 2001.

37. Coello CA. An updated survey of GA-based multiobjective optimization techniques. *ACM Computing Surveys*. 2000;32(2): 109–143. https://doi.org/10.1145/358923.358929.

38. Bektas E, Broermann K, Pecanac G, Rzepka S, Silber C, Wunderle B. Robust design optimization: on methodology and short review. In: *2017 18th International Conference on Thermal, Mechanical and Multi-Physics Simulation and Experiments in Microelectronics and Microsystems, EuroSimE 2017*. 2017. p. 1–7. https://doi.org/10.1109/EuroSimE.2017.7926290.

39. Zang TA, Hemsch MJ, Hilburger MW, Kenny SP, Luckring JM. *Needs and opportunities for uncertainty-based multidisciplinary design methods for aerospace vehicles*. 2002.

40. Yoo K, Bacarreza O, Aliabadi MHF. Multi-fidelity robust design optimisation for composite structures based on low-fidelity models using successive high-fidelity corrections. *Composite Structures*. 2021;259(July 2020): 113477. https://doi.org/10.1016/j.compstruct.2020.113477.

41. Morse L, Khodaei ZS, Aliabadi MH. Multi-fidelity modeling-based structural reliability analysis with the boundary element method. *Journal of Multiscale Modelling*. 2017;8: 1740001. https://doi.org/10.1142/S1756973717400017.

42. Schuëller GI, Jensen HA. Computational methods in optimization considering uncertainties - an overview. *Computer Methods in Applied Mechanics and Engineering*. 2008;198(1): 2–13. https://doi.org/10.1016/j.cma.2008.05.004.

43. Youn BD, Choi KK. Selecting probabilistic approaches for reliability-based design optimization. *AIAA Journal*. 2008;42(1): 124–131. https://doi.org/10.2514/1.9036.

44. Haldar A, Mahadevan S. *Probability, reliability, and statistical methods in engineering design*. Wiley; 1999.

45. Vitali R, Haftka RT, Sankar B v. Multi-fidelity design of stiffened composite panel with a crack. *Structural and Multidisciplinary Optimization*. 2002;23(5): 347–356. https://doi.org/10.1007/s00158-002-0195-1.

46. Park C, Haftka RT, Kim NH. Remarks on multi-fidelity surrogates. *Structural and Multidisciplinary Optimization*. 2017;55(3): 1029–1050. https://doi.org/10.1007/s00158-016-1550-y.

47. Burhenne S, Jacob D, Henze GP. Sampling-based on sobol sequence for monte carlo techniques applied to building simulation. In: *Proceedings of Building Simulation 2011: 12th Conference of International Building Performance Simulation Association*. Sydney; 2011. p. 1816–1823.

48. Hassoun MH. *Fundamentals of artificial neural networks*. MIT Press; 1995. https://doi.org/10.1109/tnn.1996.501738.

49. Buhmann MD. *Radial basis functions*. Cambridge University Press; 2003. https://doi.org/10.1017/CBO9780511543241.

50. Fang H, Horstemeyer MF. Global response approximation with radial basis functions. *Engineering Optimization*. 2006;38(4). https://doi.org/10.1080/03052150500422294.

51. Yaser S Abu-Mostafa, Malik Magdon-Ismail H-TL. *Learning from data*. AMLBook; 2012.

52. Rasmussen CE, Williams CKI, Bach F. *Gaussian processes for machine learning*.. vol. 2. Cambridge, MA: MIT Press.; 2006. http://www.gaussianprocess.org/gpml/chapters/RW.pdf

53. Mack Y, Goel T, Shyy W, Haftka R. Surrogate model-based optimization framework: a case study in aerospace design. In: Springer; 2007. https://doi.org/10.1007/978-3-540-49774-5_14.

54. Eason J, Cremaschi S. Adaptive sequential sampling for surrogate model generation with artificial neural networks. *Computers and Chemical Engineering*. 2014;68: 220–232. https://doi.org/10.1016/j.compchemeng.2014.05.021.

55. Simulia 3ds. *Abaqus documentation*. 2019.

56. Simulia 3ds. *Isight documentation*. Simulia; 2019. http://www.3ds.com/fileadmin/PRODUCTS/SIMULIA/PDF/whitepapers/SIMULIA-Isight-Design-Optimization-Methodologies.pdf

57. Lam R. *Surrogate modeling-based on statistical techniques for multi-fidelity optimization*. 2014. http://hdl.handle.net/1721.1/90673

58. Gano SE, Renaud JE, Sanders B. Hybrid variable fidelity optimization by using a kriging-based scaling function. *AIAA Journal*. 2008;43(11): 2422–2433. https://doi.org/10.2514/1.12466.

59. Bakr MH, Bandler JW, Madsen K, Sndergaard J. An introduction to the space mapping technique. *Optimization and Engineering*. 2001;2(4): 369–384. https://doi.org/10.1023/A:1016086220943.

60. Bakr MH, Bandler JW, Madsen K, Søndergaard J. Review of the space mapping approach to engineering optimization and modeling. *Optimization and Engineering*. 2000;1(3): 241–276. https://doi.org/10.1023/a%253a1010000106286.

61. Forrester AIJ, Sóbester A, Keane AJ. Multi-fidelity optimization via surrogate modelling. *Proceedings of the Royal Society A: Mathematical, Physical and Engineering Sciences*. 2007;463(2088): 3251–3269. https://doi.org/10.1098/rspa.2007.1900.

62. Kennedy MC, O'Hagan A. Predicting the output from a complex computer code when fast approximations are available. *Biometrika*. 2000;87(1): 1–13. https://doi.org/10.1093/biomet/87.1.1.

63. Hassanien S, Kainat M, Adeeb S, Langer D. On the use of surrogate models in reliability-based analysis of dented pipes. In: *Proceedings of the 2016 11th International Pipeline Conference*. Calgary, Alberta, Canada: ASME; 2016. p. 1–9. https://doi.org/10.1115/IPC2016-64470.

64. Lee S, Kim I-G, Cho W, Shul C. Advanced probabilistic design and reliability-based design optimization for composite sandwich structure. *Advanced Composite Materials*. 2014;23(1): 3–16. https://doi.org/10.1080/09243046.2013.862381.

65. Scarth C, Sartor PN, Cooper JE, Weaver PM, Silva GHC. Robust and reliability-based aeroelastic design of composite plate wings. *AIAA Journal*. 2017;55(10): 3539–3552. https://doi.org/10.2514/1.J055829.

66. Jin R, Chen W, Sudjianto A. On sequential sampling for global metamodeling in engineering design. In: *Proceedings of DETC'02: ASME 2002 Design Engineering Technical Conferences And Computers and ASME 2002 Design Engineering Technical Conferences*. Montreal, Canada: ASME; 2002. p. DETC2002/DAC-34092. https://doi.org/10.1115/DETC2002/DAC-34092.

67. Alexandrov NM, Lewis RM, Gumbert CR, Green LL, Newman PA. Approximation and model management in aerodynamic optimization with variable-fidelity models. *Journal of Aircraft*. 2001;38(6): 1093–1101. https://doi.org/10.2514/2.2877.

68. Goldfeld Y, Vervenne K, Arbocz J, Keulen F van. Multi-fidelity optimization of laminated conical shells for buckling. *Structural and Multidisciplinary Optimization*. 2005;30(2): 128–141. https://doi.org/10.1016/j.tws.2004.07.003.

69. Causon D, Mingham C. *Introductory finite difference methods for PDEs*. Bookboon; 2010.

70. Lee DS, Morillo C, Oller S, Bugeda G, Oñate E. Robust design optimisation of advance hybrid (fiber-metal) composite structures. *Composite Structures*. 2013;99: 181–192. https://doi.org/10.1016/j.compstruct.2012.11.033.

71. Zhou XY, Ruan X, Gosling PD. Robust design optimization of variable angle tow composite plates for maximum buckling load in the presence of uncertainties. *Composite Structures*. 2019;223(February). https://doi.org/10.1016/j.compstruct.2019.110985.

72. António CC, Hoffbauer LN. Bi-level dominance GA for minimum weight and maximum feasibility robustness of composite structures. *Composite Structures*. 2016;135: 83–95. https://doi.org/10.1016/j.compstruct.2015.09.019.

73. Keane AJ. Cokriging for robust design optimization. *AIAA Journal*. 2012;50(11): 2351–2364. https://doi.org/10.2514/1.j051391.

74. Vuruskan A, Hosder S. Impact of turbulence models and shape parameterization on robust aerodynamic shape optimization. *Journal of Aircraft*. 2019;56(3): 1099–1115. https://doi.org/10.2514/1.C035039.

75. Dodson M, Parks GT. Robust aerodynamic design optimization using polynomial chaos. *Journal of Aircraft*. 2009;46(2): 635–646. https://doi.org/10.2514/1.39419.

76. Ong YS, Nair PB, Keane AJ. Evolutionary optimization of computationally expensive problems via surrogate modeling. *AIAA Journal*. 2003;41(4): 687–696. https://doi.org/10.2514/2.1999.

77. Mohammad Nezhad A, Mahlooji H. An artificial neural network meta-model for constrained simulation optimization. *Journal of the Operational Research Society*. 2014;65(8): 1232–1244. https://doi.org/10.1057/jors.2013.73.

78. Gu X, Sun G, Li G, Mao L, Li Q. A Comparative study on multiobjective reliable and robust optimization for crashworthiness design of vehicle structure. *Structural and Multidisciplinary Optimization*. 2013;48(3): 669–684. https://doi.org/10.1007/s00158-013-0921-x.

79. Zhou Q, Wang Y, Choi SK, Jiang P, Shao X, Hu J, et al. A robust optimization approach based on multi-fidelity metamodel. *Structural and Multidisciplinary Optimization*. 2018;57(2): 775–797. https://doi.org/10.1007/s00158-017-1783-4.

80. Robinson TD, Eldred MS, Willcox KE, Haimes R. Surrogate-based optimization using multi-fidelity models with variable parameterization and corrected space mapping. *AIAA Journal*. 2008;46(11): 2814–2822. https://doi.org/10.2514/1.36043.

81. Leary SJ, Bhaskar A, Keane AJ. A constraint mapping approach to the structural optimization of an expensive model using surrogates. *Optimization and Engineering*. 2001;2(4). https://doi.org/10.1023/A:1016038305014.

82. Madsen K, Bandler JW, Dakroury SA, Bakr MH, Sondergaard J, Cheng QS, et al. Space Mapping: The State of the Art. *IEEE Transactions on Microwave Theory and Techniques*. 2004;52(1): 337–361. https://doi.org/10.1109/tmtt.2003.820904.

83. Sinha A, Malo P, Deb K. A review on bi-level optimization: from classical to evolutionary approaches and applications. *IEEE Transactions on Evolutionary Computation*. 2018;22(2): 276–295. https://doi.org/10.1109/TEVC.2017.2712906.

84. Choi S, Alonso JJ, Kroo IM. Two-level multi-fidelity design optimization studies for supersonic jets. *Journal of Aircraft*. 2009;46(3): 776–790. https://doi.org/10.2514/1.34362.

85. Liu B, Haftka RT, Akgün MA. Two-level composite wing structural optimization using response surfaces. *Structural and Multidisciplinary Optimization*. 2000;20(2): 87–96. https://doi.org/10.1007/s001580050140.

86. Stevens KA, Ricci R, Davies GAO. Buckling and postbuckling of composite structures. *Composites*. 1995;26(3). https://doi.org/10.1016/0010-4361(95)91382-F.

87. Bisagni C. Numerical analysis and experimental correlation of composite shell buckling and post-buckling. *Composites Part B: Engineering*. 2000;31(8): 655–667. https://doi.org/10.1016/S1359-8368(00)00031-7.

88. Tsai SW, Wu EM. A general theory of strength for anisotropic materials. *Journal of Composite Materials*. 1971;5(1). https://doi.org/10.1177/002199837100500106.

89. Akcin Y, Karakaya S, Soykasap O. Electrical, thermal and mechanical properties of CNT treated prepreg CFRP composites. *Materials Sciences and Applications*. 2016;07(09): 465–483. https://doi.org/10.4236/msa.2016.79041.

90. Wang C, Xu Y, Du J. Study on the thermal buckling and post-buckling of metallic sub-stiffening structure and its optimization. *Materials and Structures/Materiaux et Constructions*. 2016;49(11): 4867–4879. https://doi.org/10.1617/s11527-016-0830-8.

91. Vosoughi AR, Nikoo MR. Maximum fundamental frequency and thermal buckling temperature of laminated composite plates by a new hybrid multi-objective optimization technique. *Thin-Walled Structures*. 2015;95: 408–415. https://doi.org/10.1016/j.tws.2015.07.014.

92. Meyers CA, Hyer MW. Thermal buckling and post-buckling of symmetrically laminated composite plates. *Journal of Thermal Stresses*. 1991;14(4). https://doi.org/10.1080/01495739108927083.

93. Nawab Y, Jacquemin F, Casari P, Boyard N, Borjon-Piron Y, Sobotka V. Study of variation of thermal expansion coefficients in carbon/epoxy laminated composite plates. *Composites Part B: Engineering*. 2013;50. https://doi.org/10.1016/j.compositesb.2013.02.002.

94. Chen X, Qiu Z. Reliability assessment of fiber-reinforced composite laminates with correlated elastic mechanical parameters. *Composite Structures*. 2018;203(April): 396–403. https://doi.org/10.1016/j.compstruct.2018.05.032.

95. Sohouli A, Yildiz M, Suleman A. Efficient strategies for reliability-based design optimization of variable stiffness composite structures. *Structural and Multidisciplinary Optimization*. 2017; 1–16. https://doi.org/10.1007/s00158-017-1771-8.

96. das Neves Carneiro G, Antonio CC. A RBRDO approach based on structural robustness and imposed reliability level. *Structural and Multidisciplinary Optimization*. 2018;57(6): 2411–2429. https://doi.org/10.1007/s00158-017-1870-6.

97. Cid Montoya M, Costas M, Díaz J, Romera LE, Hernández S. A multi-objective reliability-based optimization of the crashworthiness of a metallic-GFRP impact absorber using hybrid approximations. *Structural and Multidisciplinary Optimization*. 2015;52(4): 827–843. https://doi.org/10.1007/s00158-015-1255-7.

98. Perdikaris P, Venturi D, Royset JO, Karniadakis GE. Multi-fidelity modelling via recursive co-kriging and Gaussian-Markov random fields. *Proceedings of the Royal Society A: Mathematical, Physical and Engineering Sciences*. 2015;471(2179). https://doi.org/10.1098/rspa.2015.0018.

99. Perdikaris P, Raissi M, Damianou A, Lawrence ND, Karniadakis GE. Nonlinear information fusion algorithms for data-efficient multi-fidelity modelling. *Proceedings of the Royal Society A: Mathematical, Physical and Engineering Sciences*. 2017;473(2198). https://doi.org/10.1098/rspa.2016.0751.

100. Yoo K, Bacarreza O, Aliabadi MHF. Multi-fidelity probabilistic optimisation of composite structures under thermomechanical loading using Gaussian processes. *Computers & Structures*. 2021;257. https://doi.org/10.1016/j.compstruc.2021.106655.

101. Gratiet L le. Recursive co-kriging model for design of computer experiments with multiple levels of fidelity with an application to hydrodynamic. 2012;

102. Bouhlel MA, Bartoli N, Otsmane A, Morlier J. An improved approach for estimating the hyperparameters of the kriging model for high-dimensional problems through the partial least squares method. Cuevas E (ed.) *Mathematical Problems in Engineering*. 2016;2016: 6723410. https://doi.org/10.1155/2016/6723410.